

UNIVERSIDADE FEDERAL DO RIO GRANDE DO SUL
ESCOLA DE ENGENHARIA
PROGRAMA DE PÓS- GRADUAÇÃO EM ENGENHARIA DE MINAS, METALÚRGICA E
MATERIAIS - PPGE3M

VÍTOR OTACÍLIO DE ALMEIDA

**PROCESSAMENTO HIDROMETALÚRGICO DE
REJEITOS DE MINÉRIO DE FERRO**

Porto Alegre
2023

VÍTOR OTACÍLIO DE ALMEIDA

**PROCESSAMENTO HIDROMETALÚRGICO DE
REJEITOS DE MINÉRIO DE FERRO**

Trabalho realizado no Laboratório de Tecnologia Mineral e Ambiental (LTM) da Escola de Engenharia da UFRGS, dentro do Programa de Pós-Graduação em Engenharia de Minas, Metalúrgica e de Materiais (PPGE3M), como parte dos requisitos para obtenção do título de Doutor em Engenharia.

Orientador: Ivo André Homrich Schneider

Porto Alegre
2023

CIP - Catalogação na Publicação

Almeida, Vitor Otacilio de
PROCESSAMENTO HIDROMETALÚRGICO DE REJEITOS DE MINÉRIO DE
FERRO / Vitor Otacilio de Almeida. --2023.
194 f.

Orientador: Ivo André Homrich Schneider.

Tese (Doutorado) -- Universidade Federal do Rio
Grande do Sul, Escola de Engenharia, Programa de Pós-
Graduação em Engenharia de Minas, Metalúrgica e de
Materiais, Porto Alegre, BR-RS, 2023.

1. Hidrometalurgia. 2. Rejeito de minério de ferro.
3. Óxidos de ferro. 4. Silica. 5. Aproveitamento de
resíduos. I. Homrich Schneider, Ivo André, orient. II.
Título.

Esse trabalho será julgado para obtenção do título de Doutor em Engenharia, na área de concentração em Tecnologia Mineral, Ambiental e Metalurgia Extrativa do Programa de Pós-Graduação em Engenharia de Minas, Metalúrgica e de Materiais pela seguinte banca examinadora:

Orientador: Prof. Dr. Ivo André Homrich Schneider

Banca Examinadora:

Prof^a. Dr^a. Virginia Sampaio Teixeira Ciminelli

Prof. Dr. Neymayer Pereira Lima

Prof. Dr. Carlos Otávio Petter

Prof. Dr. Rodrigo de Lemos Peroni
Coordenador do PPGE3M

Dedico esse trabalho à Tia Ana (*in memoriam*).

AGRADECIMENTOS

Gratidão a Deus pela perseverança diante dos momentos difíceis; pela inspiração e crença neste sonho e pelas bençãos que recebo todos os dias.

Agradeço a Tia Ana, minha madrinha, amiga, inspiração e referência; por nunca ter saído do meu lado e me ensinado que o amanhã pode ser melhor que hoje e que a fé é a maior de todas as forças.

À minha mãe, por lutar ao meu lado e por ter dedicado muito a um futuro que hoje se faz presente. Obrigado por ser a luz dos meus sonhos!

Meus agradecimentos ao meu orientador Ivo Schneider, que me ajudou a dar voz a objetivos que guardei por muito tempo. Grato por todas as oportunidades e confiança no meu trabalho. Sua orientação, conselhos e dedicação aos desafios que construímos juntos foram decisivos para que eu pudesse chegar até aqui.

Aos meus familiares e amigos, que são minha referência de amizade, fraternidade e companheirismo. Ao Anderson e Isabel Müller que me abraçaram em sua família e me tornaram parte dela.

Ao Tito por trazer leveza e harmonia para cada instante do meu dia e por me ensinar o amor na forma mais pura.

Aos colegas do Laboratório de Tecnologia Mineral e Ambiental (LTM); em especial a Jessica Weiler e Karine Batista que permitiram que os “cebolas” dividissem momentos únicos juntos; no trabalho, nas conversas, nos cafés e almoços de RU.

A CAPES, CNPq, VALE, UFRGS, PPGE3M e LTM, pelo incentivo à pesquisa, recursos disponibilizados e infraestrutura.

A todos que fizeram e fazem parte do meu caminho; alegrando a vida e permitindo que essa jornada seja leve e inesquecível.

Minha Gratidão!

“São nossas escolhas, mais do que as nossas capacidades, que mostram quem realmente somos - Alvo Dumbledore”
(ROWLING, 2000).

RESUMO

O gerenciamento de rejeitos de minério de ferro é um dos principais desafios do setor mineral, especialmente pelos volumes gerados e pelos riscos decorrentes de sua disposição. Nesse contexto, o objetivo deste trabalho foi discutir os efeitos da disposição de rejeitos, as alternativas de aproveitamento e as oportunidades associadas ao processamento hidrometalúrgico. A lixiviação, com uso de ácido clorídrico (HCl) à quente, foi investigada e os parâmetros de temperatura, concentração ácida, relação sólido-líquido e tempo avaliados. Através da lixiviação foi possível obter uma elevada recuperação do ferro no licor (>99%), além de uma fração sólida rica em sílica (>90%). Um estudo cinético foi realizado a partir do modelo de núcleo encolhido (*shrinking core model - SC*) e constatou-se que o processo é regido, majoritariamente, pela reação de difusão interna. Os produtos do processamento hidrometalúrgico foram caracterizados e avaliados sob a perspectiva do seu aproveitamento em segmentos estratégicos. O licor férrico (FeCl_3) foi testado como coagulante e apresentou resultados satisfatórios para o tratamento de água. Esse produto também foi avaliado como precursor para síntese de óxidos de ferro, resultando em um produto isento de sílica, composto basicamente por hematita (92%) e com propriedades compatíveis com aplicações no âmbito da indústria de pigmentos e na siderurgia. Para tal, uma rota simplificada de precipitação/conversão térmica foi desenvolvida, a qual resultou em uma recuperação metalúrgica de ferro de 84%. A fração sólida, rica em sílica, foi investigada como material cimentício suplementar que proporcionou uma substituição de até 20% do cimento Portland, sem causar prejuízos na resistência à compressão das pastas de cimento. Ainda, a incorporação do rejeito após a lixiviação representou uma redução de 21% na emissão de CO_2 . Além da exequibilidade técnica, discutiram-se os aspectos econômicos e de produtividade da rota proposta, os quais apontam indícios favoráveis para a obtenção de produtos com valor agregado significativo. Assim, pode-se concluir que a hidrometallurgia é uma alternativa promissora para o aproveitamento de rejeitos de minério de ferro, garantindo a máxima recuperação de recursos naturais, a integração de setores industriais estratégicos e a geração de valor para materiais que atualmente são negligenciados na forma de passivos ambientais, aspectos esses condizentes com o desenvolvimento sustentável, as práticas ESG e a perspectiva da mineração zero resíduos.

Palavras-chave: hidrometallurgia; rejeito de minério de ferro, óxidos de ferro; sílica; aproveitamento de resíduos

ABSTRACT

The management of iron ore tailings is one of the main challenges of the mineral sector, especially due the volumes generated and the risks arising from their disposal. In this context, the objective of this work was to discuss the effects of tailings disposal, the alternatives of use, and the opportunities associated with hydrometallurgical processing. Leaching, with the use of hydrochloric acid (HCl), was investigated and the parameters of temperature, acid concentration, solid-liquid ratio, and time evaluated. Through leaching it was possible to obtain a high recovery of iron in the liquor (>99%), and a silica-rich solid fraction (>90%). A kinetic study was performed from the shrinking core model, and it was found that the process is governed, mostly, by the internal diffusion reaction. The products of the hydrometallurgical processing were characterized and evaluated from the perspective of their use in strategic segments. Ferric liquor (FeCl_3) was tested as a coagulant and showed satisfactory results for water treatment. This product was also evaluated as a precursor for the synthesis of iron oxides, resulting in a silica-free product, composed basically of hematite (92%) and with properties compatible with applications in the pigment and steel industry. For that purpose, a simplified precipitation/thermal conversion route has been developed, which resulted in an iron metallurgical recovery of 84%. The solid fraction, rich in silica, was investigated as a supplementary cementitious material that provided a replacement of up to 20% of Portland cement, without causing losses in the compressive strength of cement pastes. In addition, the incorporation of tailings after leaching represented a 21% reduction in the emission of CO_2 . Beyond technical feasibility, the economic and productivity aspects of the proposed route were discussed, which indicate favorable markers for obtaining products with substantial added value. Thus, it can be concluded that hydrometallurgy is a promising alternative for processing iron ore tailings, ensuring maximum recovery of natural resources, the integration of strategic industrial sectors, and the generation of value for materials that are currently neglected in the form of environmental liabilities. These points are consistent with sustainable development, ESG practices and the perspective of zero waste mining.

Keywords: hydrometallurgy; iron ore tailings, iron oxides; silica; waste recovery

LISTA DE ILUSTRAÇÕES

CAPÍTULO I - AVALIAÇÃO DAS PUBLICAÇÕES TÉCNICO-CIENTÍFICAS SOBRE RESÍDUOS DA MINERAÇÃO DE FERRO: ANÁLISE BIBLIOMÉTRICA E INTEGRAÇÃO DOS ARTIGOS

Figura I.01. Benefícios oriundos do uso de rejeitos minerais	29
Figura I.02. Configuração da pesquisa na plataforma CAPES e os principais resultados obtidos.	30
Figura I.03 - Resultados da triagem e segmentação dos artigos selecionados para análise.....	32
Figura I.04 - Evolução das publicações sobre resíduos de minério de ferro no período de 2000- 2023	32
Figura I.05 - Países que mais publicaram no âmbito de aproveitamento de resíduos de ferro	33
Figura I.06 - Palavras-chave mapeadas nos artigos selecionados, no período de 2016 a 2023	34
Figura I.07 - Indicadores dos artigos sobre resíduos de minério de ferro. (A) Participação por área na categoria de aproveitamento. (B) Principais subáreas da construção civil. (C) Participação por área na categoria de disposição. (D) Principais subáreas de impactos ambientais.	36
Figura I.08 - Foco das investigações dos países que mais publicaram sobre resíduos de ferro no período de 2000-2023.....	37
Figura I.09 - Universidades brasileiras com maior número de publicações relacionados à disposição/aproveitamento de resíduos da mineração de ferro.	38
Figura I.10 - Metodologias tradicionais para síntese de diferentes óxidos de ferro...40	
Figura I.11 - Integração dos artigos utilizados no desenvolvimento deste trabalho. .42	

CAPÍTULO II - ON THE EFFECTS OF IRON ORE TAILINGS MICRO/NANOPARTICLES IN EMBRYONIC AND LARVAL ZEBRAFISH (*Danio rerio*)

Graphical abstract	52
Figure II.01. Representative turbidity of iron ore tailing suspension collected 5 cm from the surface as a function of settling time. (NTU: nephelometric turbidity units).	56

Figure II.02. Zebrafish survival and hatching rate during 6-day exposure to iron ore tailings (IOT) in suspension. (A) Survival curve (estimated according to the Kaplan-Meier method) and (B) hatching rate for full IOT exposure, from up to 4 until 144 hpf (hours post-fertilization). Error bars represent standard error (* $p\leq 0.05$, two-way ANOVA followed by Bonferroni post-hoc, n=400/group, three independent experiments).....61

Figure II.03. Effect of zebrafish embryos and larvae exposure to iron ore tailings (IOT) micro/nanoparticles in suspension. Results for (A) embryonic spontaneous tail movements at 24 hpf (n=36/group); (B) heart rate at 48 hpf (n=36/group); larval morphology in terms of body length (C), ocular distance (D), and ocular surface area (E), analyzed at 120 hpf (n=36/group) and larval behavior, evaluated at 144 hpf, in terms of distance traveled (F), mean velocity (G), and mean absolute turn angle (H) (n=80/group). Column bars represent mean \pm standard error (of three independent experiments, * $p\leq 0.05$, one-way ANOVA followed by Bonferroni post-hoc for A-G, Kruskal-Wallis followed by Dunn's post-hoc for H).....62

Figure II.04. Effect of iron ore tailing (IOT) suspensions exposure to zebrafish chorion. Representative FESEM images of 24 and 48 hpf embryos showing cumulative time- and concentration-dependent IOT particles deposits on the fish chorion. The dotted-line square identifies the representative EDS measurement area for analysis and element identification is informed at the bottom, for each experimental group. Scale bar: 500 μ m. (FESEM: field-emission scanning electron microscopy, EDS: energy dispersive X-ray spectroscopy, voltage: 20,000 kV, magnitude: 200 x, spot: 4.0, working distance: 10.4 mm).....64

Figure II.05. Turbidity range of the iron ore tailing suspension compared to environmental background values of Doce River basin before (2010-2015) and one year after (2016) the Fundão dam disaster. (*Source: IGAM, 2018 - turbidity range values were graphically constructed based on 25-90 percentile of the dataset).....66

Appendix II.01. Determination of Zeta Potential of iron ore tailing (IOT) particles as function of pH. The isoelectric point (IEP) of IOT particles was identified at the pH of 9.7. The analysis was carried out in ZetaSizer Nano ZS by the electrophoretic light scattering technique. The suspension with the IOT particles presented original pH 7.0 \pm 0.1 and ionic strength of 157.6 μ S. Adjustment for the acid and basic ranges were performed by the addition of hydrochloric acid (4.0 mol L $^{-1}$) and sodium hydroxide (4.0 mol L $^{-1}$), respectively.187

Appendix II.02. X-ray diffraction (XRD) pattern of iron ore tailing (IOT) particles in suspension. XRD analysis performed on Siemens X-ray diffractometer, equipped with a fixed Cu anode tube. Hematite and quartz represent the sample major mineralogical components.....188

Appendix II.03. Effect of iron ore tailing (IOT) suspensions exposure to zebrafish chorion. Representative FESEM detailed images of 48 hpf embryo (magnitude: 10.000 x) showing massive IOT deposits on the fish chorion surface (right) when compared to control group (left). Left top corner images show the entire embryo (magnitude: 200 x; voltage: 20,000 kV, spot: 4.0).....188

CAPÍTULO III - PRODUCTION OF A FERRIC CHLORIDE COAGULANT BY LEACHING AN IRON ORE TAILING

Graphical abstract	78
Figure III.01. Location of the Quadrilátero Ferrífero in Minas Gerais – Brazil.....	81
Figure III.02. Solubilization of iron contained in the IOT as a function of temperature and HCl concentration at a leaching time of 2 hours.....	85
Figure III.03. Solubilization of iron contained in the IOT as a function of time at a temperature of 80°C and hydrochloric acid concentration of 10.8 mol L ⁻¹	85

CAPÍTULO IV - SIMPLIFIED HYDROMETALLURGICAL ROUTE FOR THE SYNTHESIS OF SILICA-FREE HEMATITE FROM IRON ORE TAILINGS

Graphical abstract	95
Figure IV.01. Sequence of operations involved in the production of silica-free iron oxides.....	102
Figure IV.02. Thermogravimetric analysis (TGA) of the iron sludge obtained by selective precipitation at pH values of 3.6, 3.8, and 4.0.	104
Figure IV.03. Differential thermal analysis (DTA) of the iron sludge obtained by selective precipitation at pH values of 3.6, 3.8, and 4.0.	105
Appendix IV.02. Solid fraction obtained after leaching and washing of iron ore tailings, followed by drying at 60°C.....	190
Appendix IV.03. Granulometric distribution of iron oxides synthetised from the iron sludge obtained by selective precipitation at pH values of 3.6, 3.8, and 4.0, followed by thermal treatment (550 °C) and hot water washing.	191
Appendix IV.04. (A) X-ray diffractograms of the iron sludge obtained by selective precipitation at pH values of 3.6, 3.8, and 4.0 and after drying at 60°C, and (B) X-ray diffractograms of iron oxides synthetised from the iron sludge obtained by selective precipitation at pH values of 3.6, 3.8, and 4.0, followed by thermal treatment (550°C) and hot water washing.	192

Appendix IV.05. SEM of the silica-free iron oxy-hydroxy precipitate at pH 3.8 and after drying at 60°C; and hematite particles synthesised at pH 3.8, following thermal treatment (550°C) and hot water washing.193

Appendix IV.06. Silica-free hematite powder produced from iron ore tailings by means of the simplified hydrometallurgical route developed in this work.193

CAPÍTULO V - APPLICATION OF LEACHED IRON ORE TAILINGS TO PRODUCE SUSTAINABLE CEMENTS

Graphical abstract	120
Figure V.01. Rheometer (a) and parallel-plate geometry (b) used in the rotational rheometry tests.....	126
Figure V.02 - Thermogravimetric analysis of leached IOT	129
Figure V.03 - XRD patterns of leached IOT before and after thermal activation.....	130
Figure V.04 - SEM images at 1,000 x magnification. (A) Raw sample of IOT. (B) IOT leached. (C) IOT after leaching and thermal activation.	130
Figure V.05 - Descending flow curves (shear stress vs. shear rate) of cement pastes	131
Figure V.06 - Heat flow and cumulative heat of IOT cement pastes.....	133
Figure V.07 - Compressive strength of cement pastes at 3, 7, and 28 days	134
Figure V.08 - XRD patterns of L-IOT cement pastes at (a) 3 days, (b) 7 days, and (c) 28 days (E - ettringite, Hc - hemicarboaluminate, M – monocarboaluminate, P – portlandite, Q – quartz, C – calcite).....	135
Figure V.09 - Selected range of XRD patterns from 5-15° 2θ of cement pastes at 3, 7, and 28 days (E – ettringite, F - ferrite Hc – hemicarboaluminate, M – monocarboaluminate).....	136
Figure V.10 - Bound water (a) and portlandite (b) contents of cement pastes after 3, 7, and 28 days determined by TGA. The standard deviation was adopted based on Scrivener et al. [44].	137
Figure V.11 - Evolution of AFm phases in IOT cement pastes after 3, 7, and 28 days of hydration, as determined by TGA.....	137
Figure V.12 - CO ₂ -eq intensity (kg CO ₂ -eq/MPa .m ³ of paste) at 3, 7, and 28 days	139

CAPÍTULO VI - HYDROMETALLURGICAL PROCESSING OF IRON ORE TAILINGS (IOT): KINETICS OF IRON EXTRACTION BY HYDROCHLORIC ACID LEACHING

Graphical abstract	152
Figure VI.01. Leaching products and iron dissolving behaviour	157
Figure VI.02. Effect of temperature on the dissolution of iron present in the IOT. Conditions: HCl concentration of 7.2 mol L ⁻¹ , solid-liquid ratio of 1:3, and stirring speed of 100 rpm	158
Figure VI.03. Results of fitting the experimental data into the SC model: (A) chemical reaction process, (B) internal diffusion, and (C) interfacial transfer and diffusion through the product layer.....	159
Figure VI.04. Arrhenius plot for iron dissolution at leaching temperatures from 60 to 90 °C, HCl concentration of 7.2 mol L ⁻¹ , solid-liquid ratio of 1:3; and stirring speed of 100 rpm.....	160
Figure VI.05. Effect of HCl concentration on the dissolution of iron present in the IOT. Conditions: temperature 80 °C, solid-liquid ratio 1:3, and stirring speed of 100 rpm.	161
Figure VI.06. Results of fitting of experimental kinetics data into SC model. (A) Chemical reaction process. (B) Internal diffusion. (C) Interfacial transfer and diffusion through the product layer	161
Figure VI.07. Relationship between ln k and ln [C _{HCl}] based on the internal diffusion model	162
Figure VI.08. Effect of the solid-liquid ratio on the dissolution of iron present in the IOT. Conditions: temperature of 80 °C, HCl concentration of 7.2 mol L ⁻¹ , and stirring speed of 100 rpm	163
Figure VI.09. Results of fitting of experimental kinetics data of solid-liquid ratio into SCM model. (A) Chemical reaction process. (B) Internal diffusion. (C) Interfacial transfer and diffusion through the product layer	163
Figure VI.10. Relationship between ln k–ln ε _{S/L} based on the internal diffusion model.	164
Figure VI.11. The relationship between 1-2/3X-(1-X)2/3 and CHCl1.29εS/L – 1.94exp[-44584/(RT)].....	165

**CAPÍTULO VII - ASPECTOS ECONÔMICOS E PRODUTIVOS DO
PROCESSAMENTO HIDROMETALÚRGICO DE REJEITOS DE MINÉRIO DE
FERRO E AS PERSPECTIVAS FUTURAS SOBRE O APROVEITAMENTO DO IOT.**

Figura VII.01. Esquema do processo hidrometalúrgico para produção de óxidos de ferro e sílica a partir de rejeitos de minério de ferro.173

Figura VII.02. Cenário produtivo do Quadrilátero Ferrífero para geração de IOT e segmentos que podem incorporar tais resíduos.....175

LISTA DE TABELAS

CAPÍTULO I - AVALIAÇÃO DAS PUBLICAÇÕES TÉCNICO-CIENTÍFICAS SOBRE RESÍDUOS DA MINERAÇÃO DE FERRO: ANÁLISE BIBLIOMÉTRICA E INTEGRAÇÃO DOS ARTIGOS

Tabela I.01 - Estrutura de classificação da análise em área e subárea.....34

CAPÍTULO II - ON THE EFFECTS OF IRON ORE TAILINGS MICRO/NANOPARTICLES IN EMBRYONIC AND LARVAL ZEBRAFISH (*Danio rerio*)

Table II.01. Characteristics of the micro/nanoparticles of iron ore tailing (IOT) suspension.....59

CAPÍTULO III - PRODUCTION OF A FERRIC CHLORIDE COAGULANT BY LEACHING AN IRON ORE TAILING

Table III.01 - Characteristics of the iron ore tailing (IOT) sample.....84

Table III.02. Density and chemical composition of the ferric chloride coagulant produced by acid leaching of IOT (FC/IOT) and a conventional ferric chloride coagulant produced from iron scrap (FC/IS) and from mill scale (FC/MS).....86

Table III.03. Characteristics of raw water and treated water with the coagulant FC/IOT.....86

CAPÍTULO IV - SIMPLIFIED HYDROMETALLURGICAL ROUTE FOR THE SYNTHESIS OF SILICA-FREE HEMATITE FROM IRON ORE TAILINGS

Table IV.01. Properties of the iron sludge obtained by selective precipitation at pH values of 3.6, 3.8, and 4.0 and after drying at 60°C.....102

Table IV.02. Characteristics of iron oxides synthetised from the iron sludge obtained by selective precipitation at pH values of 3.6, 3.8, and 4.0, followed by thermal treatment (550°C) and hot water washing.....106

Table IV.03. Statistical analysis performed by the ANOVA method ($p \leq 5\%$) for the parameters of iron concentration, metallurgical recovery, and mass of synthesised oxides ($n = 3$).....107

Table IV.04. The $L^*a^*b^*$ chromaticity colour spaces of the synthesised iron oxides.....109

Appendix IV.01. Elemental analysis of iron ore tailings by microwave assisted digestion (U.S. EPA 3052 Method*) and ICP/OES.....189

CAPÍTULO V - APPLICATION OF LEACHED IRON ORE TAILINGS TO PRODUCE SUSTAINABLE CEMENTS

Table V.01 - Chemical composition and physical properties of OPC	124
Table V.02 - Mix proportions of cement pastes	125
Table V.03 - Elemental composition by XRF and particle size distribution.....	129
Table V.04 - Mini-slump and rheological parameters of cement pastes	131

CAPÍTULO VI - HYDROMETALLURGICAL PROCESSING OF IRON ORE TAILINGS (IOT): KINETICS OF IRON EXTRACTION BY HYDROCHLORIC ACID LEACHING

Table VI.01. Shrinking core model comparison by correlation coefficient (R^2) for temperature results.	159
Table VI.02. Shrinking core model comparison by correlation coefficient (R^2) for concentration HCl results.	161

CAPÍTULO VII - ASPECTOS ECONÔMICOS E PRODUTIVOS DO PROCESSAMENTO HIDROMETALÚRGICO DE REJEITOS DE MINÉRIO DE FERRO E AS PERSPECTIVAS FUTURAS SOBRE O APROVEITAMENTO DO IOT.

Tabela VII.01. Faixa de preço dos principais coprodutos da lixiviação de IOT.	176
Tabela VII.02. Rendimento e valor dos coprodutos por tonelada de IOT.....	178

LISTA DE ABREVIATURAS E SIGLAS

- ANM - Agência Nacional de Mineração
CAPEX - capital expenditure
ESG - *environmental, social and governance*
FC - *Ferric Chloride*
IEP - *isoelectric point*
IOT - *iron ore tailings*
IOTL - *iron ore tailings leached*
IPEA - Instituto de Pesquisa Econômica Aplicada
L-IOT – iron ore tailing leached heat treated
MG - Minas Gerais
Mt - milhões de toneladas
ODS - objetivos do desenvolvimento sustentável
rpm - rotação por minuto
S/L - solid-liquid
SC - *shrinking core model*
SCM - *supplementary cementitious material*
t - tonelada
TGA - *thermogravimetric analysis*
XRD - *X-ray diffraction*
XRF - *X-ray fluorescence*

SUMÁRIO

CAPÍTULO I - PROBLEMA DE PESQUISA E AVALIAÇÃO DAS PUBLICAÇÕES TÉCNICO-CIENTÍFICAS SOBRE RESÍDUOS DA MINERAÇÃO DE FERRO: ANÁLISE BIBLIOMÉTRICA E INTEGRAÇÃO DOS ARTIGOS.....	22
1. INTRODUÇÃO	23
1.1. Objetivos	25
1.1.1 Objetivo Geral	25
1.1.2. Objetivos específicos	25
2. ANÁLISE BIBLIOMÉTRICA.....	26
REFERÊNCIAS.....	43
CAPÍTULO II - ON THE EFFECTS OF IRON ORE TAILINGS MICRO/NANOPARTICLES IN EMBRYONIC AND LARVAL ZEBRAFISH (DANIO RERIO).....	50
ABSTRACT.....	52
GRAPHICAL ABSTRACT	52
1. INTRODUCTION.....	53
2. MATERIALS AND METHODS.....	55
2.1. Preparation of IOT suspension.....	55
2.2. Characterization of iron ore suspension	56
2.3. <i>In vivo</i> exposure and toxicological endpoints	58
2.4. Scanning electron microscopy (SEM) analysis	58
2.5. Statistical analysis	59
3. RESULTS AND DISCUSSION.....	59
4. CONCLUSIONS	67
ACKNOWLEDGEMENTS.....	67
REFERENCES.....	68

**CAPÍTULO III - PRODUCTION OF A FERRIC CHLORIDE COAGULANT BY
LEACHING AN IRON ORE TAILING**.....**76**

ABSTRACT..........**78**

GRAPHICAL ABSTRACT**78**

1. INTRODUCTION..........**79**

2. MATERIAL AND METHODS**80**

 2.1. Iron ore tailing (IOT)

.....**80**

 2.2. Reagents.....

.....**81**

 2.3. Ferric chloride production.....

.....**81**

 2.4. Water treatment

.....**82**

 2.5. Ferric chloride production residue

.....**83**

 2.6. Statistical analysis

.....**83**

3. RESULTS AND DISCUSSION..........**83**

4. CONCLUSION**88**

ACKNOWLEDGMENTS**88**

REFERENCES..........**89**

**CAPÍTULO IV - SIMPLIFIED HYDROMETALLURGICAL ROUTE FOR THE
SYNTHESIS OF SILICA-FREE HEMATITE FROM IRON ORE TAILINGS**.....**93**

ABSTRACT..........**95**

GRAPHICAL ABSTRACT**95**

1. INTRODUCTION..........**96**

2. MATERIAL AND METHODS**98**

 2.1. Reagents and Materials

.....**98**

 2.2. Leaching process

.....**99**

 2.3. Iron precipitation.....

.....**99**

 2.4. Thermal conversion and washing.....

.....**100**

 2.5. Characterization of ferric precipitates and iron oxides.....

.....**100**

 2.6 Statistical analysis.....

.....**101**

3. RESULTS AND DISCUSSION..........**101**

4. CONCLUSIONS	109
ACKNOWLEDGMENTS	110
REFERENCES	111
CAPÍTULO V - APPLICATION OF LEACHED IRON ORE TAILINGS TO PRODUCE SUSTAINABLE CEMENTS	118
ABSTRACT.....	120
GRAPHICAL ABSTRACT	120
1. INTRODUCTION.....	121
2. MATERIAL AND METHODS	123
2.1. Iron ore tailings.....	123
2.2. IOT leaching process	123
2.3. Thermal activation.....	124
2.4. Mix proportions and sample preparation	124
2.5 Test Methods	125
3 RESULTS AND DISCUSSION.....	128
3.1. Leaching and thermal activation.....	128
3.2. Fresh-state of cement pastes.....	131
3.3. Isothermal calorimetry.....	132
3.4. Compressive strength	133
3.5. XRD analysis of L-IOT cement pastes	134
3.6. TGA analysis of L-IOT cement pastes	137
3.7. CO ₂ analysis and scale of use	138
4. CONCLUSION	140
ACKNOWLEDGEMENTS	141
REFERENCES	142

CAPÍTULO VI - HYDROMETALLURGICAL PROCESSING OF IRON ORE TAILINGS (IOT): KINETICS OF IRON EXTRACTION BY HYDROCHLORIC ACID LEACHING	150
ABSTRACT	152
GRAPHICAL ABSTRACT	152
1. INTRODUCTION	153
2. EXPERIMENTAL SETUP	154
2.1 Iron Ore Tailings (IOT)	154
2.2 Leaching procedure	154
2.3 Analysis	155
2.4 Shrinking core model (SCM)	156
3. RESULTS AND DISCUSSION	157
3.1 Effect of temperature on iron dissolution in IOT	158
3.2 Effect of HCl concentration on iron dissolution in IOT	160
3.3 Effect of solid-liquid ratio on iron dissolution in IOT	162
3.4 Leaching kinetics of IOT with HCl for iron extraction	164
4. CONCLUSION	165
REFERENCES	166
CAPÍTULO VII - ASPECTOS ECONÔMICOS E PRODUTIVOS DO PROCESSAMENTO HIDROMETALÚRGICO DE REJEITOS DE MINÉRIO DE FERRO E AS PERSPECTIVAS FUTURAS SOBRE O APROVEITAMENTO DO IOT.	170
1. BENEFÍCIOS ECONÔMICOS E PERSPECTIVAS FUTURAS	171
2. CONSIDERAÇÕES FINAIS	179
REFERÊNCIAS	183

CAPÍTULO I

PROBLEMA DE PESQUISA E AVALIAÇÃO DAS PUBLICAÇÕES TÉCNICO-CIENTÍFICAS SOBRE RESÍDUOS DA MINERAÇÃO DE FERRO: ANÁLISE BIBLIOMÉTRICA E INTEGRAÇÃO DOS ARTIGOS

1. INTRODUÇÃO

O minério de ferro é uma commodity determinante para o desenvolvimento econômico e qualidade de vida. Segundo dados da STATISTA (2022), a produção média mundial de minério de ferro, no período de 2015 a 2022, foi em torno de 2,5 bilhões de toneladas métricas com, aproximadamente, 1,54 bilhões de toneladas de ferro contido. Os maiores produtores mundiais são a Austrália e o Brasil, produzindo 880 e 410 milhões de toneladas métricas, respectivamente, no ano de 2020.

No Brasil, o minério de ferro representa cerca de 80% da produção econômica das substâncias metálicas. Sua significância econômica pode ser visualizada pelo impacto no PIB nacional, o qual sofreu uma queda de 3,3% no ano de 2019, após o rompimento da barragem de Córrego do Feijão (ANM, 2022; IPEA, 2019).

Frente a relevância da indústria do ferro, torna-se crucial a incorporação de preceitos da sustentabilidade nas decisões do segmento, assim como a adoção das práticas ESG (*Environmental, Social and Governance*). Para tal, o uso de tecnologias sustentáveis para redução dos impactos relacionados à mineração tem sido alvo de diversas investigações.

Os impactos da mineração de ferro acompanham toda a cadeia produtiva e vão desde a supressão vegetal para início das atividades de lavra até os riscos associados ao rompimento de uma barragem (DE SOUSA *et al.*, 2020). Riscos esses, que foram vivenciados em dois episódios catastróficos da mineração brasileira: Fundão (2015) e Córrego do Feijão (2019).

Os dois eventos ocorreram no estado de Minas Gerais e marcaram a história como as maiores tragédias socioambientais brasileiras relacionadas à mineração. O colapso da barragem de Fundão foi precursor de uma série de discussões e medidas, as quais não foram suficientes para evitar, ou ao menos minimizar, os danos ocorridos no rompimento da barragem de Córrego do Feijão (ALMEIDA, 2019).

Aliado a isso, os atuais sistemas de gerenciamento de rejeitos, que utilizam barragens e empilhamento a seco, não priorizam a maximização do aproveitamento dos recursos naturais explorados. As barragens e pilhas são grandes passivos ambientais, que oferecem riscos, comprometem grandes áreas e detêm quantidades significativas de minerais de interesse.

No entanto, nos últimos anos (a partir de 2015), há um crescente interesse na busca por soluções sustentáveis para o aproveitamento desses rejeitos, a fim de mitigar os impactos negativos e explorar seu potencial benéfico. Os rejeitos de minério de ferro (*iron ore tailings - IOT*) são fonte de elementos como ferro, silício, alumínio, dentre outros. Investigar e adotar práticas voltadas para incorporação de rejeitos de minério de ferro na indústria é uma pauta que promove inúmeros benefícios. Tal proposta incentiva práticas sustentáveis no âmbito da mineração; especialmente pela inserção de conceitos fundamentais como a produção mais limpa, economia circular e simbiose industrial; além de prover benefícios sociais que integram a concepção dos preceitos ESG.

Assim, pode-se afirmar, que atualmente, os rejeitos de ferro são materiais negligenciados pela indústria mineral, por não se adequarem nos parâmetros de comercialização desse metal. Apesar disso, apresentam potencial de serem explorados por rotas adjacentes. Para tal, é fundamental identificar as principais propriedades destes materiais e elencar as possíveis alternativas de aproveitamento. Diante do exposto, esta pesquisa propõe a investigação do panorama associado a gestão de rejeitos de minério de ferro e a possibilidade de processamento dos IOT por via hidrometalúrgica, visando a recuperação dos componentes ferro e sílica.

A lixiviação do ferro foi estudada ao longo dos anos, sendo o ferro usualmente considerado como contaminante em rotas hidrometalúrgicas de diversos minerais (DAVEY; SCOTT, 1976; ISMAEL; CARVALHO, 2003; PRADEL et al., 1993). De modo inverso, propõe-se nesta pesquisa investigar as variáveis que norteiam a lixiviação do ferro como elemento de valor presente nos rejeitos; parametrizando as melhores condições para solubilização deste metal.

Este trabalho é baseado na lixiviação ácida a quente com uso de ácido clorídrico (HCl), para dissolução do ferro presente nos rejeitos provenientes do Quadrilátero Ferrífero (MG), e tem como objetivo apresentar as condições do processamento hidrometalúrgico, os benefícios e as possibilidades de uso dos coprodutos oriundos da mineração de ferro.

Os resultados serão apresentados em cinco capítulos que pautaram: os impactos da disposição de rejeitos no ambiente (Artigo 1); os parâmetros e o modelo cinético que governam a lixiviação ácida do ferro por HCl (Artigos 2 e 5); a síntese de

óxidos de ferro livres de sílica para incorporação na indústria mineral (Artigo 3) e a incorporação do rejeito lixiviado como material cimentício suplementar (*supplementary cementitious material* – SCM) (Artigo 4).

1.1. Objetivos

1.1.1 Objetivo Geral

Investigar o potencial associado ao aproveitamento de rejeitos de minério de ferro através de uma rota hidrometalúrgica, para síntese de óxidos de ferro e produção de sílica.

1.1.2. Objetivos específicos

- Contextualizar as temáticas de investigação associadas aos resíduos da mineração de ferro e integrar dos artigos apresentados, nesta tese, no cenário técnico científico atual.
- Avaliar os efeitos toxicológicos de micro/nanopartículas de minério de ferro, no organismo teste *zebra-fish* (*Danio rerio*), em condições normais de disposição de rejeitos.
- Determinar os parâmetros para produção de cloreto férrico a partir de rejeitos de minério de ferro e sua aplicação no tratamento de água de abastecimento.
- Sintetizar óxidos de ferro, livres de sílica, a partir de rejeitos de minério de ferro por uma rota simplificada de precipitação/tratamento térmico.
- Investigar o potencial de aplicação da fração sólida da lixiviação dos rejeitos como material cimentício suplementar.
- Entender o mecanismo cinético da lixiviação do rejeito de minério de ferro com uso de ácido clorídrico.
- Avaliar benefícios técnico-econômicos do aproveitamento de rejeitos e discorrer sobre as perspectivas futuras para o gerenciamento destes coprodutos minerais.

2. ANÁLISE BIBLIOMÉTRICA

A mineração é um setor estratégico para toda cadeia industrial e contribui substancialmente para diversas economias. Em paralelo, é um segmento industrial conhecido por seu histórico de impactos socioambientais e que carece de avanços efetivos no que tange à sustentabilidade (DUBIŃSKI, 2013; MORAN et al., 2014). Com o objetivo de minimizar os riscos associados aos desafios da mineração e providenciar mudanças que efetivamente contribuam para a sustentabilidade do setor, as empresas têm incorporado os princípios ESG em suas operações (MAYBEE; LILFORD; HITCH, 2023). De um modo geral, os princípios ESG direcionam as decisões dos empreendimentos de mineração com intuito a agregar benefícios sociais e ambientais aos resultados econômicos por meio de uma boa governança corporativa.

Entretanto, o avanço efetivo rumo a práticas de desenvolvimento sustentável tem sido lento e de baixa amplitude, pois tais mudanças dependem de investigações específicas para o setor e demandam de políticas, investimentos e estratégias voltadas para a pesquisa e desenvolvimento tecnológico dedicado a este ramo industrial (BÖHLING; MURGUÍA; GODFRID, 2019). Tal contexto, é claramente evidenciado nos atuais desafios vivenciados pela indústria mineral. Segundo relatório da Ernest Young (2022), os riscos ambientais e sociais são os mais críticos enfrentados pela mineração; seguidos pela descarbonização e pelo licenciamento de novos projetos.

Por essa razão, a inserção de práticas de sustentabilidade na indústria mineral depende de soluções que contribuam para as esferas sociais, ambientais e econômicas, segundo às especificidades de cada empreendimento mineiro (ALVES; FERREIRA; ARAÚJO, 2021).

Os desafios ambientais, por sua vez, representam um aspecto de grande criticidade, já que são intrínsecos às atividades de produção mineral. Envolvem danos aos ecossistemas locais através da degradação do solo, poluição do ar, contaminação da água e perda da biodiversidade (ADIANSYAH et al., 2015; EDRAKI et al., 2014; MILLER; GHISOLFI; BARROSO, 2023)

Estes impactos ambientais assumiram uma proporção ainda mais grave após o colapso das barragens de Fundão (2015) e Córrego do Feijão (2019). Os acidentes com barragens degradaram grandes áreas de mata nativa, destruíram quilômetros de rios, afetaram a fauna e desestabilizaram o ecossistema nas áreas atingidas (ALMEIDA; SCHNEIDER, 2018; GOMES *et al.*, 2017; IBAMA, 2019; NASCIMENTO *et al.*, 2022; SCHOENBERGER, 2016).

O desenvolvimento da perspectiva ambiental deve ser uma das prioridades para adoção de conceitos sustentáveis na mineração. Para Kogel (2015), a adoção de práticas de reciclagem e utilização de resíduos minerais são uma forte alternativa ao panorama atual de gerenciamento de rejeitos. Mundialmente, a indústria mineral é responsável pela geração de bilhões de toneladas de resíduos sólidos (XU *et al.*, 2019), os quais representam um passivo ambiental colossal e demandam de soluções eficazes para o seu gerenciamento. Se não forem gerenciados adequadamente, os resíduos da mineração podem gerar poluição significativa, a qual pode variar desde a geração de poeira até a ocorrência de danos irreversíveis, como o colapso de uma barragem (Tayebi-Khorami *et al.*, 2019).

Dentre os resíduos de mineração, os rejeitos de minério de ferro representam cerca de 50% de todos os resíduos sólidos gerados no setor (LI *et al.*, 2023; ZHAO *et al.*, 2021). Na China, um dos maiores produtores de minério de ferro no mundo, o volume de armazenamento de rejeitos de ferro ultrapassou 5 bilhões de toneladas e está aumentando a uma taxa de mais de 300 milhões de toneladas por ano. Entretanto, o país utiliza menos de 20% deste resíduo (LU *et al.*, 2020a; LV *et al.*, 2021), destinando esse material, majoritariamente, para a construção civil. O Brasil, outro *player* mundial da produção de minério de ferro, gera em torno de 200 milhões de toneladas de IOT por ano (MENDES *et al.*, 2019) e ainda não possui indicadores de utilização para este resíduo industrial.

Além da grande quantidade de rejeitos de minério de ferro gerada e do baixo aproveitamento destes resíduos, outro aspecto crítico é a forma que estes materiais são gerenciados. A maior parte do volume de IOT produzido é destinada para disposição em barragens, as quais são enormes passivos ambientais e que fomentam sérios problemas de saúde, segurança e meio ambiente (LIU *et al.*, 2010; MENG *et al.*, 2023).

Cabe destacar que as barragens representam um custo expressivo para as atividades de produção mineral. Segundo LIU *et al.* (2010), os custos de construção de barragens variam de USD 0,29 a USD 0,44 por capacidade de armazenamento (t). A manutenção de barragens ativas representa um custo de USD 0,44 a USD 0,74 por tonelada de rejeito. Considerando a produção de rejeitos do Brasil, apenas o armazenamento de rejeitos de minério de ferro gera custos anuais de manutenção na ordem de centenas de milhões de dólares, sem considerar o CAPEX direcionado para a construção destas estruturas.

Por todos esses impactos, ambientais, sociais e financeiros; que o aproveitamento de resíduos minerais se tornou uma ação estratégica para a indústria da mineração. Alinhado com os objetivos de desenvolvimento sustentável das Nações Unidas (ODS), especialmente em relação ao ODS 12 - Produção e consumo responsável; o aproveitamento de rejeitos de mineração agrega uma série de benefícios para o setor mineral e para a sociedade diretamente envolvida no ecossistema dos projetos de mineração. De forma indireta, outros benefícios sustentáveis são obtidos a partir das estratégias de reuso/reciclagem de rejeitos: (i) ODS 8 - Trabalho decente e crescimento econômico; (ii) ODS 9 - Indústria, inovação e infraestrutura; e (iii) ODS 11 - Cidades e comunidades sustentáveis (UNITED NATIONS, 2015).

No âmbito da mineração de ferro, esses aspectos ganham uma relevância ainda maior, graças ao tamanho desse segmento industrial e a quantidade de rejeitos passível de ser utilizada (TAYEBI-KHORAMI *et al.*, 2019; XU *et al.*, 2019; ZHAO *et al.*, 2021). Tal configuração permite a incorporação de várias oportunidades de aproveitamento, o estabelecimento de parcerias com diversos segmentos industriais, além da possibilidade integrar práticas sustentáveis na gestão de um dos principais resíduos sólidos gerados na indústria mineral (ALMEIDA; SCHNEIDER, 2018; ZHANG *et al.*, 2022b). Tal perspectiva contribui de forma variada e favorece substancialmente várias esferas no âmbito socioambiental (Figura 1).

Em linhas gerais, pode-se dizer o aproveitamento de resíduos compõe uma boa estratégia ESG, visto que proporciona diversos benefícios, como: (i) maximização do uso de recursos naturais; (ii) geração de emprego e renda devido ao desenvolvimento de novas oportunidade de negócio; (iii) modernização da cadeia produtiva através da

adoção de novas tecnologias; (iv) menores custos de capital e operação relacionados à disposição dos rejeitos; e (v) uma boa visibilidade de mercado em relação à responsabilidade corporativa.

Figura I.01. Benefícios oriundos do uso de rejeitos minerais.



As vantagens oriundas do aproveitamento de rejeitos têm mobilizado vários estudos acerca do uso de IOT e tem mostrado resultados promissores no que diz respeito ao potencial de incorporação destes resíduos. As investigações são diversas, como: uso de rejeitos para recuperação de ferro em rotas de reprocessamento (ARAUJO *et al.*, 2020; PANDIRI *et al.*, 2022; PEREIRA *et al.*, 2021); obtenção de geopolímeros (DO CARMO E SILVA DEFÁVERI *et al.*, 2019; LI *et al.*, 2022); incorporação de rejeitos para produção de cerâmicas (AMARAL; PRAT; REIS, 2020; CECHIN *et al.*, 2022; MENDES *et al.*, 2019); utilização de rejeitos como agregado em substituição a areia (HUANG *et al.*, 2023; MENDES PROTASIO *et al.*, 2021); incorporação como material cimentício suplementar (DUARTE *et al.*, 2022; LING *et al.*, 2021); produção de pigmentos (ALMEIDA; SCHNEIDER, 2022; GALVÃO *et al.*, 2018), remoção de poluentes (AUGUSTO *et al.*, 2018; PUIATTI *et al.*, 2021), e no saneamento básico (ALMEIDA; SCHNEIDER, 2020a).

Dentre os segmentos que discutem o aproveitamento de rejeitos de minério de ferro, a construção civil é precursora dentre as áreas que investigam a incorporação

de resíduos minerais em suas práticas (ALMEIDA *et al.*, 2023b; YELLISHETTY *et al.*, 2008; YI *et al.*, 2009). A maioria das aplicações do IOT é voltada para a reciclagem dos rejeitos em oportunidades próximas ao local de mineração e abrange usos que apresentam baixo valor agregado (Kinnunen *et al.*, 2018; Y. Lu *et al.*, 2020).

Essa característica impacta na efetiva incorporação destes recursos, principalmente devido a localização da maioria das empresas de mineração. Apesar da construção civil apresentar potencial de incorporação de grande parcela dos rejeitos de minério de ferro produzida no Brasil, ainda não é suficiente para absorver todo o resíduo produzido por esse ramo da produção mineral. Por essa razão, alternativas de aproveitamento precisam ser mapeadas, para que uma maior quantidade de rejeitos possa ser utilizada.

Para caracterizar as principais tendências associadas ao aproveitamento de resíduos da mineração de ferro, realizou-se uma análise bibliométrica para identificar o perfil das investigações relacionadas aos rejeitos e estéreis de minério de ferro. Para tal, as palavras-chave utilizadas na pesquisa foram “*iron ore tailing*” | “*iron ore waste*”. Com o intuito de incluir resultados das duas palavras-chave, o operador “*or*” foi aplicado na busca. Para seleção da base de dados, um levantamento prévio com esses termos foi realizado na plataforma CAPES (Figura 2).

Figura I.02. Configuração da pesquisa na plataforma CAPES e os principais resultados obtidos.

The screenshot shows the CAPES Periodicals search interface. At the top, there's a header with the gov.br logo and 'Ministério da Educação/CAPES'. Below it, the CAPES logo and the text '.periodicos.' are displayed. A message says 'Você tem acesso ao conteúdo gratuito do Portal de Periódicos da CAPES' and 'Acesso CAFE ▾'. The main search area has a dark blue header with a house icon and 'Acervo'. Below it, there are two search fields: 'Qualquer campo ▾ contém ▾ "iron ore tailing"' and 'OU ▾ Qualquer campo ▾ contém ▾ "iron ore waste"'. There are also buttons for '+ ADICIONAR OUTRO CAMPO' and 'LIMPAR'. To the right of these fields are dropdown menus for 'Tipo de material' (set to 'Artigos'), 'Idioma' (set to 'Qualquer idioma'), 'Data de publicação' (set to 'Últimos 20 anos'), and a 'BUSCAR' button. On the far right, there are three columns of filters: 'Tipo de recurso' (Artigos 565), 'Assunto' (Science & Technology 448, Technology 298, Iron Ores 212, Engineering 202, Materials Science 166), and 'Coleção' (Elsevier ScienceDirect Journals 265, Science Citation Index Expanded (Web of Science) 225, DOAJ Directory of Open Access Journals 146, SpringerNature Complete Journals 85, PubMed 75). At the bottom left, it says '1-10 of 565 Resultados ▾'.

A busca baseada nos parâmetros indicados resultou em 565 artigos. Dentre estes resultados, foi possível identificar que as temáticas predominantes foram:

Science & Technology (448), *Technology* (298) e *Iron ores* (212). O levantamento indicou que as publicações estão concentradas principalmente no banco de dados da Elsevier (*Scopus*).

Diante disso, os parâmetros de busca mencionados acima foram replicados na base de dados da *Scopus* para uma avaliação detalhada do perfil de publicações associadas a temática de rejeitos/resíduos da mineração de ferro. Os parâmetros de pesquisa utilizados foram:

- Palavras-chave: “*iron ore tailing*” | “*iron ore waste*”
- Período: 2000-2023;
- Tipo de documento: Artigo de pesquisa;
- Idioma: Inglês;
- Data do download do banco de dados: 07 de julho de 2023.

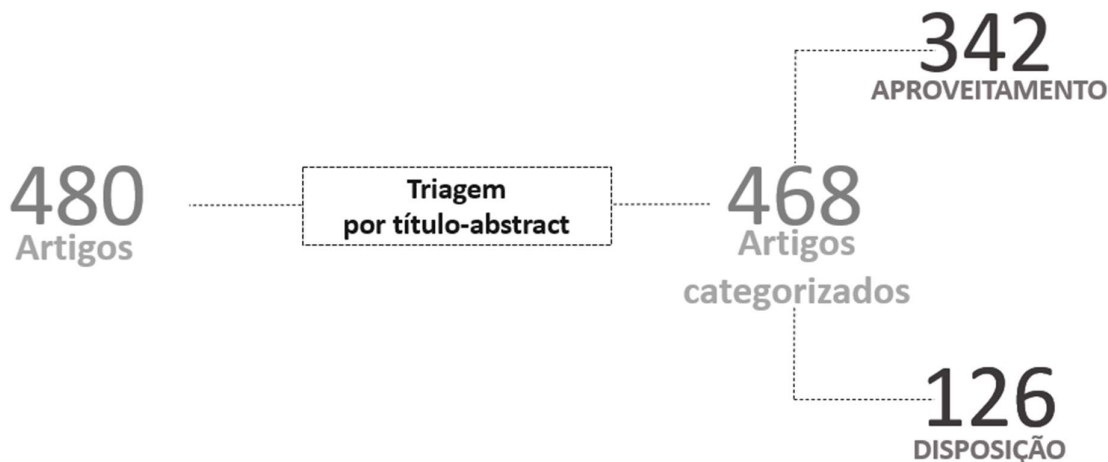
Tais filtros resultaram no seguinte algoritmo de pesquisa:

(*TITLE-ABS-KEY* (“*iron ore tailing*”) OR *TITLE-ABS-KEY* (“*iron ore waste*”)) AND (*LIMIT-TO* (*DOCTYPE* , “ar”)) AND (*LIMIT-TO* (*PUBYEAR* , 2023) OR *LIMIT-TO* (*PUBYEAR* , 2022) OR *LIMIT-TO* (*PUBYEAR* , 2021) OR *LIMIT-TO* (*PUBYEAR* , 2020) OR *LIMIT-TO* (*PUBYEAR* , 2019) OR *LIMIT-TO* (*PUBYEAR* , 2018) OR *LIMIT-TO* (*PUBYEAR* , 2017) OR *LIMIT-TO* (*PUBYEAR* , 2016) OR *LIMIT-TO* (*PUBYEAR* , 2015) OR *LIMIT-TO* (*PUBYEAR* , 2014) OR *LIMIT-TO* (*PUBYEAR* , 2013) OR *LIMIT-TO* (*PUBYEAR* , 2012) OR *LIMIT-TO* (*PUBYEAR* , 2011) OR *LIMIT-TO* (*PUBYEAR* , 2010) OR *LIMIT-TO* (*PUBYEAR* , 2009) OR *LIMIT-TO* (*PUBYEAR* , 2008) OR *LIMIT-TO* (*PUBYEAR* , 2006) OR *LIMIT-TO* (*PUBYEAR* , 2005) OR *LIMIT-TO* (*PUBYEAR* , 2004) OR *LIMIT-TO* (*PUBYEAR* , 2001) OR *LIMIT-TO* (*PUBYEAR* , 2000)) AND (*LIMIT-TO* (*LANGUAGE* , “English”))

Esse levantamento resultou em 480 documentos, os quais foram utilizados como referência para a análise quantitativa-qualitativa. Os artigos foram submetidos a uma triagem para validação da relação do referido resultado aos temas da pesquisa. Na triagem realizada por título e *abstract* foram identificados 12 artigos com temas

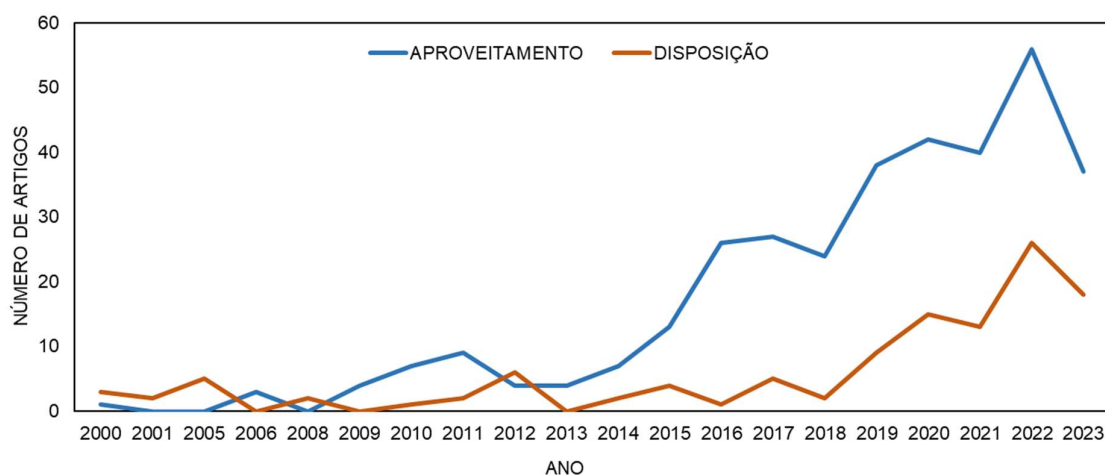
não efetivamente vinculados aos resíduos da mineração de ferro, por essa razão foram suprimidos da etapa de categorização. Deste modo, 468 publicações foram analisadas para categorização e obtenção de indicadores bibliométricos. O escopo da metodologia qualitativa pode ser visualizado na figura 03.

Figura I.03 - Resultados da triagem e segmentação dos artigos selecionados para análise.



A partir dos artigos classificados nos segmentos de aproveitamento e disposição, verificou-se como as investigações em relação a resíduos de minério de ferro evoluíram na última década, especialmente para os estudos que objetivaram o aproveitamento (Figura 04).

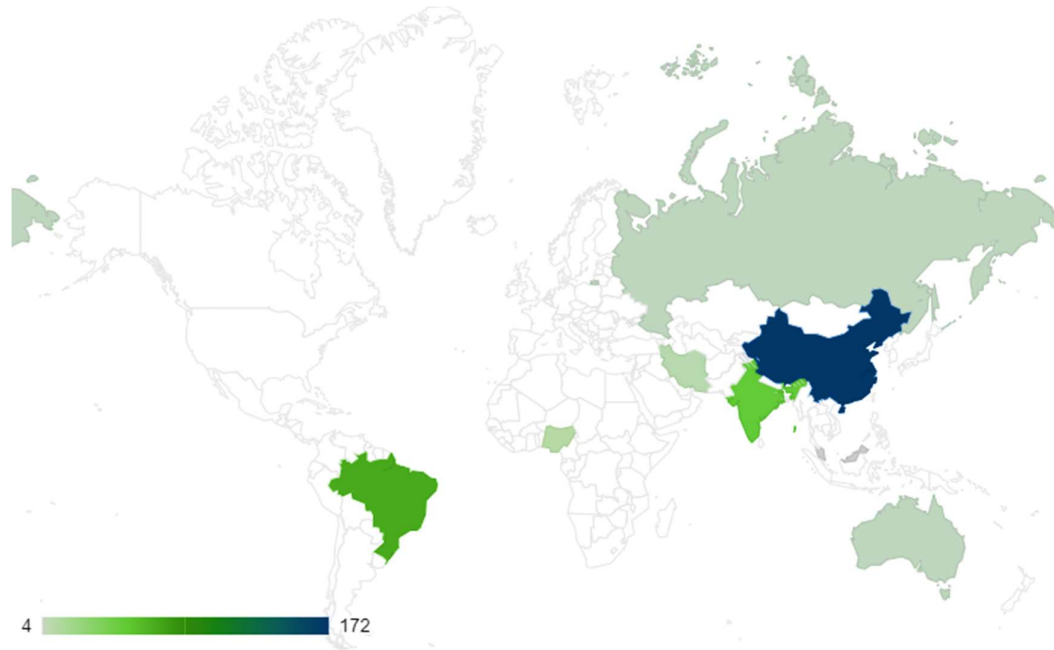
Figura I.04 - Evolução das publicações sobre resíduos de minério de ferro no período de 2000- 2023.



Nota-se que mais de 85% das publicações foram realizadas no período de 2015-2023, com expressivo destaque para trabalhos voltados para o aproveitamento dos rejeitos, os quais representam cerca de 75% dos artigos do período. Os países

que mais publicaram foram China (39%), Brasil (30%) e Índia (15%), respondendo juntos por cerca de 80% dos trabalhos identificados. Outros países desse grupo podem ser verificados na figura 05.

Figura I.05 - Países que mais publicaram no âmbito de aproveitamento de resíduos de ferro.



Para uma melhor perspectiva do perfil de cada uma destas categorias, foi realizada uma classificação por área e subárea. Para tal, o banco de dados obtido na plataforma SCOPUS foi importado no software VOSviewer -*Visualizing scientific landscapes*, que é uma ferramenta utilizada para construção e visualização de redes Bibliográficas. Através do tratamento de dados, foram elencadas as principais palavras-chave citadas nos artigos selecionados. Considerando o período de 2016 a 2023, pode-se observar alguns eixos principais de pesquisa vinculados aos rejeitos de minério de ferro, conforme Figura 6. Observa-se que nos anos de 2017 a 2019, as palavras-chave estão vinculadas a linhas de pesquisa predominantemente associadas ao aproveitamento do IOT. Enquanto, no período de 2020 a 2023 muitos estudos retomam termos associados a impactos ambientais, viés atrelado ao rompimento da barragem de Córrego do Feijão. Por meios das palavras-chave, foi possível categorizar as publicações em área e subárea, conforme Tabela 01.

Figura I.06 - Palavras-chave mapeadas nos artigos selecionados, no período de 2016 a 2023.

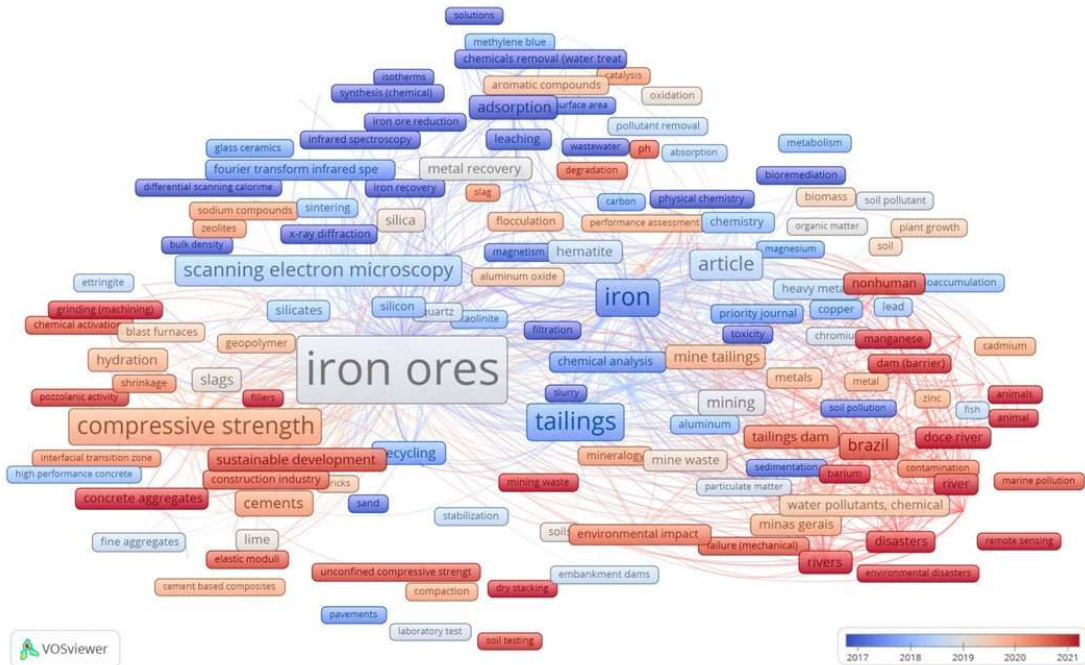


Tabela 01 - Estrutura de classificação da análise em área e subárea.

Categoria	Área	Subárea
Aproveitamento	Construção Civil	Agregado/ Cerâmica / Geopolímeros / Pavimentação/ Outros
	Ciência dos materiais	Adsorção de poluentes / Catalisador / Síntese de Materiais
	Mineração	Processamento de rejeitos / Caracterização
	Lixiviação	Síntese de materiais / Estudos de purificação / Produção de coagulantes
	Gestão de rejeitos	Práticas de sustentabilidade / Sistemas de gerenciamento
	Outros	Outros
Disposição	Recuperação de áreas	Revegetação / Fitoestabilização
	Impactos ambientais	Acidentes com barragens / Poluição de recursos hídricos / Poluição do solo / Ecotoxicidade
	Métodos de disposição	Formas de disposição de rejeitos
	Gestão de rejeitos	Sistemas de classificação
	Outros	Outros

A área da construção civil assume a dianteira na classificação dos artigos, sendo responsável por 54% dos trabalhos voltados para aproveitamento e 40% de todo o conjunto amostral. A China, país com o maior número de publicações identificadas, foca substancialmente em pesquisas que possibilitem o uso de rejeitos na construção civil.

As principais linhas de pesquisa, dentro do contexto da construção civil, estão voltadas para utilização dos rejeitos como agregado (MATHEUS CARVALHO EUGÊNIO *et al.*, 2023; MYMRIN *et al.*, 2021), aplicação como material cimentício suplementar (EUGENIO *et al.*, 2023; ZHANG *et al.*, 2022a) e na produção de cerâmicas (H.K.; HOSSINEY, 2022; WEISHI *et al.*, 2018). Juntas, essas linhas de pesquisa respondem por 80% das subáreas de estudos dentro da área da construção civil.

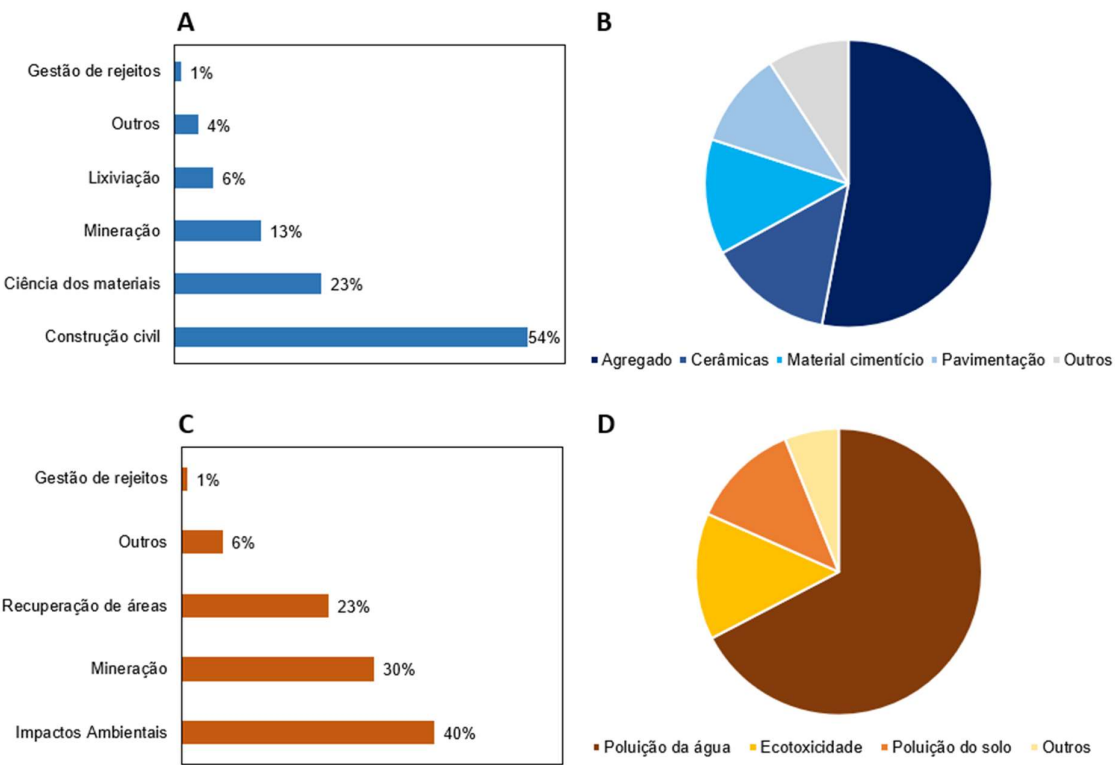
Outra área com destaque no âmbito de aproveitamento é a de Ciência dos Materiais (23% das publicações sobre aproveitamento), em que os rejeitos de minério de ferro são avaliados quanto a propriedades físicas e químicas, que permitem sua utilização como insumo para síntese materiais (GONG *et al.*, 2023; SU *et al.*, 2022), como catalisadores em processos químicos (LUCIANO *et al.*, 2022; SILVA *et al.*, 2020) e como materiais adsorventes para remoção de poluentes (FANG *et al.*, 2021; LIU *et al.*, 2020).

A mineração, segmento que inclui estudos sobre beneficiamento dos rejeitos, é um nicho que responde por 13% dos artigos identificados na análise bibliométrica, os quais objetivam o processamento de rejeitos para aproveitamento do ferro disponível. Nestes estudos são avaliados, principalmente, processos de flotação e separação magnética (BAI *et al.*, 2018; PANDIRI *et al.*, 2022; PEREIRA *et al.*, 2021).

Ainda no contexto de artigos vinculados ao aproveitamento de rejeitos de minério de ferro, foram identificados artigos que pautam o uso de rotas hidrometalúrgicas para o processamento do IOT. Essas publicações representam cerca de 6% dos artigos mapeados e elucidam o uso da lixiviação como alternativa para síntese de novos materiais, purificação de matrizes minerais e produção de coagulantes.

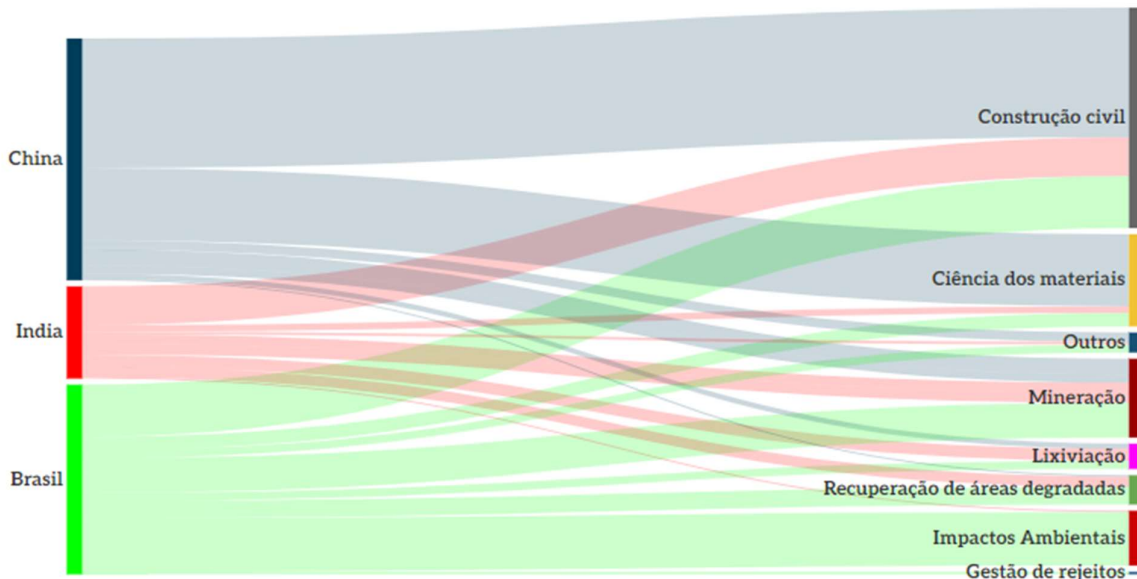
Na categoria de disposição, os estudos relacionados a impactos ambientais representam 40% dos artigos selecionados. São pesquisas que abordam a poluição do solo, das águas e os efeitos toxicológicos dos rejeitos de minério de ferro no ambiente (ALMEIDA *et al.*, 2023a; DAROS *et al.*, 2022; SIQUEIRA *et al.*, 2022). O segundo viés investigativo com maior número de publicações está vinculado aos métodos de disposição de rejeitos (30%). Nesse segmento foram incluídos artigos que abordam aspectos relacionados a construção de barragens, avaliação geotécnica dos rejeitos e soluções associadas a filtragem e empilhamento a seco (GOMES; DE TOMI; ASSIS, 2016; MMBANDO; FOURIE; REID, 2023; SERVI *et al.*, 2022). Os indicadores obtidos nessa análise bibliométrica podem ser verificados na figura 7.

Figura 1.07 - Indicadores dos artigos sobre resíduos de minério de ferro. (A) Participação por área na categoria de aproveitamento. (B) Principais subáreas da construção civil. (C) Participação por área na categoria de disposição. (D) Principais subáreas de impactos ambientais.



Avaliando o panorama dos países que mais publicaram no período de 2000 a 2023 sobre resíduos de minério de ferro, observa-se que cada um deles apresenta linhas de pesquisas prioritárias (Figura 8). A China foca predominantemente em estudos voltados para Construção Civil (54%) e Ciência dos materiais (30%).

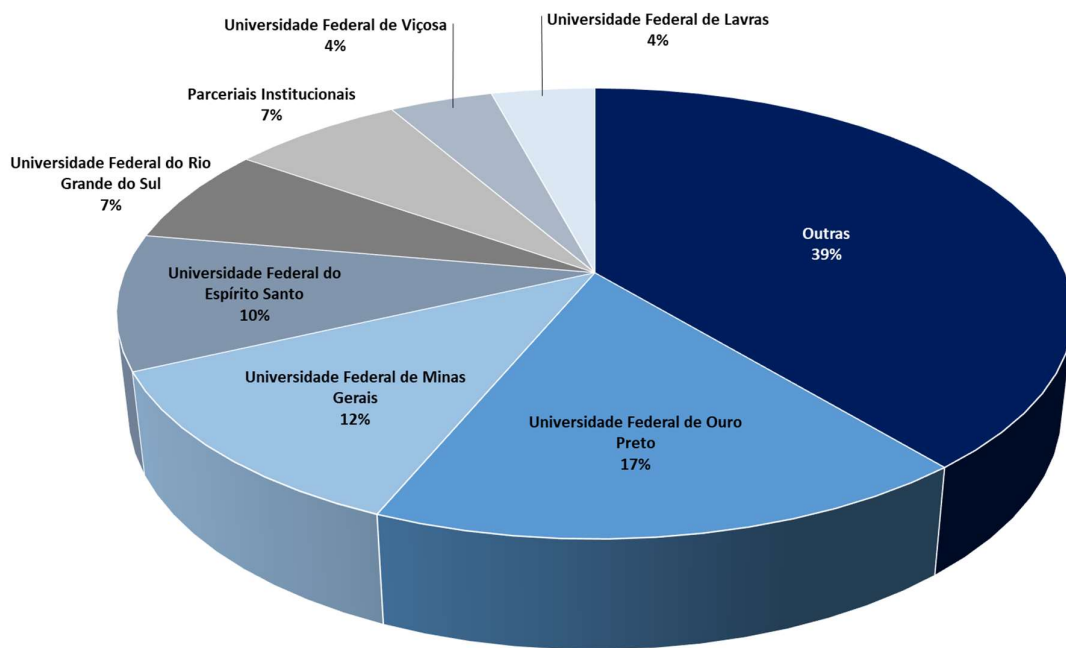
Figura I.08 - Foco das investigações dos países que mais publicaram sobre resíduos de ferro no período de 2000-2023.



O Brasil, por sua vez, apresenta um perfil de publicações mais heterogêneo, com artigos atrelados aos temas: Impactos Ambientais (28%), Construção Civil (27%), Mineração (18%) e Recuperação de Áreas Degradadas (9%). No caso da Índia, o foco das pesquisas também é variado, com destaque para os tópicos aproveitamento de rejeitos na construção civil e reprocessamento do IOT em processos de concentração mineral, que representam juntos cerca de 65% das publicações deste país.

No cenário brasileiro, as universidades que mais publicaram foram Universidade Federal de Ouro Preto - UFOP (17%) e a Universidade Federal de Minas Gerais - UFMG (12%), ambas com objetivos múltiplos no âmbito de aproveitamento e disposição (Figura 9). Outras universidades que apresentaram destaque nesse levantamento foram a Universidade Federal do Espírito Santo - UFES (10%), com inúmeras publicações atreladas aos impactos ambientais decorrentes de acidentes de barragens e a Universidade do Rio Grande do Sul - UFRGS (7%), com pesquisas direcionadas ao aproveitamento de resíduos por processamento químico e estudos voltados para as melhores práticas de disposição de rejeitos de minério de ferro. Algumas das investigações são provenientes de parcerias de diversas universidades brasileiras, as quais representam 7% dos artigos selecionados.

Figura 1.09 - Universidades brasileiras com maior número de publicações relacionados à disposição/aproveitamento de resíduos da mineração de ferro.



Por meio destes dados, foi possível relacionar os artigos apresentados nesta tese aos segmentos de pesquisa elencados na análise bibliométrica. Foram elaboradas investigações que pautaram tanto a disposição de rejeitos (Artigo 1) quanto diferentes abordagens para o aproveitamento destes materiais como coprodutos (Artigo 2 - 4).

O artigo 1 “*On the effects of iron ore tailings micro/nanoparticles in embryonic and larval zebrafish (*Danio rerio*)*” está categorizado como um trabalho vinculado a disposição de rejeitos, com foco nos impactos ambientais (Disposição → Impactos Ambientais → Ecotoxicidade). No âmbito da Ecotoxicidade foram identificados 7 artigos ao todo, dos quais 5 foram publicados no Brasil nos anos de 2021 e 2022. Em sua maioria, os artigos avaliaram organismos teste impactados pelo rompimento de barragens (MERÇON *et al.*, 2021; SIQUEIRA *et al.*, 2022)

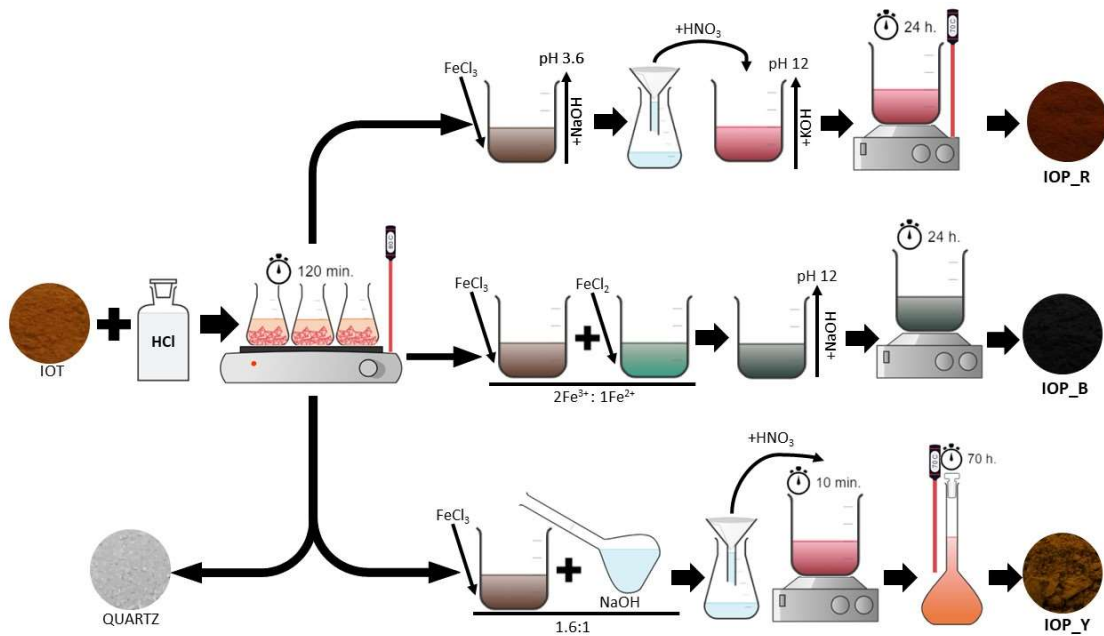
Apesar da relevância destes artigos, um questionamento fica em aberto: quais os efeitos dos rejeitos de ferro nas áreas circundantes da mineração, em condições normais de disposição em barragens e/ou empilhados a seco? Para responder essa questão, o artigo 1 investigou os efeitos de nano-micropartículas de rejeitos de minério de ferro, suscetíveis ao transporte pela chuva e pelo vento, no organismo teste Zebra-

fish (*Danio rerio*). O diferencial desta pesquisa foi mapear, em ambiente controlado e com um organismo teste de referência, os efeitos das partículas de rejeito que podem atingir o entorno, e por sua vez, provocar impactos toxicológicos. Considerando os resultados da análise bibliométrica e até onde sabemos, esse é o único estudo a combinar a caracterização completa da fração micro/nano de uma amostra de rejeito de minério de ferro e seus efeitos *in vivo* em peixes.

O artigo 2 “*Production of a ferric chloride coagulant by leaching an iron ore tailing*” é uma investigação no âmbito de aproveitamento de rejeitos e foca no processamento químico para obtenção de novos produtos. Através de uma rota de lixiviação foi possível recuperar o ferro e utilizá-lo como agente coagulante na forma de cloreto férrico (FeCl_3). Na subárea “Lixiviação”, foram mapeados 20 trabalhos, que correspondem 6% das publicações categorizadas como Aproveitamento (Aproveitamento → Lixiviação → Coagulantes). Nesse viés foi identificado mais um artigo voltado a obtenção de FeCl_3 a partir do IOT e foi publicado no mesmo ano do artigo 2 aqui retratado (LI *et al.*, 2020). Além da produção do cloreto férrico, o artigo 2 avaliou a aplicação deste insumo para o tratamento de água de abastecimento, evidenciando a eficácia do reagente FeCl_3 /IOT na remoção de cor e turbidez da água bruta utilizada para abastecimento público (ALMEIDA; SCHNEIDER, 2020). A aplicação do produto gerado para uma finalidade com relevância ambiental e que beneficia diretamente a população local é um aspecto que potencializa a sustentabilidade dessa alternativa e agrupa impactos positivos nas esferas ambiental, social e econômica.

Ainda no contexto da lixiviação, o Artigo 3 “*Simplified hydrometallurgical route for the synthesis of silica-free hematite from iron ore tailings*” investigou o uso do cloreto férrico para síntese de óxidos de ferro livres de sílica (Aproveitamento → Lixiviação → Síntese de materiais). Estudos sobre a síntese de materiais, representam 70% dos artigos da subárea Lixiviação e há uma forte tendência para síntese de partículas magnéticas (36% das publicações sobre síntese de materiais). De um modo geral, essas pesquisas aproveitam os rejeitos de minério de ferro via lixiviação e aplicam metodologias diversas para obtenção dos óxidos de ferro. ALMEIDA e SCHNEIDER (2022), investigaram as metodologias tradicionais para síntese de óxidos de ferro propostas por (SCHWERTMANN; CORNELL, 2000), utilizando os rejeitos de minério de ferro como insumos precursores (Figura 10).

Figura I.10 - Metodologias tradicionais para síntese de diferentes óxidos de ferro.



Os procedimentos gerais de síntese de óxidos de ferro, normalmente, envolvem várias etapas e diferentes reagentes, o que reforça a importância de buscar alternativas simplificadas de processamento, que sejam compatíveis com o grande volume de rejeitos gerenciados pela indústria de processamento mineral (ALMEIDA; SCHNEIDER, 2022). Deste modo, o Artigo 3 propõe e caracteriza os produtos de uma rota simplificada para produção de hematita e pauta a utilização deste processo para obtenção de um produto com características compatíveis ao uso na indústria siderúrgica. Tal possibilidade, potencializa a adoção do processamento químico como extensão do beneficiamento do ferro e viabiliza um nicho de incorporação com capacidade compatível ao grande volume de rejeito gerado.

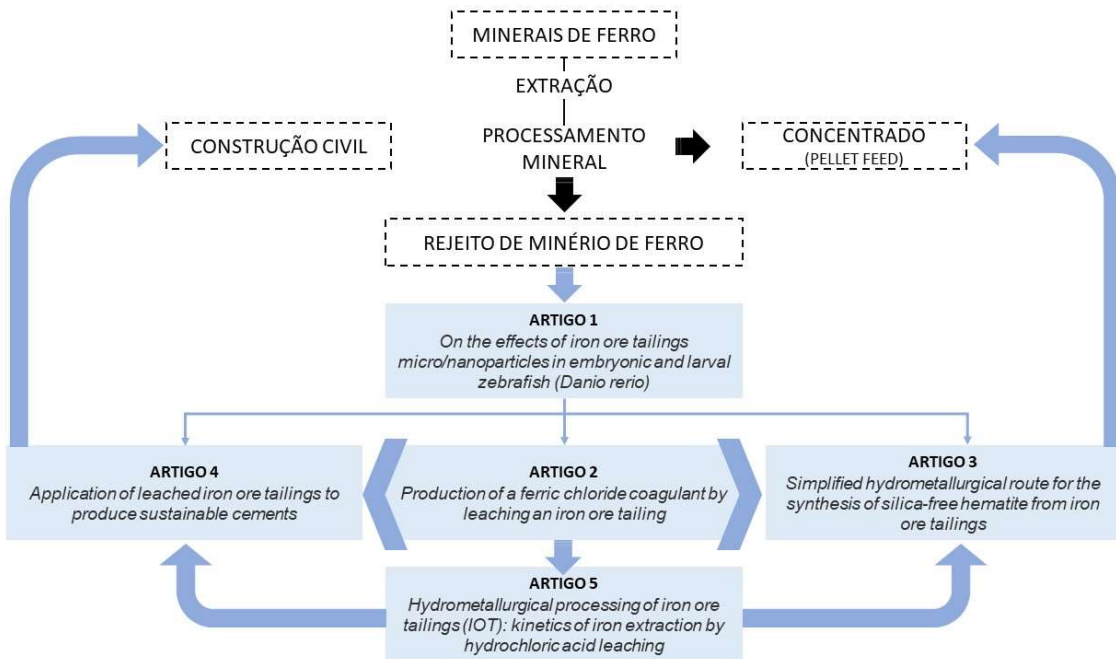
Outro produto da lixiviação é a fração insolúvel ao ácido clorídrico a quente, o qual foi caracterizado e avaliado como material cimentício suplementar no artigo 4. A publicação “*Application of leached iron ore tailings to produce sustainable cements*” está inclusa nos estudos voltados para aplicação de coprodutos da mineração na construção civil, sendo que a subárea material cimentício suplementar corresponde a 13% dos artigos da área Construção civil (Figura 7). Nessa subárea, o Brasil detém 30% dos artigos e foca, majoritariamente, na incorporação direta dos rejeitos como SCM. Diferentemente destes trabalhos, o artigo 4 utiliza um coproduto proveniente do

processamento químico do IOT, fator que potencializa a concentração de quartzo e caulinita e favorece a substituição do cimento Portland sem prejudicar a resistência à compressão das pastas de cimento. Segundo nosso conhecimento, esse é primeiro estudo que investiga a substituição do cimento pelo rejeito de minério de ferro preparado por lixiviação ácida para reduzir o teor de Fe_2O_3 (~2%), visando produzir materiais cimentícios sustentáveis.

Na continuidade, com intuito de entender os aspectos que governam a lixiviação, o Capítulo 5 “*Hydrometallurgical processing of iron ore tailings (IOT): kinetics of iron extraction by hydrochloric acid Leaching*” objetiva avaliar o modelo cinético que melhor se ajusta aos resultados experimentais de dissolução do ferro. Na análise bibliométrica, não foi identificado nenhum artigo que avaliasse a cinética de lixiviação voltada para o aproveitamento do ferro via lixiviação ácida. Por essa razão, os resultados deste estudo contribuem para o melhor entendimento dos parâmetros que governam o processamento hidrometalúrgico dos rejeitos de minério de ferro e os aspectos que podem ser otimizados para máxima recuperação das espécies minerais disponíveis no IOT.

Assim, pode-se justificar a integração dos artigos apresentados, enfatizando que os riscos associados a disposição de rejeitos têm mobilizado avanços crescentes para o aproveitamento destes materiais, juntamente com as oportunidades econômicas oriundas das inúmeros aplicações passíveis de serem incorporadas na gestão destes materiais. O processamento hidrometalúrgico é um viés ainda pouco explorado, mas que apresenta inúmeros aspectos que corroboram para a valorização dos rejeitos, além de ser uma abordagem adequada do ponto de vista sustentável e do gerenciamento dos resíduos sólidos. O fluxograma a seguir sintetiza a integração dos artigos (Figura 11).

Figura I.11 - Integração dos artigos utilizados no desenvolvimento deste trabalho.



REFERÊNCIAS

- ADIANSYAH, J. S. et al. A framework for a sustainable approach to mine tailings management: disposal strategies. *Journal of Cleaner Production*, v. 108, p. 1050–1062, dez. 2015.
- ALMEIDA, P. I. N. DE et al. The microbial profile of rivers and lagoons three years after the impact of the world's largest mining disaster (Fundão dam, Brazil). *Environmental Research*, v. 216, p. 114710, jan. 2023a.
- ALMEIDA, V. O. DE. Produção de Cloreto Férrico a partir de Rejeito de Minério de Ferro: Um estudo de caracterização e aplicabilidade. Porto Alegre: Dissertação de mestrado, 2019.
- ALMEIDA, V. O. DE; SCHNEIDER, I. A. H. Hydrometallurgical Processing of Brazilian Iron Ore Tailings for the Synthesis of Pigments. *Geomaterials*, v. 12, n. 02, p. 30–36, 2022.
- ALMEIDA, V. O. et al. Application of leached iron ore tailings to produce sustainable cements. *Construction and Building Materials*, v. 377, p. 131095, maio 2023b.
- ALMEIDA, V. O.; SCHNEIDER, I. A. H. Desafios rumo ao gerenciamento e aplicação sustentável dos rejeitos da indústria mineral: um estudo estatístico dos rejeitos das produções acadêmicas e inovações no segmento. 11º Simpósio Internacional de qualidade ambiental. Anais...Porto Alegre: 2018.
- ALMEIDA, V. O.; SCHNEIDER, I. A. H. Production of a ferric chloride coagulant by leaching an iron ore tailing. *Minerals Engineering*, v. 156, 2020.
- ALVES, W.; FERREIRA, P.; ARAÚJO, M. Challenges and pathways for Brazilian mining sustainability. *Resources Policy*, v. 74, p. 101648, dez. 2021.
- AMARAL, I. B. C.; PRAT, B. V.; REIS, A. B. DOS. Effect of iron mining tailings as a red ceramic additive for decreased sintering temperature. *Matéria (Rio de Janeiro)*, v. 25, n. 4, 2020.
- ANM. ANUÁRIO MINERAL BRASILEIRO PRINCIPAIS SUBSTÂNCIAS METÁLICAS. Brasília: [s.n.]. Disponível em: <<https://www.gov.br/anm/pt-br/centrais-de-conteudo/publicacoes/serie-estatisticas-e-economia-mineral/anuario-mineral/anuario-mineral-brasileiro/PreviaAMB2022.pdf>>. Acesso em: 15 jul. 2023.
- ARAUJO, V. A. et al. Column reverse rougher flotation of iron bearing fine tailings assisted by HIC and a new cationic collector. *Minerals Engineering*, v. 156, p. 106531, set. 2020.
- AUGUSTO, T. DE M. et al. Iron ore tailings as catalysts for oxidation of the drug paracetamol and dyes by heterogeneous Fenton. *Journal of Environmental Chemical Engineering*, v. 6, n. 5, p. 6545–6553, out. 2018.

- BAI, S.-J. et al. Novel method for iron recovery from hazardous iron ore tailing with induced carbothermic reduction-magnetic flocculation separation. *Clean Technologies and Environmental Policy*, v. 20, n. 4, p. 825–837, 10 maio 2018.
- BÖHLING, K.; MURGUÍA, D. I.; GODFRID, J. Sustainability Reporting in the Mining Sector: Exploring Its Symbolic Nature. *Business & Society*, v. 58, n. 1, p. 191–225, 11 jan. 2019.
- CECHIN, L. et al. Ceramics composites from iron ore tailings and blast furnace slag. *Ceramics International*, v. 48, n. 8, p. 10506–10515, abr. 2022.
- DAROS, F. A. et al. Fish otolith microchemistry as a biomarker of the world's largest mining disaster. *Science of The Total Environment*, v. 807, p. 151780, fev. 2022.
- DAVEY, P. T.; SCOTT, T. R. Removal of iron from leach liquors by the “Goethite” process. *Hydrometallurgy*, v. 2, n. 1, p. 25–33, jul. 1976.
- DE SOUSA, S. S. et al. Iron ore mining areas and their reclamation in Minas Gerais State, Brazil: impacts on soil physical properties. *SN Applied Sciences*, v. 2, n. 10, p. 1659, 9 out. 2020.
- DO CARMO E SILVA DEFÁVERI, K. et al. Iron ore tailing-based geopolymer containing glass wool residue: A study of mechanical and microstructural properties. *Construction and Building Materials*, v. 220, p. 375–385, set. 2019.
- DUARTE, M. S. et al. Influence of mechanical treatment and magnetic separation on the performance of iron ore tailings as supplementary cementitious material. *Journal of Building Engineering*, v. 59, p. 105099, nov. 2022.
- DUBIŃSKI, J. Sustainable Development of Mining Mineral Resources. *Journal of Sustainable Mining*, v. 12, n. 1, p. 1–6, 2013.
- EDRAKI, M. et al. Designing mine tailings for better environmental, social and economic outcomes: a review of alternative approaches. *Journal of Cleaner Production*, v. 84, p. 411–420, dez. 2014.
- ERNEST YOUNG. Top 10 business risks and opportunities for mining and metals in 2023. Disponível em: <https://www.ey.com/en_gl/mining-metals/risks-opportunities>. Acesso em: 30 maio. 2023.
- EUGENIO, T. M. C. et al. Study on the use of mining waste as raw material for extruded fiber cement production. *Journal of Building Engineering*, v. 63, p. 105547, jan. 2023.
- FANG, N. et al. Toward broader applications of iron ore waste in pollution control: Adsorption of norfloxacin. *Journal of Hazardous Materials*, v. 418, p. 126273, set. 2021.
- GALVÃO, J. L. B. et al. Reuse of iron ore tailings from tailings dams as pigment for sustainable paints. *Journal of Cleaner Production*, v. 200, p. 412–422, 1 nov. 2018.

GOMES, L. E. DE O. et al. The impacts of the Samarco mine tailing spill on the Rio Doce estuary, Eastern Brazil. *Marine Pollution Bulletin*, v. 120, n. 1–2, p. 28–36, jul. 2017.

GOMES, R. B.; DE TOMI, G.; ASSIS, P. S. Iron ore tailings dry stacking in Pau Branco mine, Brazil. *Journal of Materials Research and Technology*, v. 5, n. 4, p. 339–344, out. 2016.

GONG, L. et al. Novel red composite pigment with high thermostability from iron ore tailings: Synthesis and coloring mechanism. *Ceramics International*, v. 49, n. 3, p. 5066–5076, fev. 2023.

H.K., T.; HOSSINEY, N. Alkali-activated bricks made with mining waste iron ore tailings. *Case Studies in Construction Materials*, v. 16, p. e00973, jun. 2022.

HUANG, S. et al. Utilization of high-sulfur iron ore tailings in cement mortar by considering the influence of curing temperature and tailing content. *Journal of Building Engineering*, v. 74, p. 106826, set. 2023.

IBAMA. Rompimento de barragem da Vale em Brumadinho (MG) destruiu 269,84 hectares. Disponível em: <https://www.gov.br/ibama/pt-br/assuntos/noticias/copy_of_noticias/noticias-2019/rompimento-de-barragem-da-vale-em-brumadinho-mg-destruiu-269-84-hectares>. Acesso em: 30 maio. 2023.

IPEA. Carta de conjuntura Nº 43. Rio de Janeiro: [s.n.]. Disponível em: <https://portalantigo.ipea.gov.br/portal/images/stories/PDFs/conjuntura/200825_cc_43.pdf>. Acesso em: 15 jul. 2023.

ISMAEL, M. R. C.; CARVALHO, J. M. R. Iron recovery from sulphate leach liquors in zinc hydrometallurgy. *Minerals Engineering*, v. 16, n. 1, p. 31–39, jan. 2003.

KINNUNEN, P. et al. Recycling mine tailings in chemically bonded ceramics – A review. *Journal of Cleaner Production*, v. 174, p. 634–649, fev. 2018.

KOGEL, J. E. Sustainable Development and the Minerals Industry. Em: *Engineering Solutions for Sustainability*. Cham: Springer International Publishing, 2015. p. 25–34.

LI, X. et al. Effect of Fe²⁺/Fe³⁺ on high-strength ceramsite prepared by sintering geopolymers using iron ore tailings. *Ceramics International*, v. 48, n. 4, p. 5681–5688, fev. 2022.

LI, Y. et al. Comprehensive reutilization of iron in iron ore tailings: preparation and characterization of magnetic flocculants. *Environmental Science and Pollution Research*, v. 27, n. 29, p. 37011–37021, 23 out. 2020.

LI, Y. et al. Recovery and preparation of high-grade silica from iron ore tailings by S-HGMS coupling with acid leaching technology: Description of separation mechanism and leaching kinetics. *Powder Technology*, v. 424, p. 118523, jun. 2023.

LING, G. et al. Utilizing Iron Ore Tailing as Cementitious Material for Eco-Friendly Design of Ultra-High Performance Concrete (UHPC). *Materials*, v. 14, n. 8, p. 1829, 7 abr. 2021.

LIU, J. et al. Removal of Orange II using an adsorbent-supported zero-valent iron as a heterogeneous Fenton-like catalyst. *DESALINATION AND WATER TREATMENT*, v. 175, p. 273–281, 2020.

LIU, Y. et al. Production of lightweight ceramisite from iron ore tailings and its performance investigation in a biological aerated filter (BAF) reactor. *Journal of Hazardous Materials*, v. 178, n. 1–3, p. 999–1006, jun. 2010.

LU, C. et al. Utilization of iron tailings to prepare high-surface area mesoporous silica materials. *Science of The Total Environment*, v. 736, p. 139483, set. 2020a.

LU, Y. et al. Synthesis of iron red hybrid pigments from oil shale semi-coke waste. *Advanced Powder Technology*, v. 31, n. 6, p. 2276–2284, 1 jun. 2020b.

LUCIANO, V. A. et al. Thermal cracking of oleic acid promoted by iron species from iron ore tailings for the production of ketones and fuels. *Fuel*, v. 310, p. 122290, fev. 2022.

LV, X. et al. Environmental impact, durability performance, and interfacial transition zone of iron ore tailings utilized as dam concrete aggregates. *Journal of Cleaner Production*, v. 292, p. 126068, abr. 2021.

MATHEUS CARVALHO EUGÊNIO, T. et al. Study on the feasibility of partial replacement of cement with IOT in extruded concrete roof tiles production. *Construction and Building Materials*, v. 393, p. 132129, ago. 2023.

MAYBEE, B.; LILFORD, E.; HITCH, M. Environmental, Social and Governance (ESG) risk, uncertainty, and the mining life cycle. *The Extractive Industries and Society*, v. 14, p. 101244, jun. 2023.

MENDES, B. C. et al. Technical and environmental assessment of the incorporation of iron ore tailings in construction clay bricks. *Construction and Building Materials*, v. 227, 10 dez. 2019.

MENDES PROTASIO, F. N. et al. The use of iron ore tailings obtained from the Germano dam in the production of a sustainable concrete. *Journal of Cleaner Production*, v. 278, p. 123929, jan. 2021.

MENG, J. et al. Synthesis of schorl doped iron ore tailings glass-ceramics with superior performance. *Journal of Non-Crystalline Solids*, v. 600, p. 122034, jan. 2023.

MERÇON, J. et al. Evidence of reproductive disturbance in *Astyanax lacustris* (Teleostei: Characiformes) from the Doce River after the collapse of the Fundão Dam

in Mariana, Brazil. *Environmental Science and Pollution Research*, v. 28, n. 47, p. 66643–66655, 7 dez. 2021.

MILLER, M. E.; GHISOLFI, R. D.; BARROSO, G. F. Remote sensing monitoring of mining tailings in the fluvial-estuarine-coastal ocean continuum of the Lower Doce River Valley (Brazil). *Environmental Monitoring and Assessment*, v. 195, n. 5, p. 542, 5 maio 2023.

MMBANDO, E.; FOURIE, A.; REID, D. Mechanics of an Iron Ore Tailings Exhibiting Transitional Behaviour. *Geotechnical and Geological Engineering*, v. 41, n. 3, p. 2211–2220, 18 maio 2023.

MORAN, C. J. et al. Sustainability in mining, minerals and energy: new processes, pathways and human interactions for a cautiously optimistic future. *Journal of Cleaner Production*, v. 84, p. 1–15, dez. 2014.

MYMRIN, V. et al. Physical-chemical processes of sustainable construction materials structure formation with iron ore processing tailings and aluminum anodizing sludge. *Construction and Building Materials*, v. 298, p. 123698, set. 2021.

NASCIMENTO, R. L. et al. The Fundão dam failure: Iron ore tailing impact on marine benthic macrofauna. *Science of The Total Environment*, v. 838, p. 156205, set. 2022.

PANDIRI, S. et al. Enhanced Iron Recovery from Ultrafine Iron Ore Tailing Through Combined Gravitational and Magnetic Separation Process. *Transactions of the Indian Institute of Metals*, v. 75, n. 9, p. 2435–2442, 18 set. 2022.

PEREIRA, A. R. M. et al. Direct hematite flotation from an iron ore tailing using an innovative biosurfactant. *Separation Science and Technology*, v. 56, n. 17, p. 2978–2988, 22 nov. 2021.

PRADEL, J. et al. Ferric hydroxide oxide from the goethite process: characterization and potential use. *Industrial & Engineering Chemistry Research*, v. 32, n. 9, p. 1801–1804, 1 set. 1993.

PUIATTI, G. A. et al. Reuse of iron ore tailings as an efficient adsorbent to remove dyes from aqueous solution. *Environmental Technology*, p. 1–12, 17 dez. 2021.

SCHOENBERGER, E. Environmentally sustainable mining: The case of tailings storage facilities. *Resources Policy*, v. 49, p. 119–128, set. 2016.

SCHWERTMANN, U.; CORNELL, R. M. Iron oxides in the laboratory: Preparation and Characterization. New York: Wiley-VCH, 2000.

SERVI, S. et al. Mechanical response of filtered and compacted iron ore tailings with different cementing agents: Focus on tailings-binder mixtures disposal by stacking. *Construction and Building Materials*, v. 349, p. 128770, set. 2022.

SILVA, R. C. F. et al. Use of iron mining tailings from dams for carbon nanotubes synthesis in fluidized bed for 17 α -ethinylestradiol removal. Environmental Pollution, v. 260, p. 114099, maio 2020.

SIQUEIRA, D. et al. Terrestrial and aquatic ecotoxicity of iron ore tailings after the failure of VALE S.A mining dam in Brumadinho (Brazil). Journal of Geochemical Exploration, v. 235, p. 106954, abr. 2022.

STATISTA. Production volume of usable iron ore worldwide from 2010 to 2022(in million metric tons). Disponível em: <[https://www.statista.com/statistics/589945/iron-ore-production-gross-weight-worldwide/#:~:text=In%202022%2C%20the%20total%20volume,tons%20of%20usable%20iron%20ore.](https://www.statista.com/statistics/589945/iron-ore-production-gross-weight-worldwide/#:~:text=In%202022%2C%20the%20total%20volume,tons%20of%20usable%20iron%20ore.>)>. Acesso em: 15 jul. 2023.

SU, Z. et al. Preparation of Iron Ore Tailings-Based Superhydrophobic Coatings. Materials, v. 15, n. 12, p. 4235, 15 jun. 2022.

TAYEBI-KHORAMI, M. et al. Re-Thinking Mining Waste through an Integrative Approach Led by Circular Economy Aspirations. Minerals, v. 9, n. 5, p. 286, 10 maio 2019.

UNITED NATIONS. Sustainable Development Goals.

WEISHI, L. et al. The properties and formation mechanisms of eco-friendly brick building materials fabricated from low-silicon iron ore tailings. Journal of Cleaner Production, v. 204, p. 685–692, dez. 2018.

XU, D.-M. et al. A critical review on environmental implications, recycling strategies, and ecological remediation for mine tailings. Environmental Science and Pollution Research, v. 26, n. 35, p. 35657–35669, 15 dez. 2019.

YELLISHETTY, M. et al. Reuse of iron ore mineral wastes in civil engineering constructions: A case study. Resources, Conservation and Recycling, v. 52, n. 11, p. 1283–1289, set. 2008.

YI, Z. et al. Iron ore tailings used for the preparation of cementitious material by compound thermal activation. International Journal of Minerals, Metallurgy and Materials, v. 16, n. 3, p. 355–358, jun. 2009.

ZHANG, Y. et al. Mechanochemical activation of iron ore tailing-based ternary supplementary cementitious materials. Construction and Building Materials, v. 346, 5 set. 2022a.

ZHANG, Y. et al. Filling of iron ore tailings into poly(vinyl chloride) based composites: Surface modification effect and performance enhancement. Materials Chemistry and Physics, v. 292, p. 126834, dez. 2022b.

ZHAO, J. et al. An evaluation of iron ore tailings characteristics and iron ore tailings concrete properties. Construction and Building Materials, v. 286, p. 122968, jun. 2021.

CAPÍTULO II

ON THE EFFECTS OF IRON ORE TAILINGS MICRO/NANOPARTICLES IN

EMBRYONIC AND LARVAL ZEBRAFISH (*Danio rerio*)

ARTIGO 1

On the effects of iron ore tailings micro/nanoparticles in embryonic and larval zebrafish (*Danio rerio*)

Vítor Otacílio de Almeida¹, Talita Carneiro Brandão Pereira^{2,3}, Lilian de Souza Teodoro^{2,3}, Manuella Escobar², Carolina Junqueira Ordovás², Karine Batista dos Santos¹, Jéssica Weiler¹, Maurício Reis Bogo^{2,3,4*}, Ivo André Homrich Schneider^{1*}

1. Laboratório de Tecnologia Mineral e Ambiental, Programa de Pós-Graduação em Engenharia de Minas, Metalúrgica e de Materiais, Escola de Engenharia, Universidade Federal do Rio Grande do Sul (UFRGS). Av. Bento Gonçalves, 9500. CEP-91501-970. Porto Alegre, RS, Brasil.

2. Laboratório de Biologia Genômica e Molecular, Pontifícia Universidade Católica do Rio Grande do Sul (PUCRS). Av. Ipiranga, 6681. CEP: 90.619.900. Porto Alegre, RS, Brasil.

3. Programa de Biologia Celular e Molecular, Escola de Ciências da Saúde e da Vida, PUCRS. Av. Ipiranga, 6681. CEP: 90.619.900. Porto Alegre, RS, Brasil.

4. Programa de Medicina e Ciências da Saúde, Escola de Medicina, PUCRS. Av. Ipiranga, 6690. CEP: 90.610-000. Porto Alegre, RS, Brasil.

*Corresponding authors (emails: ivo.andre@ufrgs.br; mbogo@pucrs.br).

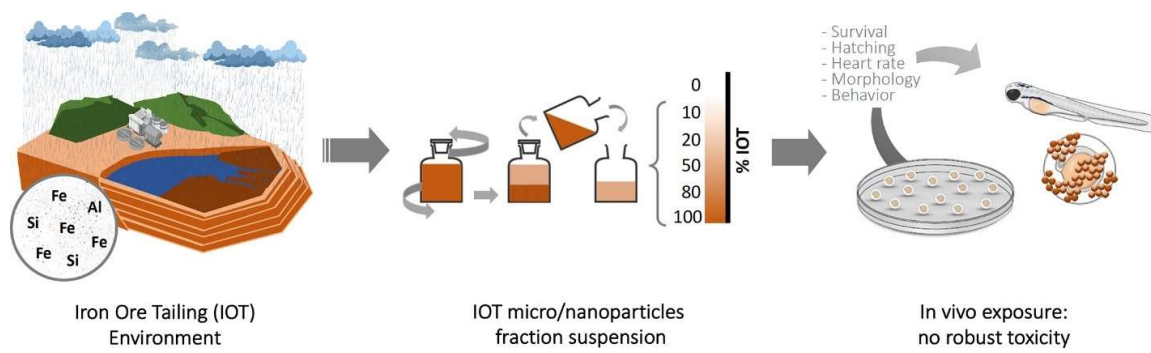
Artigo publicado na *Science of The Total Environment* (ISSN: 1879-1026 | Impact Factor 9.8 | Qualis A1 – Quadriênio 2017-2020)

ABSTRACT

Iron ore tailings (IOT) represent a major problem in the mining industry worldwide due to large volumes of waste disposed in mine sites. IOT are exposed to the environment and subjected to wind and water dispersion, even under non-catastrophic scenarios as dam collapses, and the effects of these particles to the biota are still mostly unknown. This work aimed to prepare and to characterize a suspension containing the finest (micro/nano range) particles of IOT and to evaluate its effects on development and behavior of zebrafish (*Danio rerio*), at both embryonic and larval stages. IOT suspension comprised 37 mg L⁻¹ of a multi-mineral material mainly composed by hematite and quartz, in a size-range of 33 - 1400 nm. Regarding in vivo toxicological assays, no robust alterations were recorded in functional, morphological and behavioral end-points analyzed, although a significant adhesion of IOT particles on zebrafish chorion was observed, without a prejudice of embryo hatching. Under applied conditions, iron ore particles did not present harmful effects to the initial stages of zebrafish development, and the particle size range and potential interactions with SiO₂ content might be behind such effect.

Keywords: mining; environmental toxicity, hematite, quartz, iron ore suspension, econanotoxicology.

GRAPHICAL ABSTRACT



1. INTRODUCTION

Iron ore is an important commodity of the mineral industry being vital in the modern economy (Su et al., 2017). It is exploited in several countries, of which Australia, Brazil, and China stand out as world leaders (WA Iron ore profile, 2019). Another characteristic of the iron ore industry is the large generation of tailings. In the Quadrilátero Ferrífero region (Brazil), it is estimated that for every metric ton of iron ore extracted, 40% of the mass is rejected (Mendes et al., 2019). This proportion results in a environmental problem regarding waste disposal.

The IOT has been an important focus of concern following Brazilian dam disasters. The collapse of the Fundão dam in 2015 and the Córrego do Feijão dam in 2019 caused social and environmental impacts of great magnitude. Related studies have emphasized general and large-scale impacts in terms of socio-economics (Fernandes et al., 2016), extent of contamination (Marta-Almeida et al., 2016; Carmo et al., 2017; Hatje et al., 2017, Davila et al., 2020), characterization and treatment of water resources (Segura et al., 2016; Gomes et al., 2017; Oliveira et al; 2019), impact on forest resources (Omachi et al., 2018), and possible causes of dam collapse (Armstrong et al., 2019; Palmer, 2019; Rotta et al., 2020), but they did not evaluated specific effects of IOT particles, which are important to assist mining endeavors in waste management and environmental risk studies.

The IOT are composed of fine particles, essentially a mixture of silica, iron oxides, and clay minerals (Pires et al., 2003; Galvão et al., 2018). Particle characteristics and the large volume of tailings allow these materials to be easily diffuse into the surrounding areas, through surface runoff and dust (Breshears et al., 2003; Schaider et al., 2007; Hayes et al., 2012; Geng et al., 2020). The transport of fine particles by wind is a recurring problem for mining regions. The same problems arise in pluvial transport in which the particles of colloidal size remain in water suspension, easily dispersed and traveling long distances (Hayes et al, 2012; Bratby, 2016). These factors could have ecotoxicological effects: increasing bioavailability of metals in soil and water (Rodgher et al., 2013; Bori et al., 2016); metal accumulation in tissues of aquatic organisms (Wong and Li, 1977); endocrine disruption (Van Ree and Payne, 2005), even in a non-collapse dam scenario, since climatic conditions, river basin profile and density of mining units/sites affect the input of sediments in aquatic systems

(Brazil, 2006; Macklin et al. 2006; Chalov, 2014; Pietroń et al., 2017). For instance, Pereira et al. (2008) investigated metal bioavailability in water, sediments and aquatic invertebrates field samples of coastal lagoon adjacent to iron-ore mining and processing sites. They identified that these mining operations were a potential source of metal-containing suspended particulates.

Ecotoxicological studies are important to evaluate the possible effects of the interaction between IOT and the biota. Water resources affected in both Brazilian dam collapses were targeted for studies of cytotoxicity and genotoxicity and assessing the potential damage associated with the interaction of these tailings in the environment. Quadra et al. (2019) collected water along the Doce River 10 days after the Fundão disaster at two impacted sites and one non-impacted site. Sampling points were located hundreds of kilometers downstream of the collapsed dam. Water samples were used for trace element quantification and to run toxicological analyses using *Allium cepa*. The authors observed cytogenotoxic effects such as alterations in mitotic and phase indexes and enhanced frequency of chromosomal aberrations. Weber et al. (2020) assessed the effects due to the rupture of the Fundão dam on two native fish species (*Hoplias intermedius* and *Hypostomus affinis*) from the same river. The study demonstrates that the release of mineral residues from the rupture of the dam provokes hepatic damage in the fish and induces the expression of proteins and enzymes related to metal contamination. Thompson et al. (2020) published the results of biogeochemical, microbiological, and ecotoxicological analyses to reveal the short-term impact of the Brumadinho dam rupture on the Paraopeba River. Immediately after the disaster, the water turbidity increased dramatically, allowing an increase in iron tolerant microbial activity. Ecotoxicological analyses using zebrafish indicated high embryo mortality in the river, although it may not be exclusively related to the dam failure. They noted that the causal nexus of mortality may be associated with other factors (e.g., local sewage pollution) and suggest that independent monitoring programs are needed to promote the recovery of the degraded sites. In fact, all above mentioned studies were performed with water samples collected directly from river sites under the influence of other anthropogenic factors, not just the iron ore flooding.

In this context, considering that (i) IOT are permanently exposed to the environment, (ii) its mineral components are subjected to wind and water dispersion, most likely reaching aquatic ecosystems even under non-catastrophic scenarios of

dam collapses and (iii) the effects of exposure to fine fraction of IOT particles in the biota is mostly unknown, this work aimed to evaluate *in vivo* toxicity of fine IOT particles present in water suspension using zebrafish embryos and larvae as testing organism. The IOT sample was collected from a mining site that uses exclusively magnetic separation as the iron ore concentration method (to avoid possible interference with mining chemicals, such as those used in flotation and thickening) and then, it was submitted to thorough physical-chemical characterization. The zebrafish (*Danio rerio*) was chosen as the *in vivo* model because it is a well-recognized vertebrate ecotoxicological model commonly applied as a tool to address environmental health or toxicity in aqueous systems (Bambino and Chu, 2017; Horzmann and Freeman, 2018) with a robust set of quantifiable developmental end-points available (Pereira et al., 2020a).

2. MATERIALS AND METHODS

2.1. Preparation of IOT suspension

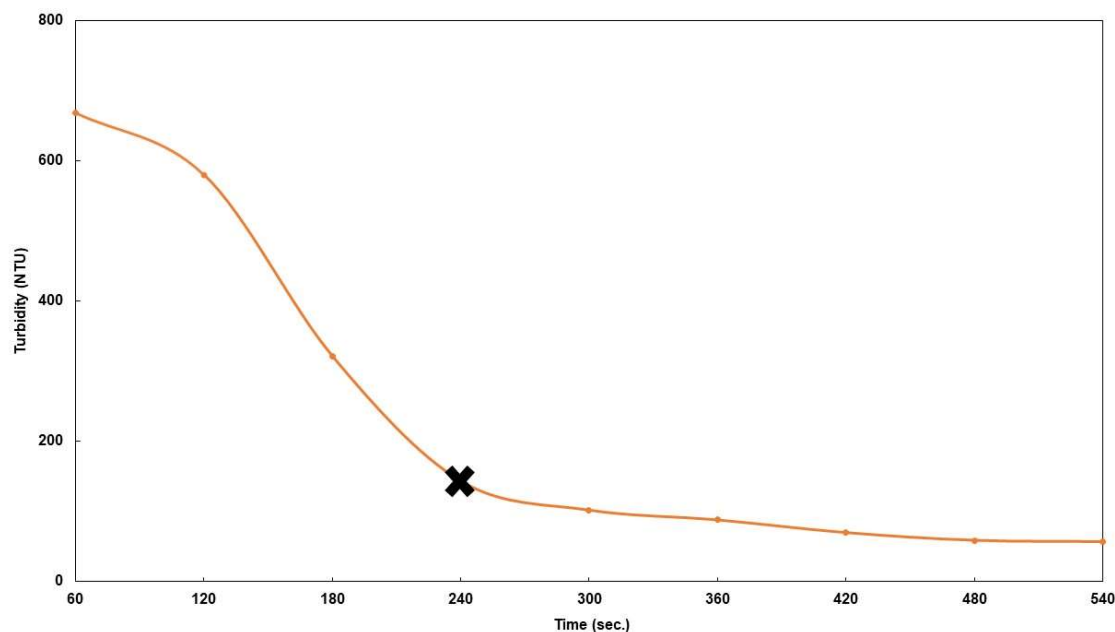
The IOT samples were provided by a company that operates the extraction and beneficiation of iron ore in the Quadrilátero Ferrífero, Minas Gerais, Brazil. This mine is located geologically in the Cauê Formation ($20^{\circ}25'37"S$, $43^{\circ}52'29"W$), consisting of siliceous itabirite, carbonatic itabirite, amphibolitic itabirite, and manganiferous itabirite, with high hematite content (Trzaskos et al, 2011).

The iron ore concentration is accomplished by magnetic separation without the addition of any chemicals in any step of the concentration system. The micro and nano particles were obtained by gravity settling of the IOT collected from the underflow of a deep cone thickener used for dewatering. This pulp presented 40% solids in suspension (mass/volume, m/v), a top size of 300 μm , and the following elemental composition: Si-31.0%, Fe-17.0%, Al-1.6%, Ti-0.07%, Mn-0.02%, Mg-0.004%, and P-0.04%; a typical constitution of IOT from the Quadrilátero Ferrífero region.

The procedure used in this work aimed to represent the stable fraction of colloidal particles present in an aqueous environment. To achieve this objective, preparation of a fine particle IOT suspension was carried out by following the steps:

(a) 2 L of 40% m/v pulp was placed in a glass bottle with a lid, (b) the bottle was manually shaken for complete homogenization of the suspension, (c) the bottle was left to rest allowing the particles to settle, and (d) the supernatant was collected after 240 s resting time. The time of 240 s was chosen because turbidity tends to be approximately constant after this period of time (Figure 1). This suspension was then characterized and used for following toxicological tests.

Figure II.01. Representative turbidity of iron ore tailing suspension collected 5 cm from the surface as a function of settling time. (NTU: nephelometric turbidity units).



2.2. Characterization of iron ore suspension

The characterization of the suspension included pH, conductivity, turbidity, suspended solids concentration, particle size distribution, and determination of the isoelectric point. The pH of the suspension was measured using a bench pH meter (AKSO model 86505, São Leopoldo, BRA). Calibration of the equipment was performed with buffer solutions for pH of 4.0, 7.0, and 10.0 (Dinâmica, Indaiatuba, BRA). Conductivity was determined with a multiparameter analyzer (AKSO model AK88, São Leopoldo, BRA) and calibration carried out with a standard conductivity solution of 12.88 mS/cm (AKSO, São Leopoldo, BRA). Turbidity was analyzed using a portable turbidimeter (Digimed, São Paulo, BRA) and calibration was performed with

standard solutions of 10, 100, and 500 NTU (Digimed, São Paulo, BRA). The concentration of suspended solids was measured using the evaporation method as described in SMWW 2540 Solids (APHA, 2017). The hydrodynamic particle size and the isoelectric point were attained using a Zetasizer Nano ZS (Malvern Panalytical, Malvern, UK). To measure the mean size of the particles, the zetasizer (with a particle size measurement coverage from 0.3 nm to 10 µm) held a dynamic light scattering method that monitors the diffusion of particles in Brownian motion and converts this signal to equivalent diameters according to the Stokes-Einstein relationship. The isoelectric point (IEP) was determined by zeta potential analysis for the pH range 2-10. This instrument uses a laser doppler micro-electrophoresis technique, in which an electric field is applied to the dispersion of particles that migrate at a velocity that depends on the zeta potential. This velocity was measured using laser interferometry-M3-PALS (phase analysis light scattering), which enables the calculation of electrophoretic mobilities and converts them into a zeta potential (millivolts) using Smoluchowski's equation (Hunter, 1981). For pH adequacy in the range of 2-6, a 4 mol L⁻¹ hydrochloric acid (analytical grade, Química Moderna, Barueri, BRA) solution was used. For the range of 8-10, the pH was adjusted with sodium hydroxide (Dinâmica, Indaiatuba, BRA) at a concentration of 4 mol L⁻¹.

Further characterization of the solid particles in suspension was carried out in terms of crystalline composition by X-ray diffraction (XRD) and elemental composition by X-ray fluorescence (XRF). For this, several batches of the suspension were prepared and centrifuged (Fanem, Excelsa Baby model-206 R, BRA) at 4000 rpm for 2 min to attain approximately 20 g of solids. The centrifuged solid was dried at 60 °C and the clods dismantled in a porcelain mortar with a pestle to below 37 µm to meet the specifications for the analyses. The XRD was carried out using an X-ray diffractometer (Siemens, Bruker AXS, USA) model D-5000 (θ -2 θ) equipped with a fixed Cu anode tube and operated at 40 kV and 25 mA, with an incident radiation of 1.5406 Å. The angular range analyzed was from 3° to 80°, 2 θ with a step size of 0.02°/3 s using divergence and anti-scattering slits of 2 mm and 0.2 mm in the detector, respectively. Chemical characterization was carried out by XRF using a spectrometer XRF Rigaku (Siemens, Bruker AXS, USA) model RIX 2000, equipped with a rhodium X-ray tube. The XRF analysis was performed using a fused bead with a calibration curve from rock patterns.

2.3. *In vivo* exposure and toxicological endpoints

Exposure suspensions were freshly prepared daily in 10, 20, 50, 80, and 100 % of the original characterized suspension, diluted with recirculating system water using a volumetric flask; representing the turbidity levels of 14, 29, 72, 115, and 143 NTU, respectively. Zebrafish eggs were obtained by breeding wild-type AB-line adults, maintained in automated recirculating systems (Zebtec - Tecniplast, ITA) under optimal standard water conditions (27 ± 1 °C, pH = 7.0-8.0, conductivity = 500-800 µS, 14-10 h light-dark cycles and room temperature 26 ± 1 °C) and fed thrice a day with dry flake food (TetraMin Tropical Flake - Tetra, USA), supplemented with brine shrimp (*Artemia* sp.) during evening feeding. Reproduction was performed at a ratio of 2 males to 1 female, and healthy viable embryos were collected and randomly distributed among all six experimental groups petri dishes, in a density of ≤ 2 embryo/mL, and maintained at 28.5°C in a bio-oxygen demand (BOD) incubator during the 6-day exposure protocol. The exposure solutions and previously sterilized plates were substituted every 24 h, from 4 up to 144 hpf (hours post-fertilization), when larvae were euthanized through cryoanesthesia. Conductivity and pH of pre- and post-exposure solutions were recorded daily for water quality control. All *in vivo* protocols followed current national legislation and international guidelines and were approved by the institutional ethics committee on animal use (CEUA/PUCRS, 9003). Survival and hatching rates were recorded daily, while spontaneous movement, heart rate, larval morphology, and locomotor activity were analyzed at 24, 48, 120, and 144 hpf, respectively, as previously reported (Pereira et al., 2020a).

2.4. Scanning electron microscopy (SEM) analysis

To investigate interactions of IOT suspensions with fish embryo chorion, field-emission scanning electron microscopy (FESEM) and energy dispersive X-ray spectroscopy (EDS) were performed on chorion surface at 24 and 48 hpf (n=10/group). Fish embryos were fixed in 25% glutaraldehyde phosphate buffered for at least one week before preparation. After 0.2 M phosphate buffer washes, samples were dehydrated in an acetone series up to 100%, and the critical-point-dried and sputter-coated with gold in carbon tape-covered stubs. Inspect F50 microscope (FEI

Company, EUA) coupled with an Oxford X-Act detector combined with AZtec software (Oxford Instruments, UK) were employed for EDS analysis. Exposure suspensions were also submitted to FESEM-EDS analysis to confirm major elements detection by placing a drop of homogenized solution in carbon tape-covered stubs, which were then air-dried and sputter-coated with gold before examination.

2.5. Statistical analysis

The Shapiro-Wilk normality test was performed on all *in vivo* parameters. The Kaplan-Meier test was applied to the survival curve and two-way analysis of variance (ANOVA) followed by Bonferroni post-hoc was used to assess hatching rate. Non-parametric results were analyzed with the Kruskal-Wallis test followed by Dunn's post-hoc test, while parametric data were evaluated by one-way ANOVA followed by the Bonferroni post-hoc test; $p \leq 0.05$ was considered statistically significant.

3. RESULTS AND DISCUSSION

The physical-chemical characteristics of the IOT suspension are presented in Table 1.

Table II.01. Characteristics of the micro/nanoparticles of iron ore tailing (IOT) suspension.

Physical Characteristics		Mineralogical Composition XRD	Elemental composition (%) XRF	
Suspension pH	7.0	Major	Fe	33.0
Conductivity (μS)	157.6	Hematite - $\alpha\text{-Fe}_2\text{O}_3$	Si	15.7
Particle size (nm)	33-1400	Quartz - SiO_2	Al	8.8
Total solids (mg L^{-1})	37	Minor	Ti	0.29
Turbidity (NTU)	143	Goethite - FeO.OH	Mn	0.05
IEP (pH)	9.7	Kaolinite - $(\text{Al}_2(\text{Si}_2\text{O}_5)(\text{OH})_4$	Mg	0.43
			P	0.07

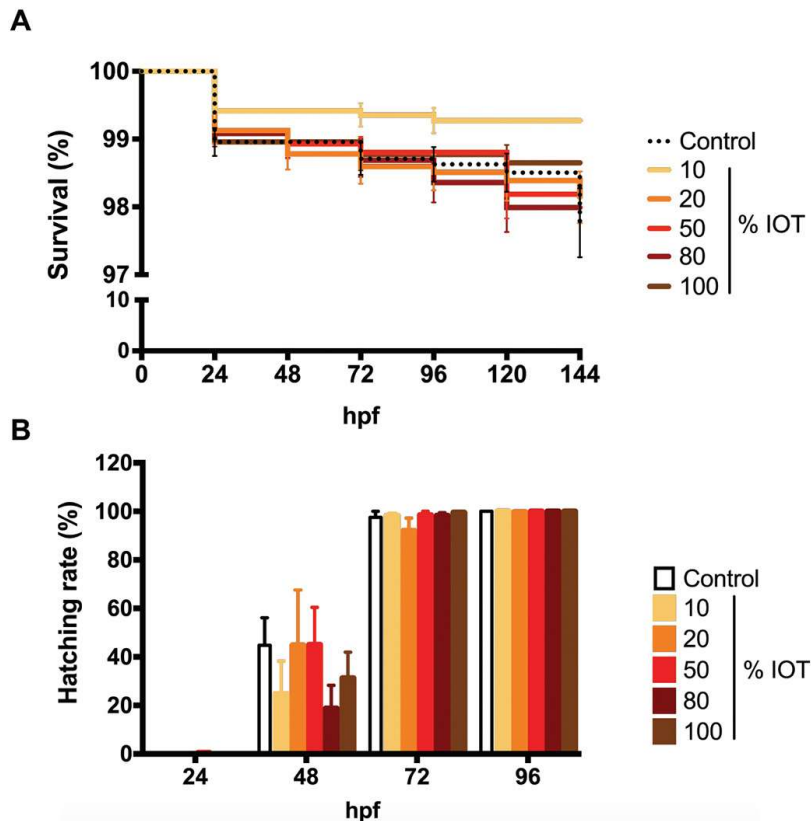
The sample had a granulometric distribution within the range of 33 to 1400 nm, with total solids concentration of 37 mg L⁻¹. The granulometric distribution of the suspension had a top size about 200 times smaller than the top size of the original tailings pulp (the underflow of a deep cone thickener - depicted in section 2.1) and falls within 10% of the finest range of the sample (D₁₀) and within the range of fluvial suspended sediments (Walling and Moorehead, 1989). The IEP of the IOT suspension was 9.7 (ANEXO I - Appendix 1), slightly above the IEP band of iron oxides, which ranges from pH 6 to 9 (Schwertmann and Taylor, 1989; Kosmulski, 2001; Cornell and Schwertmann, 2003).

The XRD analysis of the solid phase present in the IOT suspension showed hematite and quartz as predominant phases, with incidental occurrence of other minerals such as goethite and kaolinite (ANEXO I - Appendix 2). After the settling process, the iron oxide particles constituted the majority of the composition, as compared to the original sample in which quartz was the major component. The amount of kaolinite also rose since the Al concentration increased from 1.6% in the original sample to 8.8% in the suspension.

In vivo exposure to 10, 20, 50, 80, and 100% of IOT in suspension exhibited no robust toxicity to embryos or larvae under the described conditions, with no significant differences between 100%-IOT suspension and control group in any parameter analyzed. All experimental groups presented more than 97% survival and normal hatching rates, between 48 and 72 hpf (Fig. 2).

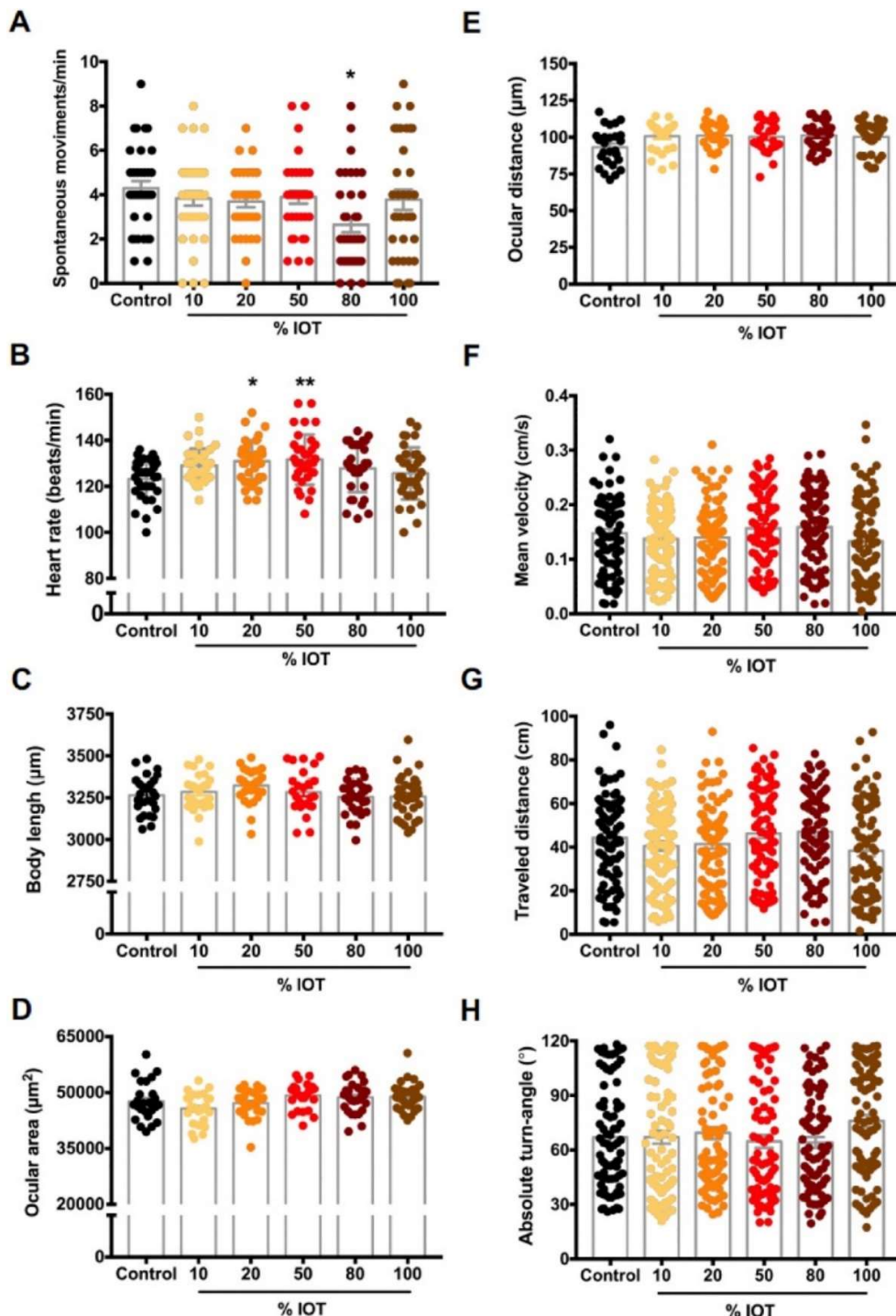
Embryonic spontaneous movement showed a statistical decrease only for the 80% group (Fig. 3A) and heart rate a statistical increase in both 20 and 50% groups at 48 hpf (Fig. 3B) when compared to control. Analysis of larval morphology (in terms of body length, ocular area and ocular distance) and locomotor behavior (in terms of distance travelled, mean velocity and mean absolute turn angle) did not record any significant alterations among all experimental groups (Fig. 3C-H).

Figure II.02. Zebrafish survival and hatching rate during 6-day exposure to iron ore tailings (IOT) in suspension. (A) Survival curve (estimated according to the Kaplan-Meier method) and (B) hatching rate for full IOT exposure, from up to 4 until 144 hpf (hours post-fertilization). Error bars represent standard error (* $p\leq 0.05$, two-way ANOVA followed by Bonferroni post-hoc, n=400/group, three independent experiments).



Previous studies with lab-synthesized iron-based nanoparticles, such as hematite, reported *in vivo* toxicity in developing zebrafish (Zhu et al, 2012; Pereira et al, 2020b). These studies evaluated pure suspensions of very small average size particles (< 100 nm), which are considerably smaller than zebrafish chorion pores (500 to 700 nm) (Rawson et al., 2001). In contrast, in the present work, particle size distribution is quite large, ranging from 33 to 1400 nm, and more importantly, in a suspension of a multi-mineral composition from a mineral processing operation; majorly of iron oxide- and silica-based particles.

Figure II.03. Effect of zebrafish embryos and larvae exposure to iron ore tailings (IOT) micro/nanoparticles in suspension. Results for (A) embryonic spontaneous tail movements at 24 hpf ($n=36/\text{group}$); (B) heart rate at 48 hpf ($n=36/\text{group}$); larval morphology in terms of body length (C), ocular distance (D), and ocular surface area (E), analyzed at 120 hpf ($n=36/\text{group}$) and larval behavior, evaluated at 144 hpf, in terms of distance traveled (F), mean velocity (G), and mean absolute turn angle (H) ($n=80/\text{group}$). Column bars represent mean \pm standard error (of three independent experiments, * $p\leq 0.05$, one-way ANOVA followed by Bonferroni post-hoc for A-G, Kruskal-Wallis followed by Dunn's post-hoc for H).



The nature of the iron particles and the presence of silica may alter the symptomatic array. It is well known that α -hematite (the major crystalline component of the IOT sample) is one of the most stable forms of iron oxides found in the environment (Cornell and Schwertmann, 2003). Silica, when associated with iron oxides surface, can reduce iron oxide particles' reactivity by either partial liberation of the multiphase mineral composition, or electrostatic attraction between SiO_2 and $\alpha\text{-Fe}_2\text{O}_3$ (Taylor, 1995; Jones et al., 2009). Indeed, SiO_2 is a classical coating material for engineered iron-oxide nanoparticles aiming to enhance dispersion and to reduce toxicity (Arias et al, 2018). Thus, our findings reinforce that not only particle size but also suspension conditions and composition play important role *in vivo* toxicity outcomes.

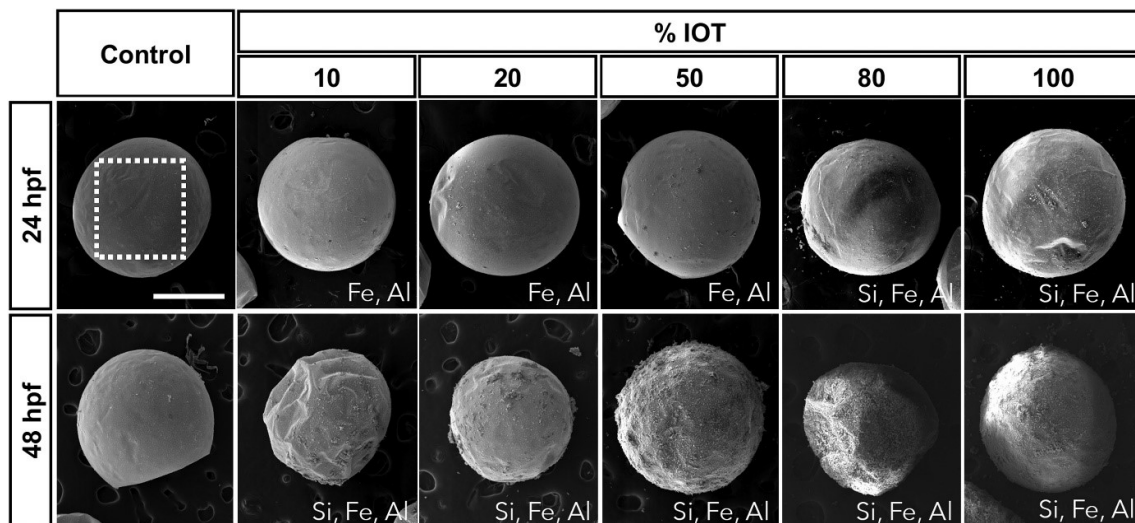
It is current understanding that nanoparticles physical-chemical characteristics, including size, shape, chemical and surface composition, aggregation and concentration impact their behavior (Zoroddu et. al, 2014; Sukhanova et. al, 2018), and accumulating evidence indicate that nanoparticles environmental risk assessment should also focus beyond their inherent core toxicity. Interactions with other environmental compounds or contaminants are important players since they might result in additive, synergistic or antagonistic responses, altering the bioavailability, bioconcentration, and consequently, the toxicity of nanoparticles (Canesi et al., 2015).

Despite IOT suspension exposures show no lethality or indication of robust toxicity, it was visible that IOT-exposed embryos had a substantial number of particles attached to the animals' chorion (Fig. 4 and ANEXO I - Appendix 3, for detail). Indeed, FESEM images clearly illustrate both time- and concentration- dependent envelopment of zebrafish embryo chorion exposed to IOT in suspension. Furthermore, EDS analysis identified that Fe, Si, and Al are the main elements present in the envelopment layer (Fig. 4), consistent with the suspensions' pre-characterization (Table 1 and EDS control).

Interestingly, Si was not identified in animals exposed to lower concentrations of IOT in suspension (namely, 10, 20, and 50%) on the first day of exposure (24 hpf), indicating, at least in the initial steps of adhesion, a preferential adhesion of iron oxide particles. This initial step of adhesion may occur due to interactions between iron oxides and the functional groups of zebrafish chorion. Gu et al. (1995) summarized six

possible mechanisms for organic matter (OM) adsorption on mineral surfaces, with electrostatic attraction and ligand exchange between hydroxyl groups on the iron oxide surface and carboxyl or hydroxyl groups in the biological material being the two primary mechanisms for most OM and iron oxide systems.

Figure II.04. Effect of iron ore tailing (IOT) suspensions exposure to zebrafish chorion. Representative FESEM images of 24 and 48 hpf embryos showing cumulative time- and concentration-dependent IOT particles deposits on the fish chorion. The dotted-line square identifies the representative EDS measurement area for analysis and element identification is informed at the bottom, for each experimental group. Scale bar: 500 µm. (FESEM: field-emission scanning electron microscopy, EDS: energy dispersive X-ray spectroscopy, voltage: 20,000 kV, magnitude: 200 x, spot: 4.0, working distance: 10.4 mm).



Indeed, chorion bonding of iron oxide particles is likely to occur by electrostatic attraction, because at pH 7.0, the mineral particles present a positive charge and fish chorion a negative charge (Peterson and Martin-Robichaud, 1987; Eddy et al., 1989). Also, we may assume a simultaneous mechanism of adsorption by surface complex formation and hydrogen bonding, supported by the fact that both zebrafish chorion (Bonsignorio et al, 1996) and iron oxide surfaces have hydroxyl groups capable of interacting in a similar way that occurs with starches and hematite (Weissenborn et al., 1995; Peres e Correa, 1996; Pavlovic and Brandão, 2003; Shrimali et al., 2018; Peçanha et al., 2019).

A cumulative effect is reinforced by the proportional increase of particulates found on the chorion as IOT concentration increases. From a macro perspective, aggregation in zebrafish embryos result similar to a flocculation process. The precise mechanism that iron oxide nanoparticles interact with the chorion is still unclear, as

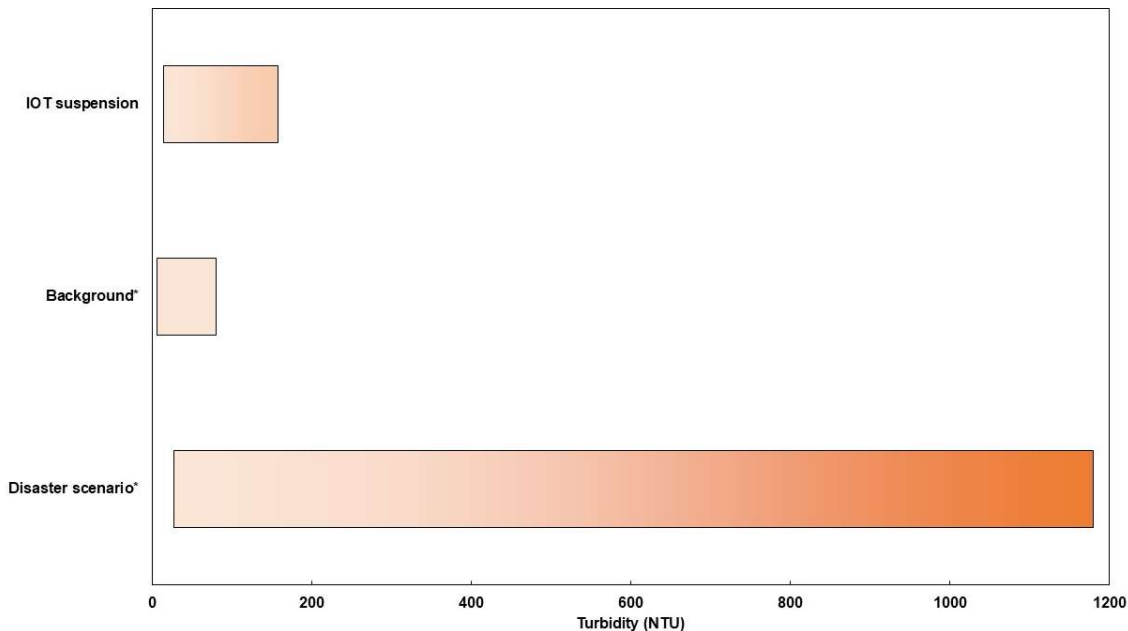
also pointed out by recent reports with lab-engineered nanoparticles (Pereira et al, 2020b).

The results indicate that the presence of micro/nano IOT particles in water suspensions alone do not impair the initial development of zebrafish. These findings, however, do not disregard toxicological effects associated with later developmental stages of zebrafish and/or other organisms, especially due to the potential long-term cumulative effect of mineral exposure. For example, Veronez et. al (2016) investigated the toxicity of an iron ore suspension ($\leq 75 \mu\text{m}$) with high metal content, majorly Fe and Mn, in bullfrog tadpoles' metamorphosis.

Exposure to these metals (in combination or alone) did not lead to mortality but induced tissue bioaccumulation, resulting in morphological, developmental, genotoxic and biochemical adverse effects. Effect of metal fraction was the study main objective, and so, non-metal composition such as silica, was not reported for the studied sample (Veronez et. al., 2016). Among negative ecological effects reported for IOT in water streams are: changes in river mud composition and toxic metal release from the mud into the water (Segura et al., 2016); increase in iron tolerant microbial communities (Thompson et al., 2020); decrease in the photosynthesis rate due to increased turbidity (Cordeiro et al., 2019); and fish death (Fernandes et al., 2016, Gomes et al., 2017).

Nevertheless, most of these observations were consequence of the catastrophic scenarios that reached the Gualaxo do Norte, Carmo, and Doce rivers in 2015 and the Paraopeba River in 2019, characterized by the release of massive amounts of mud. IOT suspensions used in this work presented low concentrations of suspended solids and turbidity levels, just above background range of rivers in sampling region (Figure 5) and, therefore, most likely consistent with wind dispersion and/or limited water flooding events during normal mining activities associated with tailing dams or dry stacking procedures.

Figure II.05. Turbidity range of the iron ore tailing suspension compared to environmental background values of Doce River basin before (2010-2015) and one year after (2016) the Fundão dam disaster. (*Source: IGAM, 2018 - turbidity range values were graphically constructed based on 25-90 percentile of the dataset).



Finally, it is important to highlight that physical-chemical characteristics of both nanoparticles and environment will determine the fate and behavior of the suspended solids. The solids may remain suspended or compose aggregates that settle when reach a sufficient size (Sharma et al., 2015; Lei et al., 2018; Ma et. al, 2018). This is especially important in environmental toxicity evaluation because there is a very heterogenic mixture of macromolecules forming natural organic matter, with substantial geographic and seasonal variability, that will influence aggregates structure and their stability, mobility and transformation thought aquatic system. Furthermore, environmental contaminants may be 'trapped' within these aggregates and contribute to additional toxicological concerns (Farré et al., 2009; Sharma et al., 2015; Lei et al., 2018; Ma et al., 2018).

4. CONCLUSIONS

To the best of our knowledge, this is the very first study to combine thoroughly characterization of micro/nano fraction of an IOT sample and its in vivo effects in fish. The IOT water suspension showed 37 mg L⁻¹ of solids containing hematite, quartz, goethite, and kaolinite particles, ranging 33-1400 nm in size and turbidity of 143 NTU. Under this multi-mineral composition of micro/nanoparticles, no significant differences in early zebrafish development were observed in IOT-exposed groups compared to the control group. Despite the prominent adhesion of micro/nano particles on zebrafish embryo chorion, no consistent adverse effects were recorded among all the developmental, morphological and behavioral end-points analyzed, suggesting a complex interaction net between IOT nanoparticles and biota. Therefore, we speculate that toxicity levels found in water courses due to IOT flooding in catastrophic periods are most likely associated with massive concentration of solids in the aquatic system. In short, the control and monitoring programs of particulates in areas adjacent to the disposal of mineral tailings should be encouraged along with the importance of toxicological evaluations to identify borderline conditions, as an active tool in mining-related endeavors and econanotoxicology.

ACKNOWLEDGEMENTS

The authors are grateful to *Ferro + Mineração* for providing the IOT samples, to LabCEMM/PUCRS for FESEM-EDS technical assistance, and to CEMBE/PUCRS for fish facility operation. This work was supported by Brazilian funding agencies: *Fundação de Amparo à Pesquisa do Rio Grande do Sul* (FAPERGS); *Conselho Nacional de Desenvolvimento Científico e Tecnológico* (CNPq); *Instituto Nacional de Ciência e Tecnologia em Doenças Cerebrais, Excitotoxicidade e Neuroproteção* (INCT-EN); *Financiadora de Estudos e Projetos* (FINEP); and *Coordenação de Aperfeiçoamento de Pessoal de Nível Superior* (CAPES)-Finance Code 001. I.A.H.S. and M.R.B are Research Career Awardees of CNPq.

REFERENCES

- APHA. American Public Health Association, 2018. 2540 Solids (2017). Standard Methods for the Examination of Water and Wastewater.
- Arias LS, Pessan JP, Vieira APM, Lima TMT, Delbem ACB, Monteiro DR.; 2018 Iron Oxide Nanoparticles for Biomedical Applications: A Perspective on Synthesis, Drugs, Antimicrobial Activity, and Toxicity. *Antibiotics* 7 (2), 46.
- Armstrong, M., Petter, R., Petter, C., 2019. Why have so many tailings dams failed in recent years? *Resources Policy* 63, 101412.
- Bambino, K., Chu, J., 2017. Zebrafish in Toxicology and Environmental Health, in: Current Topics in Developmental Biology. Academic Press Inc., pp. 331-367.
- Bonsignorio, D., Perego, L., Del Giacco, L., Cotelli, F. 1996. Structure and macromolecular composition of the zebrafish egg chorion. *Zygote* 4 (2), 101-108
- Bori, J., Vallès, B., Navarro, A., Riva, M.C., 2016. Geochemistry and environmental threats of soils surrounding an abandoned mercury mine. *Environmental Science and Pollution Research* 23, 12941-12953
- Bratby, J., 2016. Coagulation and Flocculation in Water and Wastewater Treatment. London: IWA Publishing, 3° ed., p. 450.
- Brazil. Ministério do Meio Ambiente, 2006. Caderno da Região Hidrográfica do São Francisco. Available at: https://www.mma.gov.br/estruturas/161/_publicacao/161_publicacao03032011023538.pdf. Accessed on June 2020.
- Breshears, D.D., Whicker, J.J., Johansen, M.P., Pinder, J.E., 2003. Wind and water erosion and transport in semi-arid shrubland, grassland and forest ecosystems: Quantifying dominance of horizontal wind-driven transport. *Earth Surface Processes and Landforms* 28(11), 1189-1209.
- Canesi, L., Ciacci, C., Balbi, T.; 2015. Interactive effects of nanoparticles with other contaminants in aquatic organisms: Friend or foe? *Marine Environmental Research*. 111, 128-134
- Carmo, F.F., Kamino, L.H.Y., Junior, R.T., de Campos, I.C., do Carmo, F.F., Silvino, G., Pinto, C.E.F., 2017. Fundão tailings dam failures: the environment tragedy of the

largest technological disaster of Brazilian mining in global context. Perspectives in ecology and conservation 15, 145-151.

Chalov, S. R., 2014. Effects of placer mining on suspended sediment budget: case study of north of Russia's Kamchatka Peninsula. Hydrological Sciences Journal 59 (5), 1081-1094.

Cordeiro, M.C., Garcia, G.D., Rocha, A.M., Tschoeke, D.A., Campeão, M.E., Appolinario, L.R., Soares, A.C., Leomil, L., Froes, A., Bahiense, L., Rezende, C.E. Almeida, D.Q.R., Thompson, M.C., Thompson, C.C., Thompson, F.L., 2019. Insights on the freshwater microbiomes metabolic changes associated with the world's largest mining disaster. Science of the Total Environment 654, 1209-1217

Cornell, R.M., Schwermann, U., 2003. The Iron Oxides: Structure, Properties, Reactions, Occurrences and Uses. (second edition) Wiley-VCH, New York, p. 705

Davila, R. B., Fontes, M. P. F., Pacheco, A. A., Ferreira, M. S., 2020. Heavy metals in iron ore tailings and floodplain soils affected by the Samarco dam collapse in Brazil. Science of the Total Environment 709, 136151.

Eddy, F.B., Ward, M.R., Talbot, C., Primmett, D., 1989. Ionic movements across the chorion in newly shed salmon eggs (*Salmo salar* L.). Journal of Comparative Physiology B 159, 771-776.

Farré, M., Gajda-Schrantz, k., Kantiani, L., Barceló, D., 2009. Ecotoxicity and analysis of nanomaterials in the aquatic environment. Anal Bioanal Chem 393, 81-95.

Fernandes, G.W., Goulart, F.F., Ranieri, B.D., Coelho, M.S., Dales, K., Boesche, N., Bustamante, M., Carvalho, F.A., Carvalho, D.C., Dirzo, R., Fernandes, S., Galetti Jr., P.M., Millan, V.E.G., Mielke, C., Ramirez, J.L., Neves, A., Rogass, C., Ribeiro, S.P., Scariot, A., Soares-Filho, B., 2016. Deep in the mud: ecological and socio-economic impacts of the dam breach in Mariana, Brazil. Natureza Conservação 14, 35-45.

Galvão, J.L.B., Andrade, H.D., Brigolini, G.J., Peixoto, R.A.F., Mendes, J. C., 2018. Reuse of iron tailings from tailings dams as pigment for sustainable paints. Journal of Cleaner Production 200, 412-422.

- Geng, H., Wang, F., Yan, C., Tian, Z., Chen, H., Zhou, B., Yuan, R., Yao, J., 2020. Leaching behavior of metals from iron tailings under varying pH and low-molecular-weight organic acids. *Journal of Hazardous Materials* 383, 121136.
- Gomes, L.E.O., Correa, L.B., Sá, F., Neto, R.R., Bernardino, A.F., 2017. The impacts of the Samarco mine tailing spill on the Rio Doce estuary, Eastern Brazil. *Marine Pollution Bulletin* 120, 28-36.
- Gu, B., Schmitt, J., Chen, Z., Liang, L., McCarthy, J.F., 1995. Adsorption and desorption of different organic matter fractions on iron oxide. *Geochimica et Cosmochimica Acta* 59, 219-229
- Hatje, V., Pedreira, R.M.A., Rezende, C.E., Schettini, C.A.F., Souza, G.C., Marin, D.C., Hackspacher, P.C., 2017. The environmental impacts of one of the largest tailing dam failures worldwide. *Scientific Reports* 7, 10706.
- Hayes, S.M., Webb, S.M., Bargar, J.R., O'day, P.A., Maier, R.M., Chorover, J., 2012. Geochemical weathering Increases lead bioaccessibility in mine tailings. *Environmental Science & Technology* 46, 5834-5841.
- Horzmann, K.A., Freeman, J.L., 2018. Making waves: New developments in toxicology with the zebrafish. *Toxicological Sciences* 163, 5-12.
- Hunter, R. J., 1981. *Zeta Potential in Colloid Science: Principles and Applications*. Australia: Academic Press, 1 ed., p. 386.
- IGAM - Instituto Mineiro de Gestão das Águas (in Portuguese), 2018. Encarte especial sobre a qualidade das águas do Rio Doce após 3 anos do rompimento da Barragem de Fundão 2015-2018. Available at http://www.igam.mg.gov.br/images/stories/2018/QUALIDADE_DA_AGUA/ENCARTE_Tres_ANOS.pdf. Accessed on June 2020.
- Jones, A.M., Collins, R.N., Rose, J., Waite, T. D., 2009. The effect of silica and natural organic matter on the Fe(II)-catalysed transformation and reactivity of Fe(III) minerals. *Geochim. Cosmochim. Acta* 73, 4409-4422.
- Kosmulski, M., 2001. *Chemical Properties of Material Surfaces*. New York: Marcel Dekker, p. 768.
- Lei, C., Sun, Y., Tsang, D.C.W., Lin, D., 2018. Environmental transformations and ecological effects of iron-based nanoparticles. *Environmental Pollution* 232, 10-30.

Ma, C., Huangfu, X., He, Q., Ma, J., Huang, R.; 2018. Deposition of engineered nanoparticles (ENPs) on surfaces in aquatic systems: a review of interaction forces, experimental approaches, and influencing factors. *Environmental Science and Pollution Research* 25, 33056-33081.

Macklin, M. G.; Brewer, P. A.; Hudson-Edwards, k. A.; Bird, G.; Coulthard, T. J.; Dennis, I. A.; Lechler, P. J.; Miller, J. R.; Turner, J. N.; 2006. A geomorphological approach to the management of rivers contaminated by metal mining. *Geomorphology* 79 (3-4), 423-447.

Marta-Almeida, M., Mendes, R., Amorim, F.N., Cirano, M., Dias, J.M., 2016. Fundão Dam collapse: oceanic dispersion of River Doce after the greatest Brazilian environmental accident. *Marine Pollution Bulletin* 112 (1-2), 359-364.

Mendes, B.C., Pedroti, L.G., Fontes, M.P.F., Ribeiro, J.C.L., Vieira, C.M.F., Pacheco, A.A., Azevedo, A.R.G., 2019. Technical and environmental assessment of the incorporation of iron ore tailings in construction clay bricks. *Construction and Building Materials* 227, 116669.

Oliveira, H., Azevedo, A., Rubio, J., 2019. Innovative Precipitation-Flocculation Process for Treating Turbid Waters from Gualaxo do Norte River, Brazil. *Mining, Metallurgy & Exploration*, 36(4), 851-856.

Omachi, C.Y., Siani, S.M.O., Chagas, F.M. Mascagni, M.L., Cordeiro, M., Garcia, G.D., Thompson, C.C., Siegle, E., Thompson, F.L., 2018. Atlantic Forest loss caused by the world's largest tailing dam collapse (Fundão Dam, Mariana, Brazil). *Remote Sensing Applications Society and Environment* 12, 30-34.

Palmer, J., 2019. Anatomy of a Tailings Dam Failure and a Caution for the Future, *Engineering* 5 (4), 605-606.

Pavlovic, S., Brandao, P.R.G., 2003. Adsorption of starch, amylose, amylopectin and glucose monomer and their effect on the flotation of hematite and quartz. *Minerals Engineering* 16, 1117-1122.

Peçanha, E.R., Albuquerque, M.D.F., Simão, R.A., Filho, L.S.L., Monte, M.B.M., 2019. Interaction forces between colloidal starch and quartz and hematite particles in mineral flotation. *Colloids and Surfaces A: Physicochemical and Engineering Aspects* 562, 79-85.

- Pereira, A.A., Van Hattum, B., Brouwer, A., Van Bodegom, P.M., Rezende, C.E., Salomons, W., 2008. Effects of iron-ore mining and processing on metal bioavailability in a tropical coastal lagoon. *Journal of Soils and Sediments* 8, 239–252.
- Pereira, T.C.B., Santos, K.B., William, L., Teodoro, L.S., Almeida, V.O., Weiler, J., Schneider, I.A.H., Bogo, M.R., 2020a. Acid mine drainage (AMD) treatment by neutralization: Evaluation of physical-chemical performance and ecotoxicological effects on zebrafish (*Danio rerio*) development. *Chemosphere* 253, 126665.
- Pereira, A.C., Gonçalves, B., Brito, R., Vieira, L., Lima, E., Rocha, T.L.; 2020b. Comparative developmental toxicity of iron oxide nanoparticles and ferric chloride to zebrafish (*Danio rerio*) after static and semi-static exposure. *Chemosphere*. 254, 126792.
- Peres, A.E.C., Correa, M.I., 1996. Depression of iron oxides with corn starches. *Minerals Engineering*, 9 (12), 1227-1234.
- Peterson, R.H., Martin-Robichaud, D.J., 1987. Permeability of the isolated Atlantic salmon (*Salmo salar*) chorion to ions as estimated by diffusion potentials. *Can J Fish Aquat Sci* 44, 1635-1639.
- Pietroń, J.; Chalov, S. R.; Chalov, A. S.; Alekseenko, A. V.; Jarsjö, J.; 2017. Extreme spatial variability in riverine sediment load inputs due to soil loss in surface mining areas of the Lake Baikal basin. *Catena* 152, 82-93.
- Pires, J.M.M., Lena, J.C., Machado, C.C., Pereiram R.S., 2003. Polluting potential of Samarco Mineração S.A. Solid Waste: a Germano Dam case study. *Revista Árvore* 27(3), 393-397.
- Quadra, G.R., Roland, F., Barros, N., Malm, O., Lino, A.S., Azevedo, G.M., Thomaz, J.R., Andrade-Vieira, L.F., Praça-Fontes, M.M., Almeida, R.M., Mendonça, R.F., Cardoso, S. J., Guida, Y.S., Campos, J.M.S., 2019. Far-reaching cytogenotoxic effects of mine waste from the Fundão dam disaster in Brazil. *Chemosphere* 215, 753-757.
- Rawson, D.M., Zhang, T., Kalicharan, D., Jogeblod, W.L., 2001. Field emission scanning electron microscopy and transmission electron microscopy studies of the chorion, plasma membrane and syncytial layers of the gastrula-stage embryo of the zebrafish Brachy *Danio rerio*: a consideration of the structural and functional relationships with respect to cryoprotectant penetration. *Aquacult. Res.* 31, 325-336.

- Rodgher, S., Azevedo, H., Ferrari, C.R., Roque, C.V., Ronqui, L.B., Campos, M.B., Nascimento, M.R.L., 2013. Evaluation of surface water quality in aquatic bodies under the influence of uranium mining (MG, Brazil). *Environmental Monitoring and Assessment* 185, 2395-2406.
- Rotta, L.H.S., Alcântara, E., Park, E., Negri, R.G., Lin, Y.N., Bernardo, N., Mendes, T. S.G., Filho, C.R.S., 2020. The 2019 Brumadinho tailings dam collapse: Possible cause and impacts of the worst human and environmental disaster in Brazil. *International Journal of Applied Earth Observation and Geoinformation* 90, 102119.
- Schaider, L.A., Senn, D.B., Brabander, D.J., McCarthy, K.D., Shine, J.P., 2007. Characterization of zinc, lead, and cadmium in mine waste: Implications for transport, exposure, and bioavailability. *Environmental Science and Technology* 41(11), 4164-4171.
- Sharma, V.K, Filip, J., Zboril, R., Varma, R.S., 2015. Natural inorganic nanoparticles - formation, fate, and toxicity in the environment. *Chemical Society Reviews*. 44, 8410-8423.
- Shrimali, K., Atluri, V., Wang, Y., Bacchuwar, S., Wang, X., Miller, J.D., 2018. The nature of hematite depression with corn starch in the reverse flotation of iron ore. *Journal of Colloid Interface Science* 524, 337-349.
- Schwertmann, U., Taylor, R.M., 1989. Iron oxides. In: Minerals in soil environments. Soil Science Society of America Journal, 2 ed., 379-438.
- Segura, F.R., Nunes, E.A., Paniz, F.P., Paulelli, A.C.C., Rodrigues, G.B., Braga, G.U. L. Filho, W.R.P., Barbosa JR., F., Cerchiaro, G., Silva, F.F., Batista, B.L., 2016. Potential risks of the residue from Samarco's mine dam burst (Bento Rodrigues, Brazil). *Environmental Pollution* 218, 813-825.
- Su, C. W., Wang, K.H., Chang, H.L., Dumitrescu-Peculea, A., 2017. Do iron ore price bubbles occur? *Resources Policy* 53, 340-346.
- Sukhanova, A., Bozrova, S., Sokolov, P., Berestovoy, M., Karaulov A., Nabiev, I., 2018. Dependence of Nanoparticle Toxicity on Their Physical and Chemical Properties. *Nanoscale Research Letters* 13, 44 (2018).

- Taylor, P., 1995. Interactions of silica with iron oxides: Effects on oxide transformations and sorption properties. Atomic Energy of Canada Limited Report, AECL-11257, COG-I-95-023, 20p.
- Thompson, F., Oliveira, B.C., Cordeiro, M.C., Masi, B.P., Rangel, T.P., Paz, P., Freitas, T., Lopes, G., Silva, B.S., Cabral, A.S., Soares, M., Lacerda, D., Vergilio, C.S., Ferreira, M.L., Lima, C., Thompson, C., Rezende, E., 2020. Severe impacts of the Brumadinho dam failure (Minas Gerais, Brazil) on the water quality of the Paraopeba River. *Science of the Total Environment* 705, 135914.
- Trzaskos, B., Alkmim, F.F., Zavaglia, G., 2011. Arcabouço estrutural e microestruturas do minério de ferro da jazida de Casa de Pedra, Quadrilátero Ferrífero, MG. *Revista Brasileira de Geociências* 41, 486-497.
- Van Ree, G.E.F., Payne, J.F., 2005. Endocrine disruption in the pituitary of white sucker (*Catostomus commersoni*) caged in a lake contaminated with iron-ore mine tailings. *Hydrobiologia* 532, 221-224.
- Veronez, A.C.S., Salla, R.V., Baroni, V.D., Barcarolli,I.F., Bianchini,A., Martinez, C.B.R., Chippari-Gomes, A.R.Genetic and biochemical effects induced by iron ore, Fe and Mn exposure in tadpoles of the bullfrog *Lithobates catesbeianus*. *Aquatic Toxicology* 174, 101-108.
- WA Iron Ore profile, 2019. Western Australia Iron Ore Profile. Western Australian Department of State Development, Australia. Available in: https://www.jtsi.wa.gov.au/docs/default-source/default-document-library/wa-iron-ore-profile-0519.pdf?sfvrsn=db8701c_4
- Walling, D.E., Moorehead, P.W., 1989. The particle size characteristics of fluvial suspended sediment: an overview. *Hydrobiologia* 176, 125-149.
- Weber, A.A., Sales, C.F., Faria, F.S., Melo, R.M. C., Bazzoli, N., Rizzo, E., 2020. Effects of metal contamination on liver in two fish species from a highly impacted neotropical river: A case study of the Fundão dam, Brazil. *Ecotoxicology and Environmental Safety* 190, 110165
- Weisseborn, P.K., Warren, L.J., Dunna, J.G. 1995. Selective flocculation of ultrafine iron ore. 1. Mechanism of adsorption of starch onto hematite. *Colloids and Surfaces A. Physicochemical and Engineering Aspects* 10, 11-27.

Wong, M.H., Li, M.W., 1977. An ecological survey of the heavy metal contamination of the edible clam *Paphia* sp. on the iron-ore tailings of Tolo Harbour, Hong Kong. *Hydrobiologia* 56, 265-272.

Zhu, X., Tian, S., Cai, Z.; 2012. Toxicity Assessment of Iron Oxide Nanoparticles in Zebrafish (*Danio rerio*) Early Life Stages. *Plos One* 7(9), e46286.

Zoroddu, M.A., Medici, S., Ledda,A., Marina Nurchi, V.M., Lachowicz, J., Peana,M., 2014. Toxicity of Nanoparticles. *Current Medicinal Chemistry*, 2014, 21, 3837-3853 3837.

CAPÍTULO III

PRODUCTION OF A FERRIC CHLORIDE COAGULANT BY LEACHING AN

IRON ORE TAILING

ARTIGO 2***Production of a ferric chloride coagulant by leaching an iron ore tailing***

Vítor Otacílio de Almeida¹, Ivo André Homrich Schneider^{1*}

1. Laboratório de Tecnologia Mineral e Ambiental, Programa de Pós-Graduação em Engenharia de Minas, Metalúrgica e de Materiais, Escola de Engenharia, Universidade Federal do Rio Grande do Sul (UFRGS). Av. Bento Gonçalves, 9500. CEP-91501-970. Porto Alegre, RS, Brasil.

*Corresponding authors (email: ivo.andre@ufrgs.br).

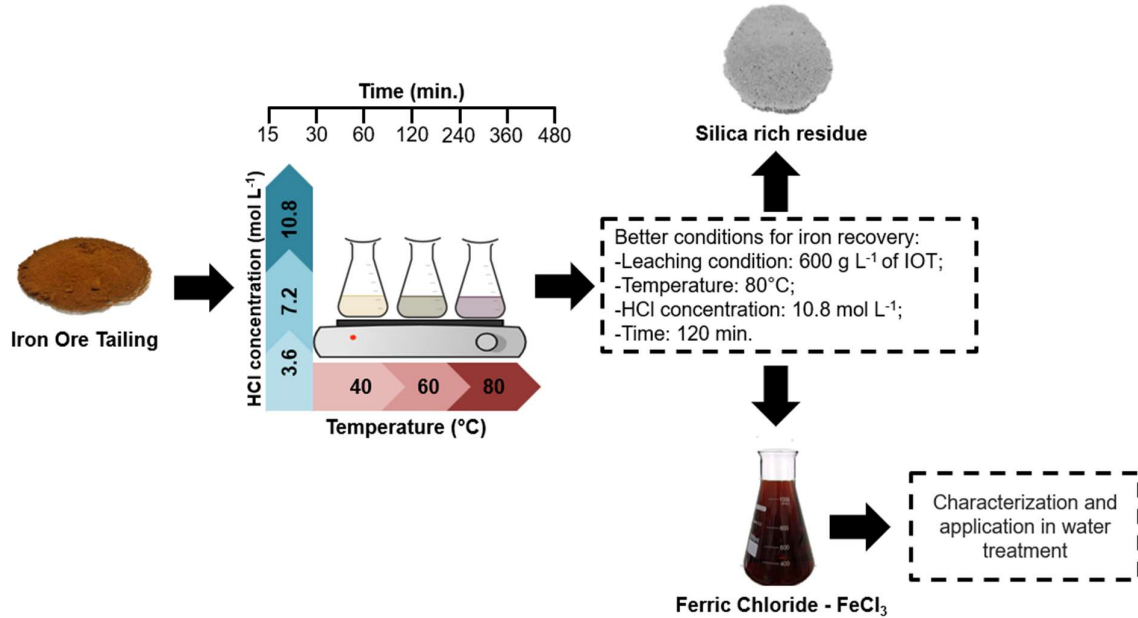
Artigo publicado na *Minerals Engineering* (ISSN: 1872-9444 | Impact Factor 4.8 | Qualis A1 - Quadriênio 2017-2020)

ABSTRACT

This work aimed at producing a ferric chloride coagulant from an iron ore tailing. The investigated variables were temperature, hydrochloric acid concentration, and heating time. The results indicated increasing solubilization of iron as a function of HCl concentration and temperature. Leaching carried out with a 10.8 mol L^{-1} of HCl at a temperature of 80°C for 120 min resulted in a 94% recovery of iron present in the iron ore tailing. The leachate presented 11% Fe in its composition and a low concentration of contaminants. This enabled the liquor to be used as a coagulant and the water treatment experiment showed the effectiveness of the reagent. The solid phase remaining from the leaching process is a fine powder replete in silica, with potential use in other industrial segments. The results indicate that the production of coagulants may be considered to extend the productive chain of iron ore extraction and to minimize the amount of tailings to be discharged in tailings dams or dry stacking.

Keywords: iron ore; tailings; sustainability; leaching; ferric chloride

GRAPHICAL ABSTRACT



1. INTRODUCTION

The disposal of mining tailings in dams is a worrisome subject in mineral processing operations. The conversion of wastes into value-added products has received great importance, as it may contribute to sustainable mining (Franks et al., 2011, Gorman and Dzombak, 2018, Wang et al., 2019) with environmental, social, and economic outcomes (Edraki et al., 2014).

Brazil generates and disposes of around 184 million tons of iron ore tailings (IOT) annually and it has become highlighted after the catastrophic failure of the dams of Fundão (November 5, 2015) and Brumadinho (January 25, 2019). The iron ore industry is investing on improvements in the maintenance and monitoring of tailings dams, tailings reduction, dry tailings disposal, and conversion of IOT into value-added products (Defáveri et al, 2019). The use of IOT in the civil construction sector has been one of the great targets. Investigations comprise cement and concrete compounds (Zhao et al., 2014, Fontes et al., 2016, Shettima et al., 2016, Young and Yang, 2019), material for road construction (Bastos et al., 2016), ceramic materials (Das et al, 2000), and pigments (Galvão et al, 2018). In addition to these applications, IOT has been considered for synthesis of magnetite nanoparticles (Darezereshki et al., 2018), as an adsorbent material for phosphorus removal (Sima et al, 2018), and as a catalyst for drug oxidation (Augusto et al, 2018). However, most studies do not consider the potential of iron recovery by hydrometallurgical processes.

Iron oxides, in general, have low to very low solubilization capacity in water and acid leaching decreases in the order of the following acids: hydrofluoric acid > hydrochloric acid > sulfuric acid > perchloric acid (Evans and Pryor, 1949, Surana, 1969). The main properties that influence iron dissolution are temperature, pH, acid concentration, specific surface area, chemical composition, and crystalline habit (Cornell and Schwertmann, 1996). These factors are relevant in the production of ferric coagulants, a group of reagents worldwide used for water and wastewater treatment (Metcalf and Eddy, 2014).

Coagulation is an essential process in the treatment of water and industrial wastewater. The reagents are divided into two categories: the aluminum base coagulants and the iron base coagulants (Sahu and Chaudhari, 2013, Bratby, 2016). Among the iron-based coagulants, one of the most applied is ferric chloride (FC),

characterized by rapidly decreasing turbidity due to the formation of strong and heavy flocs and for being applicable in a wide range of pH (Lee et al., 2011, Bratby, 2016). FC is usually produced by acid attack of iron scraps with hydrochloric acid (European Commission, 2005) but it can be also be produced from alternative sources, such as mill scale from steel production (Silva, 2013) and the residue generated from pyrite ustulation (Lopes et al., 2015).

The potential of ferric chloride production from IOT (FC/IOT) was considered in this study. We investigated, at bench scale, the main process variables, which included acid concentration, temperature, and time of reaction. The FC/IOT coagulant produced was analyzed in terms of chemical composition and then its effectiveness in water treatment was compared with a conventional FC coagulant produced from iron scrap. Finally, the silica rich solid phase remaining of the leaching process was characterized. The results are discussed in terms of the feasibility of the iron ore tailing production with regard to the market of water treatment.

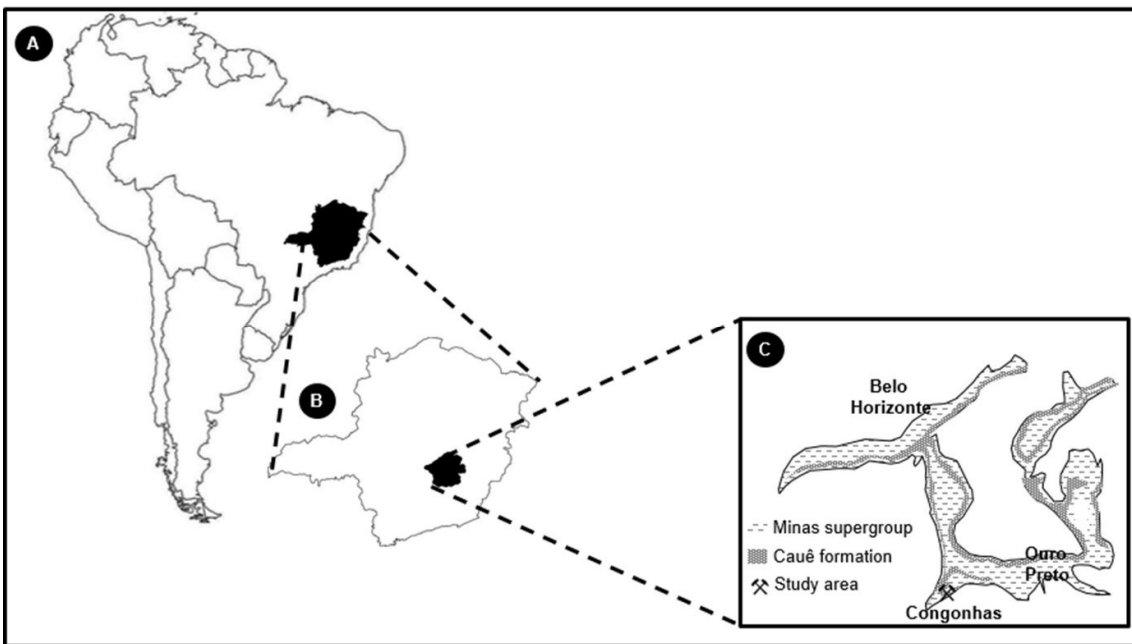
2. MATERIAL AND METHODS

2.1. Iron ore tailing (IOT)

The IOT was provided by a company that operates in the extraction and beneficiation of iron ore in the Quadrilátero Ferrífero, Minas Gerais, Brazil (Fig. 1). This area is located geologically in the Cauê Formation - coordinates are 20°25'37"S 43°52'29"W - consisting of siliceous itabirite, carbonatic itabirite, amphibolitic itabirite and manganeseiferous itabirite (Trzaskos et al, 2011). The IOT is the tailing of the magnetic concentration system, without the addition of any kind of chemical. The sample collection was conducted by the company, following the procedures of NBR 10,007 (ABNT, 2004). The IOT was physically and chemically characterized. The particle size distribution was obtained by laser diffraction using CILAS 1180 particle size analyzer. The specific surface area was determined by BET surface area measurements using Surface Area & Pore Size Analyzer (Quantachrome). Chemical characterization was carried out by X-ray fluorescence (XRF) and X-ray diffraction (XRD). X-ray fluorescence (XRF) was obtained by spectrometer X-ray fluorescence Rigaku, model RIX 2000. X-ray diffraction was carried out in a Siemens (Bruker AXS,

United States) X-ray diffractometer, model D-5000 (θ - 2θ), equipped with a fixed Cu anode tube, operating at 40 kV and 25 mA, with an incident radiation of 1.5406 Å. The angular range analyzed was from 3° to $80^\circ 2\theta$ with a step size of $0.02^\circ/3\text{s}$ using divergence and anti-scattering slits of 2 mm and 0.2 mm in the detector.

Figure III.01. Location of the Quadrilátero Ferrífero in Minas Gerais - Brazil.



2.2. Reagents

The reagent used for acid leaching studies was analytical grade HCl, supplied by Química Moderna (Barueri, SP, BRA). Distilled water was used for preparation of all solutions. Commercial ferric chloride (FC/IS), produced from scrap iron by acid chloride digestion, was obtained from “Sulfato Rio Grande” (RS/Brazil).

2.3. Ferric chloride production

The amount of hydrochloric acid required to solubilize the hematite present in the IOT was established according to reaction (1). Considering the stoichiometry, for each 1 g of the IOT ($\approx 30\%$ Fe₂O₃) it is necessary to have 1 mL of HCl 37%.



Leaching experiments were performed with 30 g of IOT for 50 mL of leaching solution. Three concentrations of HCl were evaluated: 3.6 mol L⁻¹; 7.2 mol L⁻¹; and 10.8 mol L⁻¹. These concentrations were established considering the chemical reaction (1), in which such molarities correspond, respectively, to 50%, 100%, and 150% of the amount of HCl required to dissolve 1 g of IOT. The temperatures investigated in this study were 20 °C, 40 °C, 60 °C, and 80 °C. After determining the better concentration of HCl and temperature for iron solubilization, the heating time required to obtain FC from IOT (FC/IOT) was evaluated. The leaching period of time adopted was 15, 30, 60, 120, 240, 360, and 480 min. After the leaching step, the ferric chloride was filtered to remove process residue. Each leaching condition investigated was carried out in triplicate ($n = 3$) and the results are reported in terms of average, maximum, and minimum. The FC/IOT attained at the best condition was analyzed in terms of the dissolved metals Fe, Al, Mn, Pb, Cu, Cr, Zn, and As. Metal analyses were carried out by inductively coupled plasma (ICP) spectroscopy using a Perkin Elmer Optime, model OPTIMA 8300 DV. The density was determined gravimetrically in 10 mL calibrated volumetric flasks. This liquor was used in a water treatment trial, and the undissolved material was characterized.

2.4. Water treatment

The water treatment procedure was carried out with raw water from Guaíba Lake (Porto Alegre, RS, Brazil) by using a conventional Jar Test apparatus. The coagulation procedure was accomplished by using a 1000 mL water sample. The samples of FC/IOT were added in a molar concentration of 0.001 mM (Fe + Al). The raw water was placed at an agitation of 100 rpm for 10 min and then the coagulant dosage was added. The pH was then adjusted to 7.0, using NaOH. Subsequently, the agitation was stopped and the samples were left undisturbed without any agitation for a period of 10 min to allow settling of the solids. The treated water was analyzed for: settleable solids, suspended solids, total dissolved solids, turbidity, color, hydrogen sulfide, surfactants, metals (Fe, Al, Mn, Zn, Cu, Cr, Cd, Pb, and As), and hardness. All analyses followed the procedures described in the "Standard Method for the Examination of Water and Wastewater" (APHA, 2017).

2.5. Ferric chloride production residue

The leaching stage generates a residue that was submitted to a washing procedure. Washing was carried out three times during the filtration step, using a volume of water approximately twice as that presented by the residue. After filtration, the material was dried at 100 °C and the mass was measured. The residue was characterized by laser granulometry, elemental and mineralogical composition by using the same procedures applied for IOT.

2.6. Statistical analysis

Results of iron recovery as function of HCl concentration and as function of temperature were assessed by using an Analysis of Variance (ANOVA), considering a significance level $p \leq 5\%$ and Tukey Test to compare the difference between averages.

3. RESULTS AND DISCUSSION

The general characteristics of IOT are presented in Table 1. The IOT has a size distribution in the range of 0.07 to 300 µm with a surface area of $10.66 \text{ m}^2\text{g}^{-1}$. Elemental analysis showed a material with high content of silicon, followed by iron and alumina. The DRX confirms the results, indicating quartz and hematite as the predominant crystalline phases, with the incidence of other minerals such as goethite, kaolinite, biotite, and gibbsite. The characteristics of the IOT, the iron concentration, the fine particle size, the high surface area of the material, and the low concentration of toxic elements indicated the potential for the synthesis of FC.

Fig. 2 depicts iron solubilization from IOT at 2 h leaching experiments considering different HCl concentrations and temperatures. Little variation among repetitions and an increase in iron recovery when increasing both variables were observed. Indeed, there were statistically significant differences between mean values ($p \leq 0.05$) while considering different temperatures for the same HCl concentration as well as for different concentrations for the same temperature, indicating the relevance of those conditions in the leaching process. Major results were attained at 80 °C with

7.2 mol L⁻¹ and 10.8 mol L⁻¹ of HCl, with iron dissolution mean values of 85% and 94%, respectively.

Table III.01 - Characteristics of the iron ore tailing (IOT) sample.

Property	IOT
Particle size	
Size distribution (μm)	0.07 - 300
D90 (μm)	123.6
D50 (μm)	54.5
D10 (μm)	4.5
Surface area ($\text{m}^2 \text{ g}^{-1}$)	10.66
Mineral composition	Quartz - SiO_2 (major mineral fase) Hematite - Fe_2O_3 Goethite - FeO(OH) Kaolinite - $\text{Al}_2(\text{Si}_2\text{O}_5)(\text{OH})_4$ Biotite - $\text{K}_{0.78}\text{Na}_{0.22}\text{Mg}_{1.63}\text{Fe}_{0.85}\text{Ti}_{0.33}\text{Al}_{1.35}\text{Si}_{2.84}\text{O}_{11}(\text{OH})$ Gibbsite - $\text{Al}(\text{OH})_3$
Elemental composition	Si - 31.05 Fe - 16.98 Al - 1.59 Ti - 0.07 Mn - 0.02 Mg - 0.0038 P - 0.04

Those results are in accordance with those by Schwertmann and Taylor (1989), which assert that iron oxide dissolution is maximized with HCl solutions between 6 and 12 mol L⁻¹ and heating temperatures in the order of 60 to 80 °C. Moreover, Fig. 3 shows the iron solubilization as a function of time by the addition of 10.8 mol L⁻¹ HCl at 80 °C, revealing that in about 2 h the leaching processes has stabilized to 94–95%. Thus, the concentration of 10.8 mol L⁻¹ HCl, temperature of 80 °C, and a leaching time of 2 h were the conditions adopted in this work for the production of FC from IOT.

Table 2 summarizes the characteristics of the ferric chloride solution produced by leaching the IOT. The liquor presented a density 1.32 g mL⁻¹ and the required concentration of Fe greater than 10% (mass/volume) to be commercialized as a coagulant. The coagulant is metal composed of ferric iron (98.49%) and aluminum (1.48%) and low concentrations of undesirable metals (UM) such as Mn, Pb, Cu, Cr, Zn, and As. Compared with the FC produced from an iron scrap - FC/IS and from mill scale from steel production - FC/MS (Silva, 2013), the molar mass ratio UM/(Fe + Al) of the ferric chloride produced from iron ore tailings (FC/IOT) is substantially less. This means a coagulant of better quality in terms of chemical composition, with a lower risk

of toxic metals in the treated water as well as in sludge generated in the water treatment process.

Figure III.02. Solubilization of iron contained in the IOT as a function of temperature and HCl concentration at a leaching time of 2 hours.

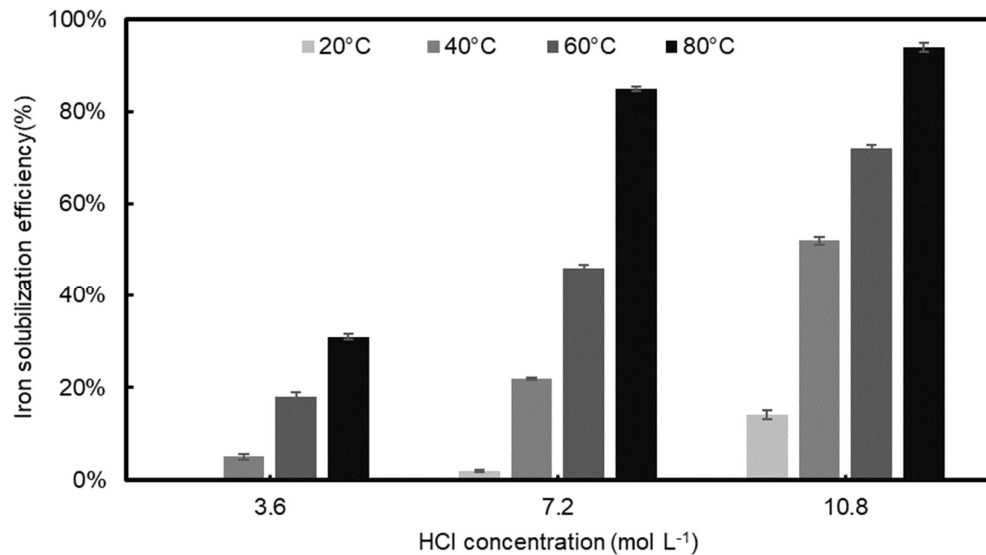


Figure III.03. Solubilization of iron contained in the IOT as a function of time at a temperature of 80°C and hydrochloric acid concentration of 10.8 mol L^{-1} .

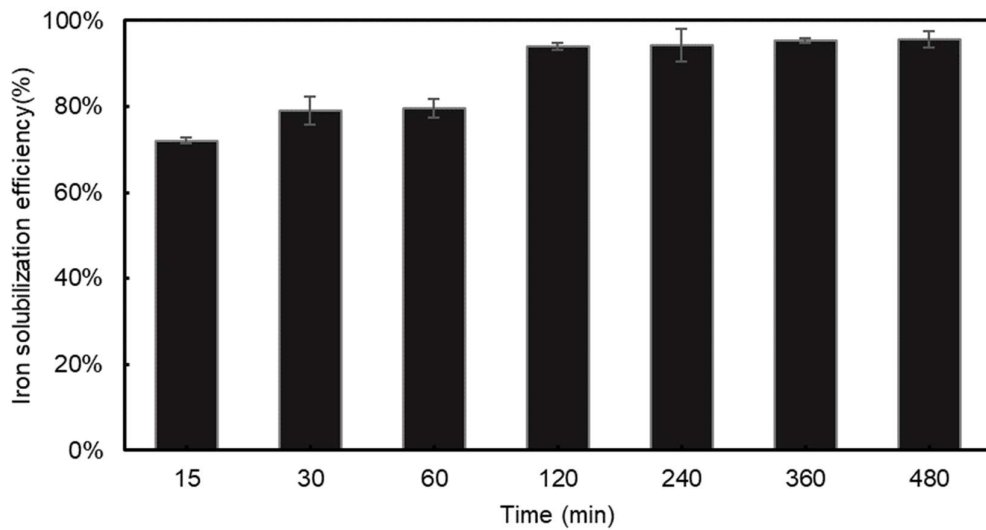


Table III.02. Density and chemical composition of the ferric chloride coagulant produced by acid leaching of IOT (FC/IOT) and a conventional ferric chloride coagulant produced from iron scrap (FC/IS) and from mill scale (FC/MS).

Parameter	FC/IOT	FC/IS	FC/MS
Density (g cm ⁻³)	1.32	1.38	1.40
Fe (mg L ⁻¹)	112,880.00	134,896.00	120,413.00
Al (mg L ⁻¹)	1,700.00	1,903.00	44.8
Mn (mg L ⁻¹)	24.00	663.00	1,008
Pb (mg L ⁻¹)	3.12	< 0.006	< 0.006
Cu (mg L ⁻¹)	2.70	25.30	96.2
Cr (mg L ⁻¹)	2.23	64.70	197.00
Zn (mg L ⁻¹)	1.58	18.00	15.8
As (mg L ⁻¹)	0.89	4.84	1.18
UM/(Fe+Al) (mol/mol x 1000)	0.28	5.65	51.59

Table 3 presents the results obtained in the water treatment test. The coagulant produced from IOT was efficient in terms of residual suspended solids, turbidity, and color removal. The residual amounts of heavy metals in the treated water were very low, meeting Brazilian standards for drinking water (Brasil, 2017).

Table III.03. Characteristics of raw water and treated water with the coagulant FC/IOT.

Parameter	Raw water	Treated with FC/IOT	Brazilian standards for drinking water
pH	6.3	7.0	-
Suspended solids (mg L ⁻¹)	20.00	< 10	-
Turbidity (NTU)	59.6	< 1	5.00
Color (uH)	< 5	< 5	15.00
Settable solids (mg L ⁻¹)	1	< 0,1	-
Total dissolved solids (mg L ⁻¹)	164	112	1000.00
Fe (mg L ⁻¹)	1.029	< 0.06	0.30
Al (mg L ⁻¹)	0.812	< 0.05	0.20
Mn (mg L ⁻¹)	0.125	0.03	0.10
Pb (mg L ⁻¹)	< 0.006	< 0.006	0.010
Cu (mg L ⁻¹)	0.011	< 0.01	0.010
Cr (mg L ⁻¹)	< 0.009	< 0.009	0.050
Zn (mg L ⁻¹)	0.082	< 0.05	5.00
As (mg L ⁻¹)	< 0.01	< 0.01	0.01
Cd (mg L ⁻¹)	< 0.004	< 0.004	0.005
BOD (mg L ⁻¹)	39.17	13.66	-
Hardness (mg L ⁻¹)	44.50	34.3	500.00
Surfactants (mg L ⁻¹)	0.67	0.32	0.50
Hydrogen sulfide (mg L ⁻¹)	0.167	<0.1	0.10
Color (uH)	< 5	< 5	15.00

The recovery of iron present in the IOT for ferric chloride production allows the utilization of 95% of the iron and 30% of the mass of the studied waste, resulting in a coagulant of quality that can be applied in basic sanitation operations, including water, sewage, and leachates from public landfills treatment systems, as well as in industrial wastewater treatment (Metcalf & Eddy, 2014, Costa et al., 2019). In relation to water for public supply, it is estimated that 1 ton of iron ore tailings allows obtaining approximately 1665 L of ferric chloride solution with 10% Fe, which is able to treat about 3000 cubic meters of water and attend more than 16,000 hab/day considering the Brazilian average consumption of water 200 L/hab.dia. For instance, taking into account a middle-sized iron ore mine production in the Quadrilátero Ferrífero region, with a mass production of IOT of approximately 1Mt year⁻¹, this corresponds to an amount of reagent that is able to attend 45.6 million people each year. It also should be considered that FC could also be a chemical precursor for the synthesis of magnetite nanoparticles (Suganthi and Kandasamy, 2017, Sawisai et al., 2019, Rizk and El-hefny, 2020) and iron-based pigments (Muller et al., 2015) as well as a leaching agent in the oxidation of metal-base sulfides ores (Victoriano et al., 1996).

The residue obtained after filtration and washing steps, about 70% of initial IOT mass, showed in the FRX analysis the following elemental composition: Si – 42.5%, Fe – 2.1%, Al – 3.1%, K – 0.3%, Ti – 0.2%, P – 0.1%, and Cl – 0.04%. Quartz was the sole crystalline phase detected by XDR and it accounts with approximately 92% of the material. Chemically, it is very similar to quartz river sand (Markovic et al., 2011, Arun and Madhan, 2018) and the concentration of chlorine was low, showing the efficiency of the washing procedure. The particle size distribution of the IOT, after the leaching procedure, comprises between 0.2 and 170 µm, presenting 40% of its mass inside the granulometric range recommended for use as fine aggregate for civil construction, which extends from 62.5 to 2000 µm (Shaffer, 2016). It should be mentioned that silica sand (SiO_2) is a desired mineral asset, since most of the extraction came from river beds and river banks. Its exploitation may cause adverse effects on the environment, such as river bank erosion, river bed degradation, and deterioration of river water quality (Jonge, 1983, Hossain et al., 2004, van Maren et al., 2015, Yao et al., 2019). Quartzitic sands are also used as a raw material in various industrial areas such as glass, casting, ceramics and refractories, paints, among others. Each of the silica

incorporation niches requires specific levels of purity (Luz and Lins, 2005), which will be the subject of our future research.

4. CONCLUSION

The leaching of the iron ore tailing (IOT) carried out with a 10.8 mol L^{-1} of HCl at a temperature of 80°C for 120 min resulted in a 94% solubilization efficiency of iron. The leachate presented 11% Fe in its composition and a low concentration of contaminants, which enabled the liquor to be used as a coagulant. The water treatment test showed the effectiveness of the FC/IOT reagent in the color and turbidity removal of raw water used for public supply. The results indicate that the production of coagulants may be considered to extend the productive chain of iron ore exploration. The benefits may include the improving of iron recovery in the iron ore sector, production of a chemical reagent that could be used in sanitary operations, and the reduction of the environmental pressure for siliceous sand.

CREDIT AUTHORSHIP CONTRIBUTION STATEMENT

Vitor O. Almeida: Conceptualization, Investigation, Formal analysis, Writing - original draft, Writing - review & editing. Ivo A.H. Schneider: Conceptualization, Resources, Writing - review & editing.

ACKNOWLEDGMENTS

The authors are grateful to CAPES and CNPq for the financial support and Ferro + Mineração S.A. for providing the IOT sample for this study.

REFERENCES

- ABNT (Associação Brasileira de Normas Técnicas), 2004. NBR 10.007: Amostragem de resíduos sólidos.
- Augusto, T. M.; Chagas, P.; Sangiorgi, D. L.; Leod, T. C. O. M.; Oliveira, L. C. A.; Castro, S. C. Iron ore tailings as catalysts for oxidation of the drug paracetamol and dyes by heterogeneous Fenton. *J. Environ Chem. Eng.*, 6 (5) (2018), pp. 6545-6553
- Bastos, L. A. C.; Silva, G. C.; Mendes, J. C.; Peixoto, R. A. F. Using iron ore tailings from tailing dams as road material. *J. Mater. Civ. Eng.*, 28 (2016), pp. 1-9
- Bratby, J. Coagulation and Flocculation in Water and Wastewater Treatment. (third edition) IWA Publishing, London (2016), p. 450
- Brasil. Ministério da Saúde. Portaria de Consolidação N° 5, Brasília (2017)
- Cornell, R. M.; Schwertmann, U. The Iron Oxides: Structure, Properties, Reactions, Occurrences and Uses. (Second edition) Wiley-VCH, New York (1996), p. 705
- Costa, R. H. R.; Villafranca, B. M.; Voltolini, C. A.; Guimarães, L. B.; Hoffmann, H.; Velho, V. F.; Mohedano, R. A. Effectiveness of phosphorus removal in an SBR using co-precipitation with ferric chloride, and its effects on microbial activity. *Braz. J. Chem. Eng.*, 36 (2) (2019), pp. 785-795
- Defáveri, K. C. S.; Santos, L. F.; Carvalho, J. M. F.; Peixoto, R. A. F.; Brigolini, G. J. Iron ore tailing-based geopolymers containing glass wool residue: A study of mechanical and microstructural properties. *Construction Build. Mater.*, 220 (2019), pp. 375-385
- Darezereshki, E.; Darban, A. K.; Abdollahy, M.; Jamshidi, A. Synthesis of magnetite nanoparticles from iron ore tailings using a novel reduction-precipitation method. *J. Alloys. Compd.*, 749 (1) (2018), pp. 336-343.
- Das, S. K.; Kumar, S.; Ramachandrara, P. Exploitation of iron ore tailing for the development of ceramic tiles. *Waste Manag.*, 20 (8) (2000), pp. 725-729

Edraki, M.; Baumgartl, T.; Manlapig, E.; Bradshaw, D.; Franks, D. M.; Moran C. J. Designing mine tailings for better environmental, social and economic outcomes: a review of alternative approaches. *J. Clean. Prod.*, 84 (2014), pp.411-420

European Commission. Additional Information submitted during the information exchange on Large Volume Inorganic Chemicals – Solid and Others Industry. Institute for Prospective Technological Studies, 2005.

Fontes, W. C.; Mendes, J. C.; Silva, S. N. D.; Peixoto, R. A. F. Mortars for laying and coating produced with iron ore tailings from tailing dams. *Constr. Build. Mater.*, 112 (2016), pp. 988-995

Franks, D. M.; Boger, D. V.; Côte, C. M.; Mulligan, D. R. Sustainable development principles for the disposal of mining and mineral processing wastes. *Resour. Policy*, 36 (2011), pp. 114-122

Galvão, J. L. B.; Andrade, H. D.; Brigolini, G. J.; Peixoto, R. A. F.; MENDES, J. C. Reuse of iron tailings from tailings dams as pigment for sustainable paints. *J. Clean. Prod.*, 200 (2018), pp. 412-422

Gorman, M. R.; Dzombak, D. A. A review of sustainable mining and resource management: Transitioning from the life cycle of the mine to the life cycle of the mineral. *Resour. Conserv. Recycl.*, 137 (2018), pp.281-291

Hossain, S.; Eyre, B. D.; McKee, L. J. Impacts of dredging on dry season suspended sediment concentration in the Brisbane River estuary, Queensland, Australia. *Estuar. Coast. Shelf Sci.*, 61 (2004), pp. 539-545

Jonge, V. N. Relations between annual dredging activities, suspended matter concentrations, and the development of the Tidal Regime in the Ems Estuary. *Can. J. Fish. Aquat. Sci.*, 40 (1983), pp. 289-300

Lee, K. E.; Teng, T. T.; Morad, N.; Poh, B. T.; MAHALINGAM, M. Flocculation activity of novel ferric choride-polyacrylamide (FeCL3- PAM) hybrid polymer. *Desalination*, 266 (2011), pp. 108-113

Lopes, F.A.; Miotelli, H.; SCHneider, I.A.H.; Menezes, J.C.S.S. Produção de coagulante cloreto férreo a partir de óxido de ferro III gerado no processo de ustulação

da pirita presente em rejeitos de mineração de carvão. XXVI Encontro Nacional de Tratamento de Minérios e Metalurgia Extrativa, Poços de Caldas, 2015.

Luz, A. B.; Lins, F. F. Rochas e Minerais Industriais. (second edition) CETEM, Rio de Janeiro (2005), p. 974

Metcalf & Eddy. Wastewater Engineering. Treatment and Resource Recovery. (Fifth edition) McGrawHill, Boston (2014), p. 2044

Muller, M.; Villaba, J. C.; Mariani, F. Q.; Dalpasquale, M.; Lemos, M. Z.; Huila, M. F. G.; Anaissi, F. J. Synthesis and characterization of iron oxide pigments through the method of the forced hydrolysis of inorganic salts. *Dyes Pigments*, 120 (2015), pp. 271-278

Evans, U. R.; Pryor, M. J. The passivity of metals. Part IX. The Solubility product of freshly precipitated ferric hydroxide. *J. Chem. Soc.*, 1949.

Rizk, H. E.; El-hefny, N. E. Synthesis and characterization of magnetite nanoparticles from polyol medium for sorption and selective separation of Pd(II) from aqueous solution. *J. Alloys. Compd*, 812(2020), 152041

Sahu, O. P.; Chaudhari, P. K. Review on chemical treatment of industrial waste water. *J. Appl. Sci. Environ. Manage.*, 17 (2) (2013), pp. 241-257

Sawisai, R.; Wanchamthuek, R.; Radchatawedchakoon, W.; Sakee, U. Simple continuous flow synthesis of linoleic and palmitic acid-coated magnetite nanoparticles. *Surfaces and Interfaces*, 17(2019), 100344

Schwertmann, U.; Taylor, R. M. Iron oxides. In: Minerals in soil environments. *Soil Sci. Soc. Am. J.*, 2 (1989), pp. 379-438

Shaffer, N. R. The time of sands: Quartz-rich sand deposits as a renewable resource. Indiana Geological Surv., USA (2016), p. 22

Shettima, A. U; Hussin, M. W.; Ahmad, Y.; Mirza, J. Evaluation of iron ore tailings as replacement for fine aggregate in concrete. *Constr. Build. Mater.*, 120 (2016), pp. 72-79

Silva, R. G. Produção do coagulante cloreto férreo a partir de carepa da indústria siderúrgica. Universidade Federal do Rio Grande do Sul, Porto Alegre (2013), p.81

Sima, T. V.; Letshwenyo, M. W.; Lebogang, L. Efficiency of waste clinker ash and iron oxide tailings for phosphorus removal from tertiary wastewater: Batch studies. Environ. Technol. Innov., 11 (2018), pp. 49-63

SUGANTHI, H. Kandasamy, R. A novel single step synthesis and surface functionalization of iron oxide magnetic nanoparticles and thereof for the copper removal from pigment industry effluent. Sep. Purif. Technol., 188 (2017), pp. 458-467

Surana, V. S. Leaching of Goethite in Acid Solutions. British Columbia University, Canadá (1969), p. 103

Trzaskos, B.; Alkmim, F. F.; Zavaglia, G. Arcabouço estrutural e microestruturas do minério de ferro da jazida Casa de Pedra, Quadrilátero Ferrífero, MG. Braz. J. Geol., 41 (3) (2011), pp. 486-497

van Maren, D. S.; van Kessel, T.; Cronin, K.; Sittoni, L. The impact of channel deepening and dredging on estuarine sediment concentration. Cont. Shelf Res., 95 (2015), pp. 1-14

Victoriano, L. I.; Gnecco, J.A.; Carbacho, H. V. Oxidation of tetramethylthiuram sulfide and iron(III) dithiocarbamates with ferric chloride. Polyhedron, 15 (1996), pp. 1315-1321

Wang, S.; Sun, L.; Huang, L.; Li, X.; Shi, Y.; Yao, J.; Du. S. Non-explosive mining and waste utilization for achieving green mining in underground hard rock mine in China. Trans. Nonferr. Metals Soc. China, 29 (9) (2019), pp. 1914-1928

Yao, J.; Zhang, D.; Li, Y.; Zhang, Q. ; Gao, J. Quantifying the hydrodynamic impacts of cumulative sand mining on a large river-connected floodplain lake: Poyang Lake. J. Hydrol., 579(2019), 124156

Young, G.; Yang, M. Preparation and characterization of Portland cement clinker from iron ore tailings. Constr. Build. Mater., 197 (2019), pp. 152-156

Zhao, S.; Fan, J.; Sun, W. Utilization of iron ore tailings as fine aggregate in ultra-high performance concrete. Constr. Build. Mater., 50 (2014), pp. 540-548

CAPÍTULO IV

SIMPLIFIED HYDROMETALLURGICAL ROUTE FOR THE SYNTHESIS OF

SILICA-FREE HEMATITE FROM IRON ORE TAILINGS

ARTIGO 3**Simplified hydrometallurgical route for the synthesis of silica-free hematite from iron ore tailings**

Vitor O. de Almeida¹, Neymayer Lima², Ivo André H. Schneider^{1*}

¹ Laboratório de Tecnologia Mineral e Ambiental, Programa de Pós-Graduação em Engenharia de Minas, Metalúrgica e de Materiais, Escola de Engenharia, Universidade Federal do Rio Grande do Sul (UFRGS). Av. Bento Gonçalves, 9500. CEP-91501-970. Porto Alegre, RS, Brasil.

² Vale Mining Company, Av. Dr. Marco Paulo Simon Jardim - 3580, ZIP Code: 34.006-200, Nova Lima, MG, Brazil

*Corresponding authors (*email*: ivo.andre@ufrgs.br).

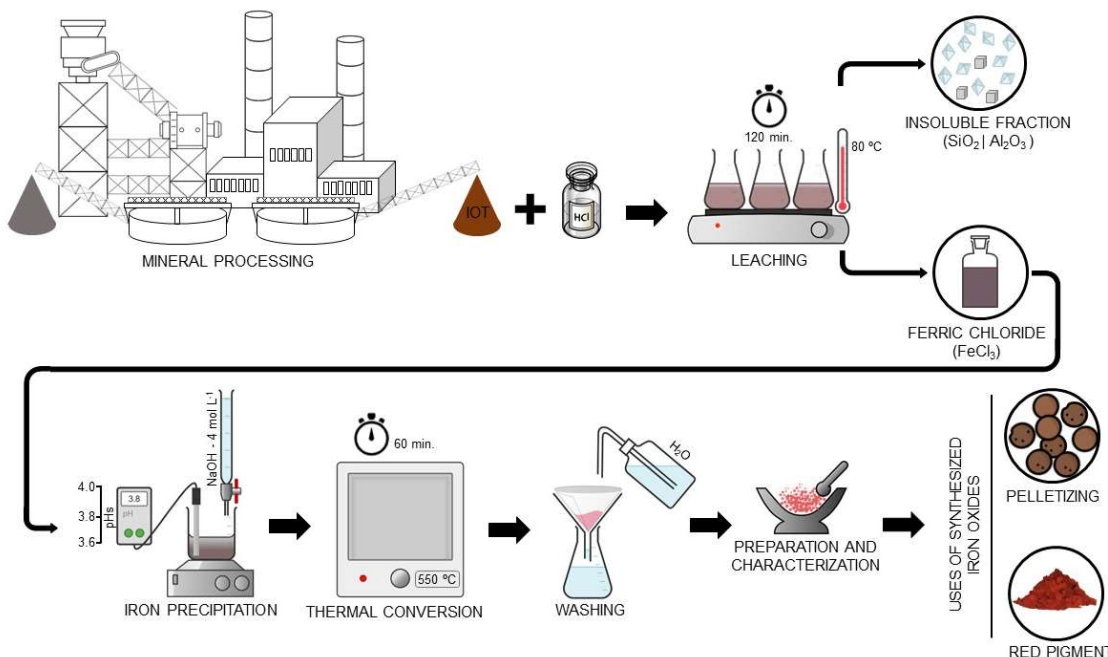
Artigo publicado na *Minerals Engineering* (ISSN: 1872-9444 | Impact Factor 4.8 | Qualis A1 - Quadriênio 2017-2020)

ABSTRACT

The processing of iron ore generates large volumes of tailings. Acid leaching enables the solubilization of iron in an aqueous solution, allowing the production of ferric liquor and a silica-rich residue. The purpose of this investigation was to use the leachate resulting from this process to synthesize high-quality iron oxide. The conducted methodology involved acid leaching, selective iron precipitation as a function of pH, and the thermal conversion of the precipitated iron oxy-hydroxides into iron oxide particles. The iron oxide consisted of micro/nano Fe_2O_3 particles which were free of silica, with iron contents of 64% and particle sizes of less than 28 μm . The process presented an overall iron recovery around 84%. The resulting material could be used as a commercial pigment or be incorporated into steel-making iron pellets. The hydrometallurgical conversion of iron ore wastes into valuable products may contribute to the future of mining and to green steel production.

Keywords: iron ore, tailings, hydrometallurgy, pigments, green steel, sustainability

GRAPHICAL ABSTRACT



1. INTRODUCTION

The iron mining industry generates millions of tons of tailings, which pose significant threats to the environment and to society. In Brazil, the Quadrilátero Ferrífero (MG) concentrates a large amount of iron ore tailings (IOT) from the processing of itabiritic ores, with 180 million metric tons of waste disposed of annually in dams or dry stacking structures. This tailings, present quartz, hematite, goethite and kaolinite as the main mineralogical components (Carmignano et al., 2021).

Indeed, IOT are associated with environmental pollution, health problems, and dam disasters. Another challenge is the growing difficulties associated with the storage and disposal of tailings (de Almeida et al., 2021, Carvalho Eugênio et al., 2021, Liu et al., 2010, Zhang et al., 2021). As a result, significant efforts are currently being made to find solutions and enable the use (Kinnunen and Kaksonen, 2019, Liu et al., 2022) or safe disposal of tailings (Adiansyah et al., 2015, UNEP, 2020).

Although waste management can be conducted through different strategies, the use and processing of waste is an option aligned with United Nations' Sustainable Development Goals (SDGs), especially in relation to the SDG12 "Responsible Consumption and Production" (UNITED NATIONS, 2015). So far, some alternative uses of IOTs have been explored (Almeida and Schneider, 2020, Duarte et al., 2022, Gong et al., 2022, Han et al., 2021, Mendes et al., 2019). However, most investigations have suggested the direct application of the tailings, resulting in initiatives with low added value, most on a small scale and with few related to mineral processing; therefore, the development of new processes should be encouraged (Lu et al., 2020).

Recent studies have investigated the hydrometallurgical processing of IOTs, showing that the latter resulted in an iron-rich liquor and a silica-rich residue (Almeida and Schneider, 2020, Li et al., 2022). The liquor can be used as iron coagulant (sometimes an iron-aluminium coagulant) or as a precursor for the synthesis of iron oxides.

The steel industry is the recipient of most of the global iron ore production, moving over 2 billion tons of this ore per year (Holmes et al., 2022, Jégourel, 2020). In

addition, steel production accounts for around 8% of global CO₂ emissions and efforts are under way to move steel production away from coal-fired furnaces (World Economic Forum, 2022). To produce the so-called “green steel”, iron ore pellets must meet specificities related to iron contents and the concentrations of gangue elements (Park and Sahajwalla, 2014, Zhu et al., 2022). Silica (SiO₂) is one of the main contaminants of iron ore and affects the productivity of metallurgical processes, especially in terms of fuel consumption and increased slag volume (Gyllenram et al., 2022, Meng et al., 2018).

To control the impact of silica on the reduction processes occurring during a blast furnace-basic oxygen furnace route and enable the use of iron ore in direct reduction, some alternatives have been worked on to maintain the SiO₂ contents at ≤ 2%. For instance, magnetic concentration and flotation processes have been combined to promote iron ore enrichment of iron ore and reduce the silica content as much as possible. Such practices have become increasingly complex and do not contribute to reducing the volume of waste (Gyllenram et al., 2022, Muslemani et al., 2021, Sparrow et al., 2022). In this context, hydrometallurgical processing is a promising alternative, as it allows the maximum recovery of the element of interest and other means to control the amount of contaminants (Habashi, 1998, Havlík, 2008).

In parallel, synthetic oxide minerals account for >60% of the pigment market (Mohapatra and Anand, 2010, Tanner, 2016) and several workers have investigated synthesis methods, reagents and iron precursors (Murthy et al., 2020, Schwertmann and Cornell, 2000, Silva et al., 2019, Tadic et al., 2019). Such research has attempted to appropriate waste as a precursor to obtaining pigments, simplify existing synthesis processes, and increase the efficiency and sustainability of production routes (Gong et al., 2022, Prim et al., 2011, Wei et al., 2005).

So, in both, the steel industry and commercial pigment applications, new productive trends demand the use of iron oxides with specifications in terms of their chemical compositions, particle size distributions, and thermal stability (Bhateria and Singh, 2019, Dheyab et al., 2020, Hradil et al., 2003). Thus, we have explored the potential uses of the iron oxide products of the hydrometallurgical processing of IOTs in the steel industry and as commercial pigments.

The hydrolysis of iron hydroxides combined with heat treatment is one of the commonly used methodologies for the synthesis of oxide minerals such as hematite and goethite (Cudennec and Lecerf, 2006, Dissanayake et al., 2019, Gialanella et al., 2010, Müller et al., 2015). However, synthesis methods typically involve multiple steps, with the usage of different reagents, pH adjustments, controlling temperature and processing times, which make the process expensive and unattractive for the mining sector (de Almeida and Schneider, 2022, Schwertmann and Cornell, 2000, Tadic et al., 2019). Given this, the development of simplified procedures, to the benefit of the mineral industry, can open markets, add value, and reduce the volume of tailings in the environment.

The aim of this work was therefore to investigate a simplified hydrolysis/thermal conversion process to obtain iron oxides from IOTs. Hydrolysis was investigated considering the use of a ferric chloride solution produced from tailings. For this, different pH values and their respective effects on the elemental compositions of the product were investigated. The ferric precipitates were submitted to thermal conversion at a temperature of 550 °C, in order to stabilise the compounds. The results were then discussed as a function of iron recovery, possible applicability to synthesised oxides, and increasing efficiency and sustainability for the mining and metallurgical sectors.

2. MATERIAL AND METHODS

2.1. Reagents and Materials

The studied IOT was derived from the Quadrilátero Ferrífero, Minas Gerais, Brazil (20°25'37"S 43°52'29"W). The sampled material was a product of the magnetic concentration stage, without the addition of any kind of chemical. The sample used in this investigation presented a specific surface area of 10.70 m²g⁻¹ and particle size distributions ranging from 0.07 to 300 µm. The mineralogical composition, obtained by X-ray diffraction (XRD), mainly consisted of quartz and hematite. Goethite, kaolinite, gibbsite, and biotite were also identified in smaller proportions. X-ray fluorescence analyses yielded the following composition: Si - 29.0%, Fe - 21.5%, Al - 3.1%, Ti - 0.11%, Mn - 0.02%, Mg - 0.0038%, and P - 0.04%. corresponding to approximate mass contents of 62% SiO₂ and 31% Fe₂O₃. These results were confirmed by chemical

extraction by Method EPA 3052 (U.S. EPA, 1996) and elemental analysis by ICP/OES (ANEXO II - Appendix 1).

Analytical grade acid hydrochloric acid (HCl) supplied by Chemistry Moderna (Barueri, SP, BRA) was used as a reagent in the acid leaching process. The sodium hydroxide (NaOH) used for the precipitation of iron hydroxide was supplied by Dinamica (Indaiatuba, SP, BRA). The commercial pigment used as a reference was supplied by Sigma-Aldrich Brazil (Cotia, SP, BRA). Deionised water was used in the preparation of all solutions. Filtration was always carried out with a Unifil qualitative filter (80 g | Ø18.5 cm).

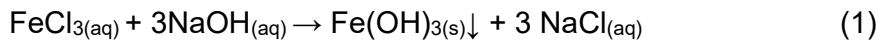
2.2. Leaching process

The dissolution of iron was performed by hot acid leaching using HCl as previously described by Almeida and Schneider (2020). The acid solution with a concentration of 10.8 mol L⁻¹ was added to the iron ore tailings in a proportion of 1.7 mL g⁻¹. Leaching was conducted at a temperature of 80°C, for a period of 120 minutes. The iron liquor was filtered, characterised, and used for the selective iron precipitation step.

The liquor was analysed by inductively coupled plasma spectroscopy (ICP), model OPTIMA 8300 DV (Perkin Elmer, United States), to determine its dissolved metal contents. The density was determined gravimetrically in 10 mL calibrated volumetric flasks.

2.3. Iron precipitation

Iron precipitation was carried out according to the following reaction:



The solubility of ferric ions decreases at pH > 1, and the recommended pH value for selective iron precipitation ranges from 3.5 to 4.0 (Menezes et al., 2010, 2009; Sawyer et al., 2003; Wei et al., 2005). In order to evaluate the effects of pH on the

quality of the ferric precipitate, pH values of 3.6, 3.8, and 4.0 were considered in this investigation.

For the precipitation, samples of 50 mL of the liquor were kept in agitation and the pH values were adjusted through the addition of NaOH (4 mol L⁻¹). The oxy-hydroxide precipitates were filtered, dried at 60°C, characterised, and submitted to thermal conversion and washing. The metallurgical recovery of iron was calculated according to the following equation:

$$R_{Fe} = \frac{\text{Iron content precipitate (\%)} * \text{mass precipitate (g L}^{-1})}{\text{Iron content IOT (\%)} * \text{mass of IOT leach (g L}^{-1})} \times 100 \quad (2)$$

2.4. Thermal conversion and washing

The iron oxy-hydroxide precipitates were subjected to thermal treatment in a muffle oven, at a temperature of 550°C for 60 minutes. After heat treatment, the samples were submitted to a hot wash process (\approx 95°C) to achieve the removal of the remaining sodium chloride. Preliminary tests showed successful washing with a hot water/solid ratio of approximately 20 mL of hot water per gram of solids.

2.5. Characterization of ferric precipitates and iron oxides

The ferric precipitates were submitted to thermogravimetric analysis (TGA) in a thermal analyzer (Shimadzu, Japan). The test parameters were a heating ratio of 10 °C.min⁻¹ and a temperature range from 25 to 1000 °C in atmospheric air. The iron oxide product was physically and chemically characterized. The particle size distribution was measured by laser diffraction using a CILAS 1180 particle size analyzer. Chemical characterization was carried out by XRF and X-ray diffraction (XRD); the XRF data was obtained with a RIX 2000 (Rigaku, Japan) XRF spectrometer; XRD analyses were carried out with an X-ray diffractometer, model D-5000 (Siemens, Germany), equipped with a fixed Cu anode tube, and operating at 40 kV and 25 mA, with an incident radiation of 1.5406 Å. The angular range analyzed was from 3° to 80° 2θ with a step size of 0.02°/3 s using divergence and anti-scattering slits of 2 mm and 0.2 mm, respectively, in the detector.

The colour of the iron oxides was analysed using a CM-2500 D colourimeter (Konica Minolta, Japan) and the CIE colourimetric values (L^* , a^* , and b^*) were utilised to evaluate the chromatic characteristics of the pigments. L^* represents the brightness ($L-100\%$ is white and $L-0\%$ is black), a^* indicates the degrees of red and green ($-a$, green/ $+a$, red), and b^* indicates the degrees of yellow and blue ($-b$, blue/ $+b$, yellow). The colourimetric differences (ΔE^*) between commercial pigments and the pigments produced in this study were calculated and interpreted according to the Technical Standard DIN 6174 (1979).

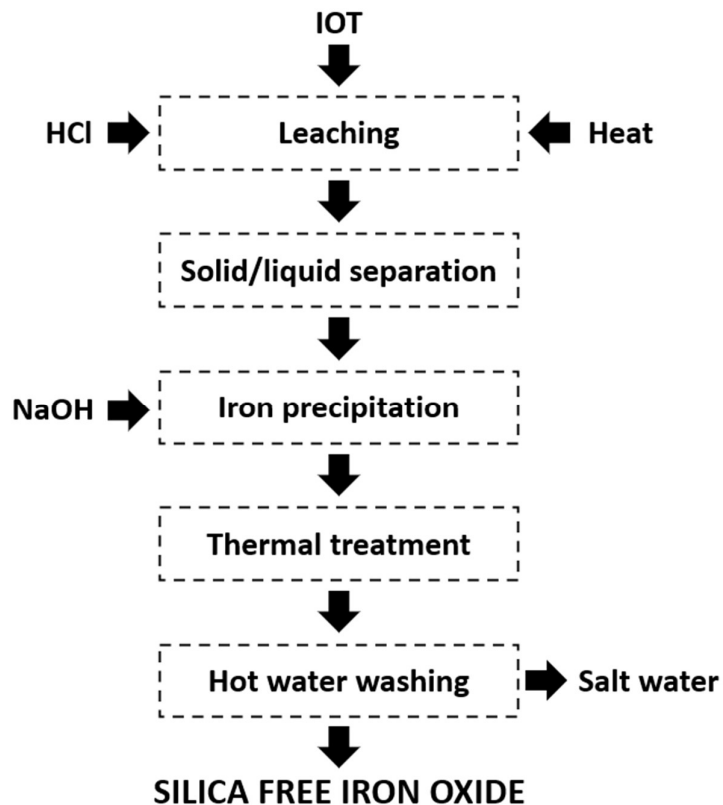
2.6 Statistical analysis

Leaching, precipitation, and thermal procedures were performed in triplicate and the results presented in terms of mean values. The results of iron contents, mass recovery, and metallurgical recovery, as a function of pH, were assessed using the mean, standard deviation, and analysis of variance (ANOVA) with a significance level $p \leq 5\%$; Tukey's test was applied to compare the differences between the means.

3. RESULTS AND DISCUSSION

Figure 1 presents a general scheme of the proposed route for the production of silica-free iron oxides. Iron dissolution via hot acid leaching was successfully performed. The ferric chloride liquor showed an iron concentration of 102 g L^{-1} and a density of 1.12 g mL^{-1} . The following elements were also identified: aluminium ($1,700 \text{ mg L}^{-1}$), barium (9.9 mg L^{-1}), lead (3.1 mg L^{-1}), sulphur (2.9 mg L^{-1}), copper (2.8 mg L^{-1}), and chromium (2.2 mg L^{-1}). The leaching and washing procedures also produced a solid fraction, whitish in colour, with particle sizes close to those of the IOT (ANEXO II - Appendix 2). Elemental analyses by XRF yielded the following composition for the silica-rich fraction: Si - 41.93% , Fe - 2.05% , Al - 3.12% , Ti - 0.15% , Cl - 0.04% , corresponding approximately to $90\% \text{ SiO}_2$ and $3\% \text{ Fe}_2\text{O}_3$. These characteristics indicate that this silica-rich fraction may be the subject of future studies.

Figure IV.01. Sequence of operations involved in the production of silica-free iron oxides.



To promote selective iron precipitation and maximize the quality of the final iron oxide product, pH values of 3.6, 3.8, and 4.0 were investigated. When increasing the pH, there was a small mass increase in the amount of precipitate formed due to an enhancement in iron recovery but also due to the partial co-precipitation of aluminium. This now silica-free oxy-hydroxy precipitate presented a reddish brown colouration and was associated with a thick layer of whitish crystals attributed to the formation of NaCl. This initially obtained sludge was amorphous and had a high thermal instability, with loss on ignition (LOI) values of 26 % at pH 3.6; 34% at pH 3.8; and 38% at pH 4.0 (Table 1).

Table IV.01. Properties of the iron sludge obtained by selective precipitation at pH values of 3.6, 3.8, and 4.0 and after drying at 60 °C.

	pH 3.6	pH 3.8	pH 4.0
Mass of ferric precipitate (kg t⁻¹ IOT)	520	542	584
Iron recovery (%)	90.80	94.31	94.60
ELEMENTAL COMPOSITION - XRF (%)			
Fe	29.12	29.00	27.00
Al	1.10	1.41	1.49
Na	29.73	29.30	28.91
Mg	0.14	0.17	0.15
LOI	25.62	33.99	38.10

Thermogravimetric and differential thermal analysis (DTA) were conducted to investigate the thermal behaviour of the precipitates (Figure 2). The profile presented four main stages of mass loss. The first stage ($\approx 25\text{--}125^\circ\text{C}$) corresponded to the removal of adsorbed water. The second stage ($\approx 175\text{--}435^\circ\text{C}$) was related to the loss of structural water through dehydration and consequent transition of hydrated oxides into more stable oxides (Földvári, 2011; Schwertmann and Cornell, 2000). The third stage ($\approx 435\text{--}590^\circ\text{C}$) was associated with the stabilisation of hematite formed during the dehydration process (Beuria et al., 2017; Földvári, 2011; Konyukhov, 2018). The fourth peak ($> 800^\circ\text{C}$) corresponded to the fusion of sodium chloride (Földvári, 2011). All these steps had an endothermic character (Figure 3).

Figure IV.02. Thermogravimetric analysis (TGA) of the iron sludge obtained by selective precipitation at pH values of 3.6, 3.8, and 4.0.

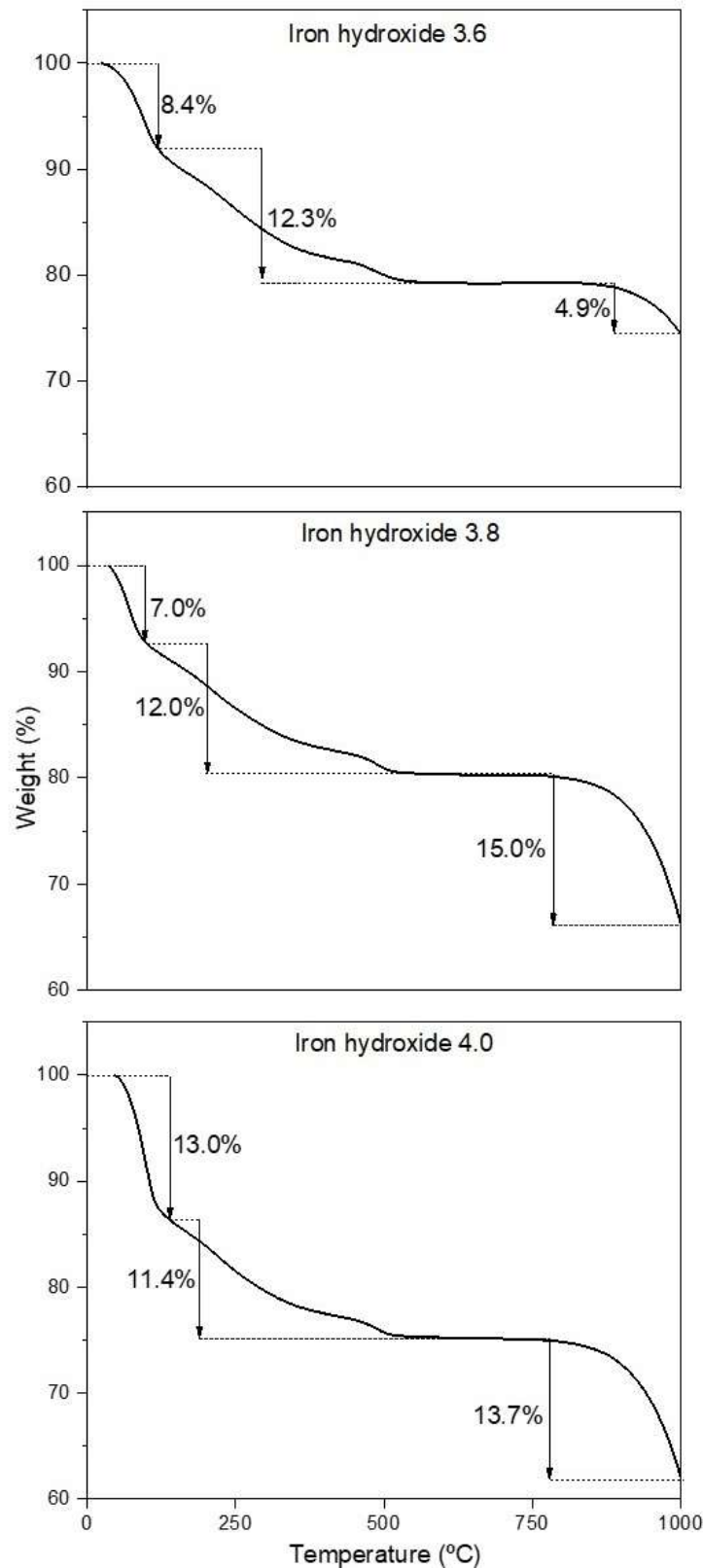
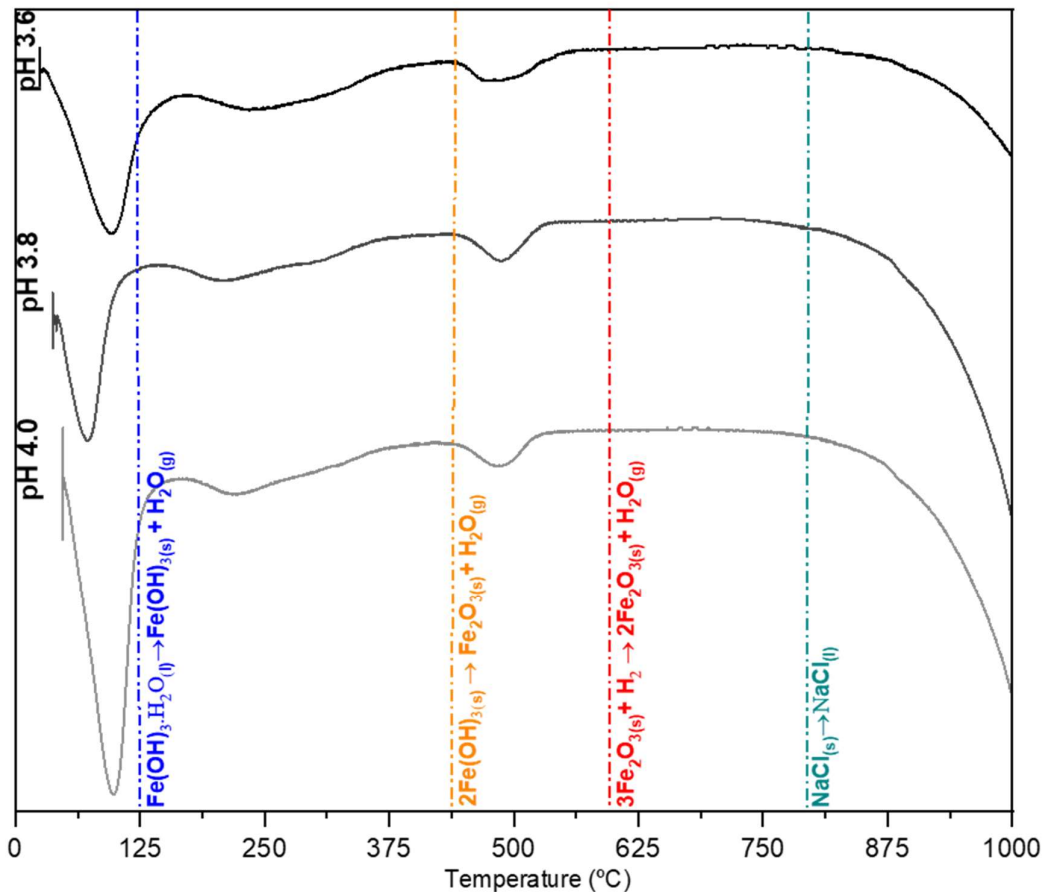


Figure IV.03. Differential thermal analysis (DTA) of the iron sludge obtained by selective precipitation at pH values of 3.6, 3.8, and 4.0.



According to the thermogravimetric profile of the samples, the temperature of 550°C was defined as optimal for the thermal conversion of iron hydroxide sludge into a more stable oxide. After calcination, hot washing ($\approx 95^\circ\text{C}$) was carried out to achieve the maximum removal of soluble compounds such as NaCl. The XRD analyses confirmed the transition of the material from amorphous iron hydroxides to hematite through the thermal treatment (ANEXO II - Appendix 3). Prior to the heat treatment/hot washing operations, the precipitates presented iron as an amorphous phase and only halite as a crystalline compound. After thermal treatment at 550°C, hematite was identified as the only crystalline component.

Table 2 summarises the main characteristics of the synthesised iron oxide considering the pH variation. All are powders with a had a reddish colouration and a fine granulometry, with maximum particle sizes of around 28 μm . The granulometric distribution of the oxides was similar for the three pH conditions investigated (ANEXO

II - Appendix 4). Two populations of particles were identified, the first with a peak in the nanometer range (350 nm) and the other in the micrometer range (18 µm).

Table IV.02. Characteristics of iron oxides synthetised from the iron sludge obtained by selective precipitation at pH values of 3.6, 3.8, and 4.0, followed by thermal treatment (550°C) and hot water washing.

	pH		
	3.6	3.8	4.0
Mass of iron oxide (kg t⁻¹ IOT)	217	234	233
Iron recovery (%)	77.59	83.74	84.11
Particle size distribution (µm)	0.04 - 28	0.04 - 28	0.04 – 28
Volumetric average diameter (µm)	5.90	5.12	4.75
ELEMENTAL COMPOSITION - XRF (%)			
Fe	63.94%	64.07%	64.50%
Al	1.84%	2.35%	2.59%
Na	0.41%	0.52%	0.62%
Mg	0.26%	0.28%	0.25%
LOI	2.57%	3.05%	3.10%
Minor elements (ppm)			
Ba	437	458	434
Cr	774	912	825
Nb	24	25	25
Zr	11.6	11.6	12.2

All materials were free of SiO₂. The hot washing procedure carried out after calcination enabled a reduction of the sodium concentration of approximately 98%. The synthesised oxides consisted primarily of iron, with Fe contents of 63.9%, 64.0%, and 64.5%, respectively, for pH values of 3.6, 3.8, and 4.0. These results conferred iron metallurgical recovery rates of 77.6%, 83.7%, and 84.1%, respectively, for the leaching/synthesis process. Table 3 shows the media, standard deviation, and the results of the statistical comparison between the media by ANOVA. The standard deviation values showed little variation between the repetitions. For ($p \leq 0.05$), there was no statistical difference between the media in terms of the iron contents of the products for the three pH conditions considered for iron precipitation. However, there was an increase in terms of the iron metallurgical recovery and mass recovery when the pH was increased from 3.6 to 3.8/4.0. Since the iron contents were the same and

the iron recovery increased, it would be logical to choose a pH adjustment of 3.8 or 4.0. However, the aluminium contents is an aspect of differentiation, as the contents increased considerably when the pH was adjusted from 3.6 to 3.8 or 4.0.

Table IV.03. Statistical analysis performed by the ANOVA method ($p \leq 5\%$) for the parameters of iron concentration, metallurgical recovery, and mass of synthesised oxides ($n = 3$).

Parameters	Iron oxide 3.6	Iron oxide 3.8	Iron oxide 4.0
Iron content			
Mean	63.94%	64.07%	64.50%
Standard deviation	0.86	0.04	0.39
Statistical difference	a	a	a
Metallurgical recovery			
Mean	77.59%	83.74%	84.11%
Standard deviation	0.24	0.62	0.76
Statistical difference	a	a b	b
Mass recovery (%)			
Mean	21.78%	23.35%	23.31%
Standard deviation	0.51	0.13	0.53
Statistical difference	a	b	a b

Values indicated by the same letter are statistically the same following ANOVA/Tukey's ($p \leq 5\%$) tests.

This should be considered depending on the destination of the product. While producing a hematite concentrate that was totally free of SiO_2 , the process was not fully selective for aluminium. Indeed, around 80-90% of Al was removed from the IOT during the leaching and selective precipitation steps.

The nature of the materials formed through the procedure was further confirmed by scanning electron microscopy (SEM) (ANEXO II - Appendix 5). Nano- and microparticles of hematite were observed but NaCl crystals were notably absent. The sizes of the particles varied on the same scale attained by laser diffraction methods. The particle morphology was angular, a characteristic that is common in hematitic oxides formed through thermal dehydration processes (Schwertmann & Cornell, 2000). A refinement of the morphological pattern and greater control of the particle size distribution of synthesised particles depends on the synthesis method and the use of reagents such as seed particles and/or surfactants (Iijima et al., 2006; Mariani et al., 2017; Schwertmann and Cornell, 2000b; Supattarasakda et al., 2013; Teja and Koh, 2009), but future studies are needed to further our understanding of this.

Given the properties of the synthesised oxides, two applications could be presented: their use as pellet feed for steel production or their marketing as pigments. The granulometry, iron content and absence of contaminants in composition of the synthesised samples indicated the potential for use of these materials as pellet feed. A fine granulometry (<40 µm), high iron contents (\approx 64%), low LOI (\approx 3.0%), and the absence of silica are desirable properties for the production of high-quality pellets (Barik et al., 2022; Patra et al., 2017; Zhu et al., 2022). The synthesised materials could be considered for (a) blending with iron ore products attained by flotation and/or magnetic separation to attend the specification for blast furnace; and/or (b) marketing as pellet feed for green steel considering direct reduction.

Gyllenram et al., 2022 highlighted the importance of the quality of raw materials for a successful migration from the blast furnace-basic oxygen furnace (BF-BOF) route to the direct reduction and Electric arc furnace (DR-EAF) one in order to reach global climate goals. It should also be mentioned that the price of raw materials with low silica and aluminium contents could double to compose the pellet feed. Still, forward thinking on the process, the conversion of the silica-free iron sludge obtained through selective precipitation into hematite could be carried out during the process of green pellet induration at 1300 °C.

Colourimetric properties are an important parameter for iron oxides, especially when it comes to their application as pigments (Cornell and Schwertmann, 2003; Mariani et al., 2017; Silva et al., 2019). In this study, colourimetric analysis was performed for a chemical grade pigment used as a reference and for the products of this investigation. Table 3 presents the L*a*b* chromaticity colour spaces for the commercial iron oxide and for the hematite samples synthesised at pH values of 3.6; 3.8, and 4.0. An image of the hematite produced is presented in the Supplementary Material (ANEXO II - Appendix 6).

The oxide minerals prepared in this work had a bright red colour similar to, but not to the same as that of the synthetic oxide used as a reference. Independently of the chosen pH, the samples synthesised from the IOT were darker than the reference, a little bit less reddish and yellowish (Table 4), and with small colour differences between them ($\Delta E^* \approx 1$). Relative to the commercial sample, the ΔE^* was 5.8 for the sample produced at pH 3.6; 5.1 for that formed at pH 3.8; and 6.3 for the sample formed

at pH 4.0. As a general rule, a delta ΔE^* value of less than 1 is barely perceptible to the human eye (DIN 6174, 1979).

Colour variations between pigment samples differ depending of the raw materials used as well as the synthesis procedures. Indeed, different colourimetric properties have been observed in other investigations using residues as precursors for the synthesis of inorganic red pigments (hematite) (Almeida and Schneider, 2022; Gong et al., 2022; Lu et al., 2020).

Table IV.04. The L*a*b* chromaticity colour spaces of the synthesised iron oxides.

Samples	L*	a*	b*
Commercial iron oxide	34.9	29.9	20.4
pH 3.6	33.2	26.4	16.9
pH 3.8	33.4	26.5	16.9
pH 4.0	32.7	26.1	15.9

The pigment market is expanding and iron-based pigments are an important product in this sector. The average price of red iron-based pigments is stable and around ten times higher than that of pellets sold for steel production (Focus on Pigments, 2022). The use of the proposed route for pigment synthesis is an interesting alternative, because there is growing interest from the pigment sector in products made from sustainable raw materials (Coatings World, 2018; Prim et al., 2011).

4. CONCLUSIONS

The hydrometallurgical processing of IOTs was successful, allowing the formation of a hematite concentrate with potential uses for the valued and expanding green steel production industry. Moreover, the iron oxide materials produced here could possibly in conditions to attend the market share of inorganic pigments based on iron oxides. The process, which included the steps of leaching, selective precipitation, thermal treatment at 550°C, and washing, enabled the production of a material with 64% Fe, which was free of silica and had aluminium contents of less than 2.5%, with an iron recovery of 84% (considering precipitation at a pH of 3.8). The maximisation of iron recovery from mineral deposits and the possible integral exploitation of the tailings are among the advantages of the hydrometallurgical processing of IOTs since this

processing results in residues rich in SiO₂. The main challenges involve the inclusion of hydrometallurgical steps in iron ore processing plants as well as the logistics behind the supply of new inputs to process the large volumes of tailings generated. Nonetheless, the inclusion of a hydrometallurgical processing step to process IOTs could help support the environmental sustainability of the iron mining and steel production sectors.

ACKNOWLEDGMENTS

The authors are grateful to UFRGS, CAPES, CNPq, and VALE for the financial support that enabled this work.

REFERENCES

- Adiansyah, J.S., Rosano, M., Vink, S., Keir, G., 2015. A framework for a sustainable approach to mine tailings management: Disposal strategies. *J Clean Prod* 108, 1050–1062. <https://doi.org/10.1016/j.jclepro.2015.07.139>
- Almeida, V.O. de, Pereira, T.C.B., Teodoro, L. de S., Escobar, M., Ordovás, C.J., dos Santos, K.B., Weiler, J., Bogo, M.R., Schneider, I.A.H., 2021. On the effects of iron ore tailings micro/nanoparticles in embryonic and larval zebrafish (*Danio rerio*). *Science of the Total Environment* 759. <https://doi.org/10.1016/j.scitotenv.2020.143456>
- Almeida, V.O. de, Schneider, I.A.H., 2022. Hydrometallurgical Processing of Brazilian Iron Ore Tailings for the Synthesis of Pigments. *Geomaterials* 12, 30–36. <https://doi.org/10.4236/gm.2022.122003>
- Almeida, V.O., Schneider, I.A.H., 2020. Production of a ferric chloride coagulant by leaching an iron ore tailing. *Miner Eng* 156. <https://doi.org/10.1016/j.mineng.2020.106511>
- Barik, K., Prusti, P., Soren, S., Meikap, B.C., Biswal, S.K., 2022. Analysis of iron ore pellets properties concerning raw material mineralogy for effective utilization of mining waste. *Powder Technol* 400. <https://doi.org/10.1016/j.powtec.2022.117259>
- Beuria, P.C., Biswal, S.K., Mishra, B.K., Roy, G.G., 2017. Study on kinetics of thermal decomposition of low LOI goethetic hematite iron ore. *Int J Min Sci Technol* 27, 1031–1036. <https://doi.org/10.1016/j.ijmst.2017.06.018>
- Bhateria, R., Singh, R., 2019. A review on nanotechnological application of magnetic iron oxides for heavy metal removal. *Journal of Water Process Engineering*. <https://doi.org/10.1016/j.jwpe.2019.100845>
- Carmignano, O.R., Vieira, S.S., Teixeira, A.P.C., Lameiras, F.S., Brandão, P.R.G., Lago, R.M., 2021. Iron Ore Tailings: Characterization and Applications. *J Braz Chem Soc*. <https://doi.org/10.21577/0103-5053.20210100>
- Carvalho Eugênio, T.M., Francisco Fagundes, J., Santos Viana, Q., Pereira Vilela, A., Farinassi Mendes, R., 2021. Study on the feasibility of using iron ore tailing (iot) on

technological properties of concrete roof tiles. *Constr Build Mater* 279. <https://doi.org/10.1016/j.conbuildmat.2021.122484>

Coatings World, 2018. Pigments Market [WWW Document]. Coatings World. URL https://www.coatingsworld.com/issues/2018-01-01/view_features/pigments-market-/ (accessed 1.14.23).

Cornell, R.M., Schwertmann, U., 2003. The Iron Oxides: Structure, Properties, Reactions, Occurrences and Uses, 2nd ed. Wiley-VCH, New York.

Cudennec, Y., Lecerf, A., 2006. The transformation of ferrihydrite into goethite or hematite, revisited. *J Solid State Chem* 179, 716–722. <https://doi.org/10.1016/j.jssc.2005.11.030>

Dheyab, M.A., Aziz, A.A., Jameel, M.S., Noqta, O.A., Mehrdel, B., 2020. Synthesis and coating methods of biocompatible iron oxide/gold nanoparticle and nanocomposite for biomedical applications. *Chinese Journal of Physics* 64, 305–325. <https://doi.org/10.1016/j.cjph.2019.11.014>

DIN 6174, 1979. Farbmehratische Bestimmung Von Farbabständen bei Körperfarben nach der CIELAB- Formel. DIN 6174.

Dissanayake, D.M.S.N., Mantilaka, M.M.M.G.P.G., Palihawadana, T.C., Chandrakumara, G.T.D., De Silva, R.T., Pitawala, H.M.T.G.A., Nalin De Silva, K.M., Amaratunga, G.A.J., 2019. Facile and low-cost synthesis of pure hematite (α -Fe₂O₃) nanoparticles from naturally occurring laterites and their superior adsorption capability towards acid-dyes. *RSC Adv* 9, 21249–21257. <https://doi.org/10.1039/c9ra03756j>

Duarte, M.S., Almada, B.S., José dos Santos, W., Lima Bessa, S.A., Cesar da Silva Bezerra, A., Paulino Aguilar, M.T., 2022. Influence of mechanical treatment and magnetic separation on the performance of iron ore tailings as supplementary cementitious material. *Journal of Building Engineering* 59. <https://doi.org/10.1016/j.jobe.2022.105099>

Focus on Pigments, 2022. European iron oxide pigment prices tracked by Vincentz. Focus on Pigments 2022, 3. <https://doi.org/10.1016/j.fop.2022.07.003>

- Földvári, M., 2011. Handbook of thermogravimetric system of minerals and its use in geological practice. Geological Institute of Hungary, Budapest.
- Gianella, S., Girardi, F., Ischia, G., Lonardelli, I., Mattarelli, M., Montagna, M., 2010. On the goethite to hematite phase transformation. *J Therm Anal Calorim* 102, 867–873. <https://doi.org/10.1007/s10973-010-0756-2>
- Gong, L., Hua, X., Yao, B., Liang, J., Tian, G., 2022. Novel red composite pigment with high thermostability from iron ore tailings: Synthesis and coloring mechanism. *Ceram Int.* <https://doi.org/10.1016/j.ceramint.2022.10.021>
- Gyllenram, R., Arzpeyma, N., Wei, W., Jönsson, P.G., 2022. Driving investments in ore beneficiation and scrap upgrading to meet an increased demand from the direct reduction-EAF route. *Mineral Economics* 35, 203–220. <https://doi.org/10.1007/s13563-021-00267-2>
- Habashi, F., 1998. *Handbook of Extractive Metallurgy*. WILEY-VCH.
- Han, X., Wang, Y., Zhang, N., Meng, J., Li, Y., Liang, J., 2021. Facile synthesis of mesoporous silica derived from iron ore tailings for efficient adsorption of methylene blue. *Colloids Surf A Physicochem Eng Asp* 617. <https://doi.org/10.1016/j.colsurfa.2021.126391>
- Havlík, T., 2008. *Hydrometallurgy: Principles and application*. CRC Press.
- Holmes, R.J., Lu, Y., Lu, L., 2022. Introduction: Overview of the global iron ore industry, in: Lu, L. (Ed.), *Iron Ore: Mineralogy, Processing and Environmental Sustainability*. Elsevier - Woodhead Publishing, Brisbane, pp. 1–56.
- Hradil, D., Grygar, T., Hradilová, J., Bezdička, P., 2003. Clay and iron oxide pigments in the history of painting. *Appl Clay Sci* 22, 223–236. [https://doi.org/10.1016/S0169-1317\(03\)00076-0](https://doi.org/10.1016/S0169-1317(03)00076-0)
- Iijima, M., Yonemochi, Y., Tsukada, M., Kamiya, H., 2006. Microstructure control of iron hydroxide nanoparticles using surfactants with different molecular structures. *J Colloid Interface Sci* 298, 202–208. <https://doi.org/10.1016/j.jcis.2005.11.061>

- Jégourel, Y., 2020. The global iron ore market: From cyclical developments to potential structural changes. Extractive Industries and Society. <https://doi.org/10.1016/j.exis.2020.05.015>
- Kinnunen, P.H.M., Kaksonen, A.H., 2019. Towards circular economy in mining: Opportunities and bottlenecks for tailings valorization. J Clean Prod 228, 153–160. <https://doi.org/10.1016/j.jclepro.2019.04.171>
- Konyukhov, Y. V., 2018. Heavy-Metal Extraction from Wastewater by Means of Iron Nanopowder. Steel in Translation 48, 135–141. <https://doi.org/10.3103/S0967091218020080>
- Li, Y., Li, S., Zhao, X., Pan, X., Guo, P., 2022. Separation and purification of high-purity quartz from high-silicon iron ore tailing: an innovative strategy for comprehensive utilization of tailings resources. Process Safety and Environmental Protection. <https://doi.org/10.1016/j.psep.2022.11.006>
- Liu, K., Wang, S., Quan, X., Jing, W., Xu, J., Zhao, N., Liu, B., 2022. Effect of iron ore tailings industrial by-product as eco-friendly aggregate on mechanical properties, pore structure, and sulfate attack and dry-wet cycles resistance of concrete. Case Studies in Construction Materials 17. <https://doi.org/10.1016/j.cscm.2022.e01472>
- Liu, Y., Du, F., Yuan, L., Zeng, H., Kong, S., 2010. Production of lightweight ceramisite from iron ore tailings and its performance investigation in a biological aerated filter (BAF) reactor. J Hazard Mater 178, 999–1006. <https://doi.org/10.1016/j.jhazmat.2010.02.038>
- Lu, Y., Xu, J., Wang, W., Wang, T., Zong, L., Wang, A., 2020. Synthesis of iron red hybrid pigments from oil shale semi-coke waste. Advanced Powder Technology 31, 2276–2284. <https://doi.org/10.1016/j.apt.2020.03.020>
- Mariani, F.Q., Borth, K.W., Müller, M., Dalpasquale, M., Anaissi, F.J., 2017. Sustainable innovative method to synthesize different shades of iron oxide pigments. Dyes and Pigments 137, 403–409. <https://doi.org/10.1016/j.dyepig.2016.10.024>
- Menezes, J.C.S.S., Silva, R.A., Arce, I.S., Schneider, I.A.H., 2010. Production of a poly-alumino-iron sulphate coagulant by chemical precipitation of a coal mining acid drainage. Miner Eng 23, 249–251. <https://doi.org/10.1016/j.mineng.2009.11.008>

Menezes, J.C.S.S., Silva, R.A., Arce, I.S., Schneider, I.A.H., 2009. Production of a poly-ferric sulphate chemical coagulant by selective precipitation of iron from acidic coal mine drainage. *Mine Water Environ* 28, 311–314. <https://doi.org/10.1007/s10230-009-0084-6>

Meng, Q. min, Li, J. xin, Wei, R. fei, Long, H. ming, Chun, T. jun, Wang, P., Di, Z. xia, Dessbesell, L., Xu, C., 2018. Effects of gangue compositions on reduction process of carbon-bearing iron ore pellets. *Journal of Iron and Steel Research International* 25, 1105–1112. <https://doi.org/10.1007/s42243-018-0168-2>

Mohapatra, M., Anand, S., 2010. Synthesis and applications of nano-structured iron oxides/hydroxides-a review, *International Journal of Engineering, Science and Technology*.

Müller, M., Villalba, J.C., Mariani, F.Q., Dalpasquale, M., Lemos, M.Z., Huila, M.F.G., Anaissi, F.J., 2015. Synthesis and characterization of iron oxide pigments through the method of the forced hydrolysis of inorganic salts. *Dyes and Pigments* 120, 271–278. <https://doi.org/10.1016/j.dyepig.2015.04.026>

Murthy, S., Effiong, P., Fei, C.C., 2020. Metal oxide nanoparticles in biomedical applications, in: Al-Douri, Y. (Ed.), *Metal Oxide Powder Technologies*. Elsevier, Amsterdam, pp. 233–251.

Muslemani, H., Liang, X., Kaesehage, K., Ascui, F., Wilson, J., 2021. Opportunities and challenges for decarbonizing steel production by creating markets for ‘green steel’ products. *J Clean Prod* 315. <https://doi.org/10.1016/j.jclepro.2021.128127>

Park, H., Sahajwalla, V., 2014. Reduction Behavior of Carbon Composite Pellets Including Alumina and Silica at 1273 K and 1373 K. *ISIJ International* 54, 1256–1265. <https://doi.org/10.2355/isijinternational.54.1256>

Patra, S., Kumar, A., Venugopal, R., 2017. THE EFFECT OF PARTICLE SIZE ON GREEN PELLET PROPERTIES OF IRON ORE FINES, *Journal of Mining and Metallurgy*, 53 A.

Prim, S.R., Folgueras, M. V., de Lima, M.A., Hotza, D., 2011. Synthesis and characterization of hematite pigment obtained from a steel waste industry. *J Hazard Mater* 192, 1307–1313. <https://doi.org/10.1016/j.jhazmat.2011.06.034>

- Sawyer, C.N., McCarty, P.L., Parkin, G.F., 2003. Chemistry for environmental engineering and science, 5th ed. McGraw-Hill, New York.
- Schwertmann, U., Cornell, R.M., 2000a. Iron oxides in the laboratory: Preparation and Characterization. Wiley-VCH, New York.
- Schwertmann, U., Cornell, R.M., 2000b. Iron Oxides in the Laboratory.
- Silva, R. de A., Secco, M.P., Lermen, R.T., Schneider, I.A.H., Hidalgo, G.E.N., Sampaio, C.H., 2019. Optimizing the selective precipitation of iron to produce yellow pigment from acid mine drainage. *Miner Eng* 135, 111–117. <https://doi.org/10.1016/j.mineng.2019.02.040>
- Sparrow, G.J., Lu, L., Lovel, R.R., 2022. Chemical separation of iron ore, in: Lu, L. (Ed.), Iron Ore: Mineralogy, Processing and Environmental Sustainability. Elsevier - Woodhead Publishing, Brisbane, pp. 397–420.
- Supattarasakda, K., Petcharoen, K., Permpool, T., Sirivat, A., Lerdwijitjarud, W., 2013. Control of hematite nanoparticle size and shape by the chemical precipitation method. *Powder Technol* 249, 353–359. <https://doi.org/10.1016/j.powtec.2013.08.042>
- Tadic, M., Trpkov, D., Kopanja, L., Vojnovic, S., Panjan, M., 2019. Hydrothermal synthesis of hematite (α -Fe₂O₃) nanoparticle forms: Synthesis conditions, structure, particle shape analysis, cytotoxicity and magnetic properties. *J Alloys Compd* 792, 599–609. <https://doi.org/10.1016/j.jallcom.2019.03.414>
- Tanner, A.O., 2016. Iron Oxide Pigments.
- Teja, A.S., Koh, P.-Y., 2009. Synthesis, properties, and applications of magnetic iron oxide nanoparticles. *Progress in Crystal Growth and Characterization of Materials* 55, 22–45. <https://doi.org/10.1016/j.pcrysgrow.2008.08.003>
- UNEP, 2020. Global Industry Standard on Tailings Management.
- UNITED NATIONS, 2015. Sustainable Development Goals [WWW Document]. <https://sdgs.un.org/goals>.

Wei, X., Viadero, R.C., Buzby, K.M., 2005. Recovery of Iron and Aluminum from Acid Mine Drainage by Selective Precipitation. *Environ Eng Sci* 22, 745–755. <https://doi.org/10.1089/ees.2005.22.745>

World Economic Forum, 2022. What is green steel and why does the world need more of it? [WWW Document]. World Economic Forum. URL <https://www.weforum.org/agenda/2022/07/green-steel-emissions-net-zero/> (accessed 1.14.23).

Zhang, N., Tang, B., Liu, X., 2021. Cementitious activity of iron ore tailing and its utilization in cementitious materials, bricks and concrete. *Constr Build Mater* 288. <https://doi.org/10.1016/j.conbuildmat.2021.123022>

Zhu, D., Pan, J., Lu, L., Holmes, R.J., 2022. Iron ore pelletization, in: Lu, L. (Ed.), *Iron Ore: Mineralogy, Processing and Environmental Sustainability*. Elsevier - Woodhead Publishing, Brisbane, pp. 539–578.

CAPÍTULO V

APPLICATION OF LEACHED IRON ORE TAILINGS TO PRODUCE

SUSTAINABLE CEMENTS

ARTIGO 4***Application of leached iron ore tailings to produce sustainable cements***

Vitor O. Almeida^a, Laura Silvestro^b, Philippe J.P. Gleize^c, Ana P. Kirchheim^d, Ivo A.H. Schneider^{a*}

^a Universidade Federal do Rio Grande do Sul (UFRGS) - LTM - DEMIN/PPGE3M, Av. Bento Gonçalves 9500, CEP: 91501-970, Porto Alegre, RS, Brasil

^b Universidade Tecnológica Federal do Paraná (UTFPR), Av. Prof^a. Laura Pacheco Bastos, 800, CEP: 85053-525, Guarapuava, PR, Brasil

^c Universidade Federal de Santa Catarina (UFSC) - Laboratório de Aplicações de Nanotecnologia em Construção Civil (NANOTEC), Rua João Pio Duarte da Silva, 205, CEP 88040-900, Florianópolis, SC, Brasil

^d Universidade Federal do Rio Grande do Sul (UFRGS) - Laboratório de Inovação em Cimentos Ecoeficientes (LINCE), Rua Engenheiro Luiz Englert, CEP 90040-040, Porto Alegre, RS, Brasil

* Corresponding author

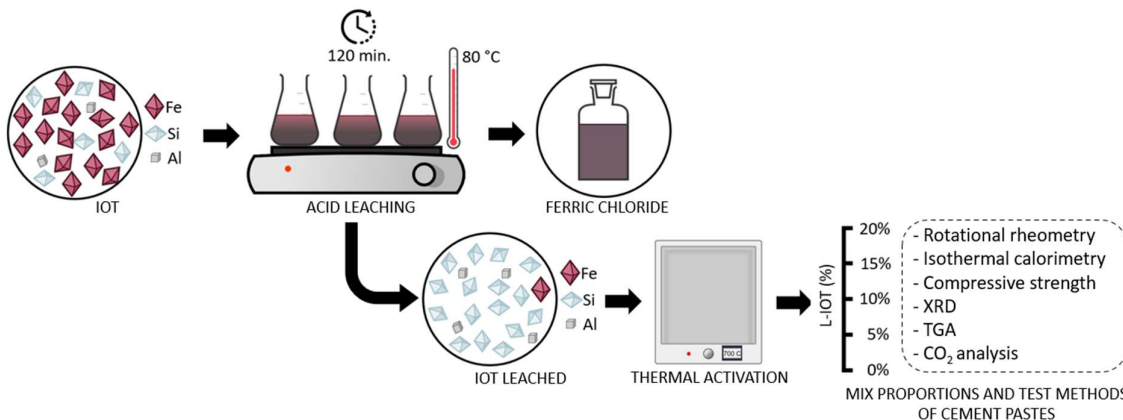
Artigo publicado na *Construction and Building Materials* (ISSN: 1879-0526 | Impact Factor 7.4 | Qualis A1 - Quadriênio 2017-2020)

ABSTRACT

The use of iron ore tailings (IOT) is a trend for the future of mining. The adoption of alternatives that minimize the disposal of natural resources and add value to production processes strongly supports this effort. Hydrometallurgy, by means of acid leaching, has been investigated as a processing route for iron recovery from IOT. After the separation of the liquor, a solid fraction of insoluble quartz and kaolinite remains (the main mineralogical phases). In the same way, the cement industry is an intensive consumer of raw materials and a major emitter of greenhouse gases. As one of the main alternatives for reducing these impacts, clinker substitution by wastes from other industries is being extensively considered. Thus, this work aims to evaluate the properties of the solid product of IOT leaching (L-IOT) and its potential to produce sustainable cements. L-IOT main composition is based on silicon ($\approx 35\%$), aluminium ($\approx 8\%$) and iron (2%). After thermal activation, the L-IOT was incorporated into pastes, replacing the cement by up to 20 wt.%. The rheological parameters, hydration kinetics, compressive strength, mineralogy through X-ray diffraction (XRD) and thermogravimetric analysis (TGA) of cement pastes were assessed. L-IOT increased cement pastes' dynamic yield stress and viscosity and anticipated its main heat flow peak by up to three hours. Replacement contents of up to 20 wt.% showed an equivalent 28-d compressive strength in the control sample, associated with carboaluminates formation. Finally, a simplified carbon dioxide equivalent emission (CO₂-eq) analysis was conducted to evaluate the L-IOT's environmental feasibility. Reductions of up to 21% CO₂-eq emissions were observed for an L-IOT content of 20 wt.%, compared to plain cement. The hydrometallurgical route allowed the recovery of 95% of the iron content in IOT, and its by-product presented technical and environmental feasibility for cement replacement in cementitious matrices.

Keywords: mining, hydrometallurgy, iron ore tailings, cement paste, CO₂ reduction, industrial symbiosis.

GRAPHICAL ABSTRACT



1. INTRODUCTION

The mining and construction industries are sectors that manage gigantic amounts of natural resources and energy, but, at the same time, they need to handle strong environmental issues. Both sectors are available to the circular economy and industrial symbioses initiatives, provided that the market and the quality of their products are maintained. Sustainable actions are essential for social license in current and new ventures (ASIM et al., 2021; ASR et al., 2019; HAN et al., 2021; MARQUES et al., 2017; WEI et al., 2022).

Iron ore is one of the main commodities and, worldwide, generates large volumes of solid waste - currently referred to as Iron Ore Tailings (IOT). In Brazil, about 200 million tons of IOT are generated annually and this number grows along with iron production (CARMIGNANO et al., 2021; MENDES et al., 2019). On the other hand, the construction sector has an increasing demand for mineral resources, especially for cement production, aggregates and ceramics manufacture (MOHAMAD et al., 2021; RAMAKRISHNA BALAJI; AZEVEDO; MADURWAR, 2022; ZHAO; FAN; SUN, 2014).

The search for multiple alternatives for solid waste is an essential path to industrial sustainability (BOSSLE et al., 2016; KRISHNA et al., 2020). There is a strong link between mining and the construction sector, mainly due to the scale compatibility between the amount of mineral waste and the demand for construction resources (ALMEIDA; SCHNEIDER, 2022; GOULART BEZERRA et al., 2021; SAFIUDDIN et al., 2010). For IOT in particular, there is a range of investigations for raw material for civil construction, including: (a) aggregates (JAYASIMHA; SUJINI; ANNAPURNA, 2022; SHETTIMA et al., 2016; ZHAO; FAN; SUN, 2014), (b) ceramics (CECHIN et al., 2022; DAS; KUMAR; RAMACHANDRARAO, 2000; FONTES et al., 2019), (c) pigments (ALMEIDA; SCHNEIDER, 2022; GALVÃO et al., 2018; GONG et al., 2021), (d) pavements (SÁ et al., 2022) and (e) supplementary cementitious material (SCM) (GOULART BEZERRA et al., 2021; YAO et al., 2020a; ZHANG et al., 2022).

SCMs are widely used to reduce the environmental impacts of Portland cement (PC) production since the PC production chain emits approximately 9% of the total carbon dioxide (CO_2) released worldwide (REIS et al., 2021). Nevertheless, the availability of typical SCM, such as fly ash and slag, could be a limiting input in large-scale usage since it depends on geographical and economic considerations

(SCRIVENER et al., 2018). Therefore, other sources of SCM need to be thoroughly investigated and evaluated as potentially feasible alternatives.

More specifically, regarding the use of IOT as SCM for cementitious matrix production, previous studies were carried out without any treatment. Thus, due to the chemical composition, high iron content, and crystallinity of the silica, IOT usually has no reactivity and acts only as a filler, which limits its incorporation into low replacement contents of Portland cement (~5 wt.%). For IOT (50.96% Fe₂O₃) contents higher than 10 wt.%, the 28-d compressive strength of cement pastes was reduced by up to 15.4% (GOULART BEZERRA et al., 2021). Similarly, (Huang et al., 2013) developed a greener engineered cementitious composite (ECCs) with IOT with a chemical composition of 22.06% of Fe₂O₃, observing reductions of 28-d compressive strength of approximately 33%, for a cement replacement content of 80%, by IOT.

Previous studies also applied a mechanical (YAO et al., 2020a) or thermal activation (MAGALHÃES et al., 2020) to enhance the potential pozzolanic activity of IOT. Nevertheless, to our knowledge, this is the first study that assess the cement substitution of IOT prepared by acid leaching to reduce the Fe₂O₃ content (~2%), to produce sustainable cementitious materials. Moreover, this approach promotes the recovery of a significant portion of iron (~95%), in the form of ferric liquor. The obtained ferric chloride (FeCl₃) can be used as a coagulant (SAHU; CHAUDHARI, 2013; SATHTHASIVAM et al., 2022), in hydrometallurgical processes (LJUBETIC; LIU, 2022; WANG; CHE; YE, 2010); as a catalyst (KUMAR SETHI et al., 2022; PATNAIK et al., 2016), and in the manufacture of other chemicals (BOUAFIA; LAOUINI, 2020).

Thus, this study aims to evaluate the properties of the solid fraction of an IOT submitted to an acid leaching process and thermal treatment, named in this work as L-IOT, and its applicability as SCM. For this purpose, several proportions of L-IOT and its rheological properties, mechanical properties, and effects on the hydration of cement pastes were evaluated.

2. MATERIAL AND METHODS

2.1. Iron ore tailings

A representative sample of 20 kg of IOT was provided by a mining company operating in the Quadrilátero Ferrífero, in the municipality of São Gonçalo do Rio Abaixo (MG), Brazil. The material was filtered, dried under ambient conditions, homogenized and finally properly divided for characterization and processing for use as SCM. The tailings sample comes from the deslaming stage, preceding flotation. This sludge is the finest fraction of iron ore processing and the most difficult to filter, considering dry staking disposal. The material is fine, with a homogeneous and controlled particle size distribution. The particle size distribution of IOT ranging from 0.04 to 36 μm , with specific surface area of $10.70 \text{ m}^2\text{g}^{-1}$. The main mineralogical components obtained via X-ray diffraction (XRD) are hematite, goethite, quartz and kaolinite.

2.2. IOT leaching process

Acid leaching of the IOT was conducted for two hours, at a temperature of 80°C, with a leaching solution of hydrochloric acid (HCl) at a concentration of 10.8 mol L⁻¹ (Almeida and Schneider, 2020). After leaching, the ferric liquor was removed by filtration (qualitative filter paper, Unifil®) and the remaining solid fraction was submitted to washing. This procedure was performed by three consecutive rinsing stages through the filter cake with deionised water, with a water volume of approximately twice the volume of the material held in the filter. After filtration, the material was dried at 60 °C and characterised.

The ferric chloride was analysed, in terms of the dissolved metals, by inductively coupled plasma (ICP) spectroscopy (Perkin Elmer - OPTIMA 8300 DV). Samples of IOT and iron ore tailings after leaching and thermal treatment (L-IOT) were physically and chemically characterised. The particle size distribution was obtained by laser diffraction (CILAS 1180). Elemental analysis was carried out by X-ray fluorescence - XRF (Rigaku - RIX 2000) and determination of crystalline species by X-ray diffraction - XRD (Bruker AXS - D 5000).

2.3. Thermal activation

A thermal activation was conducted at 700 °C for 1 h in a static calcining muffle (KK260, Linn Elektro Therm GmbH), using a heating rate of 10 °C/minute (RUVIARO et al., 2021). The characterisation of the material before and after the heat treatment was carried out through X-ray diffraction (XRD) and thermogravimetric analysis (TGA). TGA and XRD analyses were conducted with the equipment and conditions described in detail in Section 2.5. The specific surface area (SSA) of L-IOT was determined by nitrogen adsorption using an Autosorb (Quantachrome Instruments) and applying the Brunauer–Emmett–Teller (BET) method. Degassing was carried out at 300 °C for 1 h.

2.4. Mix proportions and sample preparation

Ordinary Portland cement (OPC) was used for cement paste production. The main properties of the OPC used are presented in Table 1, and the test procedure and its complete characterisation can be consulted in previous work by the authors (SILVESTRO et al., 2021).

Table V.01 - Chemical composition and physical properties of OPC

Property	OPC
<i>Chemical composition (wt.%)</i>	
SiO ₂	18.31
Al ₂ O ₃	4.46
Fe ₂ O ₃	2.84
CaO	60.76
MgO	3.37
SO ₃	3.08
Loss on ignition	3.79
Insoluble residue	0.72
<i>Physical property</i>	
D10 (µm)	3.59
D50 (µm)	15.08
D90 (µm)	35.67
Mean diameter (µm)	16.53
Density (g/cm ³)	3.09
B.E.T. Specific surface area (m ² /g)	2.22

Table 2 presents the mix design of the cement pastes evaluated. A water-to-agglomerate ratio of 0.45 was used because it provided good workability without incorporating plasticiser admixtures. Partial replacement contents of L-IOT of 5%, 10%, 15%, and 20% by cement weight were analysed. These L-IOT contents were defined based on a previous study that evaluated the incorporation of IOT as SCM in Portland cement pastes (GOULART BEZERRA et al., 2021).

For cement paste production, the water was added to (previously homogenised) anhydrous materials and mixed manually for 30 s and, after 20 s of rest, mechanically mixed for 70 s in a high-shear mixer (10,000 rpm).

Table V.02 - Mix proportions of cement pastes

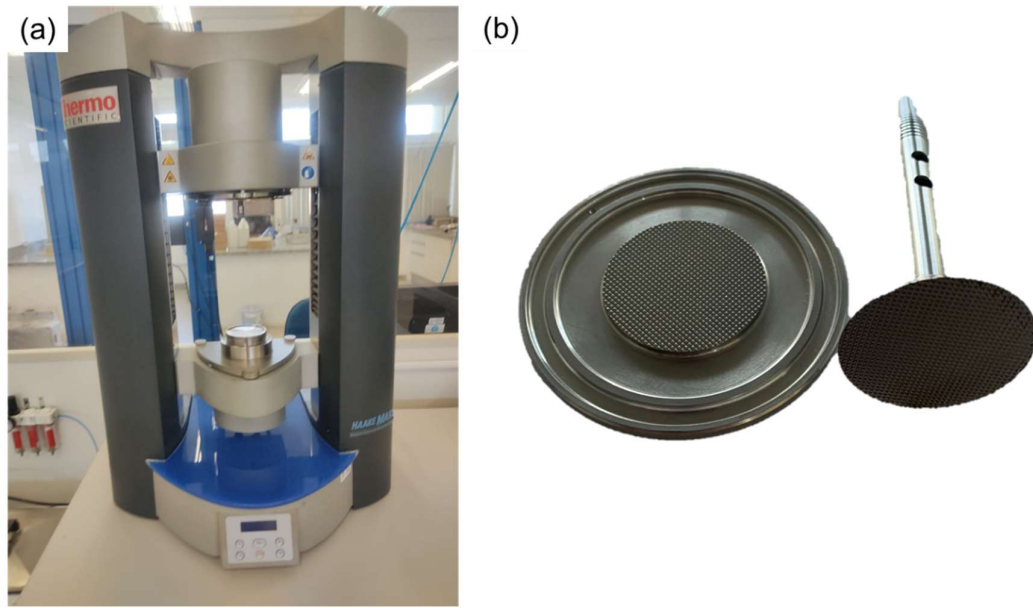
Cement Pastes	PC (wt.)	L-IOT (wt.)	Water (wt.)
0% L-IOT	1.00	0.00	0.45
5% L-IOT	0.95	0.05	0.45
10% L-IOT	0.90	0.10	0.45
15% L-IOT	0.85	0.15	0.45
20% L-IOT	0.80	0.20	0.45

2.5 Test Methods

The fresh properties of cement pastes containing L-IOT were evaluated by rotational rheometry. The tests were performed on a Haake MARS III (Thermo Fisher Scientific) rheometer with a hatched parallel-plate geometry of diameter 35 mm and a gap of 1 mm (Figure 1).

This geometry was used as it provides analytical transformation equations for shear rate and shear stress determination (WALLEVIK et al., 2015). The testing routine was as follows: (i) pre-shear of 100 s^{-1} during 60 seconds, (ii) rest for 60 seconds, (iii) increase the shear rate from 0.1 to 100.0 s^{-1} in 10 steps (ascending flow curve), (iv) decrease the shear rate from 100.0 s^{-1} to 0.1 s^{-1} at the same points (descending flow curve). A constant shear rate was applied for 10 seconds and the last 3 seconds were measured to ensure a steady state in the shear stress reading (PENG et al., 2021; WALLEVIK et al., 2015).

Figure V.01. Rheometer (a) and parallel-plate geometry (b) used in the rotational rheometry tests.



The dynamic yield stress (τ_0) was obtained by applying the Herschel-Bulkley (H-B) model (Equation 1) to the descending flow curve. The equivalent plastic viscosity (μ_{eq}) was calculated using the equation proposed by De Larrard (1996) (Equation 2).

$$\tau = \tau_0 + K \cdot \dot{\gamma}^n \quad \text{Equation 1}$$

$$\mu_{eq} = \frac{3K}{n+2} \cdot (\dot{\gamma}_{max})^{n-1} \quad \text{Equation 2}$$

where τ is the shear stress (Pa), K and n are the consistency and the pseudoplastic parameters of the Herschel-Bulkley model, respectively, $\dot{\gamma}$ is the shear rate (s^{-1}), and $\dot{\gamma}_{max}$ is the maximum shear rate applied ($100 s^{-1}$).

A TAM air calorimeter (TA Instruments) was used for the isothermal calorimetry analyses. The cement pastes were produced following the previously described procedure (see Section 2.4) and immediately added to glass ampoules, which were placed in the calorimeter. A glass ampoule with distilled water was used in the reference channel (WADSÖ, 2010). The heat flow and cumulative heat were recorded for 72 hours at 23°C .

The mechanical performance of L-IOT cement pastes was assessed through a compressive strength test after 3, 7, and 28 days of hydration following ASTM

C39/C39M. Five cylindrical specimens (20 mm diameter and a height of 26 mm) were moulded at each age evaluated, and the mean value was adopted as the compressive strength value.

Isopropanol was used for the hydration stoppage of samples for XRD and TGA analyses. Initially, cement paste samples were immersed in isopropanol for 30 min. Subsequently, the samples were vacuum filtered, dried at 40°C, ground in an agate mortar, and sieved in 45 µm-opening mesh.

The mineralogical composition of L-IOT cement pastes was evaluated by X-ray diffraction (XRD) after 3, 7, and 28 days of hydration. A Miniflex II Desktop X-Ray Diffractometer (Rigaku) with CuK radiation ($\lambda = 1.5418 \text{ \AA}$) was employed, operating at 30 kV/15 mA with the following configuration: 5° to 55° (2θ), 0.05° 2θ step size, and step time of 1 second/step.

The thermogravimetric analysis (TGA) of the paste at 7 and 28 days was performed in a TGA 2 analyser from Mettler Toledo. The samples were placed in open alumina crucibles under nitrogen flow and the temperature was increased up to 1000°C at a heating rate of 20°C/min. From TGA results, the bound water (BW) and the portlandite (CH) contents were determined according to Equations 3 and 4, considering weight loss between 50–550°C and 400–500°C, respectively (SCRIVENER; SNELLINGS; LOTHENBACH, 2018).

$$BW = \frac{(M_{50^\circ\text{C}} - M_{550^\circ\text{C}})}{M_{550^\circ\text{C}}} \times 100 \quad \text{Equation 3}$$

$$CH = CH_w \times \frac{74}{18} \times 100 \quad \text{Equation 4}$$

where BW is bound water content (%), CH is portlandite content (%), and CH_w is the weight loss in the temperature range 400–500°C.

The simplified CO₂ analysis per m³ of paste was performed according to previous studies regarding the incorporation of waste in cement-based materials (RUVIARO et al., 2021; SCOLARO et al., 2022). Briefly, a 0.892 kg CO₂-eq/kg emission was considered for Portland cement (VOTORANTIM CIMENTOS, 2016). The water CO₂-eq was insignificant and was discarded. For L-IOT, an equivalent emission

of 0.0972 kg CO₂-eq/kg was adopted, associated with the thermal activation process. To determine this value, the equipment specifications and productivity of the L-IOT activation process were considered in the energy analysis. A muffle furnace (KK260, Linn Elektro Therm GmbH) with a power of 14 kW was employed. The activation process was conducted at a heating rate of 10°C/min until 700°C was reached, remaining at this value for 1 h. Furthermore, a yield per cycle of approximately 40 kg was considered. CO₂ emission of 0.135 kg CO₂-eq/kWh was adopted for the Brazilian energy matrix (Matos et al., 2019; Schlorer et al., 2014). The IOT leaching process was discarded from CO₂ analysis since it was applied to recover iron for other uses. Thus, only the IOT beneficiation processes for application in the cement matrix were considered, i.e. thermal activation. In addition, the CO₂ emissions from mixing, batching, and transportation were discarded. A relationship between CO₂ emissions and the compressive strength of the pastes was calculated to compare the results (DAMINELLI et al., 2010).

3 RESULTS AND DISCUSSION

3.1. Leaching and thermal activation

Acid leaching, as a process of using IOT, allowed the production of ferric chloride with a concentration greater than 110 g L⁻¹ of iron, giving a recovery of this metal greater than 95%. In lower concentrations, the following elements were identified: Al (1020 mg L⁻¹); Mn (250 mg L⁻¹), P (88 mg L⁻¹) and Mg (51 mg L⁻¹). Toxic metals such as copper, zinc, nickel and lead were identified at trace levels.

The other product is the solid fraction, which comprises the elements which are insoluble in hydrochloric acid, under the evaluated conditions. This material represents about 32% of the initial IOT mass used in the hydrometallurgical route. The dissolution of the mining tailings was reflected in terms of composition and, to a lesser extent, in the particle size distribution. There was a substantial increase in Si and Al, with a decrease in Fe content. Still, the process leads to the consumption of the finer particles and the reduction of the size of the larger particles (Table V.03).

Table V.03 - Elemental composition by XRF and particle size distribution.

Element	IOT	L-IOT
Si (%), wt)	11.30	34.70
Al (%), wt)	3.60	7.90
Fe (%), wt)	41.40	1.40
Ti (%), wt)	0.17	0.36
PPC (%), wt)	7.66	0.90
Particle size distribution (μm)	0.04 – 36	0.3 – 36
D_{50} (μm)	9.7	6.4

The thermogravimetric analysis (TGA) of leached IOT presented in Figure 2 indicated a kaolinite content of 38.1%, which was calculated according to the procedure described by Ruviaro et al. (2021). The complete dehydroxylation of kaolinite was confirmed by X-ray diffraction (XRD), which indicates the absence of kaolinite reflection peaks after heat treatment (Figure 3). The specific surface area (SSA) of IOT after thermal treatment was 17.748 m^2/g .

Figure V.02 - Thermogravimetric analysis of leached IOT

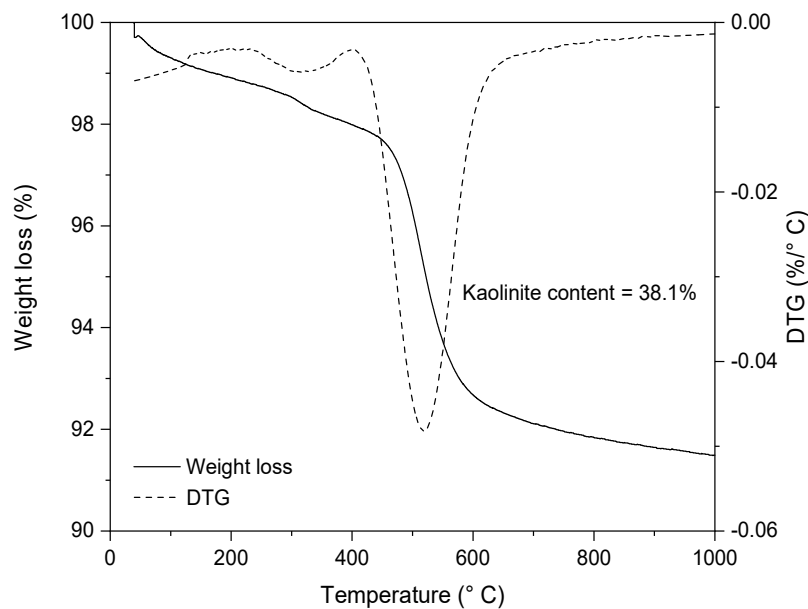
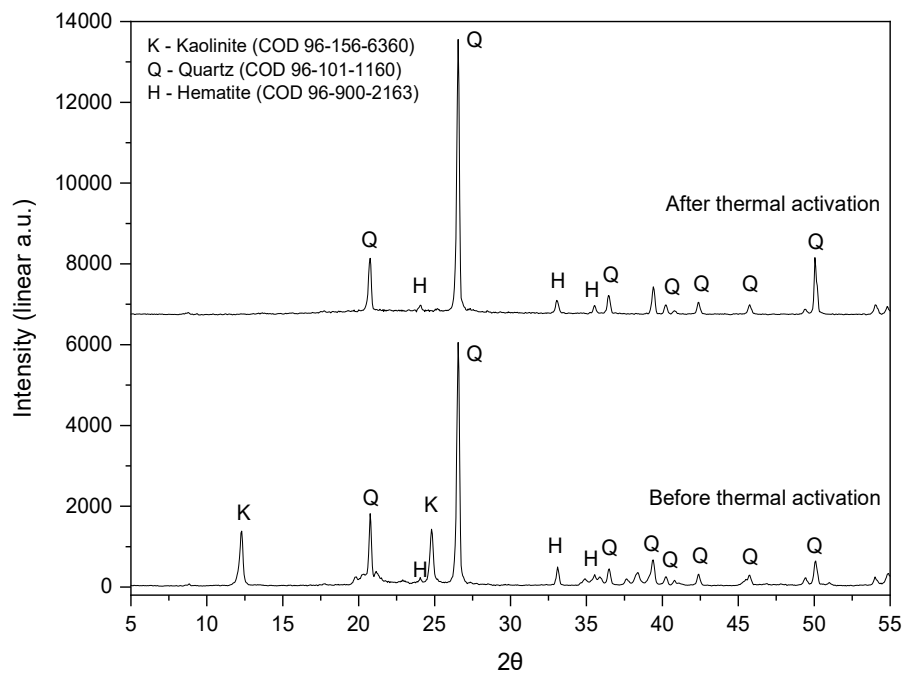
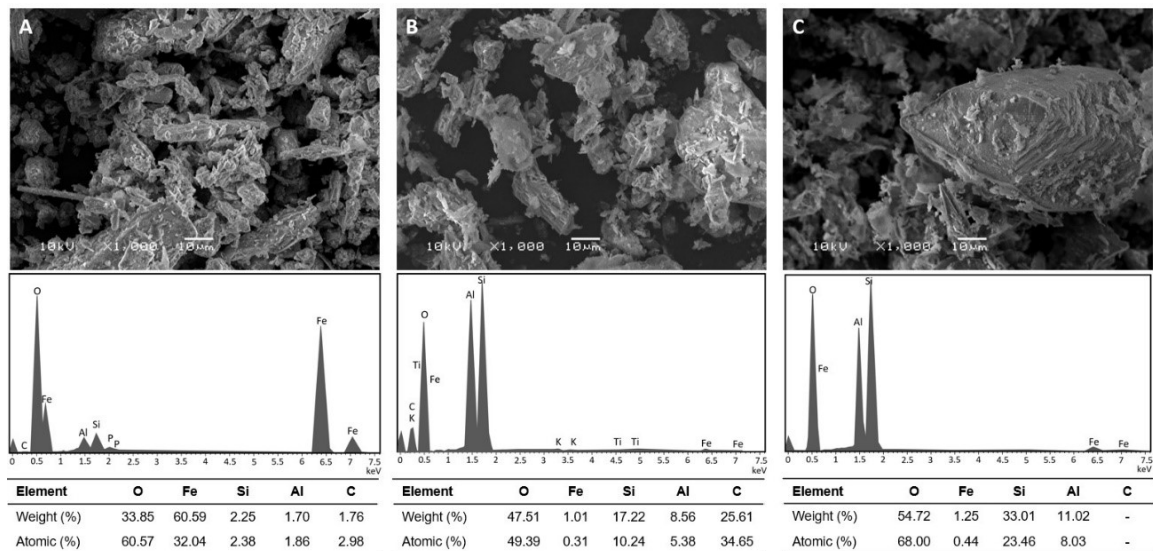


Figure V.03 - XRD patterns of leached IOT before and after thermal activation



Leaching and thermal activation did not modify the irregular morphology of IOT. However, it should be noted that, after leaching, there is a decrease in the population of ultrafine particles (nm) also observed in the particle size distribution results presented in Table 2, which corresponds to iron (Figure 4).

Figure V.04 - SEM images at 1,000 x magnification. (A) Raw sample of IOT. (B) IOT leached. (C) IOT after leaching and thermal activation.



The composition of leached IOT, combined with its granulometry and specific surface area, are compatible with chemical composition requested for use as a

supplementary cementitious material (LOTHENBACH; SCRIVENER; HOOTON, 2011a) and the consequences of the addition in the intrinsic properties of the cement paste were evaluated in this article.

3.2. Fresh-state of cement pastes

The descending flow curves of L-IOT cement pastes are presented in Fig. 5. The increase in L-IOT replacement content progressively increased the shear stress of cement pastes. A similar trend for dynamic yield stress and equivalent viscosity is presented in Table 4.

Figure V.05 - Descending flow curves (shear stress vs. shear rate) of cement pastes

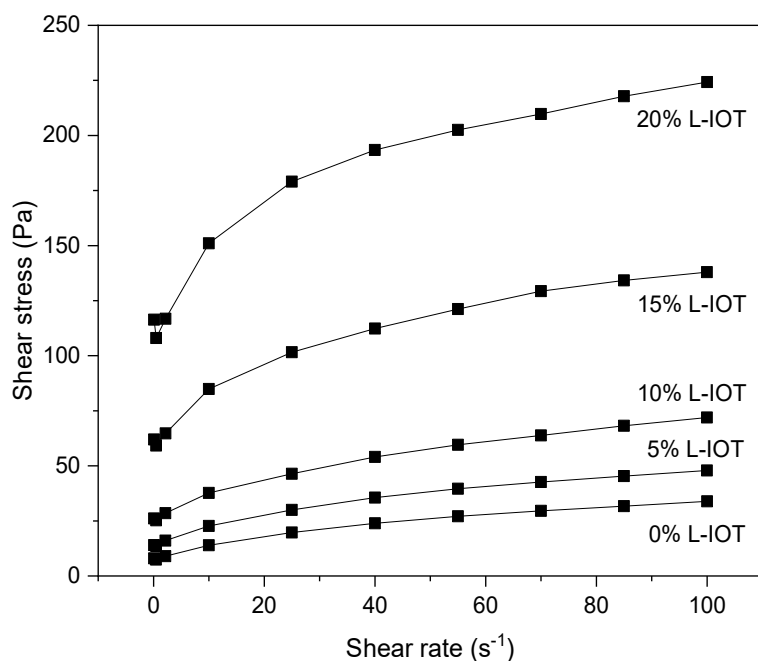


Table V.04 - Mini-slump and rheological parameters of cement pastes

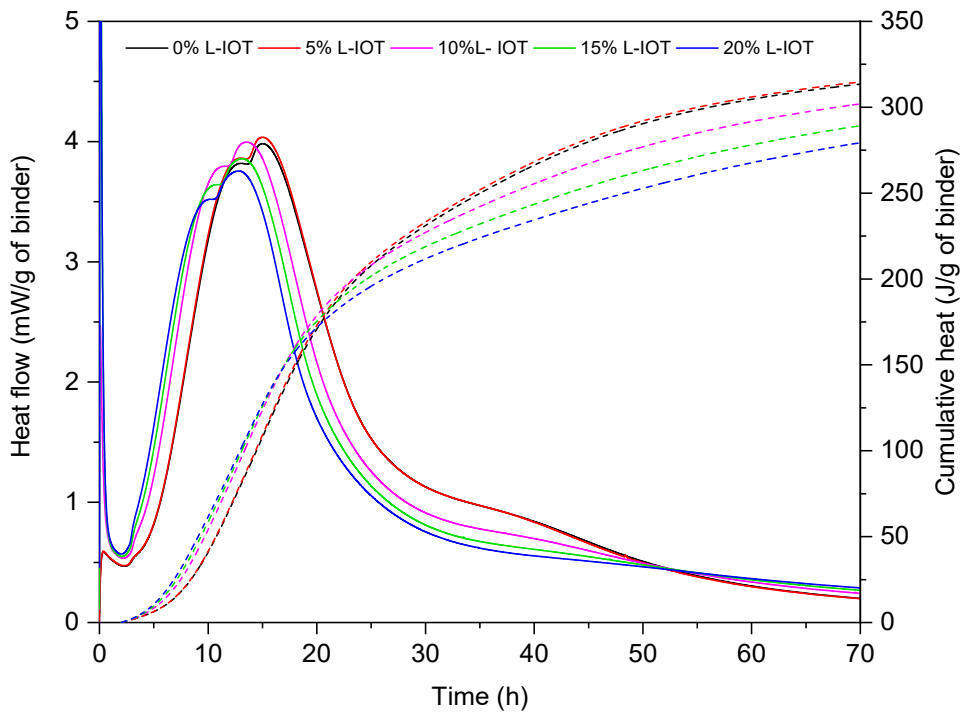
Cement Pastes	Mini-slump (mm)	Dynamic yield stress (Pa)	Equivalent viscosity (Pa.s)
0% L-IOT	88.19	6.28	0.33
5% L-IOT	79.15	11.71	0.44
10% L-IOT	70.15	21.38	0.61
15% L-IOT	56.55	53.69	1.06
20% L-IOT	53.65	97.91	1.63

For instance, increases of up to 1,450% and 393% were observed in yield stress and viscosity for 20% L-IOT, compared to plain cement paste (0% L-IOT), respectively. The rheological behaviour of cement pastes is significantly affected by the specific surface area (SSA) of particles. Thus, increasing SSA progressively reduced the workability of the cementitious material, which is in line with what was observed in this study, considering that the SSA of L-IOT is around 817% higher than CP (1.934 m²/g). Furthermore, the irregular morphology of IOT (Fig. 4) also explains this behaviour. Previous studies also reported a loss of workability with the IOT incorporation in cement-based materials (GOU; ZHOU; THEN, 2019; GOULART BEZERRA et al., 2021; ZHAO; FAN; SUN, 2014).

3.3. Isothermal calorimetry

The heat flow and cumulative heat of L-IOT cement pastes are presented in Fig. 6. Incorporation progressively anticipated the main heat flow peak by up to approximately 3 h, while slightly reducing the peak value for L-IOT contents higher than 10 wt%. In fact, reductions of 3.3% (15 wt%) and 5.8% (20 wt%) were observed in the main heat flow peak. A filler effect can explain the anticipation of the main heat flow peak (i.e. a reduction in the induction period) with the IOT incorporation. This effect is widely reported in the literature and is associated with the additional surface provided by the L-IOT, resulting in nucleation sites for calcium silicate hydrate precipitation (BERODIER; SCRIVENER, 2014; LOTHENBACH; SCRIVENER; HOOTON, 2011b). The addition also reduced the cumulative heat after 70 h of hydration. These values range from 313.5 to 279.3 J/g for L-IOT contents between 0.0 and 20.0 wt%. This is to be expected, considering the reduction in the PC content, and is in agreement with the 3-d compressive strength results presented in Fig. 7, which also indicate slightly lower compressive strength results for the compositions with L-IOT contents higher than 10 wt%. Duarte et al. (2022) also observed a reduction in hydration heat with the IOT incorporation. Similarly, Yun-hong et al. (2022) reported reductions up to 62.2% for an IOT content of 50 wt% compared to the control sample.

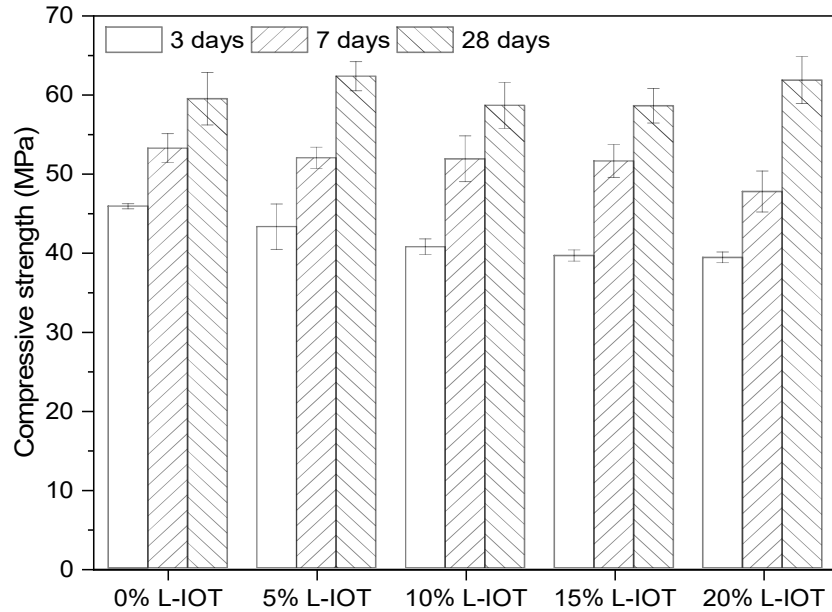
Figure V.06 - Heat flow and cumulative heat of IOT cement pastes



3.4. Compressive strength

The compressive strength at 3, 7, and 28 days of cement pastes, with L-IOT percentages of 0, 5, 10, 15, and 20 wt%, is shown in Fig. 7. At 3 days, for L-IOT contents greater than 10%, there were reductions of 13.7% in strength. This behaviour was maintained for the 7-day compressive strength values. Conversely, at 28 days, all evaluated compositions showed statistically equivalent strength. The stabilisation of ettringite and formation of carboaluminate phases in the presence of calcite (proven by the XRD and TGA results discussed ahead) leads to an increase in the total volume of the solid phases, as ettringite has a low density and, thus, a relatively large volume [56]. This explains the equivalent 28-d compressive strength of L-IOT containing cement pastes, even with lower PC contents.

Figure V.07 - Compressive strength of cement pastes at 3, 7, and 28 days



The removal of iron, combined with thermal activation, contributes to the best results of compressive strength. Li et al. (2010b) investigated roasting at high temperatures (greater than 700 °C) with combined magnetic separation for maximum iron removal available in IOT. The siliceous product (~6% Fe), obtained after iron removal, was used as cementitious material and showed better compressive strength results when compared to crude tailings, ≈25% Fe (Li et al., 2010a).

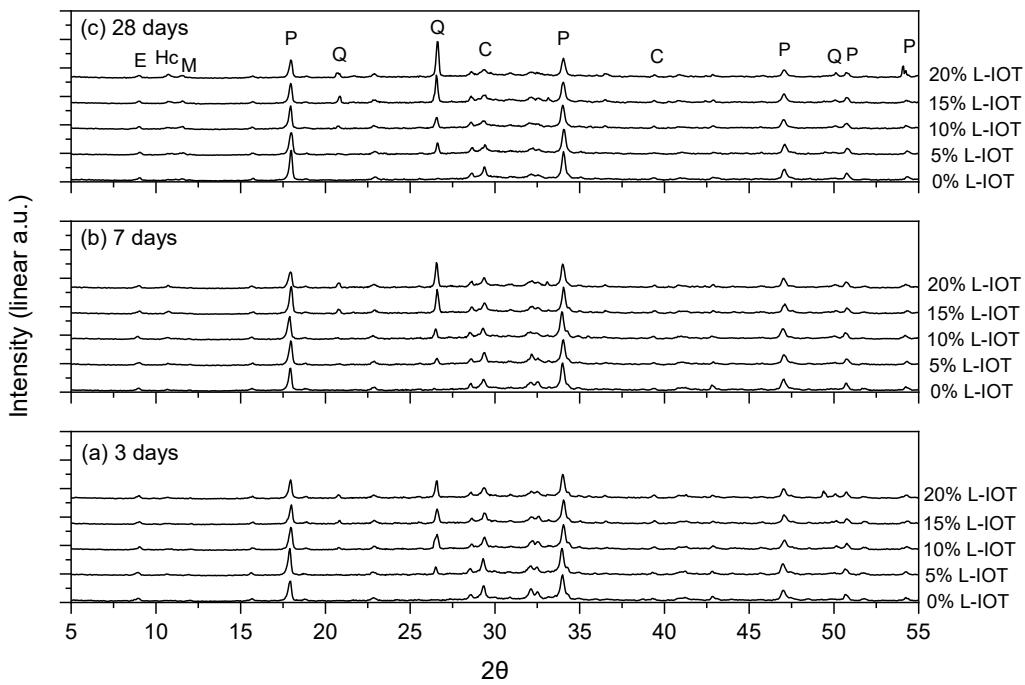
Magalhães et al. (2020) also investigated the thermal activation applied to iron ore tailings (~66% Fe) for use as SCM and showed gains in resistance concerning crude IOT. When evaluating 28-d compressive strength for the substitution ratios of 10% and 20% of IOT used in both researches, it should be noted that a sample of this study with lower iron concentration showed increases in compressive strength of 17% and 43%, respectively. These references reinforce the fact that the removal of iron by acid leaching, combined with thermal activation, contributes to obtaining a material with strong potential for use as SCM.

3.5. XRD analysis of L-IOT cement pastes

The main crystalline phases identified in the XRD patterns of cement pastes are presented in Fig. 8. The quartz peaks are attributed to L-IOT (see Fig. 3) and, thus, as

expected, a progressive increase with the SCM content. Moreover, the calcite peak identified is derived from the commercial Portland cement composition (ABNT, 2018).

Figure V.08 - XRD patterns of L-IOT cement pastes at (a) 3 days, (b) 7 days, and (c) 28 days (E - ettringite, Hc - hemicarboaluminate, M – monocarboaluminate, P – portlandite, Q – quartz, C – calcite)



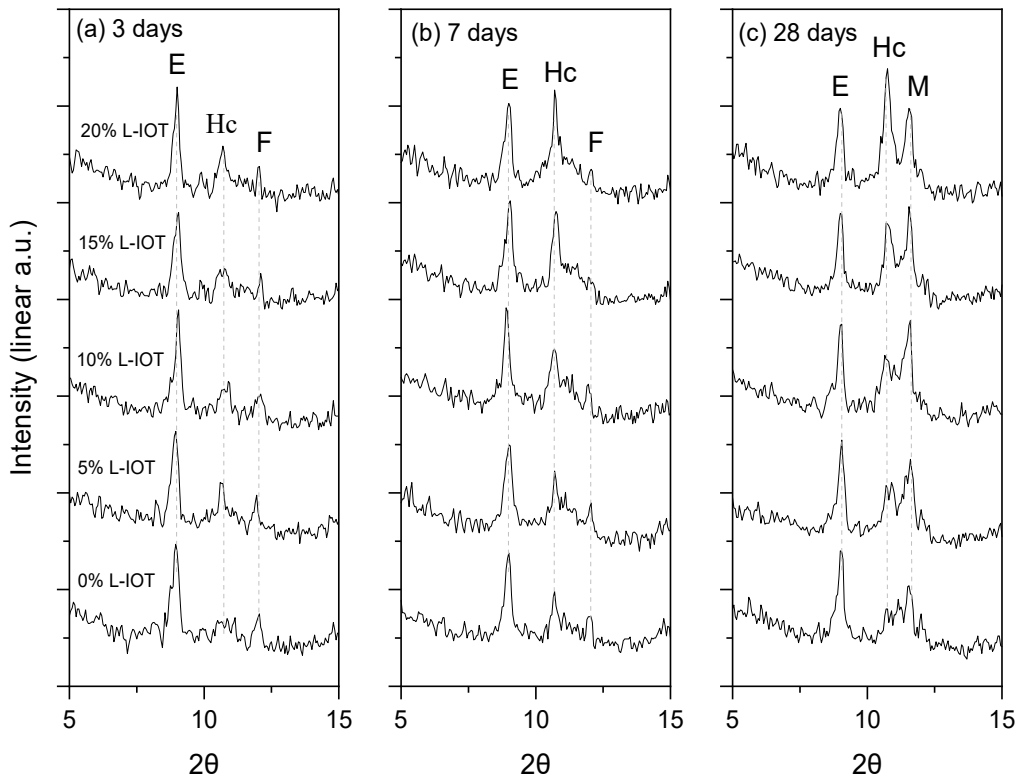
It can also be observed that the intensity of portlandite peaks progressively reduces with increasing L-IOT incorporation content, which is in agreement with the reduction in the amount of cement in the compositions. Another observation is that there are no significant changes in the intensity of the portlandite peaks over time, which suggests that the L-IOT residue does not have pozzolanic activity (further confirmed by the XRD and TGA results). This hypothesis is further confirmed with the TGA results, as discussed below. Bezerra et al. (2021) also reported that IOT did not exhibit pozzolanic activity when incorporated in cement pastes. Other studies reported similar results (PROTASIO et al., 2021; YAO et al., 2020b).

Nevertheless, it should be considered that the IOT employed in previous studies was not thermally activated. In addition, generally, the iron content of IOT in those studies was higher than the material assessed in this research, which makes the direct comparison of the results unfeasible. Another aspect that needs to be considered, that can influence the mineralogy of Portland cement pastes, is the alumina content in the L-IOT (see Section 2.1.), as will be discussed further below. In this context, it is

important to highlight that, usually, the most expected characteristic of waste for use as supplementary cementitious material is its pozzolanic activity. However, a better understanding of the formation of the carboaluminate phases (AFm phases) can change this perspective since this synergistic effect between the alumina present in some waste and the calcite (usually present in the commercial PC) can also have a positive impact on pore refinement and mechanical performance of cementitious matrices.

Fig. 9 exhibits the XRD patterns at a selected range from 5.0 to 15.0° 2θ of L-IOT cement pastes after 3, 7, and 28 days of hydration. After 3 days, ettringite (~9.0° 2θ), hemicarboaluminate (~10.8° 2θ), and ferrite (~12.0° 2θ) peaks were identified.

Figure V.09 - Selected range of XRD patterns from 5-15° 2θ of cement pastes at 3, 7, and 28 days (E – ettringite, F - ferrite Hc – hemicarboaluminate, M – monocarboaluminate)



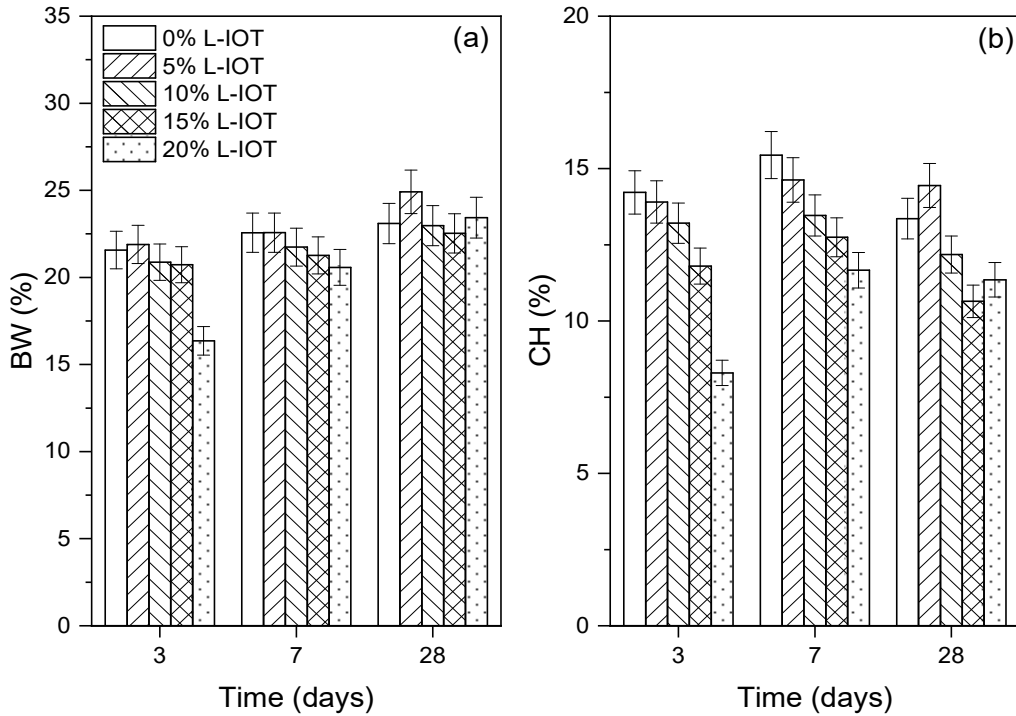
After 7 days of hydration, the hemicarboaluminate peak was significantly intensified. The aluminium in L-IOT reacted with the calcite in PC, favouring the formation of carboaluminate phases (Hc and M) instead of monosulfoaluminate (ADU-AMANKWAH et al., 2017; CARDINAUD et al., 2021; LOTHENBACH et al., 2008). In the early stages, the hemicarboaluminate is usually identified since its formation is

kinetically favoured, while the monocarboaluminate is usually identified in the latter stages (greater than 7 days) and considered to be more stable (GEORGET et al., 2022; ZAJAC et al., 2014). At 28 days, the hemicarboaluminate (H_c) peak intensity remains practically unchanged, while the monocarboaluminate (M) peak at around $11.6^\circ 2\Theta$ was also identified, indicating the progressive conversion of H_c into M .

3.6. TGA analysis of L-IOT cement pastes

The evolution of chemically bound water (BW) and portlandite content with time, determined by TGA, is shown in Fig. 10. After 3 days, the BW of 20.0 wt% L-IOT cement paste is 24.2% lower compared to the control sample. This is expected due to the reduction in cement content.

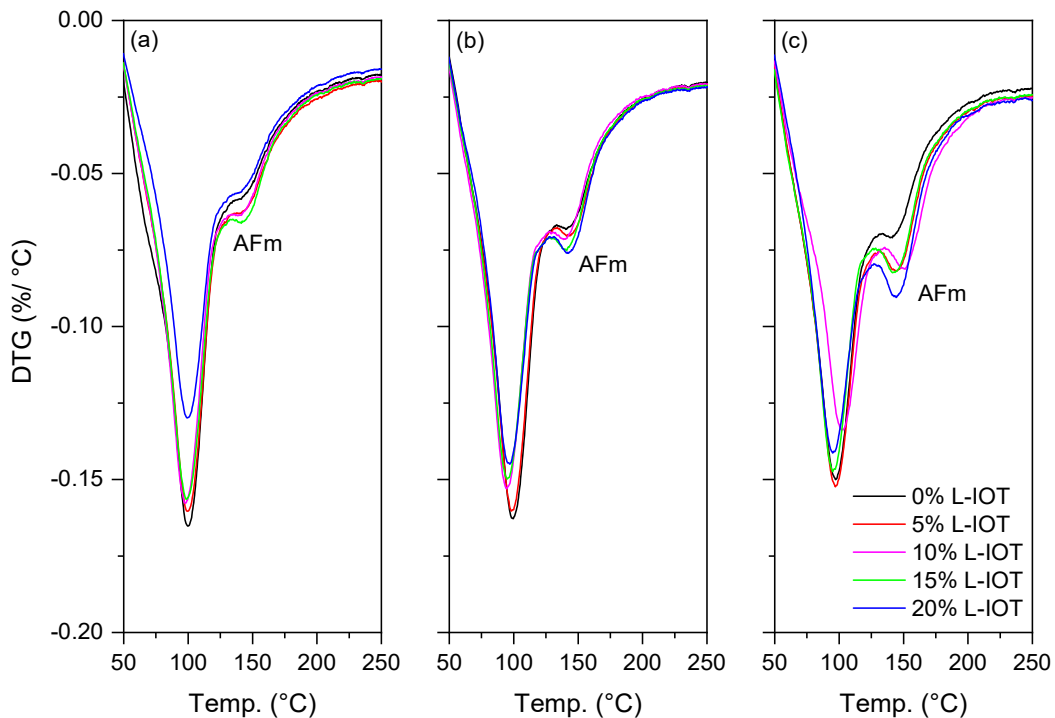
Figure V.10 - Bound water (a) and portlandite (b) contents of cement pastes after 3, 7, and 28 days determined by TGA. The standard deviation was adopted based on Scrivener et al. [44].



However, over time, there is a progressive increase in the BW content in 20 wt% L-IOT cement paste. At 28 days the chemically combined water content is equivalent to the control mix. This increase in BW is attributed to the formation of AFm phases over time, which can be identified by the increase in the peak weight loss around 150

°C indicated in Fig. 11 (SCRIVENER; SNELLINGS; LOTHENBACH, 2018). Furthermore, the evolution of portlandite content (Fig. 10b) shows that the L-IOT waste did not have a pozzolanic effect since, over time, there is no consumption of portlandite, which corroborates the XRD results.

Figure V.11 - Evolution of AFm phases in IOT cement pastes after 3, 7, and 28 days of hydration, as determined by TGA



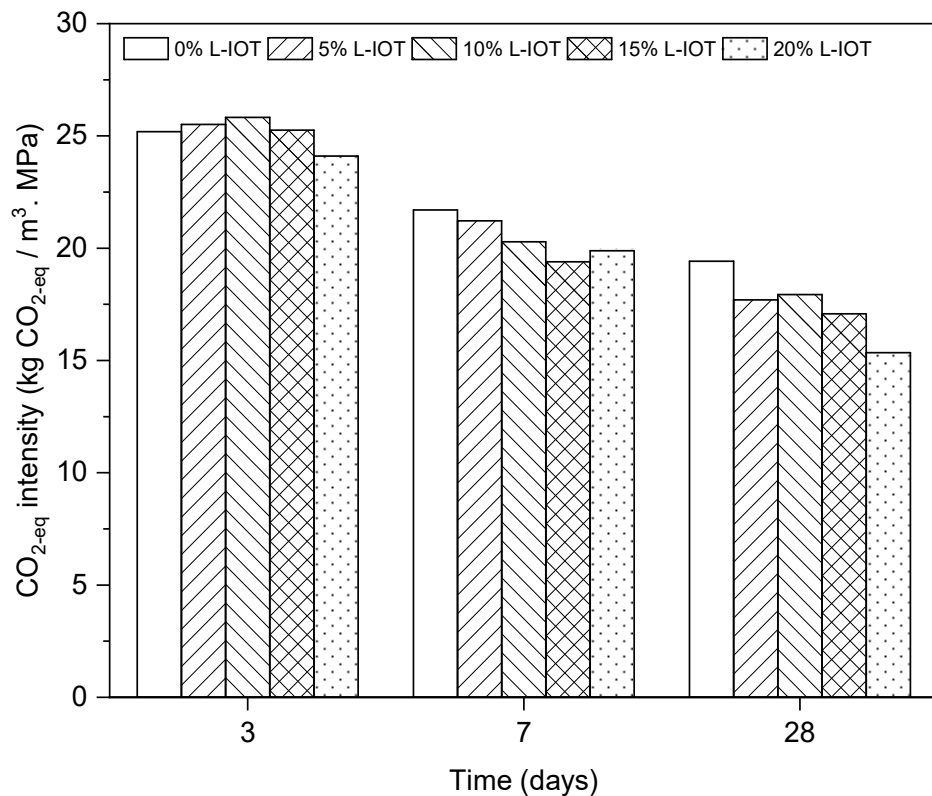
These results suggest that the activity of the L-IOT evaluated in this study is attributed, essentially, to the formation of the AFm phases and not to the pozzolanic activity, evidencing the importance of considering the synergistic effect between alumina from L-IOT and limestone filler present in commercial Portland cement. This discussion changes the perspective of evaluating the waste incorporated in cementitious matrixes.

3.7. CO₂ analysis and scale of use

The CO₂-eq intensity values of L-IOT cement pastes after 3, 7, and 28 days are presented in Fig. 12. Due to the lower compressive strength of the compositions with

IOT at 3 days, no significant changes were observed in CO₂-eq intensity compared to the plain cement paste.

Figure V.12 - CO₂-eq intensity (kg CO₂-eq/MPa · m³ of paste) at 3, 7, and 28 days



However, after 7 days, due to increases in the compressive strength of the compositions with L-IOT associated with the formation of carboaluminate phases (previously discussed in the XRD and TGA results), reductions of 2.2% (5.0% IOT), 6.5% (10.0% IOT), 10.6% (15.0% IOT), and 8.3% (20.0% IOT) in the CO₂-eq intensity were observed compared to the control sample. These values are more significant at 28 days, reaching reductions of up to 21.0% for the highest replacement content evaluated. This trend is associated with lower CO₂ emissions for IOT thermal activation compared to Portland cement production. Several authors reported similar results for other supplementary cementitious materials, such as calcined water treatment plant sludge (RUVIARO et al., 2021) and rice husk ash (GURSEL; MARYMAN; OSTERTAG, 2016). Yang et al. (2015) also reported that the CO₂ intensity decreased as the substitution replacement of the supplementary cementitious materials increased up to approximately 15–20 wt%. Specifically, regarding the IOT incorporation, this is the first

study that effectively evaluated CO₂ emissions from cementitious matrices with IOT as a partial replacement for Portland cement.

In addition to the reduction in CO₂ emissions, the use of leached IOT would allow the reduction in the amount of iron ore tailings that are destined for dams, maximising the use of natural resources. Based on Brazil's national cement production, which is approximately 60 million tons per year (SNIC, 2021), it would be possible to incorporate up to 12 million tons of leached IOT as SCM in the construction sector. In parallel, hydrometallurgical processing would also ensure the recovery of more than 15 million tons of iron oxides, currently not recovered by the mineral sector. Such applications that would allow the incorporation of about 20% of the iron ore tailings generated in Brazilian mining. These indicators reinforce the compatibility of scale between the mining and construction sectors and point out the environmental and economic benefits that can be achieved through the route proposed in this study.

4. CONCLUSION

Hot acid leaching applied to iron ore tailings is a technically feasible alternative that enables the maximum use of natural resources. The ferric liquor can be used as a coagulant in water and wastewater treatment and as a precursor for the synthesis of pure iron oxides. The solid phase, insoluble in hydrochloric acid, may contain silica content and alumina compatible with the application as supplementary cement material. In the current circumstances (L-IOT with 74% silica and 15% alumina), the mining material can replace Portland cement without impairing the compressive strength of cement pastes. The equivalent mechanical behaviour can be attributed to a synergistic effect between the alumina in the L-IOT and the limestone filler in conventional Portland cement. In this context, when waste is evaluated as SCM, besides the pozzolanic effect, the synergy that results in carboaluminate phases and a filling effect must also be considered. Moreover, in addition to an equivalent mechanical performance, the IOT incorporation reduces the equivalent CO₂ emissions by 21%, demonstrating technical and environmental feasibility. The rheological analysis indicated that the 20 wt% L-IOT incorporation increased the dynamic yield stress and equivalent viscosity of cement pastes by 1,450.0% and 393.0%, respectively. Nevertheless, it is suggested that further investigations assess the

rheological behaviour of IOT cement pastes with the incorporation of superplasticizer admixtures, aiming at the practical applicability of the material for conventional cementitious matrices. Usage of L-IOT as SCM provides a clear benefit, in terms of sustainability, which extends beyond the environmental sphere and is a possible business opportunity for the sectors involved.

ACKNOWLEDGEMENTS

Coordination for the Improvement of Higher Education Personnel (CAPES), National Council for Scientific and Technological Development (CNPq) and Foundation for Research Support of Santa Catarina (FAPESC) and Foundation for Research Support of Rio Grande do Sul (FAPERGS) are acknowledged. Artur Spat Ruviaro is recognised for his assistance in the CO₂ emission analysis.

REFERENCES

- Adu-Amankwah, S., Zajac, M., Stabler, C., Lothenbach, B., Black, L., 2017. Influence of limestone on the hydration of ternary slag cements. *Cem. Concr. Res.* 100, 96–109. <https://doi.org/10.1016/j.cemconres.2017.05.013>
- Almeida, V.O. de, Schneider, I.A.H., 2022. Hydrometallurgical Processing of Brazilian Iron Ore Tailings for the Synthesis of Pigments. *Geomaterials* 12, 30–36. <https://doi.org/10.4236/gm.2022.122003>
- Almeida, V.O., Schneider, I.A.H., 2020. Production of a ferric chloride coagulant by leaching an iron ore tailing. *Miner. Eng.* 156, 106511. <https://doi.org/10.1016/j.mineng.2020.106511>
- Asim, N., Badiei, M., Torkashvand, M., Mohammad, M., Alghoul, M.A., Gasaymeh, S.S., Sopian, K., 2021. Wastes from the petroleum industries as sustainable resource materials in construction sectors: Opportunities, limitations, and directions. *J. Clean. Prod.* 284. <https://doi.org/10.1016/j.jclepro.2020.125459>
- Asr, E.T., Kakaie, R., Ataei, M., Tavakoli Mohammadi, M.R., 2019. A review of studies on sustainable development in mining life cycle. *J. Clean. Prod.* 229, 213–231. <https://doi.org/10.1016/j.jclepro.2019.05.029>
- ASSOCIAÇÃO BRASILEIRA DE NORMAS TÉCNICAS, 2018. ABNT NBR 16697: Cimento Portland — Requisitos.
- Berodier, E., Scrivener, K., 2014. Understanding the filler effect on the nucleation and growth of C-S-H. *J. Am. Ceram. Soc.* 97, 3764–3773. <https://doi.org/10.1111/jace.13177>
- Bossle, M.B., Dutra De Barcellos, M., Vieira, L.M., Sauvée, L., 2016. The drivers for adoption of eco-innovation. *J. Clean. Prod.* 113, 861–872. <https://doi.org/10.1016/j.jclepro.2015.11.033>
- Bouafia, A., Laouini, S.E., 2020. Green synthesis of iron oxide nanoparticles by aqueous leaves extract of *Mentha Pulegium* L.: Effect of ferric chloride concentration on the type of product. *Mater. Lett.* 265, 127364. <https://doi.org/10.1016/j.matlet.2020.127364>

- Cardinaud, G., Rozière, E., Martinage, O., Loukili, A., Barnes-Davin, L., Paris, M., Deneele, D., 2021. Calcined clay – Limestone cements: Hydration processes with high and low-grade kaolinite clays. *Constr. Build. Mater.* 277, 122271. <https://doi.org/10.1016/j.conbuildmat.2021.122271>
- Carmignano, O.R., Vieira, S.S., Teixeira, A.P.C., Lameiras, F.S., Brandão, P.R.G., Lago, R.M., 2021. Iron Ore Tailings: Characterization and Applications. *J. Braz. Chem. Soc.* 32, 1895–1911. <https://doi.org/10.21577/0103-5053.20210100>
- Cechin, L., Mymrine, V., Avanci, M.A., Povaluk, A.E., 2022. Ceramics composites from iron ore tailings and blast furnace slag. *Ceram. Int.* 48, 10506–10515. <https://doi.org/10.1016/j.ceramint.2021.12.260>
- Damineli, B.L., Kemeid, F.M., Aguiar, P.S., John, V.M., 2010. Measuring the eco-efficiency of cement use. *Cem. Concr. Compos.* 32, 555–562. <https://doi.org/10.1016/j.cemconcomp.2010.07.009>
- Das, S.K., Kumar, S., Ramachandrarao, P., 2000. Exploitation of iron ore tailing for the development of ceramic tiles. *Waste Manag.* 20, 725–729. [https://doi.org/10.1016/S0956-053X\(00\)00034-9](https://doi.org/10.1016/S0956-053X(00)00034-9)
- Duarte, M.S., Almada, B.S., José dos Santos, W., Lima Bessa, S.A., Cesar da Silva Bezerra, A., Paulino Aguilar, M.T., 2022. Influence of mechanical treatment and magnetic separation on the performance of iron ore tailings as supplementary cementitious material. *J. Build. Eng.* 59, 105099. <https://doi.org/10.1016/j.jobe.2022.105099>
- Fontes, W.C., Franco de Carvalho, J.M., Andrade, L.C.R., Segadães, A.M., Peixoto, R.A.F., 2019. Assessment of the use potential of iron ore tailings in the manufacture of ceramic tiles: From tailings-dams to “brown porcelain.” *Constr. Build. Mater.* 206, 111–121. <https://doi.org/10.1016/j.conbuildmat.2019.02.052>
- Galvão, J.L.B., Andrade, H.D., Brigolini, G.J., Peixoto, R.A.F., Mendes, J.C., 2018. Reuse of iron ore tailings from tailings dams as pigment for sustainable paints. *J. Clean. Prod.* 200, 412–422. <https://doi.org/10.1016/j.jclepro.2018.07.313>

- Georget, F., Lothenbach, B., Wilson, W., Zunino, F., Scrivener, K.L., 2022. Stability of hemicarbonate under cement paste-like conditions. *Cem. Concr. Res.* 153, 106692. <https://doi.org/10.1016/j.cemconres.2021.106692>
- Gong, L., Liang, J., Kong, L., Chen, B., Li, Y., Tian, G., 2021. Synthesis of high-performance copper barium silicate composite pigment from waste iron ore tailings. *Ceram. Int.* 47, 27987–27997. <https://doi.org/10.1016/j.ceramint.2021.06.230>
- Gou, M., Zhou, L., Then, N.W.Y., 2019. Utilization of tailings in cement and concrete: A review. *Sci. Eng. Compos. Mater.* 26, 449–464. <https://doi.org/10.1515/secm-2019-0029>
- Goulart Bezerra, C., Abelha Rocha, C.A., Siqueira, I.S. de, Toledo Filho, R.D., 2021. Feasibility of iron-rich ore tailing as supplementary cementitious material in cement pastes. *Constr. Build. Mater.* 303, 124496. <https://doi.org/10.1016/j.conbuildmat.2021.124496>
- Gursel, A.P., Maryman, H., Ostertag, C., 2016. A life-cycle approach to environmental, mechanical, and durability properties of “green” concrete mixes with rice husk ash. *J. Clean. Prod.* 112, 823–836. <https://doi.org/10.1016/j.jclepro.2015.06.029>
- Han, F., Song, S., Liu, J., Wu, R., 2021. Effect of water/binder ratio and temperature on the hydration heat and properties of ternary blended cement containing slag and iron tailing powder. *J. Therm. Anal. Calorim.* 144, 1115–1128. <https://doi.org/10.1007/s10973-020-09687-8>
- Huang, X., Ranade, R., Li, V.C., 2013. Feasibility Study of Developing Green ECC Using Iron Ore Tailings Powder as Cement Replacement. *J. Mater. Civ. Eng.* 25, 923–931. [https://doi.org/10.1061/\(asce\)mt.1943-5533.0000674](https://doi.org/10.1061/(asce)mt.1943-5533.0000674)
- Jayasimha, N., Sujini, B., Annapurna, B.P., 2022. A study on durability and strength properties of high strength concrete with partial replacement of iron ore tailings with fine aggregates. *Mater. Today Proc.* <https://doi.org/10.1016/j.matpr.2022.05.163>
- Krishna, R.S., Mishra, J., Meher, S., Das, S.K., Mustakim, S.M., Singh, S.K., 2020. Industrial solid waste management through sustainable green technology: Case study insights from steel and mining industry in Keonjhar, India. *Mater. Today Proc.* 33, 5243–5249. <https://doi.org/10.1016/j.matpr.2020.02.949>

Kumar Sethi, C., Parimita Patnaik, P., Kumar Acharya, S., Nath Thatoi, D., 2022. An efficient approach for emission reduction in diesel engine with ferric chloride as catalyst and yttria stabilized zirconia as thermal barrier coating. *Mater. Today Proc.* 62, 7438–7445. <https://doi.org/10.1016/j.matpr.2022.03.317>

Li, C., Sun, H., Yi, Z., Li, L., 2010a. Innovative methodology for comprehensive utilization of iron ore tailings. Part 1: The recovery of iron from iron ore tailings using magnetic separation after magnetizing roasting. *J. Hazard. Mater.* 174, 78–83. <https://doi.org/10.1016/j.jhazmat.2009.09.019>

Li, C., Sun, H., Bai, J., Li, L., 2010b. Innovative methodology for comprehensive utilization of iron ore tailings. Part 2: The residues after iron recovery from iron ore tailings to prepare cementitious material. *J. Hazard. Mater.* 174, 71–77. <https://doi.org/10.1016/j.jhazmat.2009.09.018>

Ljubetic, K., Liu, W., 2022. Kinetic limitations of gold leaching in ferric chloride media Part I: Batch reactor studies. *Miner. Eng.* 178, 107397. <https://doi.org/10.1016/j.mineng.2022.107397>

Lothenbach, B., Le Saout, G., Gallucci, E., Scrivener, K., 2008. Influence of limestone on the hydration of Portland cements. *Cem. Concr. Res.* 38, 848–860. <https://doi.org/10.1016/j.cemconres.2008.01.002>

Lothenbach, B., Scrivener, K., Hooton, R.D., 2011. Supplementary cementitious materials. *Cem. Concr. Res.* 41, 1244–1256. <https://doi.org/10.1016/j.cemconres.2010.12.001>

Magalhães, L.F. de, França, S., Oliveira, M. dos S., Peixoto, R.A.F., Bessa, S.A.L., Bezerra, A.C. da S., 2020. Iron ore tailings as a supplementary cementitious material in the production of pigmented cements. *J. Clean. Prod.* 274. <https://doi.org/10.1016/j.jclepro.2020.123260>

Marques, B., Tadeu, A., De Brito, J., Almeida, J., 2017. A perspective on the development of sustainable construction products: An eco-design approach. *Int. J. Sustain. Dev. Plan.* 12, 304–314. <https://doi.org/10.2495/SDP-V12-N2-304-314>

Matos, P.R. de, Foiato, M., Prudêncio, L.R., 2019. Ecological, fresh state and long-term mechanical properties of high-volume fly ash high-performance self-compacting

concrete. Constr. Build. Mater. 203, 282–293.
<https://doi.org/10.1016/j.conbuildmat.2019.01.074>

Mendes, B.C., Pedroti, L.G., Fontes, M.P.F., Ribeiro, J.C.L., Vieira, C.M.F., Pacheco, A.A., Azevedo, A.R.G. d., 2019. Technical and environmental assessment of the incorporation of iron ore tailings in construction clay bricks. Constr. Build. Mater. 227, 116669. <https://doi.org/10.1016/j.conbuildmat.2019.08.050>

Mohamad, N., Muthusamy, K., Embong, R., Kusbiantoro, A., Hashim, M.H., 2021. Environmental impact of cement production and Solutions: A review. Mater. Today Proc. 48, 741–746. <https://doi.org/10.1016/j.matpr.2021.02.212>

Patnaik, P.P., Acharya, S.K., Padhi, D., Mohanty, U.K., 2016. Experimental investigation on CI engine performance using steam injection and ferric chloride as catalyst. Eng. Sci. Technol. an Int. J. 19, 2073–2080.
<https://doi.org/10.1016/j.estch.2016.07.006>

Peng, Y., Ma, K., Unluer, C., Shi, J., Long, G., 2021. Method for calculating dynamic yield stress of fresh cement pastes using a coaxial cylinder system 1–14. <https://doi.org/10.1111/jace.17979>

Protasio, F.N.M., Ribeiro de Avillez, R., Letichevsky, S., de Andrade Silva, F., 2021. The use of iron ore tailings obtained from the Germano dam in the production of a sustainable concrete. J. Clean. Prod. 278, 278.
<https://doi.org/10.1016/j.jclepro.2020.123929>

Ramakrishna Balaji, C., Azevedo, A.R.G. de, Madurwar, M., 2022. Sustainable perspective of ancillary construction materials in infrastructure industry: An overview. J. Clean. Prod. 365, 132864. <https://doi.org/10.1016/j.jclepro.2022.132864>

Reis, D.C., Quattrone, M., Souza, J.F.T., Punhagui, K.R.G., Pacca, S.A., John, V.M., 2021. Potential CO₂ reduction and uptake due to industrialization and efficient cement use in Brazil by 2050. J. Ind. Ecol. 25, 344–358. <https://doi.org/10.1111/jiec.13130>

Ruviaro, A.S., Silvestro, L., Scolaro, T.P., de Matos, P.R., Pelisser, F., 2021. Use of calcined water treatment plant sludge for sustainable cementitious composites production. J. Clean. Prod. 327, 129484. <https://doi.org/10.1016/j.jclepro.2021.129484>

- Sá, T.S.W., Oda, S., Karla Castelo Branco Louback Machado Balthar, V., Dias Toledo Filho, R., 2022. Use of iron ore tailings and sediments on pavement structure. *Constr. Build. Mater.* 342, 128072. <https://doi.org/10.1016/j.conbuildmat.2022.128072>
- Safiuddin, M., Jumaat, M.Z., Salam, M.A., Islam, M.S., Hashim, R., 2010. Utilization of solid wastes in construction materials. *Int. J. Phys. Sci.* 5, 1952–1963.
- Sahu, O., Chaudhari, P., 2013. Review on Chemical treatment of Industrial Waste Water. *J. Appl. Sci. Environ. Manag.* 17. <https://doi.org/10.4314/jasem.v17i2.8>
- Saththasivam, J., Ogunbiyi, O., Lawler, J., Al-Rewaily, R., Liu, Z., 2022. Evaluating dissolved air flotation for oil/water separation using a hybridized coagulant of ferric chloride and chitosan. *J. Water Process Eng.* 47, 102836. <https://doi.org/10.1016/j.jwpe.2022.102836>
- Schlomer, S., Bruckner, T., Fulton, L., Hertwich, E., Mckinnon, A., Perczyk, D., Roy, J., Schaffer, R., Sims, R., Smith, P., Wiser, R., 2014. Technology-specific Cost and Performance Parameters.
- Scolaro, T.P., Silvestro, L., Ruviaro, A.S., de Azevedo, A.R.G., Monteiro, S.N., Pelisser, F., 2022. Effect of Ornamental Stone Waste Incorporation on the Rheology, Hydration, Microstructure, and CO₂ Emissions of Ordinary Portland Cement. *Materials* (Basel). 15. <https://doi.org/10.3390/ma15020401>
- Scrivener, K., Martirena, F., Bishnoi, S., Maity, S., 2018a. Calcined clay limestone cements (LC3). *Cem. Concr. Res.* 114, 49–56. <https://doi.org/10.1016/j.cemconres.2017.08.017>
- Scrivener, K., Snellings, R., Lothenbach, B., 2018b. A Practical Guide to Microstructural Analysis of Cementitious Materials, Taylor & Francis Group. <https://doi.org/10.1201/b19074>
- Shettima, A.U., Hussin, M.W., Ahmad, Y., Mirza, J., 2016. Evaluation of iron ore tailings as replacement for fine aggregate in concrete. *Constr. Build. Mater.* 120, 72–79. <https://doi.org/10.1016/j.conbuildmat.2016.05.095>
- Silvestro, L., Spat Ruviaro, A., Ricardo de Matos, P., Pelisser, F., Zambelli Mezalira, D., Jean Paul Gleize, P., 2021. Functionalization of multi-walled carbon nanotubes with

3-aminopropyltriethoxysilane for application in cementitious matrix. *Constr. Build. Mater.* 311, 125358. <https://doi.org/10.1016/j.conbuildmat.2021.125358>

Sindicato Nacional da Indústria do Cimento – SNIC, 2021. Produção Nacional de Cimento por regiões e estados.

Votorantim Cimentos, 2016. EPD – Environmental Product Declaration: CP II E 40, CP III-40 RS and CP V-ARI.

Wadsö, L., 2010. Operational issues in isothermal calorimetry. *Cem. Concr. Res.* 40, 1129–1137. <https://doi.org/10.1016/j.cemconres.2010.03.017>

Wallevik, O.H., Feys, D., Wallevik, J.E., Khayat, K.H., 2015. Avoiding inaccurate interpretations of rheological measurements for cement-based materials. *Cem. Concr. Res.* 78, 100–109. <https://doi.org/10.1016/j.cemconres.2015.05.003>

Wang, Z., Che, J., Ye, C., 2010. Application of ferric chloride both as oxidant and complexant to enhance the dissolution of metallic copper. *Hydrometallurgy* 105, 69–74. <https://doi.org/10.1016/j.hydromet.2010.07.013>

Wei, Z., Jia, Y., Wang, S., Li, Z., Li, Y., Wang, X., Gao, Y., 2022. Utilization of iron ore tailing as an alternative mineral filler in asphalt mastic: High-temperature performance and environmental aspects. *J. Clean. Prod.* 335, 130318. <https://doi.org/10.1016/j.jclepro.2021.130318>

Yang, K.H., Jung, Y.B., Cho, M.S., Tae, S.H., 2015. Effect of supplementary cementitious materials on reduction of CO₂ emissions from concrete. *J. Clean. Prod.* 103, 774–783. <https://doi.org/10.1016/j.jclepro.2014.03.018>

Yao, G., Wang, Q., Wang, Z., Wang, J., Lyu, X., 2020. Activation of hydration properties of iron ore tailings and their application as supplementary cementitious materials in cement. *Powder Technol.* 360, 863–871. <https://doi.org/10.1016/j.powtec.2019.11.002>

Yun-hong, C., Si-hui, Y., Jing-yu, Z., Xiao-hui, S., 2022. Test research on hydration process of cement-iron tailings powder composite cementitious materials. *Powder Technol.* 399, 117215. <https://doi.org/10.1016/j.powtec.2022.117215>

- Zajac, M., Rossberg, A., Le Saout, G., Lothenbach, B., 2014. Influence of limestone and anhydrite on the hydration of Portland cements. *Cem. Concr. Compos.* 46, 99–108. <https://doi.org/10.1016/j.cemconcomp.2013.11.007>
- Zhang, L.V., Zhang, Y., Liu, B., Gu, X., Nehdi, M.L., 2022. Mechanochemical Activation of Iron Ore Tailing-Based Ternary Supplementary Cementitious Materials. *SSRN Electron. J.* 346, 128420. <https://doi.org/10.2139/ssrn.4004685>
- Zhao, S., Fan, J., Sun, W., 2014. Utilization of iron ore tailings as fine aggregate in ultra-high performance concrete. *Constr. Build. Mater.* 50, 540–548. <https://doi.org/10.1016/j.conbuildmat.2013.10.019>

CAPÍTULO VI

HYDROMETALLURGICAL PROCESSING OF IRON ORE TAILINGS (IOT):

KINETICS OF IRON EXTRACTION BY HYDROCHLORIC ACID LEACHING

ARTIGO 5**Hydrometallurgical processing of iron ore tailings (IOT): kinetics of iron extraction by hydrochloric acid leaching**

Vitor O. Almeida¹, Ivo A.H. Schneider^{1*}

¹ Universidade Federal do Rio Grande do Sul (UFRGS) - LTM - DEMIN/PPGE3M, Av. Bento Gonçalves 9500, CEP: 91501-970, Porto Alegre, RS, Brasil

* Corresponding author

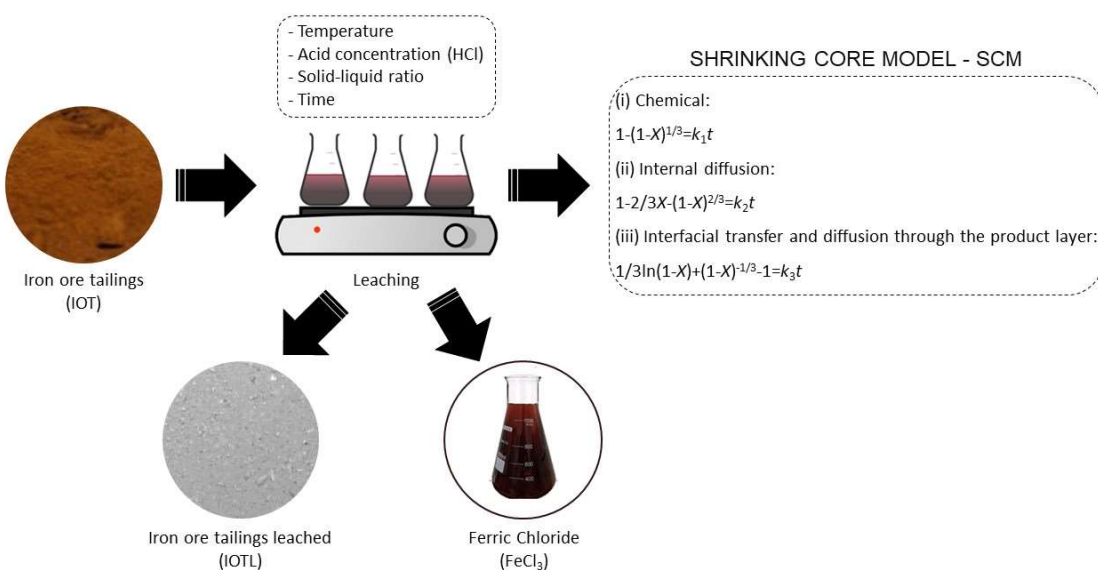
Artigo submetido na *Minerals Engineering* (ISSN: 1872-9444 | Impact Factor 4.8 | Qualis A1 - Quadriênio 2017-2020)

ABSTRACT

Hydrometallurgical processing of IOT has been used to remove iron present as an impurity and to obtain iron-rich liquors that can be used as chemical coagulants and silica-free oxides and in the synthesis of pigments. The aim of this work was to study the kinetics of iron extraction from iron ore tailings (IOT) by acid leaching. Experiments were carried out on a laboratory scale with Itabiritic Ore from Minas Gerais, Brazil, considering the effect of hydrochloric acid concentration, temperature, and the solid/liquid ratio in a batch system simulating a perfect mixed reactor. The shrinking core model was used for kinetic analysis of the leaching process. The leaching process was controlled by internal diffusion control, and the activation energy of the extraction reaction was determined to be 44.6 kJ mol⁻¹ according to the Arrhenius equation. The reaction order is 1.29 with respect to acid concentration. The conditions that configured the maximum iron recovery were a temperature of 80 °C, a solid/liquid ratio of 1:3, an acid concentration of 10.8 mol L⁻¹, and a leaching time of 150 minutes. The corresponding kinetic expression for the leaching process is $1-2/3X-(1-X)^{2/3}=35.84C_{HCl}^{1.29}\varepsilon_{S/L}^{-1.94}\exp[-44584/(RT)]$.

Keywords: iron recovery, sustainable mining, waste reuse, internal diffusion model

GRAPHICAL ABSTRACT



1. INTRODUCTION

Hydrometallurgical processing is fundamental for the production of certain mineral commodities (Habashi, 1998; Havlík, 2008). It has been increasingly suggested to process waste within the concept of “circular hydrometallurgy” (Nagarajan and Panchatcharam, 2023; Ndlovu et al., 2017; Xie et al., 2023) given the potential to reuse reagents, integrate processes, save energy, and assist in the perspective of zero waste mining (Binnemans and Jones, 2023; Doyle, 2005).

Worldwide, iron ore tailings (IOT) comprise an annual production in the order of billions of metric tons, and they are the main mineral waste produced in Brazil (Carmignano et al., 2021; Xu et al., 2019). IOTs are composed of fine mineral particles, with a chemical and mineralogical composition variable accordingly to the geology of the iron deposit and the concentration process adopted. Generally, the main components are silica, hematite, goethite, kaolinite, gibbsite, and biotite (Carmignano et al., 2021; Guimarães et al., 2012; Ferreira et al., 2022; Young and Yang, 2019).

Initiatives have been carried out to maximise the recovery of the iron available in tailings. Some investigations focused on the optimisation of flotation and magnetic separation processes or their combined use (Araujo et al., 2020; Dauce et al., 2019; Sun et al., 2020). On the other hand, according to our knowledge, other recent research touches on solutions via hydrometallurgical processes. This research considers the recovery of iron via hot acid leaching, achieving a liquor that can be used as a coagulant (Almeida and Schneider, 2020), in pigments (Almeida and Schneider, 2022), and as a source of high-purity silica-free iron oxide (Almeida et al., 2023a). The remaining solid phase has characteristics that make it useful as cementitious supplementary material (Almeida et al., 2023b) and high-grade silica (Li et al., 2023a, 2023b).

Almeida and Schneider (2020) showed that a good condition for acid leaching of Brazilian iron tailings occurs with a 10.8 mol L^{-1} hydrochloric acid solution at a temperature of 80°C and with a reaction time of approximately 2 hours, reaching iron recovery levels of 95%. However, these are not necessarily the best conditions since high iron recoveries can be reached by varying acid concentration, temperature, and time. It should also be noted that there is also information in the literature about iron leaching since iron is reported in extractive metallurgy as a critical contaminant in the

processing of some minerals (Havlík, 2008; Hoeber and Steinlechner, 2021; Ismael and Carvalho, 2003; Monhemius, 2017).

From this perspective, the central objective of this study is to model the kinetics and understand the mechanism of iron leaching from IOT, aiming to contribute to the scenario of iron ore tailings utilisation. The conditions of temperature, solid-liquid ratio, stirring speed, and hydrochloric acid (HCl) concentration in a leaching system at atmospheric pressure were evaluated to find an equation that relates these parameters with iron recovery.

2. EXPERIMENTAL SETUP

2.1 Iron Ore Tailings (IOT)

The iron ore tailings (IOT) came from a mine in the Quadrilátero Ferrífero (Minas Gerais, Brazil). The sample presented an average particle size of around 55 µm, with particle size distribution ranging from 0.04 to 250 µm. The specific surface area, measured by the BET method, was 11.90 m² g⁻¹. Typically, the particles presented a rounded to sub-rounded shape. The sample was predominantly composed of silica (62%) and hematite (31%), confirmed by the results of XRF and ICP-OES. The complete characterisation of the IOT was presented in Almeida and Schneider (2020). It should be noted that the chemical and mineralogical composition is compatible with the common characteristics of iron ore tailings from Minas Gerais, as presented in Carmignano et al. (2021).

2.2 Leaching procedure

The reagent used for acid leaching studies was analytical grade HCl, supplied by Química Moderna (Barueri, SP, BRA). Distilled water was used for the preparation of all solutions.

The dissolution process was carried out in 100 mL volumetric flasks heated on a hot plate equipped with a magnetic stirrer. The volume of solution to be used for leaching was set at 25 mL. The temperature of the solution was continuously monitored

by a thermometer. During leaching experiments, one of the parameters was varied while other parameters were maintained constant. At the end of the leaching, the slurry was filtered with a Unifil qualitative filter (80 g | Ø18.5 cm).

Each leaching condition investigated was carried out in triplicate ($n = 3$), and the results are reported in terms of average, maximum, and minimum. The variables evaluated were as follows: (i) acid concentration (HCl) 7.2, 9.6, and 10.8 mol L⁻¹; (ii) temperature 60 °C, 70°C, 80 °C, and 90 °C; (iii) solid-liquid (S/L) ratio 1:1.5, 1:3, and 1:4 g mL⁻¹; and (iv) time 15 min, 30 min, 60 min, 90 min, 120 min, and 150 min.

Stirring intensity and particle size were also considered as possible parameters that could influence the process. Preliminary tests allowed us to identify that the agitation speed has a positive effect on the leaching of iron, but only in the first 60 minutes of leaching. After this period, there is a stabilisation between the different velocities evaluated. Therefore, the trials were conducted with the adoption of a stirring speed of 100 rpm as a fixed parameter for the tests. The effect of particle size on iron dissolution also had a minor effect on the rate of dissolution under the studied conditions. The same behavior was observed by ZHANG and NICOL (2010) working in a particulate sample for iron dissolution from ilmenite in a particle size range similar to those of this study. Thus, the trials were conducted without dividing the sample into sizes fractions.

2.3 Analysis

The solutions produced in the leaching of the IOT were analysed as a function of the concentration of dissolved iron in the form of Fe_{total}, according to the method presented in VOGEL (1981).

The efficiency of iron leaching (R_{Fe}) was calculated by Equation 1:

$$R_{Fe} = \frac{V * C_{Fe}}{m * w_{Fe}} * 100 \quad (1)$$

where C_{Fe} is the iron concentration in the filtrate as g L⁻¹; V is the volume of the iron chloride solution in litres; m is the mass of the IOT load used in each individual experiment in grams; w_{Fe} is the per cent of iron in the crude IOT.

The liquor was analysed by inductively coupled plasma spectroscopy (ICP), using an OPTIMA 8300 DV model (Perkin Elmer, United States) to determine the dissolved metal contents.

2.4 Shrinking core model (SC)

The shrinking core model (SC) is always applied to describe the leaching kinetics where there is a reduction in both the mass and the particle size of the solid during leaching. The IOT after leaching can have a mass loss of up to 30% and a reduction in the granulometric range from 0.04 to 300 to 0.2 to 170 μm (with the consequent reduction in the average particle size from 54.5 μm to 46.4 μm) after acid leaching process (Almeida et al., 2023b; Almeida and Schneider, 2020).

For this, the particles are assumed to be perfectly homogeneous spherical solids (Alafara et al., 2015; Sultana and Kurny, 2012). The Following equations were used in this study:

$$1-(1-X)^{1/3}=k_1t \quad (4)$$

$$1-2/3X-(1-X)^{2/3}=k_2t \quad (5)$$

$$1/3\ln(1-X)+(1-X)^{-1/3}-1=k_3t \quad (6)$$

Where X is the rate of Fe leaching; k_i is the apparent leaching rate constant; and t is the leaching time. Equation (4) is a chemical reaction-controlled process. Equation (5) describes the processes limited by internal diffusion, and Equation (6) is a modified SCM that describes the kinetics controlled by interfacial transfer and diffusion through the product layer, according to Valeev et al. (2021).

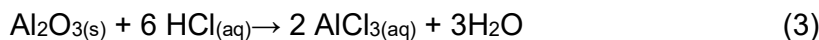
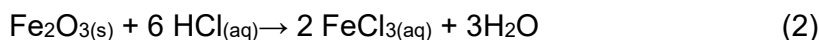
The apparent activation energy can be calculated using the Arrhenius equation:

$$k = k_0 \exp [-E_a/(RT)] \quad (7)$$

where k is the reaction rate constant represented by the slope of the leaching kinetic curve resulting from inserting the experimental data into Eq. (5); k_0 is the pre-exponential factor (min^{-1}); E_a is the activation energy (kJ mol^{-1}); R is the mole gas constant ($8.314 \text{ J}/(\text{mol}\cdot\text{K})$); and T is the reaction temperature (K).

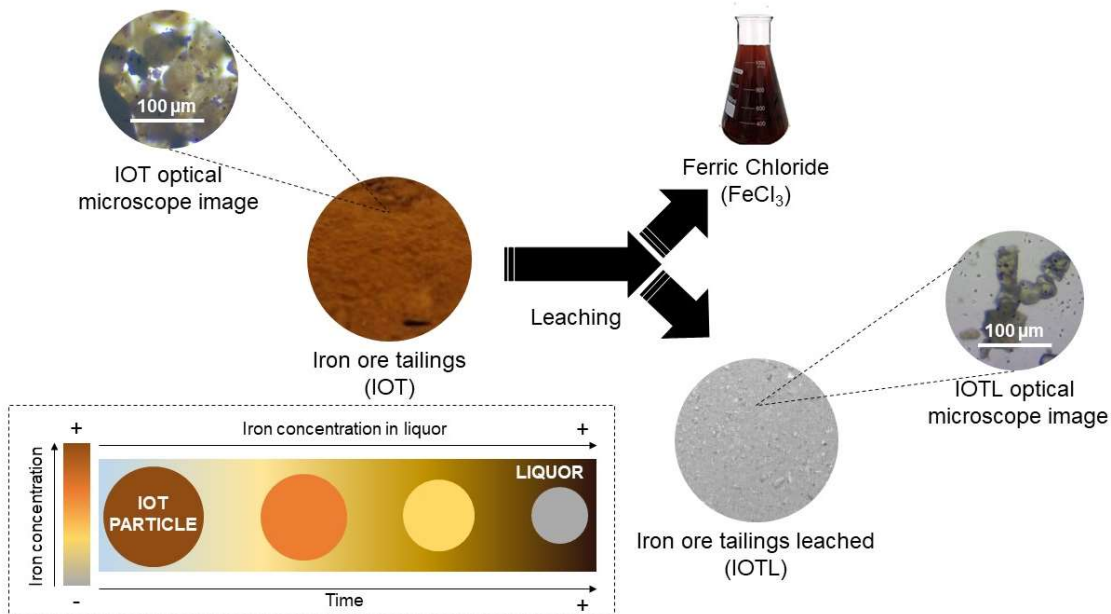
3. RESULTS AND DISCUSSION

The chemical analysis of the tailings allowed the identification of Si, Fe, and Al as the main components, which correspond, in the form of their respective oxides, to about 99% of the composition of this residue. In addition, the material has a fine grain size and a high specific surface area. These aspects corroborate the use of a hydrometallurgical process to recover the elemental species present in the IOT. Considering acid leaching with hydrochloric acid, the main chemical reactions evidenced in this process are shown in Equations 2 and 3:



Beyond iron and aluminium, the other major component of this waste is silica, which does not react with hydrochloric acid under the conditions investigated. For this reason, the leaching results in two products: a ferric liquor and a solid phase rich in silica (Figure 1).

Figure VI.01. Leaching products and iron dissolving behaviour.



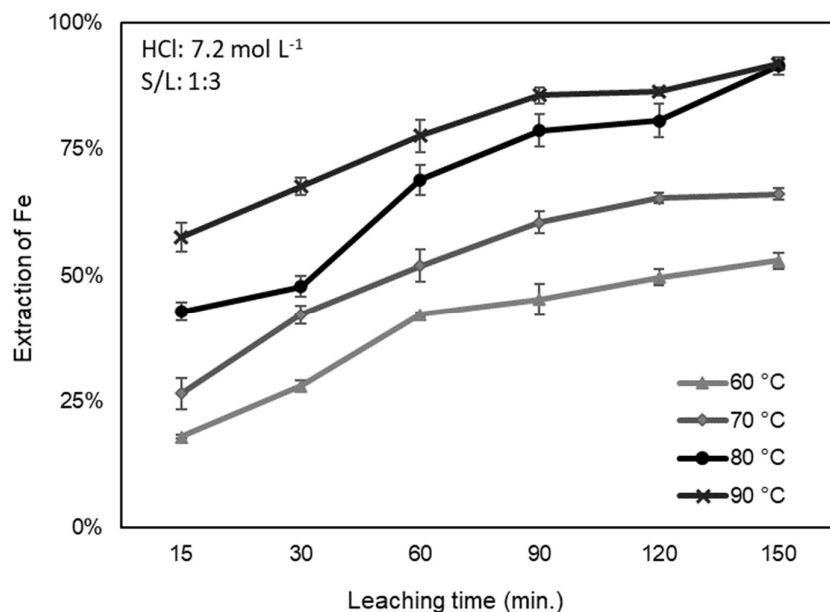
According to Almeida and Schneider (2020), the ferric liquor presented a concentration of 113 g L^{-1} of iron, which corresponds to the dissolution of 95% of the iron present in the IOT. To a lesser extent, 35% of the aluminium is recovered in the

liquid phase. In the temperature range investigated (60 °C to 90°C), low extraction of Al was observed, which is a result of the low reactivity of the mineral phases that contain this element (Paul et al., 2006; Seferinoglu, 2003). In parallel, the solid phase concentrated the SiO₂ (90%) and the remainder of the non-solubilized Al₂O₃ (6%). Also, it contained around 3% residual Fe₂O₃ (Almeida and Schneider (2020)). The constraints that govern this process and its respective kinetic model were investigated and will be discussed below.

3.1 Effect of temperature on iron dissolution in IOT

The temperature was evaluated in the leaching behaviour of the iron ore tailings, and the results can be seen in Figure 2. Temperature is an important factor affecting the kinetics of leaching, and higher temperatures are used to increase the leaching rate (WANG et al., 2019). It is observed that raising the temperature has a significant effect on the dissolution of iron and confers an increase in iron extraction. The percentage of iron dissolution was 53% and 66% for temperatures of 60 °C and 70 °C, respectively, at a concentration of 7.2 mol L⁻¹ of HCl and a solid-liquid ratio of 1:3. At temperatures above 80 °C, it was possible to obtain greater than 90% recovery of the iron in the liquor.

Figure VI.02. Effect of temperature on the dissolution of iron present in the IOT. Conditions: HCl concentration of 7.2 mol L⁻¹, solid-liquid ratio of 1:3, and stirring speed of 100 rpm.



From the temperature data, the kinetic models that best represent the dissolution of iron by HCl were evaluated. The data from the leaching curves in Figure 2 were fitted to the models (Eqs. 4–6), and the results of the mathematical modelling are presented in Figure 3. The correlation coefficient (R^2) showed the deviation of the experimental data from the ideal straight curve for the three SC models (Table 1).

Figure VI.03. Results of fitting the experimental data into the SC model: (A) chemical reaction process, (B) internal diffusion, and (C) interfacial transfer and diffusion through the product layer.

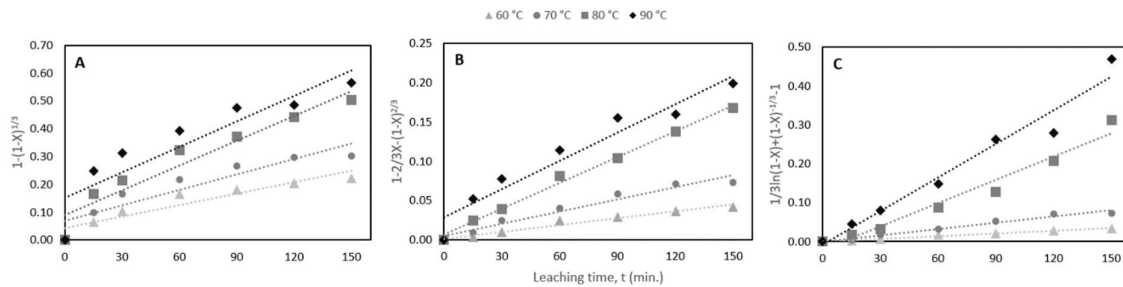


Table VI.01. Shrinking core model comparison by correlation coefficient (R^2) for temperature results.

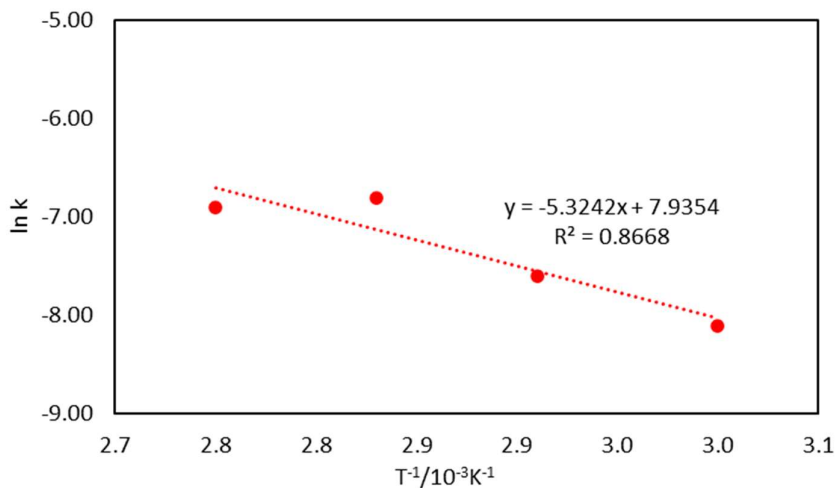
Temperature	$1-(1-X)^{1/3}$	$1-2/3X(1-X)^{2/3}$	$1/3\ln(1-X)+(1-X)^{-1/3}-1$
60 °C	0.9055	0.9585	0.9792
70 °C	0.9036	0.9476	0.9713
80 °C	0.9839	0.9951	0.9651
90 °C	0.9594	0.9676	0.9524

The correlation coefficients were >0.90 for the three calculated models. It is observed that the correlation coefficients present higher values at temperatures of 80 °C and 90 °C. Among the models, the internal diffusion model (Eq. 5) provided the best fit, even if very close to the interfacial transfer and diffusion through the product layer (Eq. 6) and the chemical reaction process (Eq. 4), showing that the process of leaching is controlled by the physical structure of the grains. This result is in accordance with the work of Huang et al (2013) and Yang and Li (2020), who identified internal diffusion as the best kinetic model to describe hot acid iron leaching (Huang et al., 2013; Yang and Li, 2020).

Based on these data, the mathematical model of internal diffusion was selected for evaluation of the activation energy (E_a) associated with the reaction of IOT leaching by HCl. To calculate the E_a , the values of $\ln k$ were plotted as a function of $T^{-1} / 10^{-3} K^{-1}$

¹, where k was the reaction rate constant represented by the slope of the curve (Figure 4). The data indicate an endothermic reaction with activation energy (E_a) of 44.58 kJ/mol calculated from the Arrhenius Equation (Eq. 7). This value is very close to the value of 45.37 kJ/mol attained by Huang et al. (2013) studying the leaching kinetics of iron from quartz sand.

Figure VI.04. Arrhenius plot for iron dissolution at leaching temperatures from 60 to 90 °C, HCl concentration of 7.2 mol L⁻¹, solid-liquid ratio of 1:3; and stirring speed of 100 rpm.



3.2 Effect of HCl concentration on iron dissolution in IOT

As well as the temperature, the concentration of hydrochloric acid (HCl) positively influences the increase in iron extraction (Figure 5). It is noteworthy that the type and concentration of the leaching agent are the parameters with the greatest influence on the leaching rate (Faraji et al., 2022). It is observed that in 60 minutes, iron extraction reaches more than 80% for the concentration of 9.0 mol L⁻¹ and 10.8 mol L⁻¹, the highest concentrations, whilst it reaches 65% for 7.2 mol L⁻¹ and only 51% at the concentration of 5.4 mol L⁻¹. Iron extraction values over 95% were just attained with a concentration of 10.8 mol L⁻¹ after 120 min of leaching. These results were adjusted in the mathematical models (Eqs. 4–6), and the respective correlation coefficients are listed in the Table 5. The experimental results of leaching as a function of acid concentration also showed a higher mathematical correlation with the internal diffusion model (Figure 6).

Figure VI.05. Effect of HCl concentration on the dissolution of iron present in the IOT. Conditions: temperature 80 °C, solid-liquid ratio 1:3, and stirring speed of 100 rpm.

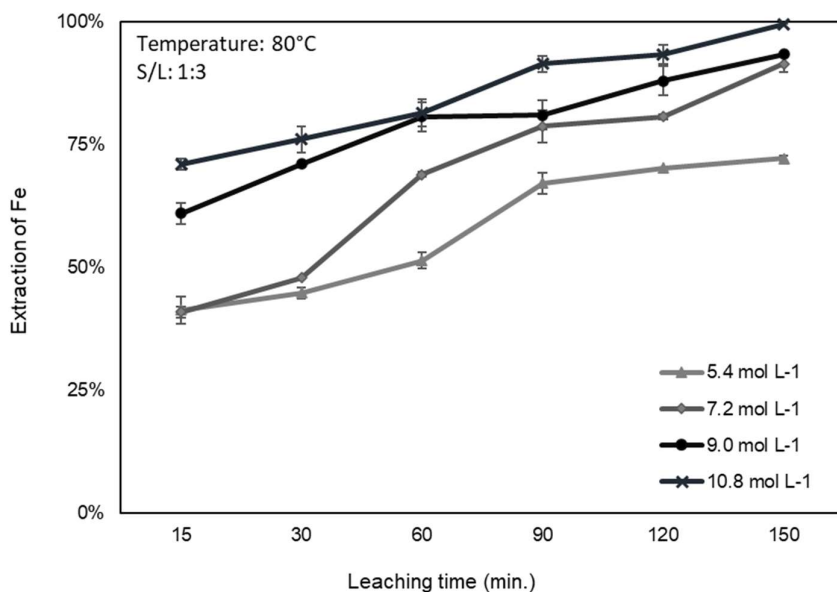


Figure VI.06. Results of fitting of experimental kinetics data into SC model. (A) Chemical reaction process. (B) Internal diffusion. (C) Interfacial transfer and diffusion through the product layer.

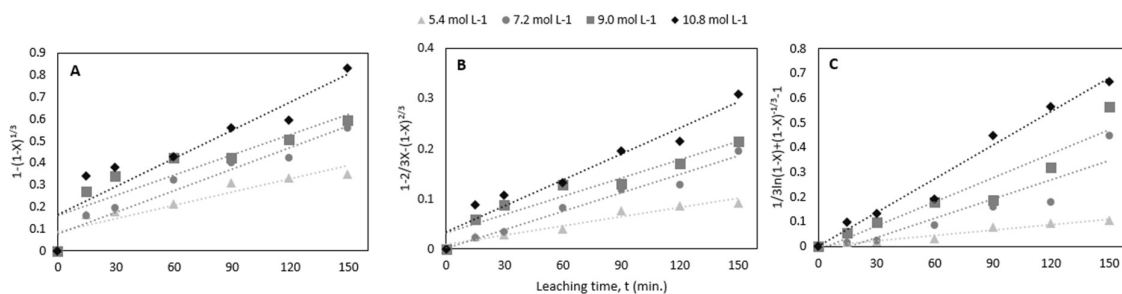


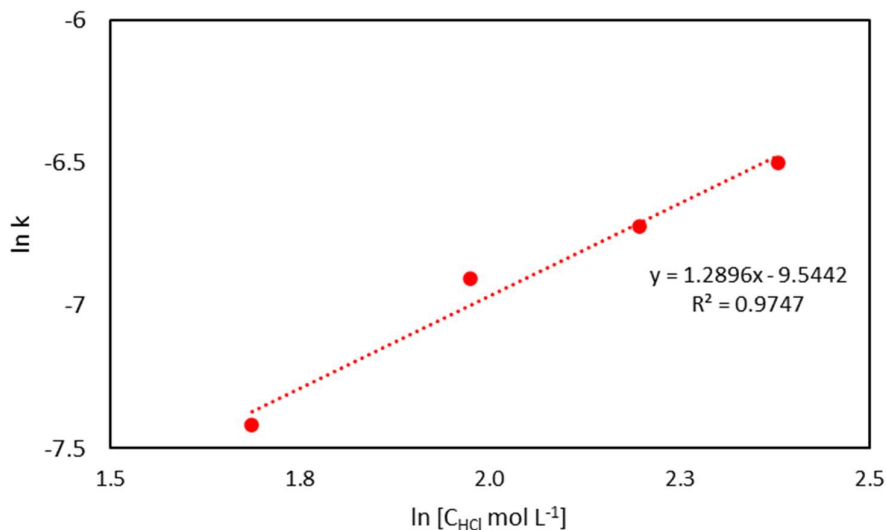
Table VI.02. Shrinking core model comparison by correlation coefficient (R^2) for concentration HCl results.

HCl concentration	$1-(1-X)^{1/3}$	$1-2/3X-(1-X)^{2/3}$	$1/3\ln(1-X)+(1-X)^{-1/3}-1$
5.4 mol L⁻¹	0.9315	0.9530	0.9668
7.2 mol L⁻¹	0.9577	0.9607	0.8809
9.0 mol L⁻¹	0.9685	0.9677	0.8471
10.8 mol L⁻¹	0.9404	0.9424	0.9486

Thus, the internal diffusion model was used as a reference to determine the empirical order of the reaction regarding the HCl concentration ($\ln k - \ln [C_{HCl}]$), as Figure 7. The

correlation of acid concentration data ($\ln [C_{HCl}]$) and dissolution of iron ($\ln k$) resulted in an empirical reaction order of 1.29.

Figure VI.07. Relationship between $\ln k$ and $\ln [CHCl]$ based on the internal diffusion model.

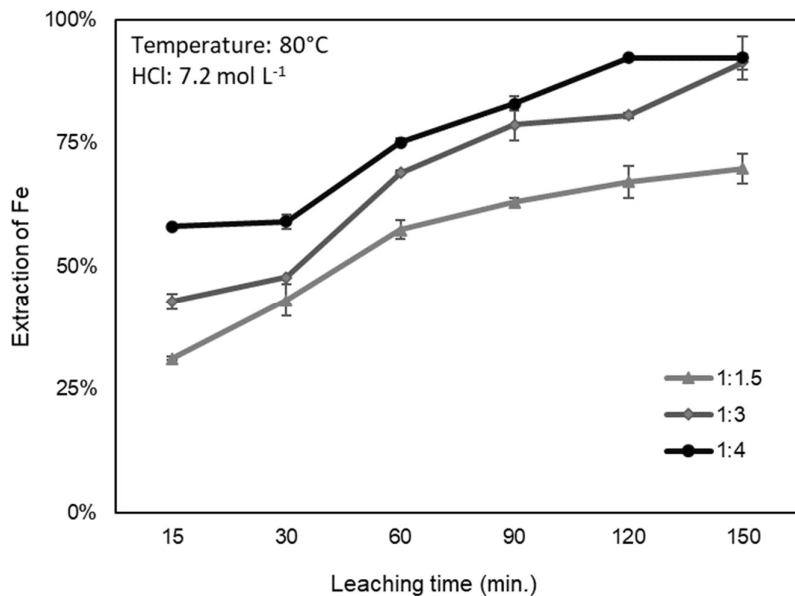


3.3 Effect of solid-liquid ratio on iron dissolution in IOT

Another determining parameter for the efficiency of leaching processes is the solid-liquid ratio (Figure 8). It is observed that the increase in the solid-liquid ratio affects the dissolution of iron. The ratios of 1:3 and 1:4 resulted in higher percentages of iron dissolution, reaching recoveries of around 90% in 150 min.

On the other hand, the ratio of 1:1.5 showed a lower recovery (70%) under the same conditions. This is due to the increase in the number of particles in suspension, which leads to less contact between the particles containing iron and the leaching agent. In addition, there is an increase in active species available, which can reduce the iron ions in the leaching solution through substitution reactions (Chen et al., 2015; Kocan and Hicsonmez, 2019; SADEGHI et al., 2017)

Figure VI.08. Effect of the solid-liquid ratio on the dissolution of iron present in the IOT. Conditions: temperature of 80 °C, HCl concentration of 7.2 mol L⁻¹, and stirring speed of 100 rpm.



The experimental data were plotted in the models evaluated in this article, and the internal diffusion model also presented a higher correlation coefficient ($R^2=0.9604$), to the detriment of the others analysed (Figure 9). The adjustment curves of experimental kinetics in the internal diffusion model (Figure 9.B) and the $\ln k - \ln \varepsilon_{S/L}$ ($\varepsilon_{S/L}$ is the S/L ratio) relationship regarding the S/L ratio (Figure 10) can be checked below. The correlation of solid-liquid ratio data ($\ln \varepsilon_{S/L}$) and dissolution of iron ($\ln k$) resulted in an empirical reaction order of 1.94.

Figure VI.09. Results of fitting of experimental kinetics data of solid-liquid ratio into SC model. (A) Chemical reaction process. (B) Internal diffusion. (C) Interfacial transfer and diffusion through the product layer.

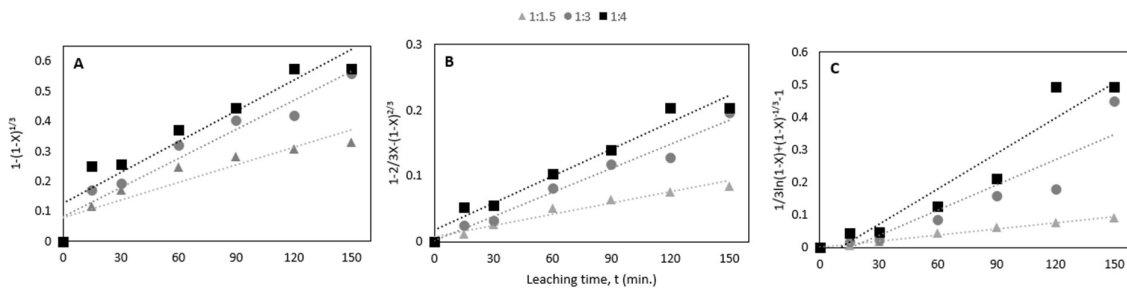
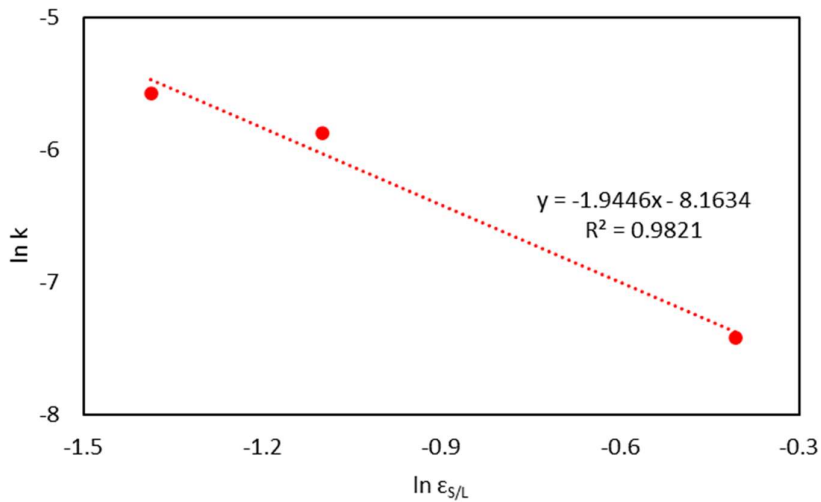


Figure VI.10. Relationship between $\ln k$ – $\ln \varepsilon_{S/L}$ based on the internal diffusion model.



3.4 Leaching kinetics of IOT with HCl for iron extraction

As a result of fitting the experimental data from Figs. 9B and 10, into a linear dependence, the empirical reaction order for C_{HCl} is calculated to be 1.29. The empirical reaction order for the S/L ratio was calculated to be -1.94. By substituting Eq. (7) into Eq. (5), the following Equation 8 could be obtained:

$$1-2/3X-(1-X)^{2/3} = k_0 \exp[-E_a/(RT)]^*t \quad (8)$$

where k_0 is dependent on the initial process parameters, including the initial C_{HCl} and S/L ratio, and the reaction time. Equation (9) could be rewritten as follows:

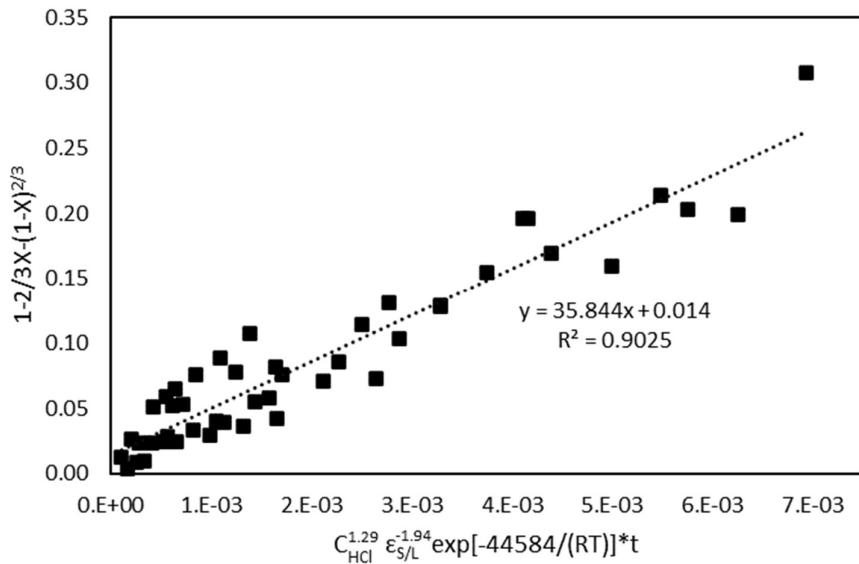
$$1-2/3X-(1-X)^{2/3} = k_0 C_{HCl}^{n_1} \varepsilon_{S/L}^{n_2} \exp[-44584/(RT)]^*t \quad (9)$$

where n_1 is the reaction order of the C_{HCl} and n_2 is the order of the S/L ratio. Based on the results calculated, the HCl leaching of Fe from the IOT in the temperature range of 60°C–90 °C could then be described by the following equation:

$$1-2/3X-(1-X)^{2/3} = k_0 C_{HCl}^{1.29} \varepsilon_{S/L}^{-1.94} \exp[-44584/(RT)]^*t \quad (10)$$

Taking $C_{HCl}^{1.29} \varepsilon_{S/L}^{-1.94} \exp[-44584/(RT)]$ as the ordinate and $1-2/3X-(1-X)^{2/3}$ as the abscissa, a fitted straight line was obtained with the correlation coefficient $R^2 = 0.903$, as shown in Figure 11.

Figure VI.11. The relationship between $1-2/3X-(1-X)^{2/3}$ and $C_{HCl}^{1.29} \varepsilon_{S/L}^{-1.94} \exp[-44584/(RT)]$.



The value of k_0 in Eq. (10) was calculated to be 35.84 according to the slope. The substitution of calculated values into Eq. (10) resulted in the final semi-empirical Eq. (11) to describe the overall HCl-leaching of iron present in IOT:

$$1-2/3X-(1-X)^{2/3} = 35.84 C_{HCl}^{1.29} \varepsilon_{S/L}^{-1.94} \exp[-44584/(RT)] * t \quad (11)$$

1. CONCLUSION

In the present study, the shrinking core model was used to study iron dissolution kinetics from IOT using HCl as a leaching medium. Iron leaching from the IOT has shown satisfactory results, resulting in a Fe recovery of more than 99% in the following configuration: 80° C, $C_{HCl} = 10.8 \text{ mol L}^{-1}$, S/L ratio = 1:3, and 150 minutes. The kinetics study showed that the iron leaching process is controlled by an internal diffusion model, with a correlation coefficient of 0.9612. Under experimental conditions, the activation energy, the apparent reaction order of hydrochloric acid, and the apparent reaction order of solid-liquid ratio were determined to be 44.58 kJ/mol, 1.29, and -1.94, respectively. The semi-empirical equation was theoretically equated to describe the deironization process as a function of the HCl concentration, S/L ratio and temperature as follows: $1-2/3X-(1-X)^{2/3} = 35.84 C_{HCl}^{1.29} \varepsilon_{S/L}^{-1.94} \exp[-44584/(RT)] * t$.

REFERENCES

- Alafara, A., Kuranga, I., Rafiu, B., Folahan, A., 2015. Quantitative leaching of a Nigerian chalcopyrite ore by nitric acid. *Bayero Journal of Pure and Applied Sciences* 7, 115. <https://doi.org/10.4314/bajopas.v7i2.20>
- Almeida, V.O. de, Schneider, I.A.H., 2022. Hydrometallurgical processing of Brazilian iron ore tailings for the synthesis of pigments. *Geomaterials* 12, 30–36. <https://doi.org/10.4236/gm.2022.122003>
- Almeida, V.O., Lima, N., Schneider, I.A.H., 2023a. Simplified hydrometallurgical route for the synthesis of silica-free hematite from iron ore tailings. *Miner Eng* 200, 108140. <https://doi.org/10.1016/j.mineng.2023.108140>
- Almeida, V.O., Schneider, I.A.H., 2020. Production of a ferric chloride coagulant by leaching an iron ore tailing. *Miner Eng* 156. <https://doi.org/10.1016/j.mineng.2020.106511>
- Almeida, V.O., Silvestro, L., Gleize, P.J.P., Kirchheim, A.P., Schneider, I.A.H., 2023b. Application of leached iron ore tailings to produce sustainable cement. *Constr Build Mater* 377, 131095. <https://doi.org/10.1016/j.conbuildmat.2023.131095>
- Araujo, V.A., Lima, N., Azevedo, A., Bicalho, L., Rubio, J., 2020. Column reverse rougher flotation of iron bearing fine tailings assisted by HIC and a new cationic collector. *Miner Eng* 156, 106531. <https://doi.org/10.1016/j.mineng.2020.106531>
- Binnemans, K., Jones, P.T., 2023. The twelve principles of circular hydrometallurgy. *Journal of Sustainable Metallurgy* 9, 1–25. <https://doi.org/10.1007/s40831-022-00636-3>
- Carmignano, O.R., Vieira, S.S., Teixeira, A.P.C., Lameiras, F.S., Brandão, P.R.G., Lago, R.M., 2021. Iron ore tailings: Characterization and applications. *J Braz Chem Soc.* <https://doi.org/10.21577/0103-5053.20210100>
- Chen, M., Huang, J., Ogunseitan, O.A., Zhu, N., Wang, Y., 2015. Comparative study on copper leaching from waste printed circuit boards by typical ionic liquid acids. *Waste Management* 41, 142–147. <https://doi.org/10.1016/j.wasman.2015.03.037>

- Douce, P.D., Castro, G.B. de, Lima, M.M.F., Lima, R.M.F., 2019. Characterisation and magnetic concentration of an iron ore tailings. *Journal of Materials Research and Technology* 8, 1052–1059. <https://doi.org/10.1016/j.jmrt.2018.07.015>
- Doyle, F.M., 2005. Teaching and learning environmental hydrometallurgy. *Hydrometallurgy* 79, 1–14. <https://doi.org/10.1016/j.hydromet.2004.10.022>
- Faraji, F., Alizadeh, A., Rashchi, F., Mostoufi, N., 2022. Kinetics of leaching: a review. *Reviews in Chemical Engineering* 38, 113–148. <https://doi.org/10.1515/revce-2019-0073>
- Ferreira, I.C., Galéry, R., Henriques, A.B., Paula de Carvalho Teixeira, A., Prates, C.D., Lima, A.S., Souza Filho, I.R., 2022. Reuse of iron ore tailings for production of metakaolin-based geopolymers. *Journal of Materials Research and Technology* 18, 4194–4200. <https://doi.org/10.1016/j.jmrt.2022.03.192>
- Habashi, F., 1998. *Handbook of Extractive Metallurgy*. WILEY-VCH.
- Havlík, T., 2008. *Hydrometallurgy: Principles and application*. CRC Press.
- Hoeber, L., Steinlechner, S., 2021. A comprehensive review of processing strategies for iron precipitation residues from zinc hydrometallurgy. *Clean Eng Technol* 4, 100214. <https://doi.org/10.1016/j.clet.2021.100214>
- Huang, H., Li, J., Li, X., Zhang, Z., 2013. Iron removal from extremely fine quartz and its kinetics. *Sep Purif Technol* 108, 45–50. <https://doi.org/10.1016/j.seppur.2013.01.046>
- Ismael, M.R.C., Carvalho, J.M.R., 2003. Iron recovery from sulphate leach liquors in zinc hydrometallurgy. *Miner Eng* 16, 31–39. [https://doi.org/10.1016/S0892-6875\(02\)00310-2](https://doi.org/10.1016/S0892-6875(02)00310-2)
- Kocan, F., Hicsonmez, U., 2019. Leaching kinetics of celestite in nitric acid solutions. *International Journal of Minerals, Metallurgy, and Materials* 26, 11–20. <https://doi.org/10.1007/s12613-019-1705-0>
- Li, Y., Li, S., Pan, X., Zhao, X., Guo, P., 2023^a. Eco-friendly strategy for preparation of high-purity silica from high-silica IOTs using S-HGMS coupling with ultrasound-

assisted fluorine-free acid leaching technology. *J Environ Manage* 339, 117932. <https://doi.org/10.1016/j.jenvman.2023.117932>

Li, Y., Li, S., Pan, X., Zhao, X., Guo, P., Zhao, Z., 2023b. Recovery and preparation of high-grade silica from iron ore tailings by S-HGMS coupling with acid leaching technology: Description of separation mechanism and leaching kinetics. *Powder Technol* 424, 118523. <https://doi.org/10.1016/j.powtec.2023.118523>

Monhemius, A.J., 2017. The iron elephant: A brief history of hydrometallurgists' struggles with element no. 26. *CIM Journal* 8. <https://doi.org/10.15834/cimj.2017.21>

Nagarajan, N., Panchatcharam, P., 2023. Cost-effective and eco-friendly copper recovery from waste printed circuit boards using organic chemical leaching. *Heliyon* 9, e13806. <https://doi.org/10.1016/j.heliyon.2023.e13806>

Ndlovu, S., Simate, G.S., Matinde, E., 2017. Waste Production and Utilization in the Metal Extraction Industry, 1 st. ed. CRC Press, Boca Raton.

Paul, M., Seferinoğlu, M., Ayçık, G.A., Sandström, Å., Smith, M.L., Paul, J., 2006. Acid leaching of ash and coal: Time dependence and trace element occurrences. *Int J Miner Process* 79, 27–41. <https://doi.org/10.1016/j.minpro.2005.11.008>

SADEGHI, N., MOGHADDAM, J., OJAGHI ILKHCHI, M., 2017. Kinetics of zinc sulfide concentrate direct leaching in pilot plant scale and development of semi-empirical model. *Transactions of Nonferrous Metals Society of China* 27, 2272–2281. [https://doi.org/10.1016/S1003-6326\(17\)60253-X](https://doi.org/10.1016/S1003-6326(17)60253-X)

Seferinoglu, M., 2003. Acid leaching of coal and coal-ashes*. *Fuel* 82, 1721–1734. [https://doi.org/10.1016/S0016-2361\(03\)00132-7](https://doi.org/10.1016/S0016-2361(03)00132-7)

Sultana, U.K., Kurny, A.S.W., 2012. Dissolution kinetics of iron oxides in clay in oxalic acid solutions. *International Journal of Minerals, Metallurgy, and Materials* 19, 1083–1087. <https://doi.org/10.1007/s12613-012-0674-3>

Sun, Y., Zhang, X., Han, Y., Li, Y., 2020. A new approach for recovering iron from iron ore tailings using suspension magnetization roasting: A pilot-scale study. *Powder Technol* 361, 571–580. <https://doi.org/10.1016/j.powtec.2019.11.076>

VALEEV, D., PANKRATOV, D., SHOPPERT, A., SOKOLOV, A., KASIKOV, A., MIKHAILOVA, A., SALAZAR-CONCHA, C., RODIONOV, I., 2021. Mechanism and kinetics of iron extraction from high silica boehmite–kaolinite bauxite by hydrochloric acid leaching. *Transactions of Nonferrous Metals Society of China* 31, 3128–3149. [https://doi.org/10.1016/S1003-6326\(21\)65721-7](https://doi.org/10.1016/S1003-6326(21)65721-7)

VOGEL, A.I., 1981. *Química Analítica Quantitativa*, 5 ed. Ed. Editora Mestre, São Paulo.

WANG, G., LIU, Y., TONG, L., JIN, Z., CHEN, G., YANG, H., 2019. Effect of temperature on leaching behavior of copper minerals with different occurrence states in complex copper oxide ores. *Transactions of Nonferrous Metals Society of China* 29, 2192–2201. [https://doi.org/10.1016/S1003-6326\(19\)65125-3](https://doi.org/10.1016/S1003-6326(19)65125-3)

Xie, B., Liu, C., Wei, B., Wang, R., Ren, R., 2023. Recovery of rare earth elements from waste phosphors via alkali fusion roasting and controlled potential reduction leaching. *Waste Management* 163, 43–51. <https://doi.org/10.1016/j.wasman.2023.03.029>

Xu, D.-M., Zhan, C.-L., Liu, H.-X., Lin, H.-Z., 2019. A critical review on environmental implications, recycling strategies, and ecological remediation for mine tailings. *Environmental Science and Pollution Research* 26, 35657–35669. <https://doi.org/10.1007/s11356-019-06555-3>

Yang, C.-Q., Li, S.-Q., 2020. Kinetics of iron removal from quartz under ultrasound-assisted leaching. *High Temperature Materials and Processes* 39, 395–404. <https://doi.org/10.1515/htmp-2020-0081>

Young, G., Yang, M., 2019. Preparation and characterization of Portland cement clinker from iron ore tailings. *Constr Build Mater* 197, 152–156. <https://doi.org/10.1016/j.conbuildmat.2018.11.236>

CAPÍTULO VII

**ASPECTOS ECONÔMICOS E PRODUTIVOS DO PROCESSAMENTO
HIDROMETALÚRGICO DE REJEITOS DE MINÉRIO DE FERRO E AS
PERSPECTIVAS FUTURAS SOBRE O APROVEITAMENTO DO IOT.**

1. BENEFÍCIOS ECONÔMICOS E PERSPECTIVAS FUTURAS

Apesar do valor de construção e manutenção de barragens/pilhas de rejeitos ser bem consolidado nos projetos de mineração (GOUVEIA, 2020; LIU *et al.*, 2010); ainda há muitas incertezas relacionadas aos custos reais decorrentes dos riscos dessas estruturas. Essa incerteza tem colocado em *check* a viabilidade de muitos projetos e gerado questionamentos por meio dos *stakeholders* envolvidos na decisão de investir ou não em tais empreendimentos (ARMSTRONG *et al.*, 2019).

O aproveitamento dos rejeitos é uma solução que minimiza os riscos associados a tais decisões, reduz os custos de disposição e ainda agrega valor ao sistema pela comercialização de coprodutos. Além disso, tais medidas convertem os custos da sustentabilidade, que se referem a todos os recursos voltados para restauração dos danos ambientais decorrentes da atividade de mineração; para benefícios financeiros (JAFARPOUR; KHATAMI, 2021; XU *et al.*, 2018).

Assim, mudanças visando uma mineração com resíduos zero devem ser pensadas de forma sistêmica; com o objetivo de garantir interações sinérgicas que agregue valor ao longo de toda cadeia produtiva. Conforme discutido no capítulo 1, são inúmeras as iniciativas no âmbito científico que ressaltam a viabilidade técnica do aproveitamento de rejeitos de minério de ferro. Dentre as alternativas, há uma predominância de investigações que consideram o uso dos rejeitos como matéria-prima para construção civil, principalmente na forma de agregados (ALMEIDA *et al.*, 2023; ALMEIDA; SCHNEIDER, 2018).

Essa característica pode ser justificada pela compatibilidade de volumes entre a indústria da mineração e da construção civil e pelo fato de tais aplicações não demandarem de operações complexas de processamento/adequação dos rejeitos (ALLY *et al.*, 2021; CARMIGNANO *et al.*, 2021). Em contrapartida, o baixo valor agregado associado a tais aplicabilidades restringe a destinação dos rejeitos para áreas próximas as minas, o que limita o mercado consumidor e a quantidade de rejeitos efetivamente utilizada (SOBOTKA; JASKOWSKI; CZARNIGOWSKA, 2012). Esse aspecto, corrobora com a busca por aplicações que aumentem os benefícios econômicos associados à incorporação de rejeitos como coprodutos (LU *et al.*, 2020) e que viabilizem a destinação destes resíduos para outros mercados.

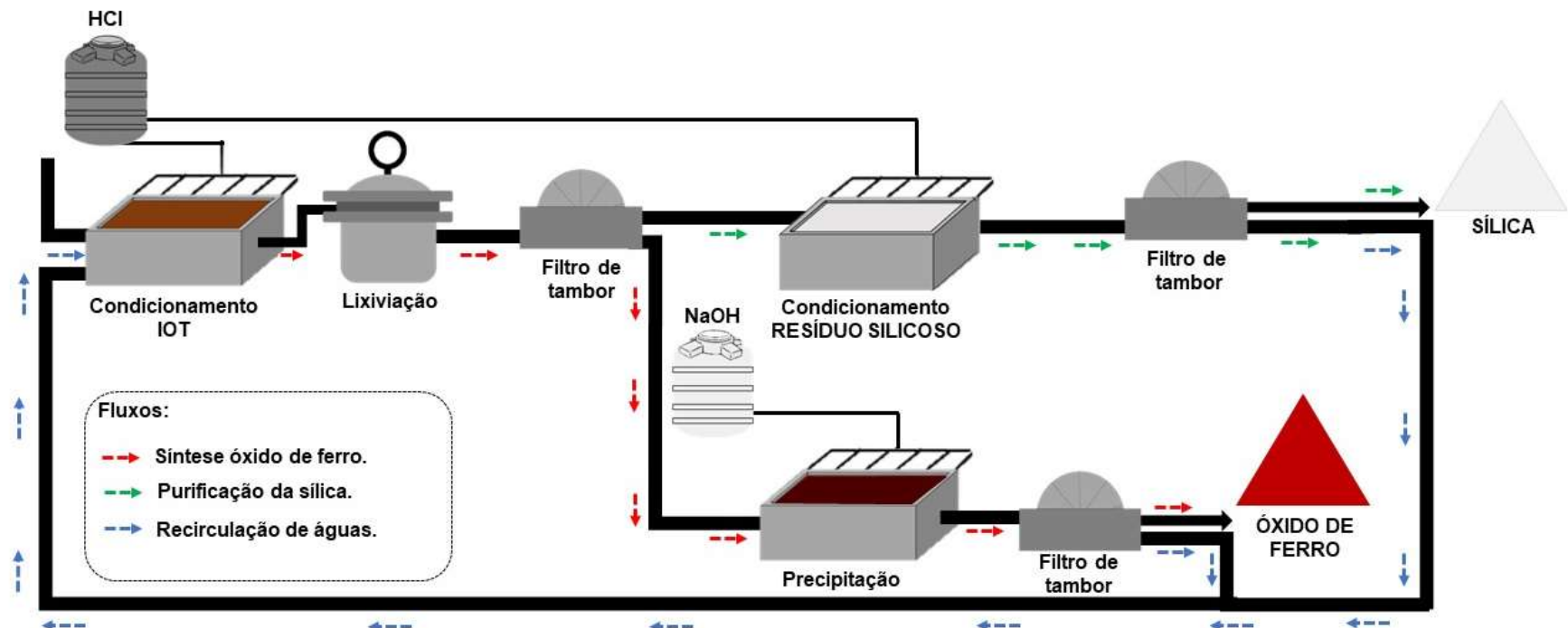
O processamento hidrometalúrgico possibilita a recuperação do ferro e da sílica, os quais podem ser utilizados para finalidades com maior valor agregado. O ferro pode ser comercializado na forma de cloreto férrico (ALMEIDA; SCHNEIDER, 2020; LI *et al.*, 2020), de óxidos magnéticos (USMAN *et al.*, 2019), como pigmento (ALMEIDA; SCHNEIDER, 2022) e como produto para siderurgia (ALMEIDA; LIMA; SCHNEIDER, 2023). A sílica pode ser utilizada como material cimentício suplementar (ALMEIDA *et al.*, 2023) e ainda pode ser purificada (LI *et al.*, 2023).

Diante disso, avaliar o valor de mercado dos coprodutos obtidos a partir da rota hidrometalúrgica, estimar o rendimento do processo e apontar as principais operações unitárias que devem ser conjugadas é determinante para compreensão das perspectivas futuras associadas a essa oportunidade.

Por meio da lixiviação, os rejeitos de minério de ferro podem ser processados e, segundo o escopo deste trabalho, resultar em dois produtos principais: licor férrico (FeCl_3) e material silicoso (SiO_2). O cloreto férrico pode ser utilizado para tratamento de água e/ou aplicado na siderurgia, na metalurgia extractiva e na indústria química. A partir do licor férrico também é possível a síntese de óxidos de ferro, livres de sílica, os quais podem ser utilizados tanto como insumo para siderurgia, como para a indústria de pigmentos. A sílica, por sua vez, pode ser utilizada como agregado fino; material cimentício suplementar e/ou destinada para finalidades mais nobres.

Segundo as investigações expostas nos capítulos anteriores, o processamento hidrometalúrgico dos rejeitos de minério de ferro contempla estágios de condicionamento, lixiviação ácida, precipitação e separação sólido-líquido. São operações comuns ao beneficiamento de minérios e que podem ser facilmente integradas na cadeia de produção do minério de ferro (Figura 1).

Figura VII.01. Esquema do processo hidrometalúrgico para produção de óxidos de ferro e sílica a partir de rejeitos de minério de ferro.



Segundo WILLS e FINCH (2016), por meio do condicionamento é possível obter o controle de vazão da polpa, a concentração de sólidos, teor de ferro e adição adequada de reagentes. Esses fatores são essenciais para uma boa eficiência na etapa de lixiviação. Outra vantagem é na utilização e controle dos recursos utilizados: água, energia, insumos, entre outros.

Para obtenção dos óxidos de ferro, o condicionamento também é de fundamental importância, pois garante o tempo, a agitação e a quantidade necessária de reagentes para obtenção do precipitado férrico. Segundo a METSO (2018), os tanques de condicionamento aumentam a eficiência e controle de circuitos de processamento de minérios, por atuarem como uma etapa de amortecimento ao circuito, além de garantir o controle das características da polpa antes de ser alimentada nos reatores de lixiviação. Essas características são essenciais ao processo hidrometalúrgico, ainda mais quando se refere a um processo que poderá atuar de forma conectada a um sistema produtivo tradicional de beneficiamento do minério de ferro.

Também serão necessárias operações de separação sólido-líquido nas etapas que seguem a lixiviação como também no estágio de precipitação do óxido de ferro. Em todas essas etapas, a máxima remoção do filtrado e lavagem da fase sólida deve ser priorizada. Filtros a vácuo, do tipo filtro a disco ou filtro de tambor são opções a serem escolhidas. De acordo com WILLS e FINCH (2016), o filtro de tambor é uma opção para sistemas em que a lavagem da torta é necessária.

Nesse sistema produtivo também devem estar contempladas unidades de armazenamentos dos reagentes utilizados: ácido clorídrico e hidróxido de sódio. Tais unidades devem cumprir os parâmetros de segurança necessários para o armazenamento de reagentes controlados.

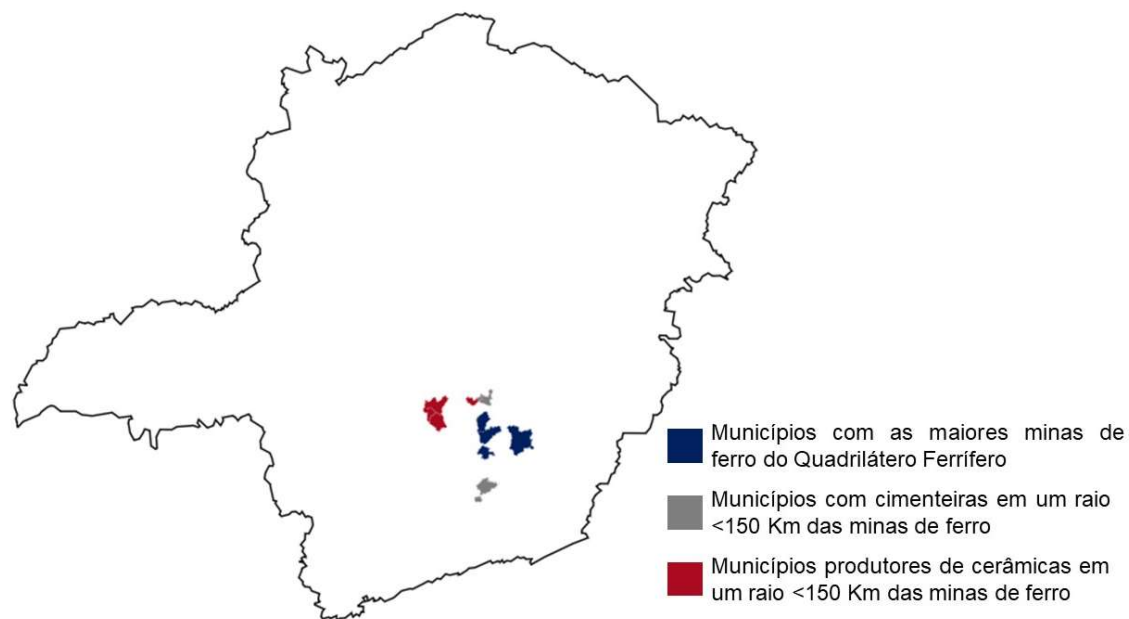
Ainda, sobre a infraestrutura de produção, a unidade de processamento hidrometalúrgica de rejeitos de minério de ferro pode ser equipada com *skids* de eletrólise de HCl de modo a reduzir os custos com insumos e maximizar a produtividade do sistema. O mesmo pode ser adotado para a obtenção do hidróxido de sódio (THYSSENKRUPP, 2023). O ácido clorídrico ainda pode ser regenerado ao

longo da cadeia de produção, maximizando a sustentabilidade do processo e reduzindo substancialmente os custos operacionais (DEMOPOULOS *et al.*, 2008).

Diante do volume de rejeitos gerados na indústria do ferro, integrar as operações hidrometalúrgicas ao sistema tradicional reduz os custos operacionais do novo processo, melhora a produtividade e minimiza os custos de implantação. Além disso, os coprodutos poderão ser comercializados através do mesmo sistema logístico adotado para o minério de ferro. Tais ações aumentam a sinergia de aproveitamento dos rejeitos e potencializam os benefícios-

Avaliando o cenário de produção de ferro do Quadrilátero Ferrífero, que é o maior gerador de rejeitos de minério de ferro do país, e os segmentos que podem absorver os coprodutos da mineração de ferro; observa-se vantagens em relação a localização destas unidades produtivas e a infraestrutura logística da região (Figura 2).

Figura VII.02. Cenário produtivo do Quadrilátero Ferrífero para geração de IOT e segmentos que podem incorporar tais resíduos.



É possível verificar a proximidade geográfica das maiores unidades de produção de minério de ferro, no estado de MG, com indústrias cimenteiras e cerâmicas (ANM, 2023; GOVERNO DE MINAS GERAIS, 2020). Tal aspecto favorece

oportunidades de simbiose industrial e facilitam a integração entre diferentes segmentos industriais.

Observa-se que há unidades produtivas de grande porte, em um raio de 150 km dos municípios que apresentam as maiores arrecadações da CFEM para o minério de ferro (ANM, 2023; GOVERNO DE MINAS GERAIS, 2020; VICTORIA, 2018; VISEDO; PECCHIO, 2019). Tal proximidade favorece a obtenção de menores custos logísticos. Para mais, os benefícios ainda podem ser potencializados pela proximidade do mercado consumidor da região metropolitana de Belo Horizonte. A infraestrutura ferroviária que atende Minas Gerais é outro aspecto favorável a distribuição dos produtos hidrometalúrgicos.

Diante do potencial regional de Minas Gerais, compreender o valor associado a cada um dos produtos da rota hidrometalúrgica é fundamental para o entendimento do potencial deste processo. A faixa de preços dos coprodutos foi obtida com base em pesquisas de mercado, considerando a seguintes especificidades: os preços do agregado fino e do material cimentício suplementar foram obtidos a partir dos valores por tonelada da areia fina, na região de Minas Gerais (ANM, 2017; SILVA, 2020; WELBERT, 2016) e do cimento em âmbito nacional (FILHO; NETO, 2018; VISEDO; PECCHIO, 2019). Destaca-se que o preço de tais insumos pode variar muito entre as regiões brasileiras e que seu valor está diretamente relacionado aos valores de transporte e a dinâmica de oferta e demanda regional.

Tabela VII.01. Faixa de preço dos principais coprodutos da lixiviação de IOT.

Coproduto	Preço (R\$/t)
Produtos silicosos	
Agregado fino	30 - 70
Material cimentício suplementar	350 - 470
Sílica de alta pureza (99%)	14000 - 24000
Produtos à base de ferro	
Cloreto Férlico (FeCl ₃)	1500 - 2500
Óxido de ferro para siderurgia	395 - 728
Óxido de ferro para pigmentos	4500 - 10000

A sílica de alta pureza, por sua vez, é um produto de valor agregado expressivo e que segue a dinâmica internacional de preços, especialmente devido ao seu uso em alta tecnologia (THE MANUFACTURER, 2023; VATALIS; CHARALAMBIDES; BENETIS, 2015). Além dessa aplicação, pode-se destacar o seu potencial de uso para: produção de vidro, fundição, cerâmica/refratário, tintas, borracha, plástico, filtração e fraturamento hidráulico. Tais usos apresentam requisitos específicos, com teores variados (93,5 - 99% de SiO₂) e seguem dinâmicas de mercado específicas (ALMEIDA, 2019).

Para os produtos à base de ferro; foram utilizados dados de cotações públicas e preços do mercado internacional. O cloreto férrico é um produto amplamente utilizado em estações de tratamento de água e adquirido através de pregões. A faixa de preço do cloreto férrico, indicada na tabela 1, foi obtida a partir de dados abertos de licitações públicas, realizadas nos anos de 2021 a 2023 (CESAMA, 2021; SAEP, 2023).

Para o óxido de ferro compatível com uso na siderurgia, foram mapeados os preços praticados no mercado internacional, nos anos de 2022 e 2023. Nesse período, o menor preço do minério de ferro foi em torno de US\$ 84 (Outubro/2022) e o maior preço do período foi de US\$ 155 (Fevereiro/2022) (TRADING ECONOMICS, 2023). Para precificação dos pigmentos à base de ferro, foram elencados dados provenientes de anuários do setor e análises de mercado (FOCUS ON PIGMENTS, 2022; INDEXBOX, 2023; LANXESS, 2021). Os pigmentos à base de ferro apresentam valores variando de R\$ 4.000,00 a R\$ 10.000,00. Destaca-se que para ajustar os preços internacionais em reais (R\$), foi utilizada a cotação média do dólar em julho de 2023 de US\$ 1,00 - R\$ 4,70.

Considerando os aspectos de lixiviação para obtenção de uma recuperação de Fe superior a 95%, é necessário um consumo de 1.8 t de HCl por tonelada de IOT. Esse processo, por sua vez, resulta em cerca de 2.2 t de FeCl₃, correspondentes a 1667 litros de licor férrico, por tonelada de rejeito.

O cloreto férrico é um produto por si só, mas pode ser direcionado para a síntese dos óxidos de ferro (Capítulo 3). Para tal, o consumo específico do hidróxido de sódio é em torno de 0.5 t por tonelada de IOT e resulta em 0,220 t de óxido de ferro livre de sílica, para um rejeito com 31% de Fe₂O₃. Outro coproduto é o material

silicoso, o qual representa aproximadamente 70% da massa de IOT lixiviada. A produtividade dos coprodutos, estimada, por tonelada de rejeitos e o valor obtido para cada um dos produtos como base nos valores médios, pode ser verificado na tabela 2.

Tabela VII.02. Rendimento e valor dos coprodutos por tonelada de IOT.

Coprodutos da lixiviação	Rendimento por ton. de IOT (t)	Preço médio (R\$)
Cloreto férrico (FeCl_3) - 10% Fe	2,20	4.400,00
Agregado fino	0,680	34,00
Material cimentício suplementar	0,680	410,00
Sílica da alta pureza (~99%)	0,610	11.600,00
Oxido de ferro para siderurgia	0,215	120,70
Oxido de ferro para pigmentos	0,215	1560,00

Vale salientar que cada produto apresenta uma especificação e que há variações significativas de mercado. Assim, tais considerações devem ser avaliadas de forma sistêmica através de um estudo de viabilidade econômica.

Diante do exposto, algumas perspectivas futuras para continuidade dessa pesquisa são:

- avaliação da variável pressão para otimização dos processos de lixiviação;
- identificação de reagentes alternativos que potencializem a dissolução do ferro;
- aplicação de soluções de geração/regeneração de HCl para adoção nesse processo hidrometalúrgico;
- validação dos resultados de bancada em escala piloto;
- análise de competitividade econômica do processo.

Em síntese, são inúmeros os indícios do potencial da rota hidrometalúrgica para aproveitamento de rejeitos de minério de ferro, especialmente em relação à obtenção de produtos de qualidade e que atendam aos quesitos de produção compatíveis com práticas de sustentabilidade, economia circular e produção mais limpa. Esses elementos contribuem para o atual gerenciamento de resíduos da mineração de ferro e que podem potencializar a capacidade produtiva e econômica dos atuais sistemas de beneficiamento.

2. CONSIDERAÇÕES FINAIS

O Brasil, como segundo maior produtor mundial de minério de ferro, é responsável por gerar grandes volumes de rejeitos, os quais representam milhões de toneladas de um material particulado fino, rico em ferro, sílica e alumínio. O Quadrilátero Ferrífero, no estado de Minas Gerais, concentra a geração de rejeitos de minério de ferro, devido aos teores atualmente explotados e aos processos de beneficiamento adotados. Como parte do atual sistema produtivo, a disposição em barragens e/ou empilhamento a seco são as técnicas comumente adotadas para o gerenciamento de rejeitos.

A disposição destes resíduos sólidos é um viés que caminha em sentido contrário ao da sustentabilidade do setor e é responsável pelas maiores catástrofes da mineração brasileira: Fundão (2015) e Córrego do Feijão (2019). Embora a utilização de sistemas de separação sólido-líquido e empilhamento a seco sejam soluções que minimizam os riscos geotécnicos e moderam os impactos decorrentes a disposição de rejeitos, essas alternativas não contemplam o máximo aproveitamento dos recursos naturais.

O capítulo 1 dessa tese reforça esse contexto, principalmente pelo crescimento de investigações que pautam o aproveitamento dos rejeitos de minério de ferro e demonstram os benefícios decorrentes dessa prática. Processar o IOT para sua aplicação, visando evitar sua disposição na natureza, é uma solução preventiva, segura e ambientalmente positiva; pois permite agregar os preceitos sustentáveis não apenas no âmbito da mineração, mas também em setores adjacentes que incorporem os rejeitos em suas cadeias produtivas.

Nessa tese, o processamento hidrometalúrgico dos rejeitos foi investigado, visando a dissolução do ferro e obtenção de uma fração sólida rica em sílica. Os produtos da lixiviação foram caracterizados e avaliados quanto a viabilidade técnica para obtenção dos seguintes coprodutos: (i) cloreto férrico - coagulante aplicado para o tratamento de água; (ii) óxido de ferro livre sílica - material com potencial para uso como pigmento ou como insumo para a siderurgia; (iii) IOT lixiviado - coproduto rico em sílica avaliado como material cimentício suplementar. Também foram discutidas as perspectivas vinculadas a disposição de rejeitos e seus efeitos na natureza

(Capítulo 2) e as tendências técnico-científicas vinculadas aos resíduos sólidos da mineração de ferro.

A lixiviação mostrou-se factível para recuperação do ferro e, nas investigações aqui apresentadas, foram mapeados os parâmetros de maior relevância na dissolução desse metal (Capítulo 3 e 6). Os artigos, de um modo geral, objetivaram demonstrar os benefícios do processamento químico do IOT, especialmente em relação à versatilidade desse processo e seu potencial de maximizar a recuperação das diversas espécies minerais que compõem os rejeitos de minério de ferro.

Os ensaios de lixiviação ácida a quente com uso de ácido clorídrico, resultaram em recuperações superiores a 95% de ferro e obtenção de uma fração sólida rica em sílica (>90%). O licor férrico produzido apresentou concentrações de ferro superiores a 110 g L⁻¹ e baixa concentração de outros elementos: Al (1700 mg L⁻¹); P (66 mg L⁻¹) e Mn (24 mg L⁻¹). Destaca-se, que elementos potencialmente tóxicos como chumbo, cromo e arsênio; ficaram abaixo dos limites estipulados para aplicação como coagulante. Já a fração silicosa apresentou a seguinte composição: SiO₂ (90%), Al₂O₃ (6%); Fe₂O₃ (3%). Tais propriedades viabilizam diversas aplicações para os produtos da lixiviação, das quais algumas foram avaliadas nessa investigação.

O licor férrico foi aplicado para o tratamento de água e demonstrou eficiência para adequação de uma amostra de água bruta aos padrões de potabilidade. O mesmo licor foi empregado como precursor de ferro para produção de óxidos de ferro. Através da precipitação química e conversão térmica dos oxi-hidróxidos de ferro foi possível sintetizar micro- nanopartículas de hematita (Fe₂O₃) isentas de sílica. Essa rota permitiu uma recuperação global de 84% do Fe e obtenção de um material com propriedades favoráveis ao seu uso como pigmento comercial ou como insumo para fabricação de aço. Nesta aplicação, o aproveitamento do IOT maximiza a recuperação do ferro da jazida, acumula benefícios financeiros para a cadeia produtiva da mineração de ferro pela obtenção de um produto com valor agregado substancial e apoia preceitos sustentáveis tanto para a mineração como para a siderurgia.

A fração sólida, por sua vez, após a lixiviação apresentou o quartzo e a caulinita como principais fases mineralógicas; as quais compreendem componentes que são úteis para as cimenteiras. Dessa forma, no Capítulo 5, o rejeito lixiviado foi submetido a uma ativação térmica realizada a 700 °C, e foi avaliado quanto ao seu potencial de

uso como material cimentício suplementar. Nas condições investigadas, observou-se que é possível substituir até 20% do cimento pelo IOT lixiviado; sem que haja prejuízo na resistência à compressão. Essa substituição permite a destinação de resíduos da mineração para uma finalidade ambientalmente amigável e ainda resulta em uma diminuição de 21% na emissão de CO₂, caso esse cimento sustentável seja aplicado. Tais aspectos corroboram os efeitos positivos do processamento hidrometalúrgico, pois conectam dois setores reconhecidos pela demanda de grandes volumes de matérias-primas e que tem buscado fortemente por soluções que pautem os preceitos de produção mais limpa.

Para viabilizar tais alternativas, o entendimento do processo de lixiviação e a compreensão dos parâmetros de maior relevância no processo é fundamental. Por essa razão, a cinética envolvida na lixiviação dos rejeitos de minério de ferro, com uso de ácido clorídrico, foi alvo de uma investigação específica (capítulo 6). Avaliando os parâmetros de temperatura, concentração de ácido clorídrico, relação sólido/líquido e tempo observou-se que a temperatura e a concentração de ácido são os parâmetros de maior influência na extração do ferro. A partir do modelo de núcleo encolhido (*Shrinking Core Model - SC*), a cinética da lixiviação dos rejeitos de minério de ferro foi avaliada. Verificou-se que a reação de difusão interna apresentou maior correlação com os dados experimentais da lixiviação. A partir desse modelo, calculou-se uma energia de ativação de 44,58 KJ/mol, configurando uma reação endotérmica para dissolução do ferro. Nas condições investigadas, foi possível obter uma recuperação do ferro superior a 99%, nas seguintes condições: temperatura de 80 °C, concentração de HCl de 10,8 mol L⁻¹, relação sólido-líquido 1:3; agitação de 100 rpm e tempo de 150 minutos. Através dessas condicionantes é possível obter parâmetros para otimização do processo e ajuste da rota visando atender a especificação do produto desejado.

A partir dos resultados obtidos, estimou-se que para cada tonelada de rejeitos processada por via hidrometalúrgica é possível obter cerca de 2,2 toneladas de cloreto férrico e 0,7 t de material silicoso, com consumo específico de 1,8 t de HCl. Caso o cloreto férrico venha a ser convertido em óxidos de ferro, livres de sílica, é possível produzir cerca de 0,2 t por tonelada de IOT. Extrapolando tais resultados para o montante anual de rejeitos de minério de ferro de 200 Mt, o processamento hidrometalúrgico é capaz de prover, aproximadamente, 50 Mt a mais de ferro para o

mercado. Tal produto é compatível com as matérias-primas desejadas para siderurgia verde (*green steel*), por minimizar o consumo energético, reduzir a geração de escória e emissão de CO₂.

Assim, o processo hidrometalúrgico de rejeitos de minério de ferro fomenta aspectos relacionados ao máximo aproveitamento de recursos minerais, redução de passivos ambientais e simbiose industrial para a utilização de resíduos. Tais benefícios estão alinhados com os preceitos ESG que vem sendo incorporados na gestão da indústria mineral e fomentam práticas sustentáveis, como: economia circular, produção mais limpa, e redução na emissão de gases de efeito estufa.

REFERÊNCIAS

- ALLY, A. N. et al. Recovery of Mining Wastes in Building Materials: A Review. Open Journal of Civil Engineering, v. 11, n. 04, p. 379–397, 2021.
- ALMEIDA, V. O. DE. Produção de Cloreto Férrico a partir de Rejeito de Minério de Ferro: Um estudo de caracterização e aplicabilidade. Porto Alegre: [s.n.].
- ALMEIDA, V. O. DE; SCHNEIDER, I. A. H. Hydrometallurgical Processing of Brazilian Iron Ore Tailings for the Synthesis of Pigments. Geomaterials, v. 12, n. 02, p. 30–36, 2022.
- ALMEIDA, V. O. et al. Application of leached iron ore tailings to produce sustainable cements. Construction and Building Materials, v. 377, p. 131095, maio 2023.
- ALMEIDA, V. O.; LIMA, N.; SCHNEIDER, I. A. H. Simplified hydrometallurgical route for the synthesis of silica-free hematite from iron ore tailings. Minerals Engineering, v. 200, p. 108140, set. 2023.
- ALMEIDA, V. O.; SCHNEIDER, I. A. H. Desafios rumo ao gerenciamento e aplicação sustentável dos rejeitos da indústria mineral: um estudo estatístico dos rejeitos das produções acadêmicas e inovações no segmento. . 11° Simpósio Internacional de qualidade ambiental. Anais...Porto Alegre: 2018.
- ALMEIDA, V. O.; SCHNEIDER, I. A. H. Production of a ferric chloride coagulant by leaching an iron ore tailing. Minerals Engineering, v. 156, 1 set. 2020.
- ANM. Sumário Mineral 2017. [s.l: s.n.]. Disponível em: <https://www.gov.br/anm/pt-br/centrais-de-conteudo/publicacoes/serie-estatisticas-e-economia-mineral/sumario-mineral/sumariomineral_2017>. Acesso em: 29 jul. 2023.
- ANM. Sistema de arrecadação da CFEM. Disponível em: <<http://recursomineralmg.codemge.com.br/substancias-minerais/recursos-industria-ceramica-e-vidreira/#>>. Acesso em: 31 jul. 2023.
- ARMSTRONG, M. et al. Accounting for tailings dam failures in the valuation of mining projects. Resources Policy, v. 63, p. 101461, out. 2019.
- CARMIGNANO, O. R. et al. Iron Ore Tailings: Characterization and Applications. Journal of the Brazilian Chemical Society Sociedade Brasileira de Quimica, , 2021.
- CESAMA. Cotação Cloreto Férrico. Juiz de Fora, 2021. Disponível em: <https://www.cesama.com.br/site/uploads/arquivos_editais/2209/165477645377356459438.pdf>. Acesso em: 29 jul. 2023
- DEMOPOULOS, G. P. et al. New Technologies for HCl Regeneration in Chloride Hydrometallurgy. World of Metallurgy – ERZMETALL, v. 61, 2008.

FILHO, A. DE A. Q.; NETO, A. A. A. Cimento. [s.l.: s.n.]. Disponível em: <<https://www.gov.br/anm/pt-br/centrais-de-conteudo/publicacoes/serie-estatisticas-e-economia-mineral/sumario-mineral/pasta-sumario-brasileiro-mineral-2018/cimento>>. Acesso em: 29 jul. 2023.

FOCUS ON PIGMENTS. European iron oxide pigment prices tracked by Vincentz. Focus on Pigments, v. 2022, n. 7, p. 3, jul. 2022.

FRITHUM, G. Fe-Separation and HCl regeneration technologies for ore leaching process: New and economic route. [s.l.: s.n.]

GOUVEIA, R. Can dry tailings be economically viable? [s.l.: s.n.]. Disponível em: <https://www.metsos.com/globalassets/saleshub/documents---episerver/webinar_dry_tailings_july2020_en.pdf?r=3>. Acesso em: 28 jul. 2023.

GOVERNO DE MINAS GERAIS. DIAGNÓSTICO DO SETOR MINERAL DE MINAS GERAIS. Belo Horizonte: [s.n.]. Disponível em: <https://www.agenciaminas.mg.gov.br/ckeditor_assets/attachments/11205/130fd1adf19cc74be83c7c6c829c53b9.pdf>. Acesso em: 31 jul. 2023.

INDEXBOX. China's Iron Oxide Pigment Price Shrinks to \$1,293 per Ton . Disponível em: <<https://www.indexbox.io/blog/china-iron-oxide-pigment-price-in-september-2022/>>. Acesso em: 29 jul. 2023.

JAFARPOUR, A.; KHATAMI, S. Analysis of Environmental Costs' Effect in Green Mining Strategy Using a System Dynamics Approach: A Case Study. Mathematical Problems in Engineering, v. 2021, p. 1–18, 16 jul. 2021.

LANXESS. Lanxess raises prices for iron oxide & chromium oxide pigments. Focus on Pigments, v. 2021, n. 4, p. 3–4, abr. 2021.

LI, Y. et al. Comprehensive reutilization of iron in iron ore tailings: preparation and characterization of magnetic flocculants. Environmental Science and Pollution Research, v. 27, n. 29, p. 37011–37021, 23 out. 2020.

LI, Y. et al. Eco-friendly strategy for preparation of high-purity silica from high-silica IOTs using S-HGMS coupling with ultrasound-assisted fluorine-free acid leaching technology. Journal of Environmental Management, v. 339, p. 117932, ago. 2023.

LIU, Y. et al. Production of lightweight ceramisite from iron ore tailings and its performance investigation in a biological aerated filter (BAF) reactor. Journal of Hazardous Materials, v. 178, n. 1–3, p. 999–1006, jun. 2010.

LU, Y. et al. Synthesis of iron red hybrid pigments from oil shale semi-coke waste. Advanced Powder Technology, v. 31, n. 6, p. 2276–2284, 1 jun. 2020.

MCKINLEY, C.; GHAREMAN, A. Hydrochloric acid regeneration in hydrometallurgical processes: a review. *Mineral Processing and Extractive Metallurgy*, v. 127, n. 3, p. 157–168, 3 jul. 2018.

METSO. Are conditioning tanks making a comeback? Disponível em: <<https://www.metso.com/insights/blog/mining-and-metals/are-conditioning-tanks-making-a-comeback/>>. Acesso em: 31 jul. 2023.

SAEP. Ata de Sessão Pública Proc. Licitatório n.o 000002/23 PREGÃO PRESENCIAL n.o 2. , 2023. Disponível em: <<https://www.saep.sp.gov.br/DownloadServlet?id=esfnngylsseza9xidjdrk0efzl7qp1iy9>> . Acesso em: 29 jul. 2023

SILVA, C. Preço do material de construção varia até 179% na Grande BH. Disponível em: <https://www.em.com.br/app/noticia/economia/2020/09/28/internas_economia,1189510/preco-do-material-de-construcao-varia-ate-179-na-grande-bh.shtml#google_vignette>. Acesso em: 29 jul. 2023.

SOBOTKA, A.; JASKOWSKI, P.; CZARNIGOWSKA, A. Optimization of Aggregate Supplies for Road Projects. *Procedia - Social and Behavioral Sciences*, v. 48, p. 838–846, 2012.

THE MANUFACTURER. Rise in Demand for Semiconductors to Drive Global High Purity Quartz Market. Disponível em: <<https://www.themanufacturer.com/press-releases/rise-in-demand-for-semiconductors-to-drive-global-high-purity-quartz-market#:~:text=The%20price%20of%20high%20purity,HPQ%20on%20a%20contract%20basis>>. Acesso em: 29 jul. 2023.

THYSSENKRUPP. Chlor-Alkali Electrolysis. [s.l: s.n.]. Disponível em: <https://ucpcdn.thyssenkrupp.com/_legacy/UCPthyssenkruppBAISUhdeChlorineEngineers/assets.files/products/chlor_alkali_electrolysis/thyssenkrupp_chlor_alkali_brochure_web.pdf>. Acesso em: 31 jul. 2023.

TRADING ECONOMICS. Iron ore. Disponível em: <<https://tradingeconomics.com/commodity/iron-ore>>. Acesso em: 29 jul. 2023.

USMAN, U. A. et al. The economic potential of the African iron-ore tailings: synthesis of magnetite for the removal of trace metals in groundwater—a review. *Environmental Earth Sciences*, v. 78, n. 21, p. 615, 16 nov. 2019.

VATALIS, K. I.; CHARALAMBIDES, G.; BENETIS, N. P. Market of High Purity Quartz Innovative Applications. *Procedia Economics and Finance*, v. 24, p. 734–742, 2015.

VICTORIA, A. M. Recursos para a Indústria Cerâmica e Vidreira. Em: *Recursos Minerais de Minas Gerais*. [s.l: s.n.]

VISEDO, G.; PECCHIO, M. ROADMAP tecnológico do cimento: potencial de redução das emissões de carbono da indústria do cimento brasileira até 2050. Rio de Janeiro: [s.n.].

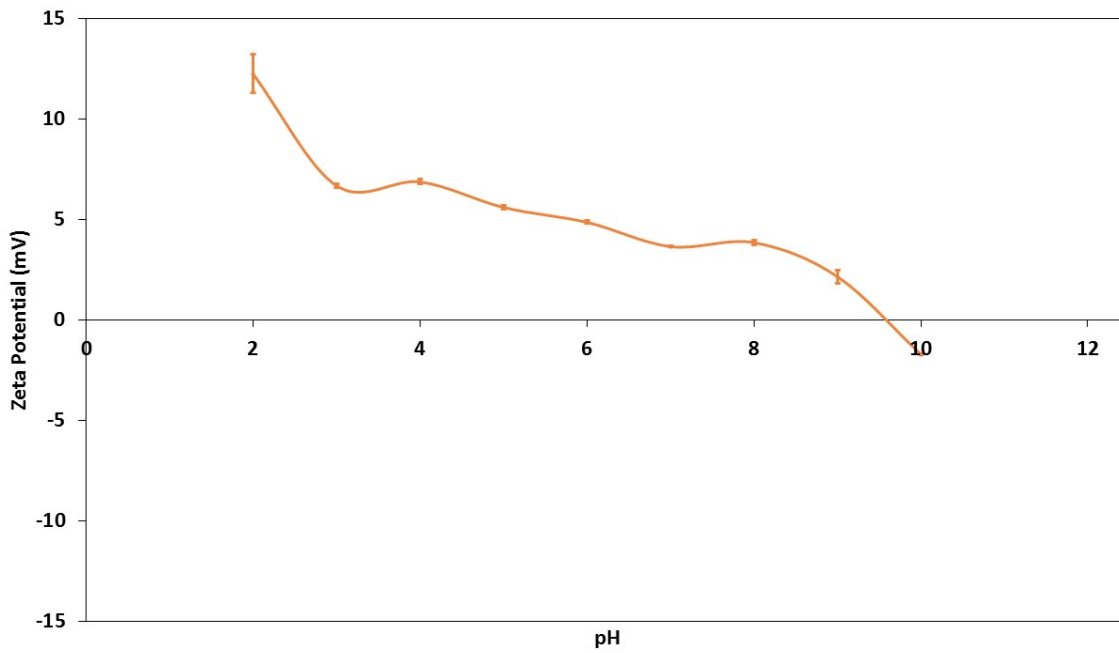
WELBERT, R. Pesquisa revela variações de preços em itens de construção em Divinópolis. Disponível em: <<https://g1.globo.com/mg/centro-oeste/noticia/2016/08/pesquisa-revela-variacoes-de-precos-em-itens-de-construcao-em-divinopolis.html>>. Acesso em: 29 jul. 2023.

WILLS, B. A.; FINCH, J. A. Wills' Mineral Processing Technology: An Introduction to the Practical Aspects of Ore Treatment and Mineral Recovery. 8. ed. [s.l.] Elsevier, 2016.

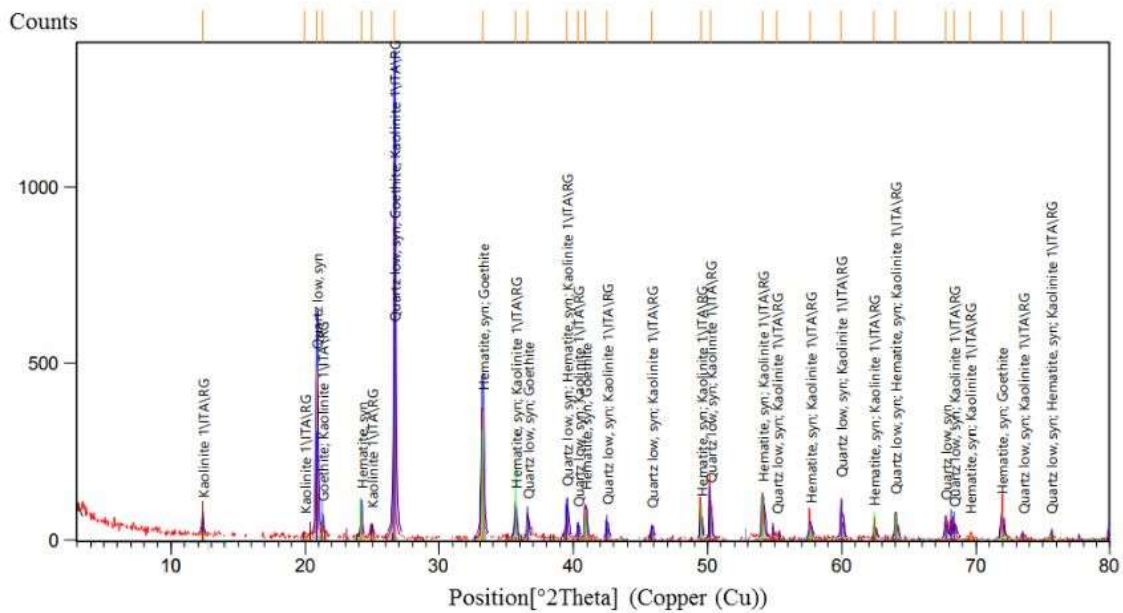
XU, X. et al. Production scheduling optimization considering ecological costs for open pit metal mines. Journal of Cleaner Production, v. 180, p. 210–221, abr. 2018.

ANEXO I – Material Suplementar Artigo 1 (Capítulo II)

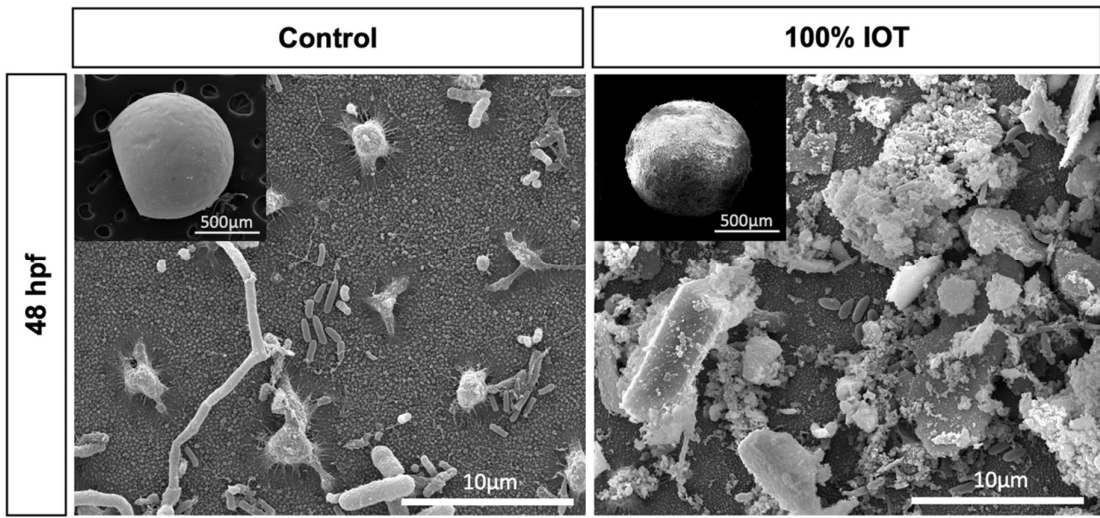
Appendix II.01. Determination of Zeta Potential of iron ore tailing (IOT) particles as function of pH. The isoelectric point (IEP) of IOT particles was identified at the pH of 9.7. The analysis was carried out in ZetaSizer Nano ZS by the electrophoretic light scattering technique. The suspension with the IOT particles presented original pH 7.0 ± 0.1 and ionic strength of $157.6 \mu\text{S}$. Adjustment for the acid and basic ranges were performed by the addition of hydrochloric acid (4.0 mol L^{-1}) and sodium hydroxide (4.0 mol L^{-1}), respectively.



Appendix II.02. X-ray diffraction (XRD) pattern of iron ore tailing (IOT) particles in suspension. XRD analysis performed on Siemens X-ray diffractometer, equipped with a fixed Cu anode tube. Hematite and quartz represent the sample major mineralogical components.



Appendix II.03. Effect of iron ore tailing (IOT) suspensions exposure to zebrafish chorion. Representative FESEM detailed images of 48 hpf embryo (magnitude: 10.000 x) showing massive IOT deposits on the fish chorion surface (right) when compared to control group (left). Left top corner images show the entire embryo (magnitude: 200 x; voltage: 20,000 kV, spot: 4.0).



ANEXO II - Material Suplementar Artigo 3 (Capítulo IV)

Appendix IV.01. Elemental analysis of iron ore tailings by microwave assisted digestion (U.S. EPA 3052 Method*) and ICP/OES.

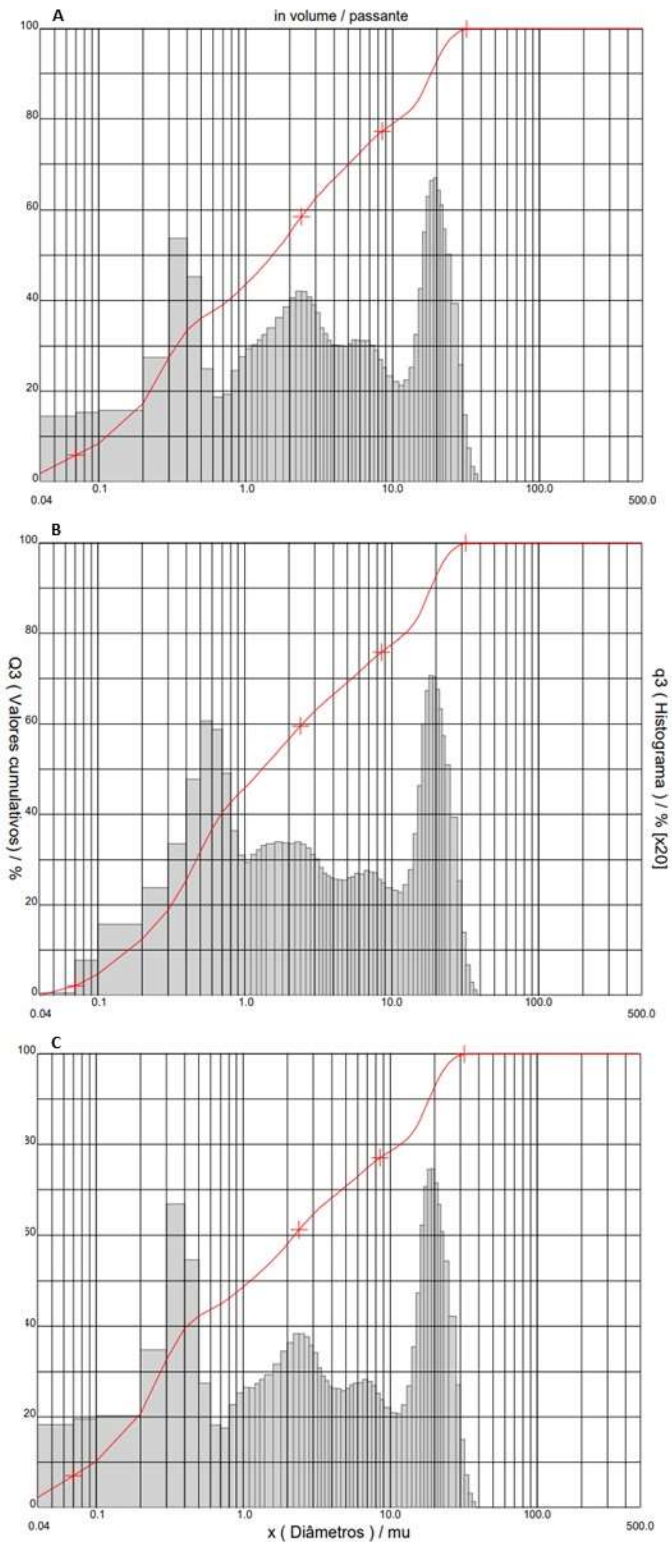
Elemental	Concentration (%)
Si	31.05
Fe	16.98
Al	1.59
Ti	0.07
P	0.04
Mn	0.02
Ca	<0.021
Ba	0.0078
Zn	0.0042
V	0.0041
Cr	0.0038
Cd	<0.0038
Mg	0.0038
As	<0.0035
Cu	0.0035
Pb	<0.0035
Sn	<0.0035
Ni	<0.0035
Na	<0.0035
Co	0.0033

*U.S. EPA. 1996. "Method 3052 (SW-846). Microwave assisted acid digestion of siliceous and organically based matrices." Revision 0, Washington, DC.

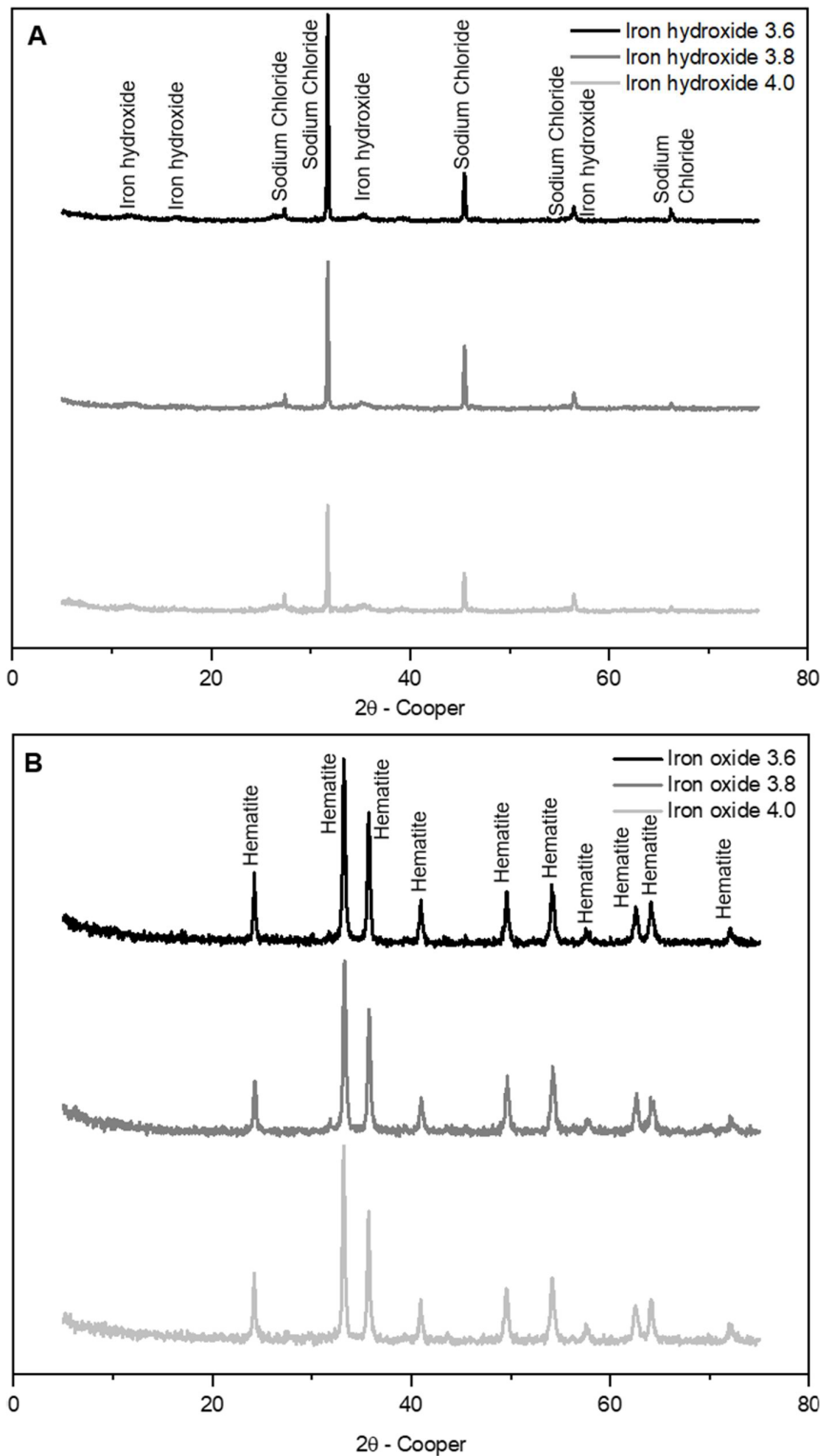
Appendix IV.02. Solid fraction obtained after leaching and washing of iron ore tailings, followed by drying at 60°C.



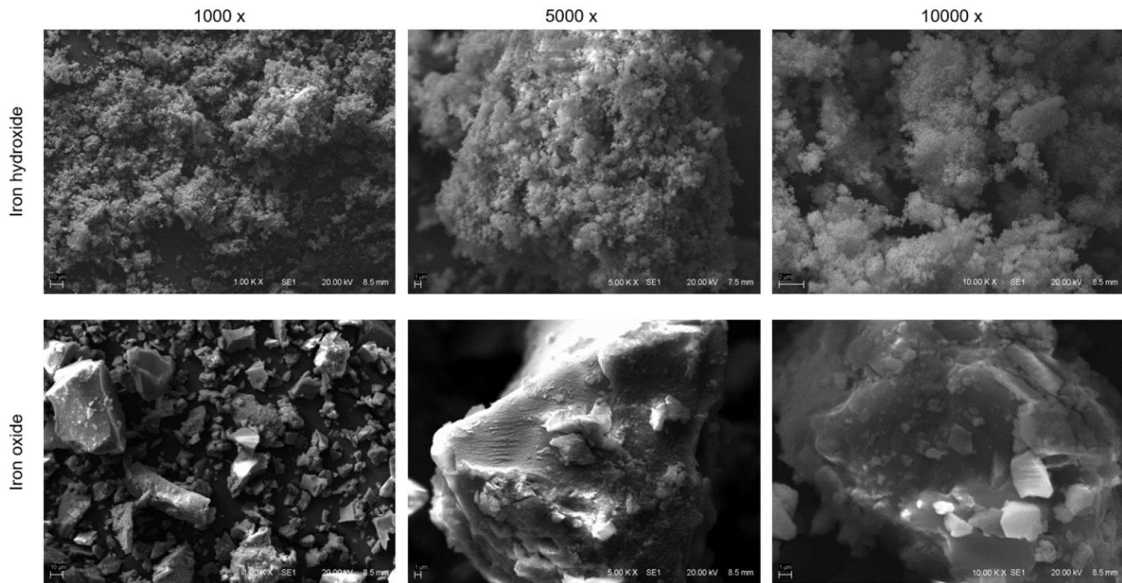
Appendix IV.03. Granulometric distribution of iron oxides synthetised from the iron sludge obtained by selective precipitation at pH values of 3.6, 3.8, and 4.0, followed by thermal treatment (550 °C) and hot water washing.



Appendix IV.04. (A) X-ray diffractograms of the iron sludge obtained by selective precipitation at pH values of 3.6, 3.8, and 4.0 and after drying at 60°C, and (B) X-ray diffractograms of iron oxides synthetised from the iron sludge obtained by selective precipitation at pH values of 3.6, 3.8, and 4.0, followed by thermal treatment (550°C) and hot water washing.



Appendix IV.05. SEM of the silica-free iron oxy-hydroxy precipitate at pH 3.8 and after drying at 60°C; and hematite particles synthesised at pH 3.8, following thermal treatment (550°C) and hot water washing.



Appendix IV.06. Silica-free hematite powder produced from iron ore tailings by means of the simplified hydrometallurgical route developed in this work.

